THE UNIVERSITY
of ADELAIDE

SUB CRUCE LUMEN

School of Biological Sciences

Department of Molecular and Biomedical Sciences

The University of Adelaide

Generation and Transcriptomic Analysis of HIF-1Alpha and HIF-2Alpha Knockout 5TGM1 Multiple Myeloma Cells

Yu Chinn Joshua Chey

A thesis submitted in fulfilment of the requirement for the degree of

Master of Philosophy

October 2019

Contents

Abstract

Multiple myeloma (MM) is a blood cancer characterised by the uncontrolled proliferation and dissemination of neoplastic plasma cells in the bone marrow (BM). As the BM is physiologically hypoxic, hypoxia may serve as a microenvironmental stimulus that drives MM disease development and progression by promoting a broad range of tumorigenic features like tumour growth, angiogenesis, metastasis and bone osteolysis. Major cellular responses and adaptation to hypoxia are mediated through Hypoxia-Inducible Factor (HIF) signalling. The HIFs are heterodimeric transcription factors that activate the transcription of hundreds of target genes in response to hypoxia. In most solid tumours, HIF signalling is co-opted to contribute to tumour survival and progression. However, the role of HIF signalling in blood cancers is less well understood, specifically the distinct roles of the major HIF-α isoforms. Given that MM PCs reside in the hypoxic BM, the HIFs are likely to play important roles in MM disease. HIF-isoform specific inhibitors are currently in development and are being tested at the clinical level, and therefore, it would of considerable interest to determine if these drugs can potentially be repurposed for MM treatment.

This research project aimed to investigate the unique and overlapping roles of HIF-1α and HIF-2α in the 5TGM1 mouse MM cell lines, which are syngeneic with the C57BL/KaLwRij mouse model. In this thesis, HIF-1α and HIF-2α inducible knockout and knocked-out 5TGM1 cells were generated using a doxycycline-inducible CRISPR/Cas9 system. Subsequently, HIF-1α and HIF-2α knockout 5TGM1 cells were characterised at the DNA, RNA and protein levels. Lastly, the *in-vitro* transcriptomes of HIF-1α and HIF-2α knockout 5TGM1 cells cultured in normoxia and hypoxia were profiled by RNA-sequencing to identify HIF-1α and HIF-2α target genes. In the 5TGM1 cells, HIF-1α was shown to regulate a broad range of target genes in response to hypoxia, with prominent roles in metabolic programming, cell-survival and transcriptional regulation. In comparison, HIF-2α appears to be expressed in very low levels and mediates more subtle roles.

Overall, the data on 5TGM1 cells in this thesis indicate that the HIFs, especially HIF-1, are likely to play important roles to support MM tumour adaptation, survival and development in the hypoxic BM microenvironment. The generated HIF-1α and HIF-2α inducible knockout and knocked-out 5TGM1 cells in this study are valuable tools for the further investigation and comparative analysis of the roles of each HIF-α isoform *in-vivo* in the syngeneic KaLwRij mouse model.

Declaration

I certify that this work contains no material which has been accepted for the award of any other degree or diploma in my name in any university or other tertiary institution and, to the best of my knowledge and belief, contains no material previously published or written by another person, except where due reference has been made in the text. In addition, I certify that no part of this work will, in the future, be used in a submission in my name for any other degree or diploma in any university or other tertiary institution without the prior approval of the University of Adelaide and where applicable, any partner institution responsible for the joint award of this degree.

I give permission for the digital version of my thesis to be made available on the web, via the University's digital research repository, the Library Search and also through web search engines, unless permission has been granted by the University to restrict access for a period of time.

Yu Chinn Joshua Chey

Acknowledgements

Life in the Peet lab is the bee's knees. Yes, I'm calling it. My two-and-a-half (technically, three) year stint here has been an absolute blast. And I owe it to all the awesome people here whom I've shared this wonderful experience with. You guys rock, and the next shout's on me.

Dan, I am grateful for your continuous support, guidance and patience throughout this research project. Thank you for agreeing to take me under your wing, and for teaching me the art of pipetting and data analysis. You're an amazing mentor and science educator, and I hope to one day incite curiosity and inquiry in others like you do. Hope you like the new indoor plant we got for you! We've named it Jerry.

To my fellow compatriots from the Peet/Whitelaw labs, I couldn't have done it without all of you. Ice, thanks for all your help and advice. You're a great teacher, and your meticulous eye for detail is truly remarkable. Cam and Joe the dynamic duo, you're a treasure trove of fresh ideas whenever I'm in an experimental pickle. Will always be as keen as a bean for our twice-weekly bouldering sessions with Tim. Lex, your lunch-time stories are always fun to listen to. Thank you for your fantastic advice for the trickiest of lab work. Tim, https://youtu.be/aFm4-joYTok. Josiah, you have my gratitude for introducing me to the wonderful world of coffee. I've been hooked ever since. Luke, your ceaseless puns never fail to amuse me. I tried to make a chemistry joke the other day but got no reaction. Nick, thanks for the lunch runs to the Hub and for constantly bewildering Ice with your brilliant remarks. It's been truly entertaining. Carla, I really appreciate your help with the final few experiments to wrap up this research project. All the best in further uncovering the mysteries of the HIFs! Lorenzo, you're an absolute mad lad. Thanks for sharing a slice of France with us. I would also like to thank Yagnesh, Nat & Jay, Emily, Rachel and Yesha for their scientific insight and great company. Also, Simon, you're a rockstar. Finally, I'd like to thank Dave and Murray, for their great advice, support and dad jokes throughout my MPhil project.

I would also like to extend my appreciation to our neighbouring virologists: Michael, Nick, Kylie, Byron, Rosa, Chuan, Emily, Ornella, Brandon, Tom and Andrew. Thank you for your infectious wholesomeness, and for lending me your qRT-PCR machine. Also, cheers to everyone on L3 MLS, including Blagojce, Kat, Joel and others, who collectively make us coolest floor in the building.

To my co-supervisor Andrew, thank you for your wonderful advice, comments and support. To Duncan, I really appreciate your help in getting started with experiments in SAHMRI, and your insight and feedback throughout. Not forgetting the members of the Myeloma Research Laboratory, Sharon, Vicki, Kryzs, Mara, Kim, Tash, Alanah and others for their generous help with all things Myeloma.

Special thanks go to my close friends Arthur, Sabrina, Shanice and Bertram for keeping me sane outside of the lab. Here's to more dinners, spontaneous coffee runs and senseless rants. To Mom, Dad and Sarah, thank you for your loving support throughout my Aussie adventures. I always love our weekly calls and banter. To my aunt Pat and aunt Ruth and their families, thank you for the lovely lunches, dinners and trips to the Barossa. It's great to have a family away from home. Finally, to my aunt Mag and family, I will forever appreciate your selflessness, kindness and generosity. Thank you for making this possible.

Formal acknowledgements

Abbreviations

5TGM1 B	5TGM1 BMX1 cells
5TGM1 BF	5TGM1 BMX1 FuCas9Cherry cells
5TGM1 BFF	5TGM1 BMX1 FuCas9Cherry FgH1tUTP cells
5TGM1 BFF m	5TGM1 BMX1 FuCas9Cherry FgH1tUTP monoclonal cells
5TGM1 BFF mK	5TGM1 BMX1 FuCas9Cherry FgH1tUTP monoclonal knockout cells
aa	Amino acid
AGRF	Australian Genome Research Facility
ARNT	Aryl hydrocarbon nuclear receptor translocator
bHLH	Basic helix-loop-helix
BM	Bone marrow
CBP	CREB-binding protein
ChIP	Chromatin Immunoprecipitation
CMV	Cytomegalovirus
CRISPR	Clustered regularly interspaced short palindromic repeats
C-TAD	C-terminal transactivation domain
Cy5	Cyanine-5
DMSO	Dimethyl sulfoxide
DNA	Deoxyribonucleic acid
Dox	Doxycycline
DP	2,2-dipyridyl
ECL	Enhance chemiluminescence
EDTA	Ethylenediaminetetraacetic acid
eGFP	Enhanced green fluorescence protein
FIH	Factor inhibiting HIF
gRNA	Guide RNA
H1E1	*Hif-1α* Exon 1
H1E2	*Hif-1α* Exon 2

H1E3	*Hif-1α* Exon 3
H2E2	*Hif-2α* Exon 2
H2E3	*Hif-2α* Exon 3
HIF	Hypoxia-inducible Factor
HRE	Hypoxia response element
HRP	Horseradish peroxidase
HSC	Haematopoietic stem cell
hUbC	Human ubiquitin C
IDT	Integrated DNA Technologies
Ig	Immunoglobulin
K_m	Michaelis constant
MGUS	Monoclonal gammaopathy of undetermined clinical significance
MM	Multiple myeloma
mmHg	Millimetres of mercury
N-TAD	N-terminal transactivation domain
ODD	Oxygen-dependent degradation domain
PAC	Motif C-terminal to PAS motifs
PAS	Per-Arnt-Sim
PBS	Phosphate buffered saline
PBS-T	Phosphate buffered saline with tween 20
PC	Plasma cell
PCR	Polymerase chain reaction
PHD	HIF Prolyl-hydroxylase
pO_2	Partial pressure of oxygen
PTC	Premature termination codon
qRT-PCR	Quantitative real time polymerase chain reaction
RCC	Renal cell carcinoma
RNA	Ribonucleic acid
RT	Room temperature
sgRNA	Single guide RNA
SMM	Smouldering multiple myeloma

spCas9	*Streptococcus pyogenes* Cas9
Tet	Tetracycline
Tet-R	Tetracycline-repressor
TF	Transcription factor
Ub	Ubiquitin
VHL	Von Hippel-Lindau

Chapter 1

Introduction

1 Introduction

1.1 Multiple Myeloma

Multiple myeloma (MM) is the ageing-associated haematological malignancy of bone marrow (BM) plasma cells (PC) (Dutta et al. 2017). Of all blood cancers, it is second only to non-Hodgkin lymphoma in prevalence and is responsible for an estimated 80 000 deaths annually worldwide (Ferlay et al. 2015; Siegel, Naishadham & Jemal 2012). About 10 000 Australians are currently affected by MM, and around 1 800 Australians are diagnosed with this malignant disease every year (Cancer Australia 2019).

MM is an area of significant research interest as it is presently incurable. Advances in treatments have increased the five-year relative survival rate of elderly American myeloma patients from 25.0% to 37.9% between the periods of 1991-2002 and 2007-2011, respectively (Uprety et al. 2017). However, MM is still universally fatal, with a median overall survival of about 7-8 years for patients diagnosed at 60 years and under (Blimark et al. 2018). The development of better patient management, therapeutic options and curative care for MM is conceivably limited by our inadequate knowledge about the aetiology of this disease.

1.1.1 Pathology

Normal PCs secrete antibodies as part of the humoral immune response to fight infection. PC precursors differentiate from B-lymphocytes in response to an antigenic challenge within the germinal centres of secondary lymphoid tissues (Suan, Sundling & Brink 2017). Precursors with high-affinity to antigens subsequently migrate to the BM, where they terminally differentiate into mature and long-living PCs (Pellat-Deceunynck & Bataille 2004).

MM is characterised as the dyscrasic proliferation of clonal neoplastic PCs in the BM that disseminate throughout the skeleton. MM PCs spread and proliferate to form myelomatous tumours at multiple BM sites, through their mobilisation and systemic recirculation from the initial lesion to distal sites (Ghobrial 2012). These tumours promote osteolytic bone destruction, reduce erythrocyte production and suppresses adaptive immune responses, leading to increased infections in patients (Dispenzieri & Kyle 2005). MM PCs also produce abundant abnormal monoclonal immunoglobulin (Ig; paraprotein), or Ig light chains (Bence-Jones protein), which is a pathognomonic feature of this disease (Djunic et al. 2014). The excess paraprotein is also nephrotoxic.

Clinically, the behaviour of MM PCs manifests as a combination of myeloma defining features known mnemonically as CRAB, which are hypercalcemia, renal insufficiency, anaemia, and bone lesions (Rajkumar et al. 2014). These symptoms are evidence of end-organ damage and negatively affect patients' quality of life. The presence of at least one CRAB feature, in addition to the presence of ≥10% clonal BM PCs or a biopsy-proven plasmacytoma (single myelomatous tumour), are indication of the requirement for MM treatment, as outlined in the recent (2014) updated guidelines by The International Myeloma Working Group (IMWG) (Rajkumar et al. 2014). Also, the presence of one or more biomarkers that are associated with the inevitable development of MM, (≥60% clonal BM PCs, ratio of involved to uninvolved serum-free Ig light chains of ≥100 or detection of ≥1 focal lesion by MRI) is now considered as an MM disease state (Rajkumar et al. 2014).

The clinical stages of MM disease development are well defined, driven by a combination of genetic mutations and environmental factors (Figure 1). Initiating genetic events provide a pre-neoplastic PC clone with a proliferative advantage, leading to an asymptomatic (no CRAB features) precursor disease state known as monoclonal gammopathy of undetermined significance (MGUS) (Korde, Kristinsson & Landgren 2011). Primary mutations that lead to the establishment of a founder PC include Immunoglobulin Heavy Chain translocations and hyperdiploidy, which confer a proliferative advantage that result in the development of MGUS (Bergsagel & Kuehl

2005; Dutta et al. 2017). Statistically, MGUS occurs in over 3% of adults over the age of 50, and they have a small risk of transitioning to MM of about 1% per year (Kyle & Rajkumar 2004; Rajkumar 2016).

Further accumulation of secondary genetic mutations and synergistic interactions with the BM microenvironment advances MGUS to an intermediate asymptomatic disease stage known as Smouldering Multiple Myeloma (SMM), and subsequently to symptomatic or progressive MM (Korde, Kristinsson & Landgren 2011). These secondary mutations include non-synonymous single nucleotide polymorphisms, copy number abnormalities and epigenetic changes, which contributes to the dysregulation of PC function and further MM disease progression (Morgan, Walker & Davies 2012). SMM patients are at a higher risk of transitioning to MM, at 10% per year for five years following diagnosis, which reduces to 3% per year over the next five years and 1.5% per year after that (Rajkumar 2016).

Most of the genetic aberrations required to give rise to MM are usually already present at SMM, implying that disease development is dependent on extrinsic factors within the BM microenvironment (Dutta et al. 2018). BM tissue located in the cavities of axial and long bones is part of the lymphatic system, and responsible for haematopoiesis. Its microenvironment supports haematopoiesis and PC longevity through the complex interplay of its various components, consisting of cells, the extracellular matrix and the liquid milieu. Among the residents of the BM are haematopoietic cells, BM stromal cells, osteoclasts, osteoblasts, and endothelial cells (Manier et al. 2012). These cells interact with each other directly through adhesion molecules, or indirectly through growth factor, cytokine and chemokine signalling (Lemaire et al. 2011). MM PCs appear to disrupt normal BM homeostasis and remodel the BM microenvironment to support its survival, proliferation and migration, leading to aberrant angiogenesis, bone degradation and treatment resistance (Hu et al. 2010; Lemaire et al. 2011).

Also, the BM microenvironment is well-accepted to be physiologically hypoxic (Martin et al. 2011). Hypoxia is the state of inadequate oxygen and is a BM feature that is

important for haematopoiesis. In recent years it has also garnered increased interest for its role in blood cancer biology, particularly in the development and progression of MM.
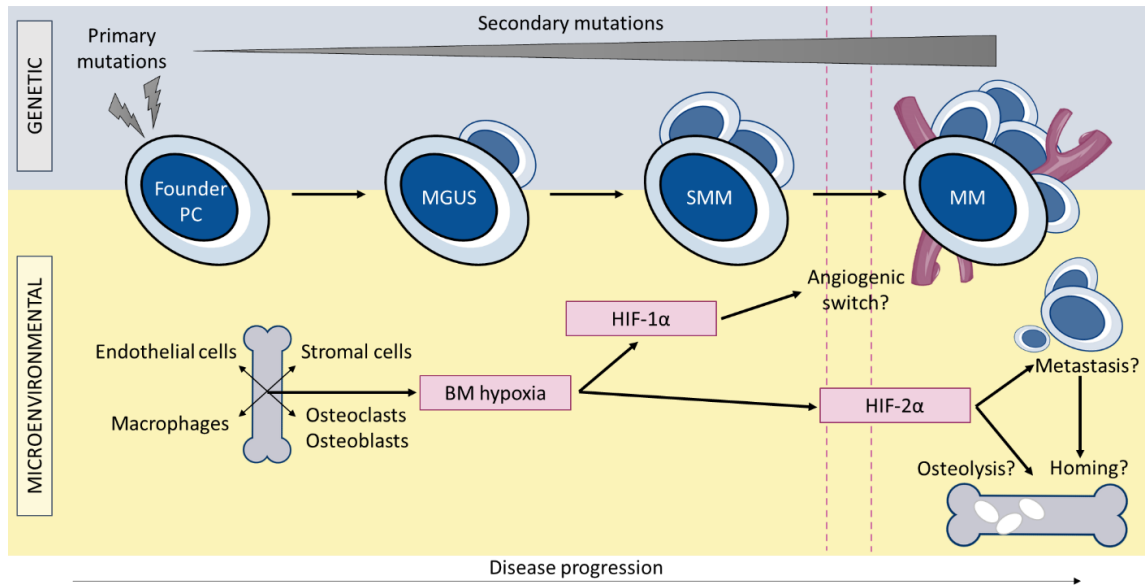
Figure 1: Microenvironmental factors drive MM disease progression in addition to genetic mutations. MM PCs interact with the many cellular residents of the BM, as well as the conditions of its surrounding microenvironment. BM hypoxia induces the expression of the HIFs in MM PCs, which elicits a broad range of responses which can contribute to disease progression. HIF-1α is thought to drive the angiogenic switch between the asymptomatic SMM and the symptomatic MM stages of the disease, while HIF-2α is thought to be important in regulating MM PC dissemination throughout the skeleton and bone osteolysis. PC, plasma cell; MGUS, monoclonal gammopathy of undetermined clinical significance; SMM, smouldering multiple myeloma; MM, multiple myeloma; HIF, hypoxia-inducible factor.

1.2 Hypoxia

Hypoxia is the state of reduced oxygen availability, brought about by insufficient oxygen supply or when cellular oxygen consumption exceeds delivery. While adequate oxygenation of most cells in an aerobic organism is essential for oxidative phosphorylation and redox reactions, hypoxic microenvironments naturally occur in regions throughout the body such as the BM and renal papilla. These areas are critical for the maintenance, proliferation, and differentiation of stem cells (Mohyeldin, Garzón-Muvdi & Quiñones-Hinojosa 2010). Hypoxia also plays essential roles in embryonic morphogenesis, such as for vascular remodelling and heart development (Dunwoodie 2009; Peng et al. 2000).

Localised hypoxia is also associated with several pathologies, such as cardiac infarction, stroke, and cancer. In many solid tumours, intratumoral hypoxia arises due to the formation of abnormal vasculature and increased diffusion distances, which is of clinical significance because it is a microenvironmental factor that selects for hypoxia-tolerant, aggressive and treatment-resistant tumour cells (Martin et al. 2011; Vaupel & Harrison 2004).

Cells need to maintain oxygen homeostasis and respond appropriately to adapt to and/or counteract a hypoxic environment. Typically, cells attempt to overcome a hypoxic challenge by altering their metabolism and microenvironment. As a general example, cells can optimise or conserve oxygen use, by favouring anaerobic glycolysis over oxidative phosphorylation for energy production and by inhibiting anabolism (Michiels 2004). Cells can also improve oxygen delivery by stimulating angiogenesis, mediated by the release of cytokines such as vascular endothelial growth factor (VEGF) and platelet-derived growth factor (PDGF) (Michiels 2004). Additionally, cells can activate autophagic cell survival processes through the induction of BCL2/adenovirus E1B 19 kDa protein-interacting protein 3 (BNIP3) (Bellot et al. 2009).

Depending on the cell or tissue type, hypoxia-induced responses can vary due to different energy requirements and sensitivities to oxygen depletion, as well as the normoxic range and other complex properties of a microenvironment. The normoxic partial pressure of oxygen (pO_2) exists as a continuum and varies between tissues. Physiological normoxia can range between ~100 mmHg in arterial blood, to as low as ~29 mmHg in the muscle (Koh & Powis 2012), and therefore the threshold for hypoxia is spatially dependent.

1.2.1   The hypoxic bone marrow microenvironment

The BM microenvironment has been generally well accepted to be physiologically hypoxic (Danet et al. 2003). Prior to reports of BM oxygen measurements, researchers had hypothesised the presence of hypoxic niches within the BM from (i) the alignment and position of long-term repopulating haematopoietic progenitors furthest from where blood enters the BM circulation, and from (ii) the desaturation of BM blood that is similar to that in the jugular vein (Cipolleschi, Dello Sbarba & Olivotto 1993; Grant & Root 1947). This notion was supported by experiments with mouse BM cell isolates, where hypoxic-incubated BM cells display better repopulation ability than normoxia-incubated cells in marrow repopulation assays (Cipolleschi, Dello Sbarba & Olivotto 1993).

Experiments performed to measure BM oxygen levels yield different results depending on the methodology used. Early techniques for measuring the pO_2 in the BM were invasive and lacked spatial resolution. Measurements performed by Watanabe *et al.* (2007) using a Clark electrode and oxygen monitor determined an average median of intramedullary oxygen tension of 12.4 mmHg within the proximal femur of patients during surgery for femoral neck fractures (Watanabe et al. 2007). Gas analysis on bone marrow aspirates of healthy volunteers by Harrison *et al.* (2002) determined a mean pO_2

of 54.9 mmHg (Harrison et al. 2002). This measurement was later found to be analogous to that of BM aspirates from MGUS, SMM and MM patients (Colla et al. 2010).

The use of non-invasive methods overcome methodological challenges to measure the heterogeneous distribution of oxygen within the BM, but with limited spatial resolution. Several groups have utilised pimonidazole, a bio-reductive marker that forms stable adducts in a hypoxic cell at pO_2 <10 mmHg, to indirectly visualise BM oxygen distribution (Hu et al. 2010; Lévesque et al. 2007; Parmar et al. 2007; Takubo et al. 2010). BM directly adjacent to the bone-BM interface (endosteal surface) displays high pimonidazole incorporation, which decreases sharply within 50 μm towards the central vascular region and is of a similar expression pattern to the hypoxia-inducible factor 1 alpha (HIF-1α)(Lévesque et al. 2007). It is thought that the more hypoxic endosteal niche maintains and supports immature and quiescent haematopoietic stem cells (HSCs) while the less hypoxic vascular niche promotes HSC self-renewal, maturation and differentiation (He et al. 2014; Martin et al. 2011).

A recent experiment by Spencer *et al.* (2014) utilised two-photon phosphorescence lifetime microscopy to directly measure BM oxygen tension in the skull of live mice with an improved spatial resolution (Spencer et al. 2014). By optically measuring the phosphorescence decay of systematically injected platinum porphyrin, pO_2 at the endosteal region was measured to be 21.9 mmHg within blood vessels, and 13.5 mmHg outside the vessels. Lower pO_2 was observed >40 μm from the endosteal surface, where values for intravascular and extravascular pO_2 were 17.7 mmHg and 9.9 mmHg respectively.

While there are discrepancies about pO_2 values and direction of oxygen gradients between different experiments, all of them support the notion that the BM is a hypoxic microenvironment.

1.3 Hypoxia-inducible Factors

Although hypoxic responses differ in extent and intensity between cell types, the primary cellular mechanism employed to monitor and respond (via targeted gene expression) to changes in oxygen tension are evolutionarily conserved in all mammalian cells (Chi et al. 2006). This mechanism is the oxygen-dependent control of a set of transcription factors (TFs) known as the Hypoxia-Inducible Factors (HIFs).

HIFs are heterodimeric TFs that play the dominant role in mediating transcriptional changes in response to hypoxia, which collectively allows individual cells and the organism as a whole to both counteract and tolerate physiological hypoxia. Consisting of an α and a β subunit, HIFs are members of the basic helix-loop-helix/Per-Arnt-Sim (bHLH/PAS) family of DNA binding proteins (Wang et al. 1995). In mammals, the oxygen-regulated α subunit of HIF consists of one of three different isoforms, namely HIF-1α, HIF-2α, and HIF-3α, while the β subunit is the constitutive, nuclear-localised aryl hydrocarbon receptor nuclear translocator (ARNT, also known as HIF-1β) (Figure 1.2). HIF-1α and HIF-2α have partly overlapping, but non-redundant functions and are the major factors responsible for hypoxic gene regulation, whereas the role of HIF-3α is more subtle and incompletely characterised (Dengler, Galbraith & Espinosa 2014). Most HIF-3α splice isoforms lack intrinsic transactivational capacity and are thought to be negative regulators of HIF-1α by inhibiting its DNA binding ability (Makino et al. 2001; Maynard et al. 2005). Given the dominant roles of HIF-1α and HIF-2α in many cancers, they are the focus of this discussion and research project.

HIF-1α and HIF-2α share similar functional domain structures. Within the N-terminal half of the proteins are the bHLH domain for DNA binding and heterodimerisation to ARNT, and the tandem PAS domains for heterodimerisation specificity and stability (Möglich, Ayers & Moffat 2009; Yang et al. 2005) (Figure 1.2). The C-terminal half contains the N-terminal transactivation domain (N-TAD) within the oxygen-dependent degradation domain (ODD) and C-terminal transactivation domain (C-TAD) (Figure 1.2). The ODD and C-TAD are modified post-translationally for the regulation of protein stability and

transactivational capacity, respectively (Figure 1.3). These modifications are mediated in normoxia by the 2-oxoglutarate-dependent oxygen-sensing hydroxylases HIF prolyl-hydroxylase (PHD) 1-3 and the asparaginyl hydroxylase Factor Inhibiting HIF (FIH) (Schofield & Ratcliffe 2004). These enzymes require oxygen, iron (Fe^{2+}), and ascorbate for their activity.

In normoxia, PHDs hydroxylate specific proline residues within the ODD of HIF-α protein, which in turn recruits the binding of the von Hippel-Lindau (VHL) tumour suppressor and components of the E3 ubiquitin-protein ligase complex (Maxwell et al. 1999; Tanimoto et al. 2000). This leads to the polyubiquitination and rapid proteasomal degradation of HIF-α protein. While they all efficiently modify and negatively regulate HIF-α in normoxia, the three PHD isoforms are not redundant as they have different cell-dependent expression profiles and exert differential effects (Takeda et al. 2008); PHD2 is known to preferentially hydroxylate HIF-1α, while PHD3 preferentially hydroxylates HIF-2α (Appelhoff et al. 2004; Fujita et al. 2012). In hypoxia, the oxygen-dependent PHDs have reduced activity, and HIF-α subsequently escapes VHL-mediated proteolysis, leading to the accumulation of HIF-α protein.

In addition to prolyl hydroxylation-mediated degradation, the C-TAD of HIF-α is also hydroxylated in normoxia at a specific asparagine residue by FIH, which prevents the recruitment and binding of the transcriptional coactivator and histone acetyltransferases CBP and p300 (Lando et al. 2002). The negative regulation of HIF-α transactivation is VHL-independent. Hypoxia abrogates FIH-mediated hydroxylation of HIF-α, which then allows for coactivator recruitment and transcriptional activation of target genes. However, in comparison to the PHDs, FIH has a lower K_m for oxygen and remains active at lower oxygen concentrations than that which would stimulate HIF accumulation (Ehrismann et al. 2007; Tarhonskaya et al. 2015).

Hypoxia-stabilised HIF-α is shuttled into the nucleus, associates with ARNT and transcriptional cofactors to form an active TF which recognises and binds to hypoxia

response elements (HRE; [A/G]CGTG) in the regulatory regions of target genes (Wenger, Stiehl & Camenisch 2005).

Additionally, HIF accumulation and activation may also occur independent of hypoxia due to growth factors and oncogenic signalling, which influences HIF translation, stabilisation and transcriptional activity in a cell and stimulus-specific manner (Singh et al. 2017). For example in many cancers, growth factors activating receptor tyrosine kinases (RTKs) can inappropriately activate the phosphatidylinositol-4,5-bisphosphate-3-kinase (PI3K) /Protein kinase B (Akt) signalling pathways which can aberrantly upregulate HIF-1α translation through downstream mammalian target of rapamycin (mTOR) signalling (Masoud & Li 2015; Semenza 2002; Treins et al. 2002). Also, RTK activation can enhance HIF-1α transactivational capacity through the mitogen-activated protein kinases (MAPK) signalling pathway. Extracellular signal-regulated kinase (ERK) activated by enhanced MAPK signalling phosphorylates p300 and enhances its transactivational activity, which facilitates its interaction with HIF-1α (Sang et al. 2003). Activated ERK also directly phosphorylates HIF-1α within the C-TAD, which promotes its nuclear accumulation (Mylonis et al. 2006).

As 'master-regulators' of cellular responses to hypoxia, the HIFs control the expression of hundreds of target genes that are responsible for a wide range of processes including metabolism, angiogenesis, erythropoiesis, vascular remodelling, iron transport and cell survival (Mole et al. 2009; Ruan, Song & Ouyang 2009). For example, HIF-1α is vital for the regulation of glycolysis, apoptosis and pH regulation (Lu, Forbes & Verma 2002; Luo et al. 2006; Magliulo & Bernardi 2018), and HIF-2α is important for epithelial-to-mesenchymal transition (EMT) and stem cell maintenance (Xu et al. 2012). HIF regulation is not limited to the direct activation of target genes, as HIF activation elicits a transcriptional cascade that triggers further responses required for oxygen homeostasis, through other TFs such as c-Myc, Notch, Ets-1 and c-Jun (Elvert et al. 2003; Gustafsson et al. 2005; Koshiji et al. 2004; Laderoute et al. 2002), as well as through regulatory RNAs including miRNAs (Camps et al. 2008; Kulshreshtha et al. 2007).
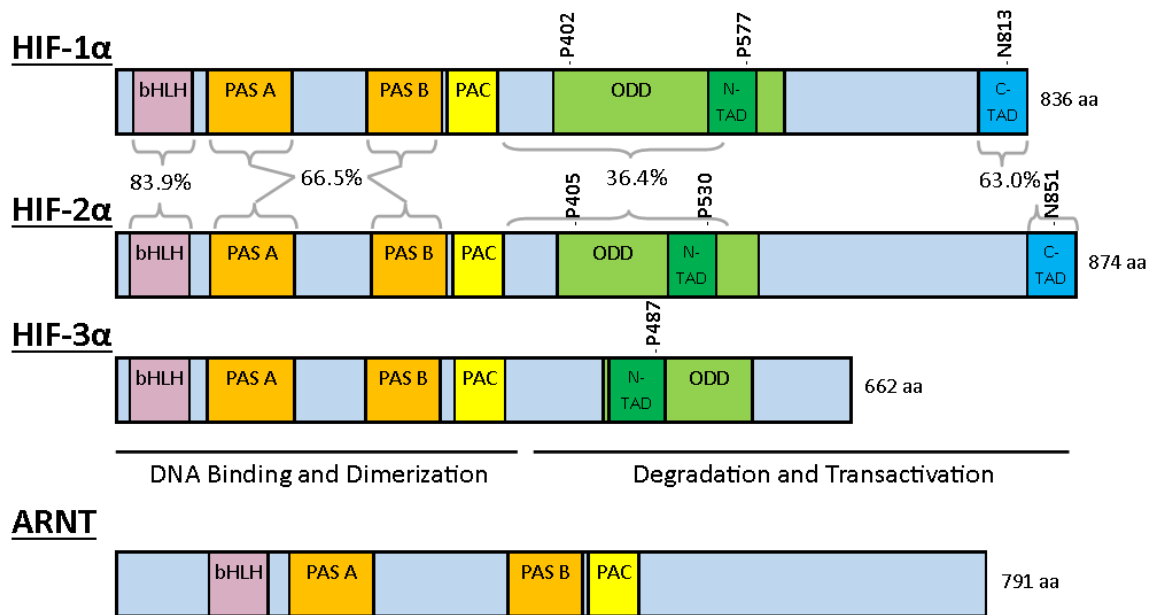
Figure 1.2: Schematic diagram of the functional domains of the mouse HIFs. Each α subunit dimerises with ARNT/HIF1β through the bHLH and tandem PAS domains. The bHLH DNA binding motif facilitates subsequent binding of the HIF heterodimers to HREs. Specific amino acids indicate residues that are post-translationally modified by oxygen-dependent hydroxylases. Percentages reflect the amino acid sequence similarity between functional regions of HIF-1α and HIF-2α (Ema et al. 1997). bHLH, basic helix-loop-helix; PAS, Per-ARNT-Sim; PAC, Motif C-terminal to PAS motifs; ODD, oxygen-dependent degradation domain; N-TAD, N-terminal transactivation domain; C-TAD, C-terminal transactivation domain.
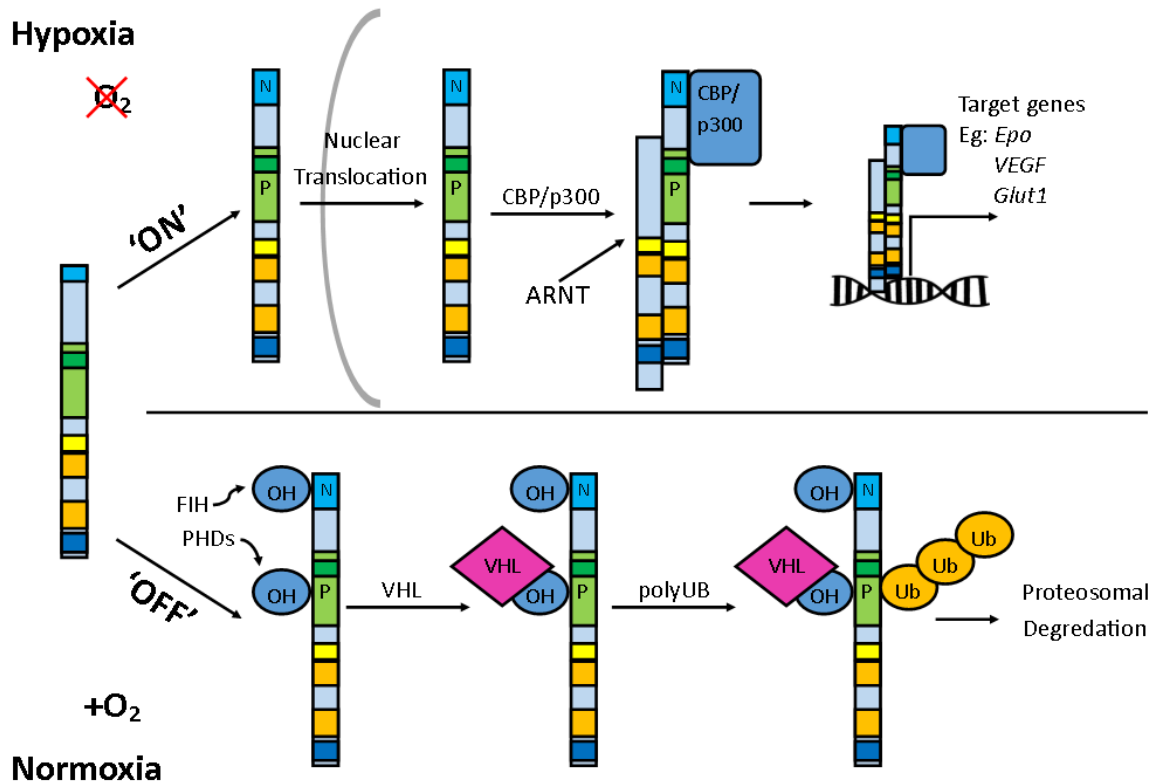
Figure 1.3: Post-translational hydroxylation regulates HIF-α activity. In normoxia, HIF-α is hydroxylated on proline residue(s) within the ODD by PHDs and on an asparagine residue within the C-TAD by FIH. The hydroxylated proline recruits the binding of VHL, leading to the subsequent polyubiquitination and degradation of HIF-α. Whereas in hypoxia, the loss of PHD and FIH activity stabilises HIF-α, leading to its accumulation and association with coactivator CBP/P300 at the C-TAD. Consequently, HIF-α translocates into the nucleus, heterodimerizes with ARNT, and regulates the expression of target genes. CBP, CREB-binding protein; VHL, Von Hippel-Lindau tumour suppressor; Ub, Ubiquitin.

1.3.1 Differential regulation of HIF-α in normal physiology

Despite sharing a consensus sequence and a high degree of structural similarity, the HIF-1α and HIF-2α isoforms are not functionally redundant. For example, they exhibit different spatial and temporal expression patterns. From early experiments of RNA *in-situ* hybridisation with mouse embryos, HIF-2α expression was initially thought to be restricted to blood vessels, where it stimulates vascularisation through the regulation of *Vegfa* (Tian, McKnight & Russell 1997). HIF-2α protein expression was then later found to be less spatially restricted and induced in many other, but not all, organs upon exposure to hypoxia, including the kidney, liver, heart, lung and intestine (Wiesener et al. 2003). In contrast HIF-1α is expressed ubiquitously. HIF-1α also mediates acute (<24 h) responses to hypoxia, whereas HIF-2α's expression is commonly associated with chronic responses to hypoxia (Dengler, Galbraith & Espinosa 2014). Also, although they are both able to bind canonical HRE sequences, chromatin immunoprecipitation (ChIP) experiments demonstrate that HIF-1α and HIF-2α bind distinct HREs in the regulatory regions of target genes, with HIF-1α commonly binding proximal to promoters, whereas HIF-2α is more frequently bound to distal sites (Smythies et al. 2019).

Presently, a complex view of HIF-mediated responses to hypoxia has developed, where both HIF-1α and HIF-2α mediate a mixture of partially overlapping and disparate responses to hypoxia in a context-dependent and complementary manner. While several distinct roles for either HIF-1α or HIF-2α have been described at the cellular and organismal level, these two isoforms do not appear to have a clear and definitive separation in the context of their overall physiological function (Bishop & Ratcliffe 2014). For example, while only HIF-1α expression is associated with the induction of glycolytic genes (Hu et al. 2003; Del Rey et al. 2017), both HIF-1α and HIF-2α have been found to promote the expression of glucose transporters such as Glut1 to complement increased levels of glycolysis (Chen et al. 2001; Huang et al. 2012; Ouiddir et al. 1999). Furthermore, both HIFs are essential for the development of the circulatory system and are not functionally redundant in knockout experiments. HIF-1α knockout mice embryos display abnormal cardiac morphogenesis, including cardiac bifida, pericardial effusion

and ventricular obstruction (Compernolle et al. 2003; Iyer et al. 1998), while HIF-2α knockout mice embryos display vascular disorganisation, haemorrhaging and bradycardia (Peng et al. 2000; Tian et al. 1998). However, both these knockouts are lethal to the developing mice embryos, denoting the non-redundancy of HIF-1α and HIF-2α.

In some instances, the two HIF-α isoforms mediate disparate or opposing responses. Murine macrophage activation and polarisation to the M1 'killer' or M2 'repair' subtypes are associated with the mRNA expression of *Hif-1α* and *Hif-2α* respectively (Takeda et al. 2010). The mediation of opposing responses by HIF-α may also occur via non-transcriptional pathways such as crosstalk with other TFs. HIF-1α, but not HIF-2α, is known to antagonistically affect c-Myc activity by competing for DNA binding to the Sp1 promoter, resulting in Sp1 de-repression (Koshiji et al. 2004). Similarly, only HIF-2α regulates the expression of erythropoietin in liver and kidney cells *in-vivo* (Takeda et al. 2008).

1.3.2   HIF-α in haematopoiesis

Increasing evidence indicates that hypoxic signalling facilitates haematopoiesis within the BM. However, the mechanisms by which HIF signalling regulates HSCs, whether through cell-autonomous mechanisms or microenvironmental cross-talk, remain controversial. Additionally, there are also differences in the roles of HIF-α subunits between mouse and human haematopoiesis.

In mice, HIF-1α and HIF-2α are essential for HSC biology. HIF-1α is an essential regulator of mHSC generation in developing mice embryos, and its conditional deletion in mHSC precursors significantly decreases HSC numbers (Imanirad et al. 2014). As downstream trans-activators of the Meis1 homeobox protein, HIF-1α and HIF-2α regulate long-term mHSC's glycolytic metabolism and antioxidant defence respectively (Kocabas et al. 2012;

Simsek et al. 2010). In a conditional knockout experiment, HIF-1α was found to regulate quiescence and tolerance to transplantation stress in mHSCs38 cells intrinsically. HIF-2α in mHSCs, however, is not essential for HSC maintenance, self-renewal or repopulation capacity (Guitart et al. 2013).

Similar to that in mice, Meis1 has been demonstrated to regulate the glycolytic metabolism of human HSCs through HIF-1α (Kocabas et al. 2015). However, the STAT5 TF was also found to promote hHSC's glycolytic metabolism, as well as self-renewal, but through the direct regulation of HIF-2α instead (Fatrai et al. 2011). Unlike mHSCs, hHSC's repopulation capacity is predominantly regulated by HIF-2α when compared to HIF-1α (Rouault-Pierre et al. 2013). *In-vitro*, hypoxia appears to favour the generation and differentiation of PC from memory B cells and drives increased plasmablast proliferation through the HIF-2α/c-Myc signalling axis (Schoenhals et al. 2017).

Collectively, the HIFs appear to exhibit complex roles in regulating normal BM haematopoiesis. Further research in this field would be valuable to further characterise the specific functions of each HIF isoform, as well as delineate their differences in normal mouse and human haematopoiesis. As the HIFs and their pathway proteins are increasingly recognised as potential therapeutic targets for various disorders including MM, it would be important to evaluate their specific roles in haematopoietic disease, and the potential side effects of these treatments to normal BM haematopoiesis and HSC function.

1.3.3 HIF-α in cancers

Hypoxia is widely recognised as a hallmark of solid tumours and plays a fundamental role in promoting solid tumour growth, survival and metastasis (Ruan, Song & Ouyang 2009). The hypoxia-mediated stabilisation and expression of the HIFαs is a well-known determinant for patient response to anti-cancer therapy and is associated with the poor

clinical prognosis of many solid cancers (Schito & Semenza 2016). Both HIF-1α and HIF-2α are expressed in a broad range of human cancers. While both HIF isoforms are frequently associated with poorer prognoses, it has been observed that the two isoforms can mediate disparate and highly divergent responses in a tumour-specific context (Keith, Johnson & Simon 2011). For instance, in neuroblastomas, HIF-1α expression is correlated with a favourable prognosis, while HIF-2α expression is correlated with poorer prognosis (Noguera et al. 2009). Understanding each HIF-α isoform's distinct function in a specific cancer type is crucial to determining the benefit of HIF-α inhibition as cancer therapy, and whether the selective inhibition of either isoform would be advantageous.

An example where selective HIF inhibition is being explored for cancer therapy is that in VHL-deficient renal cell carcinoma (RCC). In the majority of RCC tumours, the loss of functional VHL results in both HIF-1α and HIF-2α accumulation. However, HIF-2α is an oncogenic driver (Cho & Kaelin 2016), whereas HIF-1α acts as a tumour suppressor in RCC and is frequently lost in chromosome 14q deletions (Shen et al. 2011). This information has been exploited by using a novel HIF-2α specific antagonist, PT2385, in a recently completed a phase I clinical trial in advanced clear cell RCC patients where it was found to have a favourable safety profile and activity (Courtney et al. 2018). This drug is currently undergoing separate phase II clinical trials for RCC and recurrent glioblastoma (Xie et al. 2018).

Based on emerging evidence, it has been proposed that the HIFs may also play important roles that favour cancer progression in haematological malignancies like leukaemia. HIF-1α protein expression has been detected in the various forms of leukemia and is correlated with unfavourable prognosis and therapy resistance (Schito, Rey & Konopleva 2017). Consistently, BM angiogenesis, commonly mediated by HIFs, is increased in acute lymphoblastic leukemia (ALL) and acute myeloid leukemia (AML) (Ayala et al. 2009). Increased VEGF expression, a well characterised HIF target gene, in BM aspirates from chronic myeloid leukemia (CML) and ALL patients has been correlated with poorer disease prognoses and patient survival (Verstovsek et al. 2002; Wellmann et

al. 2004). The increased endothelial cell mass in leukemia has been suggested to not only improve blood perfusion to leukemic cells but to also promote their survival and proliferation by paracrine interactions, through the secretion of growth factors and cytokines (Ribatti 2009).

Furthermore, HIF activation in blood cancers is thought to further contribute to leukemic cell maintenance and progression by regulating their metabolism, metastasis, and leukemic stem cell renewal and expansion (Schito, Rey & Konopleva 2017). Leukemic stem cells are known to reside in the hypoxic BM, and experiments involving acute myelogenous leukemia stem cells have suggested that hypoxia may confer chemoresistance through HIF-1α regulated induction of quiescence and cell-cycle arrest (Matsunaga et al. 2012). Furthermore, the reduction of HIF-1α, through the inhibition of its upstream activator mTOR, has been found to chemo-sensitize hypoxic ALL cells (Frolova et al. 2012). Further research into the roles of each HIF isoform in leukemia would be valuable to delineate their distinct targetable features for the treatment of the disease.

1.4   HIF-α in MM

Given that MM PCs reside within the oxygen-deficient BM environment, hypoxic signalling through the HIFs is likely to have important roles in the initiation and progression of MM. *HIF-1α* transcript was found to be expressed in 95.4% of CD-138-purified primary MM cells from 329 untreated patients and is weakly correlated with a microarray-based proliferation index (Hose et al. 2009). From the immunohistochemical (IHC) staining of 106 MM BM biopsies, HIF-1α and HIF-2α protein have been found to be highly expressed in MM cells in 33% and 13.2% of cases respectively (Giatromanolaki et al. 2010). Further IHC experiments performed by other groups confirmed the presence of HIF-1α and HIF-2α protein expression in BM biopsy samples of MM patients (Colla et al. 2010; Martin et al. 2010). Nonetheless, the differences in HIF-1α and HIF-2α expression between normal and MM BM is unclear, as these studies do not include comparative measurements from the BM of healthy controls.

Investigations into the differences between healthy and MM BM in mice models have reported inconsistent outcomes. In experiments involving the use of the 5T33MM model, derived from C57BL6/KaLwRij mice, increased tumour growth is associated with higher pimonidazole incorporation and more IHC staining of endogenous HIF-1α in the BM (Azab et al. 2012; Hu et al. 2010). On the other hand, the levels of pimonidazole incorporation in the flushed BM of 5T2MM mice measured using flow cytometry was found to be lower than that of healthy controls, suggesting that MM-associated angiogenesis could be functional in counteracting the hypoxic BM microenvironment (Asosingh et al. 2005). However, this discrepancy could be due to inherent variations between the two different mouse MM models as well as the different methods used to quantify pimonidazole incorporation in the BM.

While the effect of MM tumours on the level of BM hypoxia has not been thoroughly elucidated, hypoxic signalling, through the HIFs, appears to be important for sustaining MM PC survival in hypoxic environments. The survival of human 8226 MM cells in hypoxia *in-vitro* is dependent on the HIFs, as the effect of siRNA mediated suppression

of either HIF-1α or HIF-2α on apoptosis is greater in hypoxic culture than in normoxic culture conditions (Gastelum et al. 2017). HIF-1α suppression in MM was also found to reduce the size of tumours in an intratibial xenograft model of JJN3 human MM cells in severe combined immunodeficiency/ nonobese diabetic (SCID-NOD) mice, through its inhibitory effect on pro-tumorigenic features such as angiogenesis and pro-osteoclastogenic cytokine signalling (Storti et al. 2013).

Interestingly, it has been reported that HIF-2α is expressed in a constitutive and oxygen-independent manner in several human MM cells, including 8226, OPM-2, H929 and U266 (Mysore et al. 2016). It is thought that the absence of PHD3 expression, which preferentially regulates HIF-2α, in these cell lines causes the normoxic stabilisation of HIF-2α, and the exogenous expression of PHD3 restores its oxygen-dependent regulation (Gastelum et al. 2017). Sustained HIF-2α activity may be important for MM PC's resistance to apoptosis and adaptation to BM hypoxia.

HIF signalling pathway components and the hypoxic BM microenvironment appear to be promising targetable features. Bortezomib and Lenalidomide, which are drugs that are currently approved for use in MM treatment, have inhibitory effects on HIF-1α (Befani et al. 2012; Lu et al. 2009; Shin et al. 2008). Dysregulated HIF-1 is associated with treatment resistance and the inhibition of which restores MM cell sensitivity to Bortezomib and Melphalan (Hu et al. 2009; Maiso et al. 2015). Additionally, a pre-clinical investigation into the disruption of HIF-1α transactivation in human MM cell lines and primary MM cells using the fungal metabolite Chetomin have reported a dose-dependent inhibition of MM cell growth (Viziteu et al. 2016). Another strategy to target the hypoxic BM niche, by the hypoxia-activated prodrug Evofostamide (TH-302), exhibited promising activity in both pre-clinical *in-vitro* and *in-vivo* MM experiments (Hu et al. 2010, 2013). Evofostamide recently underwent a phase I/II clinical trial in combination with Dexamethasone and/or Bortezomib and was reported to be well-tolerated and prolonged survival of relapsed/refractory MM patients (Laubach et al. 2019).

Despite being implicated in MM progression, there is a paucity of data for the roles of HIF-1α versus HIF-2α isoforms, especially in animal models. Therefore, there is a need to delineate their roles in an *in-vivo* system to establish if they represent promising therapeutic targets for the treatment of MM.

1.4.1   HIF-α in MM angiogenesis

HIF's role in stimulating angiogenesis is currently the best-understood arm of HIF regulated pathways in both solid tumours and MM. HIF-α activation upregulates multiple pro-angiogenic responses, notably the expression of the HIF target genes *VEGF* and *basic fibroblast growth factor 2 (bFGF*) which stimulate endothelial cell proliferation and blood vessel formation (Giuliani et al. 2011). Furthermore, HIF regulates the expression of matrix metalloproteinases (MMPs) which degrade the extracellular matrix to allow the migration of endothelial cells and angiopoietins which promote the survival, maturation and stabilisation of vascular walls (Krock, Skuli & Simon 2011; Pichiule, Chavez & LaManna 2004). Angiogenesis is crucial for the formation and progression of tumours to supply oxygen and nutrients to support the growing tumour mass. The suppression of angiogenesis in several *in-vivo* cancer models was found to inhibit tumour growth (Kim et al. 1993; Parangi et al. 1996). However, tumour blood vessels are usually structurally abnormal, disorganised and poorly functioning, resulting in regions of intratumoral hypoxia despite angiogenic activity (McDonald & Baluk 2002).

Interest in the association between angiogenesis and MM disease progression stemmed from Vacca and coworkers' 1994 observation of significantly higher microvessel densities in BM biopsies of MM patients compared to MGUS patients (Vacca et al. 1994). They also demonstrated that MM PC's increased angiogenic capacity in a chick embryo chorioallantoic membrane assay when treated with MM PC conditioned media, which is associated with increased angiogenic fibroblast growth factor (FGF) 2 levels (Vacca et al. 1999). Subsequently, several other studies have confirmed increased BM angiogenesis in

MM, which was later found to correlate with poorer disease prognosis (Bhatti et al. 2006; Rajkumar et al. 2002; Sezer et al. 2000). These observations are consistent with the idea of a switch from a non-vascular to a vascular phase during the transition from an asymptomatic to a symptomatic stage of the disease. This is also supported by findings in the 5T2MM mice model, where higher VEGF expression is associated with an increased proportion of phenotypically aggressive CD45^{-} MM cells compared to CD45^{+} MM cells (Asosingh et al. 2004).

HIF-1α is reported to be highly expressed in the hypoxic BM of MM patients, which is positively correlated with the detected serum levels of proangiogenic factors VEGF, FGF and angiopoietin 2 (Bhaskar & Tiwary 2016; Colla et al. 2010). Moreover, overexpression of either HIF-1α or HIF-2α in LP-1 human MM PCs increases vessel infiltration of subcutaneous implants *in-vivo* (Martin et al. 2010). In contrast, shRNA mediated gene silencing of *HIF-1α* human MM cell lines was found to downregulate *VEGF* and *Interleukin-8*, as well as *MMP9* and *C-C motif chemokine* (*CCL*) 2, which promote angiogenesis (Storti et al. 2013).

shRNA suppression of HIF-1α was also shown to blunt angiogenesis in subcutaneously grafted and intratibially injected JJN3 human MM PCs in SCID-NOD mice (Storti et al. 2013). Although this demonstrates HIF-1α's contribution to stimulating angiogenesis *in-vivo*, subcutaneous xenografts do not simulate the hypoxic microenvironment of the BM, and the mouse BM microenvironment may not recapitulate the various microenvironmental interactions that human MM PCs might have within the human BM. It is also important to note the increasing evidence that other BM residents can also act to support MM-associated angiogenesis. Hypoxia tolerant human MM cells have been found to shed exosomal miR-135b, which interacts with other BM cells to enhance endothelial tube formation by directly modulating the HIF-FIH signalling pathway (Umezu et al. 2014). Other investigations have also found that BM mesenchymal stromal cells, when cultured with U266 human MM cells, are involved in BM angiogenesis through the regulation of the HIF-2α integrin-linked kinase pathway (Zhang et al. 2018). Therefore, it would be of interest to replicate these findings and to further

elucidate each HIF-α specific role is in MM-associated BM angiogenesis in an animal model that has a closer resemblance to a natural model of MM disease.

1.4.2   HIF-α in MM metastasis

Metastasis is a defining feature of MM, both in its progression and relapse following therapy. Neoplastic plasma cells which have established tumours at a BM site can egress from the BM to enter the peripheral circulation, where they extravasate from blood vessels to colonise other BM niches. Although the role of hypoxia in mediating metastasis is still not well understood, increasing evidence suggests that changes in oxygen levels may regulate the different steps of this phenomenon through the epithelial-to-mesenchymal (EMT) transitional machinery and cytokine signalling (Azab et al. 2012; Roccaro et al. 2015; Vandyke et al. 2017). This idea is supported by the observation that increased BM hypoxia is positively associated with the number of circulating MM PCs *in-vivo (Azab et al. 2012)*.

The acquisition of EMT features is a fundamental process that is involved in the development of embryos and the abrogation of cell-cell adhesion leading to migratory capability (Son & Moon 2010). Pathologically, it is a phenomenon that commonly occurs in solid tumours and is linked to poorer prognosis, metastasis and cancer relapse (Son & Moon 2010). The stabilisation of HIF-1α is known to activate EMT-TFs, such as members of the SNAIL, SLUG and ZEB family of TFs that repress E-cadherin adhesion molecule expression (Lamouille, Xu & Derynck 2014; Zhang, W et al. 2015). Recent data suggest that EMT-related changes are involved in promoting MM PC metastasis and are possibly driven by the hypoxic BM microenvironment. Hypoxia is found to decrease the expression of E-cadherin on MM PCs, reducing their ability to adhere to BMSCs (Azab et al. 2012). Thus, hypoxia may play a somewhat active role in stimulating enhanced MM PC intravasation into the bloodstream throughout MM progression, which is unlike a passive shedding and passage of cells from a tumour.

The egress of MM PCs from the BM has also been suggested to be driven by the chemokine receptor CCR1, which interacts with several ligands including CCL3 and CCL5, and in response controls signalling for the mobilisation and recruitment of both normal and neoplastic immune cells. Prolonged exposure of LP-1 MM PCs to hypoxia *in-vitro* upregulates HIF-2α-induced expression of CCR1, which is postulated to stimulate their mobilisation from the BM into the peripheral blood where CCL3 levels are elevated (Terpos et al. 2003; Vandyke et al. 2017). Notably, the upregulation of CCR1 has also been found to decrease MM PC expression of E-cadherin and desensitise MM cell response to the homing and retention signal provided by CXCL12, which is expressed by BMSC (Azab et al. 2012; Vandyke et al. 2017). Since chronic hypoxia appears to stimulate MM PC egress from the BM, inhibition or loss of HIF-2α may diminish the dissemination of MM PCs.

In circulation, the reoxygenation of MM PCs is thought to re-sensitise them to CXCL12 through the recovery of its receptor CXCR4, allowing them to home to other BM niches (Vandyke et al. 2017). CXCR4 expression enhances the dissemination of MM to both the BM and extramedullary sites, and its repression delays detectable myelomatous tumour formation and progression (Roccaro et al. 2015). While most studies focus on chemokines' role in MM metastasis, there is a paucity of data on the role of HIFs in regulating the CXCR4/CXCL12 and CCR1/CCL3 axes in MM. It would thus be valuable to delineate the roles of HIF-1α and HIF-2α in regulating MM metastasis.

1.4.3   HIF-α in MM osteolysis

Normal bone is continuously produced and degraded by the coordinated efforts of osteoblasts and osteoclasts, respectively. MM PCs cause focal bone lesions by disrupting normal bone homeostasis that weakens the bones integrity, leading to symptoms of bone pain, hypercalcemia and fractures. Several hypoxia-induced cytokines have been implicated in osteolytic bone destruction in MM. CXCL12, which is upregulated by HIF-2α

in cultured MM cells, is postulated to promote the recruitment of osteoclast precursors from the peripheral blood into the BM and stimulate their activation (Grassi et al. 2004; Martin et al. 2010). The disruption of CXCL12 *in-vivo* using an antagonist for its receptor CXCR4 markedly reduced bone loss over four weeks and was associated with a lower number of osteoclasts proximal to the tumour (Diamond et al. 2009). CXCL12/CXCR4 signalling stimulates the expression of a range of osteoclast-activating genes, such as MMP9, RANK, carbonic anhydrase II, cathepsin K and TRAP (Grassi et al. 2004; Yu et al. 2003; Zannettino et al. 2005). These data suggest that HIF-2α disruption could potentially disrupt the early stages of osteoclastogenesis leading to reduced bone degradation in MM, but its role in the physiological context of MM *in-vivo* remains unclear.

Recent data suggest that hypoxia promotes the expression of the interleukin-32 (IL-32) chemokine, which is found in the extracellular vesicles secreted by MM PCs. IL-32 is described to be a novel contributor to increased osteoclastogenesis, but it is not clear if the HIFs are responsible for directly modulating IL-32 expression (Zahoor et al. 2017). Vesicles from MM PCs may also contribute to osteolysis through crosstalk with mesenchymal stem cells by suppressing their differentiation to osteoblasts with HIF-1α induced miR-210 (Saba, Soleimani & Abroun 2018).

In summary, while there is a broad appreciation for the role of hypoxia and the HIFs in MM development and progression, the specific role of each HIF isoform in crucial aspects of MM disease remain unclear. It is therefore of considerable importance to determine each HIF isoform's role in the critical features of MM disease, including angiogenesis, metastasis and osteolysis. Therefore, the research in this thesis aimed to generate an inducible-knockout 5TGM1 cell line system for each HIF-α isoform that is compatible in a syngeneic KaLwRij mouse model. Given that the HIFs are transcription factors, transcriptomic analysis of knocked-out cells would be informative as it would identify both shared and unique HIF-1α and HIF-2α target genes in the context of MM. These cells can also be further used to study the role of each HIF isoform in MM disease development and progression *in-vivo* in the KaLwRij mouse model.

1.5   The 5TGM1/KaLwRij Model

Hypoxia's contribution to MM progression can be studied using animal models that simulate the *in-vivo* behaviour of human MM neoplasms. The C57BL/KaLwRij mouse model arose spontaneously from C57BL/6 mice and frequently develops benign idiopathic paraproteinemia which is phenotypically similar to MGUS (Radl et al. 1978). At low frequency (<2% at two years of age), these mice spontaneously progress to an MM-like disease. The 5TGM1 line, derived from 5T33M myeloma cells harvested from elderly KaLwRij mice, has the genetic aberrations required to cause plasma cell disorders that accurately simulates MM, and this cell line is culturable *in-vitro*, independent of BM stroma (Hu et al. 2012). This allows for genetic modifications of this cell line to be made before injection into young syngeneic KaLwRij mice to follow MM tumour formation and disease progression *in-vivo*.

The 5TGM1/KaLwRIj model has been previously used to study other genes and proteins involved in MM disease, such as the *SAMSN1* tumour suppressor and the TSPAN7 transmembrane protein (Cheong et al. 2015; Noll et al. 2014). However, since 5TGM1 cells are already capable of establishing tumours, this model does not accurately simulate MM disease initiation. However, unlike subcutaneous xenograft models, 5TGM1 cells injected intravenously preferentially home to the BM and tumours localise mainly in the BM, just like in MM. Thus, this model is highly suitable for investigating the role of the HIFs in MM in the hypoxic BM microenvironment *in-vivo*. To specifically explore the roles of HIF-1α and HIF-2α, the genes encoding each protein will be individually disrupted ("knocked out") in the 5TGM1 cells. Transcriptomic analysis of single-HIF isoform knockout 5TGM1 cells can be used to study how each HIF isoform differentially regulates target genes in response to hypoxia. To date, there have been no published studies of HIF-1α and HIF-2α deficient 5TGM1 cells. Finally, these cells can be ultimately used in future *in-vivo* studies to determine the consequence of HIF-α deletion to critical aspects of MM disease progression in the well characterised KaLwRij mouse model.

1.6 Project Aims

1.6.1 Hypothesis

Both HIF-1α and HIF-2α play important roles in MM disease development and progression.

1.6.2 Major aim

To identify the unique and shared target genes of HIF-1α and HIF-2α in MM by transcriptomic analysis.

Aim 1: To generate HIF-1α and HIF-2α inducible-knockout 5TGM1 cells.

Aim 2: To generate and characterise HIF-1α and HIF-2α knockout 5TGM1 cells.

Aim 3: To profile the transcriptomic changes in 5TGM1 cells in response to HIF-1α and HIF-2α knockout.

1.6.3 Approach

Generate HIF-1α and HIF-2α knockout 5TGM1 cells using an inducible CRISPR/Cas9 system. Characterise HIF-1α and HIF-2α knockout 5TGM1 cells at the gene, mRNA and proteins levels by Sanger sequencing, quantitative real-time polymerase chain reaction (qRT-PCR) and western blotting. Perform transcriptomic analysis on HIF-1α and HIF-2α knockout 5TGM1 cells, cultured in normoxic and hypoxic conditions, to identify target genes.

Chapter 2

Materials and Methods

2 Materials and Methods

2.1 Materials

2.1.1 Equipment

Agarose Gel System	Sub-Cell® GT & Mini-Sub® GT	Bio-Rad
Automated Electrophoresis	2200 TapeStation	Agilent
Benchtop Centrifuge	5415D & 5417C	Eppendorf
Blotting System	Trans-Blot® Turbo™	Bio-Rad
Cell Counter	TC10™	Bio-Rad
Centrifuge	5810R	Eppendorf
Flow Cytometer	BD LSR Fortessa™ X-20	BD Biosciences
Fluorescence-Activated Cell Sorter	BD FACSAria™ Fusion	BD Biosciences
Fluorometric Quantitation	Qubit 2.0	Invitrogen
Hypoxia Workstation		Edwards Instrument Co.
Imaging System	BioDoc-It™ UV Transilluminator	UVP
Imaging System	ChemiDoc™ MP	Bio-Rad
Luminometer	GloMax® 96 Microplate	Promega
Microplate Reader	Multitaskan Ascent	Thermo Fisher
Next Generation Sequencing	NextSeq 500	Illumina
Real-Time PCR System	StepOnePlus™	Applied Biosystems
SDS-PAGE Gel System	Mini-PROTEAN®	Bio-Rad
Spectrophotometer	NanoDrop™ 2000	Thermo Fisher
Thermal Cycler	DNA Engine® PTC-0200	Bio-Rad

2.1.2 Consumables

1.5 mL Microfuge Tubes	Eppendorf
10 mL Graduated Centrifuge Tube (Screw Cap)	Technoplas
200 µL Ultraflux® Flat Cap PCR Tubes, Natural	Ssibio
50 mL Centrifuge Tubes with Screw Caps	Accumax
Anaerogen™ 2.5 L Hypoxia Sachets	Thermo Fisher
Counting Slides, Dual Chamber for Cell Counter	Bio-Rad
Microamp® Fast 96-Well Reaction Plate (0.1 mL)	Applied Biosystems
Optiplate™ -96 White	PerkinElmer
Platemax Ultraclear Sealing Film	Corning Axygen
Round-Bottom Tube with Cell Strainer Cap, 5 mL	Falcon
Tissue Culture Plasticware	Corning

2.1.3 General chemicals and reagents

1kb+ DNA Ladder	Invitrogen
2,2-dipyridyl (DP)	Sigma
40% Bis-Acrylamide Solution	Bio-Rad
Agarose Powder (Low EEO)	AppliChem
Ampicillin	Sigma-Aldrich
D-Luciferin Firefly, Potassium Salt	Biosynth
Dimethyl sulfoxide (DMSO)	Sigma-Aldrich
dNTPs	NEB
Doxycycline Hyclate (Dox)	Sigma-Aldrich
Dulbecco's Modified Eagle Medium	Gibco
Ethanol	Chem-supply
Ethidium Bromide	Sigma-Aldrich
GC Buffer	NEB

Glutamax	Invitrogen
Glycogen	Roche
HEPES	Invitrogen
Iscove's Modified Dulbecco's Medium	Sigma
Isopropanol	Chem-supply
Kanamycin	Sigma-Aldrich
Lipofectamine-2000	Invitrogen
Milli-Q water (MQ)	Millipore
Oligo-dTs	IDT
Ponceau Red	Sigma-Aldrich
Precision Plus Dual Colour Standards	Bio-Rad
Random Hexamers	IDT
RNA*later*® RNA stabilisation solution	Ambion
RNase Zap	Amersham
Triton X-100	Sigma-Aldrich
TRIzol®	Invitrogen
Tween 20	Sigma-Aldrich

2.1.4   Commercial kits

cDNA synthesis	All-in-One cDNA Synthesis SuperMix	Bimake
DNase	TURBO DNA-*free*™ Kit	Invitrogen
ECL substrate	SuperSignal™ West Femto Maximum Sensitivity Substrate	Thermo Fisher
Gel extraction	QIAquick® Gel Extraction Kit	Qiagen
Genotyping	MyTaq™ Extract PCR Kit	Bioline

mRNA-seq library kit	NuGEN Universal Plus mRNA	Tecan
PCR Cloning	pGEM®-T Easy Vector System	Promega
PCR Mastermix	MyTaq™ HS Red Mix	Bioline
PCR Mastermix	OneTaq® 2x Mastermix	NEB
PCR purification	QIAquick® PCR Purification Kit	Qiagen
Plasmid midiprep	Nucleobond® Xtra Midi Plus	Machery-Nagel
Plasmid miniprep	QIAprep® Spin Miniprep Kit	Qiagen
Precast gels	Mini-PROTEAN® TGX™ Gels	Bio-Rad
Protein assay (BCA)	Pierce™ BCA Protein Assay Kit	Thermo Fisher
Protein assay (Bradford)	Bio-Rad Protein Assay	Bio-Rad
Protein blotting system	Trans-Blot®Turbo™ Transfer System	Bio-Rad
RNA cleanup	Morarch® RNA Cleanup Kit (50 µg)	NEB
RNA extraction	*mir*Vana™ miRNA Isolation Kit	Ambion

2.1.5   Enzymes

Fast-Start Sybr-Green Mastermix (Rox)	Roche
Phusion® High-Fidelity DNA Polymerase	NEB
Restriction Enzymes	NEB
SuperScript™ III Reverse Transcriptase	Thermo Fisher
Taq Polymerase	NEB

2.1.6 Gasses

BOC supplied all gasses used for hypoxia experiments.

Carbon dioxide, compressed. Medical E.P. Grade
Nitrogen, compressed. High Purity
Oxygen, compressed. Medical E.P. Grade

2.1.7 Antibodies

Primary

HIF-1α	Novus Biologicals (NB100-449). Affinity purified rabbit polyclonal IgG that recognises the C-terminus (aa775-826) of human HIF-1α. 1:1 000 in PBS-T, 2% skim milk, incubate overnight at 4°C.
HIF-2α	Novus Biologicals (NB100-122). Affinity purified rabbit polyclonal IgG that recognises the C-terminus of mouse/human HIF-2α. 1:1 000 in PBS-T, 2% skim milk, incubate overnight at 4°C.
α- Tubulin	Novus Biologicals (NB600-506). Protein G purified rat monoclonal IgG2a that recognises the Gly-Gly-Tyr linear peptide sequence in Tyr-Tubulin. 1:1 000 in PBS-T, 2% skim milk, incubate 1 hour at RT.

Secondary

anti-rabbit	Pierce (31460). Affinity-purified goat polyclonal IgG that is conjugated to HRP. 1:20 000 in PBS-T, 2% skim milk, incubate 1 hour at RT.

anti-rat	Abcam (ab6845). Affinity-purified goat polyclonal IgG that is conjugated to HRP. 1:20 000 in PBS-T, 2% skim milk, incubate 1 hour at RT.

2.1.8 Plasmids

2.1.8.1 Retroviral transduction vectors

pEco	Human cytomegalovirus (CMV) immediate-early promoter-driven ecotropic envelope protein plasmid that is compatible with both second and third-generation packaging vectors. pEco was provided by D. Hewett, from the Zannettino lab.
psPAX2	A second-generation lentiviral packaging vector deleted for all viral auxiliary genes. psPAX2 was a gift from Didier Trono (Addgene plasmid # 12260). psPAX2 was provided by D. Hewett, from the Zannettino lab.

2.1.8.2 CRISPR/Cas9 vectors

FuCas9Cherry	A multicistronic lentiviral plasmid constitutively expressing FLAG-tagged *S. pyogenes* Cas9 and mCherry fluorescent protein, driven by the human ubiquitin C (hUbC) promoter (Aubrey et al. 2015). The two encoded genes are separated by a 'self-cleaving' T2A peptide. FUCas9Cherry was a gift from M. Herold (Addgene plasmid # 70182).
FgH1tUTG	A lentiviral plasmid encoding a tetracycline (Tet)-inducible single-guide RNA (sgRNA) cassette(Aubrey et al. 2015). The vector contains two bi-directional BsmBI restriction sites upstream of a guide RNA

	(gRNA) scaffold for the insertion of a gRNA. The plasmid also constitutively expresses Tet-Repressor (Tet-R) and enhanced green fluorescence protein (eGFP), driven by hUbC. The genes encoding these two proteins are separated by a 'self-cleaving' T2A peptide. FgH1tUTG was a gift from M. Herold (Addgene plasmid # 70183).
FgH1tUTP	Modified from FgH1tUTG, to replace the constitutively expressed eGFP with a mPlum fluorescent protein reporter. A Gibson isothermal cloning strategy was used to generate the vector. The *egfp* gene was digested out of the plasmid using BlpI and ClaI restriction enzymes, and the linearized vector backbone was purified by QIAquick gel extraction (Qiagen). Subsequently, a gBlock double-stranded DNA encoding mPlum with 40bp complementary flanking ends (IDT) was cloned via Gibson assembly into the linearised vector backbone. Successful replacement of the fluorescent reporter was confirmed by Sanger sequencing (AGRF). The following guide vectors were generated from FgH1tUTP: • FgH1tUTP mHIF1a Exon 1 (FgH1tUTP_H1E1) • FgH1tUTP mHIF1a Exon 2 (FgH1tUTP_H1E2) • FgH1tUTP mHIF1a Exon 3 (FgH1tUTP_H1E3) • FgH1tUTP mHIF2a Exon 2 (FgH1tUTP_H2E2) • FgH1tUTP mHIF2a Exon 3 (FgH1tUTP_H2E3)

2.1.8.3   In-vivo reporter

NES-TGL	A retroviral trimodal-reporter plasmid encoding GFP, firefly luciferase and Herpes Simplex Virus 1- thymidine kinase (HSV1-tk), for non-invasive imaging of transduced cells in live mice (Ponomarev et al. 2004).

	The HSV1-tk component was not utilised in this project.

2.1.8.4 Control vector

pRUFimCH2	A mCherry-expressing retroviral plasmid generated from pRUFiG2, where the IRES-GFP cassette was replaced with an IRES-mCherry cassette from pcDNA3-IRES-mCherry (Noll et al. 2014).

2.1.9 Oligonucleotides

All primers synthesised by Sigma or IDT

2.1.9.1 CRISPR sgRNA oligos

Oligo overhangs complementary to FgH1tUTP

mHIF-1α_Exon1	F	tcccgTTTCTTCTCGTTCTCGCCGC
	R	aaacGCGGCGAGAACGAGAAGAAAC
mHIF-1α_Exon2	F	tcccgAGATGTGAGCTCACATTGTG
	R	aaacCACAATGTGAGCTCACATCTC
mHIF-1α_Exon3	F	tcccGCTAACAGATGACGGCGACA
	R	aaacTGTCGCCGTCATCTGTTAGC
mHIF-2α_Exon2	F	tcccgAGAAATCCCGTGATGCCGCG
	R	aaacCGCGGCATCACGGGATTTCTC
mHIF-2α_Exon3	F	tcccgCACAGCAATGAAACCCTCCA
	R	aaacTGGAGGGTTTCATTGCTGTGC

gRNA information

gRNA	Target	PAM	Strand	On-tgt score	Off-tgt score

mHIF-1α_Exon1	TTTCTTCTCGTTCTCGCCGC	CGG	-	51.3	94.1
mHIF-1α_Exon2	AGATGTGAGCTCACATTGTG	GGG	-	65.7	67.7
mHIF-1α_Exon3	GCTAACAGATGACGGCGACA	TGG	+	64.4	88.7
mHIF-2α_Exon2	AGAAATCCCGTGATGCCGCG	AGG	+	71.7	95.6
mHIF-2α_Exon3	CACAGCAATGAAACCCTCCA	AGG	-	64.7	64.1

2.1.9.2   T7E1 primers

Primers amplify DNA region spanning CRISPR cut site

mHIF-1α_Exon1	F	CCGCCTCTGGACTTGTCTCTTT	Phusion, A = 61°C
	R	GATTACAACCAAACCCGCACGT	
mHIF-1α_Exon2	F	ACCAGTGGCTAAGGAAGTAAGC	Taq, A = 61°C
	R	CACACAGGTGCATGGACACATA	
mHIF-1α_Exon3	F	TTGTTTCTTTTCCCGTGTGCCC	Taq, A = 63°C
	R	TCTTAAATCTTGGCCACCCCC	
mHIF-2α_Exon2	F	TGGTCTGACCGTAGCTTCTTCG	Taq, A = 61°C
	R	CTGTCCTTGGTCTCTTCCCTGG	
mHIF-2α_Exon3	F	TTGGTAGTGTGCCTTTCCCTGT	Taq, A = 61°C
	R	TGGGCTATTTGTGCAGGCTTTG	

2.1.9.3   Sequencing primers for FgH1tUTP plasmid

gRNA insert		TAATACGACTCACTATAGGG
mPlum gene	F	CCCGACTACTTGAAGCTGTC
	R	GCGCACCTTCACCTTGTAGATG

2.1.9.4   Sequencing primers for amplified PCR products

mHIF-1α_Exon1	CCGCCTCTGGACTTGTCTCTTT
mHIF-1α_Exon2	CACACAGGTGCATGGACACATA
mHIF-1α_Exon3	TTGTTTCTTTTCCCGTGTGCCC

mHIF-2α_Exon2	TGGTCTGACCGTAGCTTCTTCG
mHIF-1α_Exon3	TTGGTAGTGTGCCTTTCCCTGT

2.1.9.5 Sequencing primer for PCR products cloned into pGEM®-T plasmid

T7prom_F	TAATACGACTCACTATAGGG

2.1.9.6 qPCR primers

mHIF-1α	F	CGGCGAGAACGAGAAGAA
	R	GAAGTGGCAACTGATGAGCA
mHIF-2α	F	CATAAGCTCCTGTCCTCAGTCTGC
	R	GCTGTGTCCTGTTAGTTCTACCTG
mBNIP3	F	GTAGAACTGCACTTCAGCAATGG
	R	GGGCTGTCACAGTGAGAACTC
mHPRT	F	AGTCCCAGCGTCGTGATTAGC
	R	CCAAATCCTCGGCATAATG

2.1.10 gBlocks

mplum gBlock for replacing e*gfp* of FgH1tUTG, synthesised by IDT

```
TGCTGCGGCAAGCTATTGAGTTGTTTGACCACCAAGGGGCTGAGCCTGCATTCCTTTT
TGGCCTGGAACTGATCATCTGTGGCCTGGAAAAGCAGCTGAAATGTGAGTCTGGCTCT
GGGTCCGGTGAGGGCAGAGGAAGTCTGCTAACATGCGGTGACGTCGAGGAGAATCCTG
GCCCAATGGTGAGCAAGGGCGAGGAGGTCATCAAGGAGTTCATGCGCTTCAAGGAGCA
CATGGAGGGCTCCGTGAACGGCCACGAGTTCGAGATCGAGGGCGAGGGCGAGGGCCGC
CCCTACGAGGGCACCCAGACCGCCAGGCTGAAGGTGACCAAGGGTGGCCCCCTGCCCT
TCGCCTGGGACATCCTGTCCCCTCAGATCATGTACGGCTCCAAGGCCTACGTGAAGCA
CCCCGCCGACATCCCCGACTACTTGAAGCTGTCCTTCCCCGAGGGCTTCAAGTGGGAG
CGCGTGATGAACTTCGAGGACGGCGGCGTGGTGACCGTGACCCAGGACTCCTCCCTGC
AGGACGGCGAGTTCATCTACAAGGTGAAGGTGCGCGGCACCAACTTCCCCTCCGACGG
CCCCGTAATGCAGAAGAAGACCATGGGCTGGGAGGCCTCCTCCGAGCGGATGTACCCC
GAGGACGGCGCCCTGAAGGGCGAGATGAAGATGAGGCTGAGGCTGAAGGACGGCGGCC
```

```
ACTACGACGCCGAGGTCAAGACCACCTACATGGCCAAGAAGCCCGTGCAGCTGCCCGG
CGCCTACAAGACCGACATCAAGCTGGACATCACCTCCCACAACGAGGACTACACCATC
GTGGAACAGTACGAGCGCGCCGAGGGCCGCCACTCCACCGGCGCCTAGAGCGGCCGCG
ATCTACAATTCGATATCAAGCTTATCGATAATCAACCTCTGGATTACAAAATTTGTGA
AAGATTG
```

2.1.11 Buffers and solutions

Concentrations listed are working concentrations

4x SDS load buffer	40% Glycerol, 100 mM 'SDS-PAGE separating gel' buffer, 5% SDS, 0.01% Bromophenol Blue; added fresh: 200 mM DTT
6x DNA load buffer	80% Glycerol, 0.5 M EDTA pH 8, 1% Bromophenol Blue, 0.1% Xylene Cyanol
ECL	100 mM Tris pH 8.6, 0.0001% H_2O_2, 0.225 mM p -Coumaric acid, 1.250 mM Luminol
gDNA extract buffer	100 mM NaCl, 20 mM Tris HCl pH 7.5, 10 mM EDTA, 0.5% SDS
General IP buffer	250 mM NaCl, 20 mM HEPES pH 8, 0.1% IGEPAL, 10mM EDTA
PBS	137 mM NaCl, 2.7 mM KCl, 10 mM Na_2HPO_4, 1.8 mM KH_2PO_4, pH 7.4
PBS-T	137 mM NaCl, 2.7 mM KCl, 10 mM Na_2HPO_4, 1.8 mM KH_2PO_4, pH 7.4, 0.1% Tween-20
Quick gDNA extract buffer (QT-DIE)	30 mM Tris HCl pH 8.5, 800 mM GuHCl, 1 mM EDTA, 0.36% Triton-X, 5% Tween-20
RIPA buffer	50mM Tris HCl pH 7.4, 150 mM NaCl, 1% Triton X-100, 0.5% Sodium deoxylcholate, 10 mM NaF; added fresh: 1x Protease Inhibitor, 1 mM PMSF

SDS-PAGE running buffer	25 mM Tri, 192 mM glycine, 0.1% SDS, pH 8.6

2.1.12 Bacterial strains

DH5α	An E. coli strain used for general plasmid amplification and cloning experiments. *fhuA2 lac(del)U169 phoA glnV44 Φ80' lacZ(del)M15 gyrA96 recA1 relA1 endA1 thi-1 hsdR17.*
JM109	An E. coli strain used for general plasmid amplification and cloning experiments. *F´ traD36 proA+B+ lacIq Δ(lacZ)M15/ Δ(lac-proAB) glnV44 e14- gyrA96 recA1 relA1 endA1 thi hsdR17.*

2.1.13 Mammalian cell lines

HEK293T	SV40 transformed human embryonic kidney epithelial cells, for transfection of mammalian expression plasmids and retrovirus production. ATCC® CRL-3216™. HEK293T cells were provided by D. Hewett, from the Zannettino lab.

5TGM1	Murine MM PC cells derived from spontaneously arising 5T33M MM PC cells harvested from elderly C57BL/KaLwRij mice displaying idiopathic paraproteinemia. These cells have been serially passaged in syngeneic mice before their establishment and are culturable *in-vitro* independent of BM stroma. These cells can establish MM-like disease when injected intravenously into young (6-8 weeks) syngeneic KaLwRij mice.

	5TGM1 cells also referred to a 5TGM1 parental cells, were provided by D. Hewett, from the Zannettino lab.
5TGM1 BMX1 (5TGM1 B)	5TGM1 cells transduced with the trimodal reporter vector NES-TGL. Clonal subline derived from cells recirculated in a KaLwRij mouse, harvested from the BM that exhibits BM tropism. Expresses luciferase for the non-invasive *in-vivo* bioluminescence imaging of tumours in live mice (Ponomarev et al. 2004). eGFP[+].

5TGM1 B was provided by D. Hewett, from the Zannettino lab. |
| 5TGM1 BMX1 FuCas9Cherry (5TGM1 BF) | 5TGM1 BMX1 cells transduced with the constitutively expressing, hUbC driven spCas9 vector FuCas9Cherry. eGFP[+]mCherry[+].

5TGM1 BF was provided by D. Hewett, from the Zannettino lab. |
| 5TGM1 FgH1tUTP | 5TGM1 cells transduced with the dox-inducible gRNA vector, FgH1tUTP. The vector does not contain a guide insert. This cell line was used as a control for FACS. mPlum[+]. |
| 5TGM1 BMX1 FuCas9Cherry FgH1tUTP (5TGM1 BFF) | 5TGM1 BF cells transduced with the dox-inducible gRNA vector, FgH1tUTP. For inducible-knockout lines, the vector contains a guide insert. Dox treatment of these cells induces gRNA expression, and subsequent CRISPR/Cas9 mediated cleavage of the target site within the cell genome. eGFP[+]mCherry[+]mPlum[+]. |
| 5TGM1 pRUFimCH2 | 5TGM1 cells transduced with pRUFimCH2. This cell line was used as a control for FACS. mCherry[+].

5TGM1 pRUFimCH2 was provided by D. Hewett, from the Zannettino lab. |

2.2 Methods

2.2.1 Molecular techniques

2.2.1.1 *PCR amplification*

<u>Taq Polymerase</u>

Most polymerase chain reactions were performed using commercial Taq polymerase master-mixes. A standard 25 µL reaction was set up on ice and contained 12.5 µL of 2x Polymerase master-mix, 1 µL of 10 µM forward and reverse primer mix, 1 µL of template DNA, and 10.5 µL MQ water. Reactions were scaled up as required.

General cycling parameters:

Initial denaturation	95°C	30 seconds
40 cycles	95°C 55°C - 68°C depending on primers 68°C	30 seconds 30 seconds 60 seconds per kb amplified
Final extension	68°C	5 minutes
Hold	10°C	

If necessary, primer optimisation was performed by gradient PCR, by setting a range of annealing temperatures to identify the best annealing temperature for a set of primers.

<u>Phusion Polymerase</u>

Amplification of HIF-1α Exon 1 from gDNA was performed using Phusion polymerase with GC buffer (NEB). A standard 20 µL reaction was set up on ice and contained 4 µL Phusion GC buffer, 0.4 µL of 10 mM dNTPs, 1 µL of 10 µM forward and reverse primer

mix, 1 µL of template DNA, 0.2 µL of Phusion DNA polymerase, and 13.4 µL of MQ water. Reactions were scaled up as required.

General cycling parameters:

Initial denaturation	98°C	30 seconds
40 cycles	95°C 55°C - 68°C depending on primers 72°C	10 seconds 30 seconds 25 seconds per kb amplified
Final extension	72°C	5 minutes
Hold	10°C	

2.2.1.2 A-Tailing

To A-tail Phusion PCR amplicons for pGEM-T ligations, 5 µL of PCR product was mixed with 1 µL of 10x Standard Taq Buffer, 2 µL of 1 mM dATP, 0.125 µL of Taq Polymerase and 2 µL of MQ. The reaction mixture was incubated at 70°C for 15 minutes. 2 µL of the reaction product was used for the subsequent pGEM-T ligation reaction.

2.2.1.3 T7E1 assay

Per 8.5 µL of PCR product, 1 µL of NEB Buffer 2 was added, and the sample was annealed in a thermocycler. The annealing steps consists of a 95°C incubation for 5 minutes, followed by ramping down from 95°C to 85°C at -2°C/s and from 85°C to 25°C at -0.1°C/s. 0.5 µL of 10 000 Unit/mL T7E1 enzyme was added to each sample and incubated at 37°C for 30 minutes. Cleavage products were resolved and visualised by agarose gel electrophoresis.

2.2.1.4 Agarose gel electrophoresis

DNA samples, such as plasmids, restriction digest products and PCR amplicons, as well as RNA extracts, were resolved and visualised on agarose gels via gel electrophoresis. 1%

agarose gels were made by dissolving 0.4 g agarose powder per 40 mL Tris-Borate-EDTA (TBE) and heated in a microwave. 2uL of 10 mg/mL ethidium bromide solution was added to the mixture before casting and cooling. 6x loading dye was added to samples to a concentration of x1. Samples were loaded in gel wells alongside 5 µL of 0.1 µg/µL 1kb+ DNA ladder. After loading samples, gels were run in TBE at 100-120 V for 30-40 minutes and were subsequently visualised on a UV transilluminator.

For analysing RNA samples, the gel tank, well comb and gel cast were first soaked in an SDS and sodium hydroxide solution to remove any RNases. Also, a bleach gel protocol was used for RNA samples. 800 uL of 10-15% sodium hypochlorite solution was also added to the agarose and TBE mixture and incubated at RT for 5 minutes before microwaving to remove any contaminating RNases and to help RNA denaturation (Aranda, LaJoie & Jorcyk 2012).

2.2.1.5   DNA clean-up

DNA samples were purified using the QIAquick® PCR purification kit (Qiagen) according to the manufacturer's instructions and stored at -20°C. DNA quantity and quality was assayed using the Nanodrop spectrophotometer.

2.2.1.6   Gel extraction

DNA bands were excised from agarose gels using a scalpel blade and extracted using the QIAquick® Gel extraction kit (Qiagen) according to the manufacturer's instructions. Purified DNA was stored at -20°C.

2.2.1.7   pGEM®-T ligation

Purified A-tailed PCR products were ligated to the pGEM-T vector using the pGEM®-T Vector System kit (Promega) according to the manufacturer's instructions. Ligations were performed overnight at 4°C and transformed the subsequent day using DH5α competent cells. Transformants were spread plated on X-Gal/IPTG Luria Broth (LB) +100 µg/mL Ampicillin agar plates for blue-white screening. X-Gal/IPTG plates were prepared

by spread plating LB +Amp plates with 16 µL of 50 mg/mL X-Gal and 4 µL of 1 M IPTG. Plates were incubated at 37°C overnight, and white colonies were picked for plasmid minipreps. Presence of inserts was determined by colony PCR. Cloned inserts were sequenced from prepped plasmids using AGRF's Sanger sequencing service, using the T7prom_F sequencing primer added at sample reception.

2.2.1.8   Gibson assembly

Gibson assemblies of gBlocks (IDT) into vector backbones were performed as outlined by the Miller lab's modified Gibson assembly protocol (*Gibson Assembly – Samuel Miller Lab, UW, Seattle* n.d.).

2.2.1.9   Plasmid transformation

Frozen (-80°C) chemically competent *E. coli* cells were thawed on ice. Between 1-5 µL plasmid DNA was mixed with 25 or 50 µL chemically competent cells and then incubated on ice for 20 minutes. The reaction was heat-shocked at 42°C for 45 seconds and immediately returned to the ice for 2 minutes. 250 µL SOC outgrowth medium was added to the cells before being incubated at 37°C for 1 hour for antibiotic resistance to develop. The cells were then spread plated on LB agar plates with the appropriate antibiotic for the selection of successful transformants. Plates were incubated at 37°C overnight for colonies to grow.

2.2.1.10 Plasmid mini-prep

Colonies were picked, inoculated in 4 mL LB media with the appropriate antibiotic and grown overnight on a spinner at 37°C. The culture was spun down at 3220 RCF, 4°C for 10 minutes. Plasmid DNA was extracted from cell pellets using the QIAprep® Spin Miniprep kit (Qiagen) according to the manufacturer's instructions. Plasmid quantity and quality was assayed using the Nanodrop spectrophotometer. Eluted plasmid DNA was stored at -20°C.

2.2.1.11 Plasmid midi-prep

Colonies were picked, inoculated in 50-100 mL LB media with appropriate antibiotic and grown overnight on a shaker at 37°C. The culture was spun down at 3220 RCF, 4°C for 10 minutes. Plasmid DNA was extracted from cell pellets using the NucleoBond® Xtra Plasmid Midi Plus kit (Machery-Nagel) according to the manufacturer's instructions, inclusive of the finaliser step. Plasmid quantity and quality was assayed using the Nanodrop spectrophotometer. Eluted plasmid DNA was stored at -20°C.

2.2.1.12 Colony PCR

Colonies were picked, smeared on the bottom of a PCR tube, and immediately inoculated in culture media with the appropriate antibiotic. To determine the presence of inserts, PCR reactions were performed as described in section 2.2.1.1, replacing template DNA with MQ water. The inoculated media was incubated overnight at 37°C with agitation for plasmid-prep the following day.

2.2.1.13 Restriction enzyme digest

Restriction digests were performed using NEB restriction enzymes and buffers. A general 10 μL reaction typically consists of 0.5 μL of enzyme, 1 μL of 10x restriction buffer, 1 μg of DNA and topped up with MQ water. Reactions were incubated at the recommended temperature for at least 1 hour.

2.2.1.14 Sanger sequencing

DNA was diluted within a range of concentrations for Sanger sequencing in MQ water to a volume of 11 μL, as recommended by the Australian Genome Research Facility (AGRF). 1 μL of a 100 μM sequencing primer was added to the sample, either before sample submission for custom sequencing primers or by AGRF for a selection of conventional sequencing primers. Samples were submitted to AGRF for the Purified DNA (PD) sequencing service, which covers the Big Dye Terminator reaction, clean-up and sequencing.

Sequencing traces were analysed using Benchling, aligned against reference sequences by MAFFT v7. Overlapping sequence traces were resolved manually by tracing back the peaks or by using CRISP-ID v1.1 (Dehairs et al. 2016).

2.2.1.15 gDNA extraction – Salting out method

7.5×10^3 cells were pelleted at 300 RCF, RT for 10 minutes, and washed with PBS. The cells were re-pelleted and lysed with 125 µL of gDNA extract buffer and 2.5 µL of Proteinase K. The lysate was incubated at 37°C for 4 hours. After incubation, 62.5 µL of 6M NaCl was added to the lysate, and vortexed. The lysate was then incubated on ice for 10 minutes and then centrifuged at 16 100 RCF, 4°C, for 10 minutes. The supernatant containing gDNA was transferred to a new centrifuge tube, and 500 µL of 100% Ethanol was added. The sample was inverted to mix, and centrifuged at 16 100 RCF, 4°C for 2 minutes to pellet the gDNA. The supernatant was aspirated, and the pellet was air-dried. gDNA was resuspended in 50 µL of Tris-buffered solution. 1 µL was used to set up routine PCR reactions. gDNA was stored at -20°C.

2.2.1.16 gDNA extraction – Quick method

To $1-5 \times 10^6$ cells, 50 µL of Quick gDNA extract buffer (Section 2.1.10) and 1 µL of 20 mg/mL Proteinase K were added. The lysate was incubated at 50°C for 10 minutes with occasional vortexing and heat-inactivated at 95°C for 10 minutes. Tubes were centrifuged at 16 100 RCF for 1 minute to pellet debris, and 1 µL of the supernatant containing gDNA was used to set up routine PCR reactions. gDNA was stored at -20°C.

2.2.1.17 RNA extraction – For qRT-PCR

To extract RNA for qPCR experiments, TRIzol® reagent was used. 5 mL of cell suspension was pelleted by centrifugation at 300 RCF, RT for 5 minutes. Pellets were washed in 1 mL ice-cold PBS before re-pelleting. Cell pellets were then homogenised by pipetting in 0.5 mL TRIzol® and stored at -80°C for later processing.

The frozen homogenates were later thawed, and 100 µL of chloroform was added. The tubes were shaken vigorously and incubated at RT for 10 minutes, before centrifugation at 12 200 RCF, 4°C for 15 minutes to separate the phenol-chloroform and aqueous phases. 200 µL of the upper aqueous phase was transferred to new tubes, and 0.5 mL of isopropanol and 1 µL of glycogen were added. The tubes were vortexed for 10 seconds, and incubated at RT for 10 minutes, before centrifuging at 12 200 RCF, 4°C for 8 minutes. The supernatant was aspirated from the RNA precipitate, and the precipitate was washed in 0.5 mL 75% ethanol. The tubes were centrifuged at 7 500 RCF, 4°C for 5 minutes, and the supernatant was aspirated from the RNA precipitate. The RNA pellet was air-dried and resuspended in 25 µL Tris-buffered solution. RNA quantity was assayed using the Nanodrop spectrophotometer. RNA quality was checked by running it on a 'bleach' agarose gel. RNA was stored at -80°C.

2.2.1.18 cDNA synthesis

On ice, 2 µg RNA was diluted to 9 µL in MQ water. 1 µL of 500 ng/uL Oligo-dTs, 1uL of 25 µM Random Hexamers and 1 µL of 10 mM dNTPs were added. The mixture was incubated at 65°C for 5 minutes. Following that, 4 µL of 5x First-Strand Buffer, 1 µL of 0.1 M DTT, 0.5 µL of Superscript III and 2.5 µL of MQ water was added. The mixture was incubated at 25°C for 5 minutes, 50°C for 90 minutes and 70°C for 15 minutes for the synthesis reaction. cDNA was stored at -20°C.

Alternatively, the All-in-One cDNA Synthesis SuperMix (Bimake) was used, according to the manufacturer's instructions.

2.2.1.19 Quantitative real-time PCR (qRT-PCR)

Each qRT-PCR was performed in technical triplicates for each cDNA sample, alongside a water control sample (No cDNA). Per reaction triplicate, 22.5 µL of 2x Fast-Start Sybr-Green Mastermix (Roche), 1.125 µL of 10 µM forward and reverse primer mix and 21.375 µL MQ water were combined in a tube. To the 45 µL of the master mix, 2 µL cDNA was added and mixed. The reaction mix was aliquoted to 15 µL in three wells of a Microamp® Fast 96-Well Reaction Plate, which represents three technical replicates. The

plates were cycled on a StepOnePlus™ instrument, using the default parameters for the comparative C_T experiments, with standard ramp speed (StepOne™ software v2.2/v2.3). The cycling was followed by a melt curve analysis. All qRT-PCR experiments were carried out by comparative C_T ($\Delta\Delta C_T$) analysis, using *hypoxanthine-guanine phosphoribosyltransferase* (*Hprt*) as the housekeeping gene. Previous experiments by N. Martin identified *Hprt* as a suitable housekeeping gene as it displays no significant variation to hypoxia (Martin 2018).

For analysis, C_T was baselined from cycles 3 to 15. Technical replicates with high standard deviations of >0.5 and replicates with no amplification or multiple Tm peaks were omitted. Biological replicates were combined using StepOne™ Software v2.3's study function. Outliers in replicate groups were included for analysis.

Graphs were generated, and statistics were performed on GraphPad Prism 8.0.0. Data were presented as fold change in a linear or Log2 scale, and statistics were calculated using $\Delta\Delta C_T$ values on GraphPad Prism 8.

2.2.1.20 RNA extraction and DNase treatment – For RNA-seq

Cells preserved in RNA*later* were pelleted at 1 000 RCF for 5 minutes, and the RNA*later* solution was removed by pipetting. Total RNA was extracted using the *mir*Vana miRNA Isolation Kit (Ambion), according to the manufacturer's instructions. Total RNA was eluted using nuclease-free water.

The samples were then immediately DNase treated using the TURBO DNA-*free* kit (Invitrogen), according to the manufacturer's instructions. Following DNAse inactivation, the supernatant containing RNA was purified using the Monarch RNA Cleanup Kit (NEB), according to the manufacturer's instructions.

RNA quantity was assayed using the Nanodrop spectrophotometer. 100 – 500 ng/uL RNA was submitted to The David R Gunn Genomics Facility (SAHMRI) for quality assessment using the 2200 TapeStation (Agilent).

2.2.1.21 RNA-seq

1 µg RNA in 50 µL nuclease-free water of each sample was submitted to The David R Gunn Genomics Facility (SAHMRI) for library preparation. Total RNA was converted to strand-specific Illumina compatible sequencing libraries using the NuGEN Universal Plus mRNA kit according to the manufacturer's instructions (MO1442 v2).

Briefly, 500 ng of total RNA was polyA selected and the mRNA fragmented before reverse transcription and second-strand cDNA synthesis using dUTP. The resultant cDNA is end-repaired before the ligation of Illumina-compatible barcoded sequencing adapters. The cDNA libraries were strand selected and PCR amplified for 12 cycles before assessment by Agilent 2200 TapeStation for quality and Qubit fluorescence assay for quantity. RNA was confirmed to be of adequate quality (RIN score >8). Sequencing pools were generated by mixing equimolar amounts of compatible sample libraries based on the Qubit measurements.

Sequencing of the library pool was done with an Illumina NextSeq 500 using single read 75 bp (v2.0) sequencing chemistry over four sequencing runs.

2.2.1.22 Protein extraction

Cells in suspension well pelleted by centrifugation at 300 RCF, RT for 5 minutes and the media supernatant was aspirated. The cell pellet was resuspended and washed in 1 mL ice-cold PBS, before re-pelleted by centrifugation at 300 RCF, RT for 5 minutes. The PBS was aspirated. 200 µL of RIPA buffer was added per 6 mL of initial culture volume, and the cells were homogenised by pipetting.

2.2.1.23 Protein quantification

Protein quantity in whole cell extracts was estimated using the bicinchoninic acid assay (BCA assay). All samples and standards were measured in technical triplicates. The BCA assay was carried out in the microplate format according to the manufacturer's instructions, with slight modifications: standards were prepared at 0, 1, 2, 3, 4 and 5 µg/µL, and 1 µL sample was added for each unknown sample replicate. Following

incubation at 37°C for 30 minutes, absorbances were measured on the Multitaskan Ascent plate reader at 620 nm or the Nanodrop at 562 nm.

2.2.1.24 Western blots

10-50 µg protein was mixed with 4x SDS load buffer, loaded into the wells of an SDS-PAGE gel. The gel was run at 140-160 V until the desired separation was achieved. Proteins were transferred onto a nitrocellulose membrane using the Trans-Blot® Turbo™ system. The membrane was blocked in 10% skim milk in PBS-T for 1 hour at RT, and incubated with the primary antibody in 2% skim milk in PBS-T overnight at 4°C. The following day, the membrane was washed 3x 5 minutes in PBS-T and incubated with HRP conjugated secondary antibody in 2% skim milk in PBS-T for 1 hour at RT. The membrane was washed 3x 5 minutes in PBS-T and developed using ECL before imaging on the ChemiDoc™ MP imaging system.

Optionally, nitrocellulose membranes were fixed following transfer in 50% methanol at 0°C for 30 minutes and dried at 50°C for 30 minutes to improve protein attachment.

2.2.2 Tissue culture techniques

2.2.2.1 Maintenance of cell lines

All cell lines were cultured at 37°C with 5% CO_2 and humidified conditions. For hypoxia experiments, cell lines were cultured within a humidified incubation box inside a hypoxia workstation at 37°C with 5% CO_2.

2.2.2.1.1 HEK293T

HEK293T cells were cultured in Dulbecco's Modified Eagle Medium (DMEM), supplemented with 10% foetal calf serum (FCS), 2 mM L-glutamine or 1x GlutaMAX™, 100 U/mL penicillin, 100 µg/mL streptomycin, 1 mM sodium pyruvate, and 10 mM

hydroxyethyl piperazineethanesulfonic acid (HEPES). Cells were passaged in confluency ratios of 1/10 or 1/20 every two or three days, respectively.

2.2.2.1.2   5TGM1 murine multiple myeloma cell line

5TGM1 cells were cultured in Iscove's Modified Dulbecco's Medium (IMDM) (Sigma Aldrich, Cat: I3390), supplemented with 20% FCS, 2 mM L-glutamine or 1x GlutaMAX™, 100 U/mL penicillin, 100 µg/mL streptomycin, 1 mM sodium pyruvate, and 10 mM HEPES. Cells were passaged at 5×10^5 cells/mL or 2×10^5 cells/mL every two or three days, respectively.

2.2.2.1.3   Thawing cells

Frozen vials of cells were quickly thawed in a 37°C water bath. The thawed cells were immediately added to 4 mL of media and centrifuged at 300 RCF, RT for 5 minutes. The supernatant was aspirated, and the cells were resuspended in 1 mL of supplemented media by pipetting and added to 10 mL of supplemented media in a T75 flask or 10 cm culture dish. Cells were passaged at least twice to recover before being used for experiments.

2.2.2.1.4   Freezing cells

For each vial to be frozen, between $5 \times 10^6 - 1 \times 10^7$ cells were spun down at 300 RCF, RT for 5 minutes. The supernatant was aspirated, and the cell pellet was resuspended in 1 mL of FCS, 10% DMSO. The vials were frozen at -80°C in a Mr Frosty™ Freezing Container (Thermo Fisher) overnight and transferred to the vapour phase of a liquid nitrogen tank for long-term storage.

2.2.2.2   *Modification of cell lines*

2.2.2.2.1 Lentivirus production

6×10^5 HEK293T cells were plated in a 6 cm culture dish one day before transfections. On the day of transfection, 15 μL of Lipofectamine 3000 was diluted in 0.5 mL IMDM media (without supplements) and incubated at RT for 15 minutes. In another tube, 3.33 μg each of pEo lentivirus envelope vector, psPAX2 lentivirus expression vector and FgH1tUTP lentiviral guide RNA vector was diluted in 0.5 mL IMDM media (without supplements). The two tubes were combined and incubated at RT for 10-15 minutes. The mixture was then added dropwise to the HEK293T cells. Following a two-day incubation, the media containing viruses was harvested and filtered through a 0.22 μM syringe filter. The virus was used immediately for cellular transduction.

Any consumables in contact with live virus or liquids containing live virus were decontaminated with Virkon before disposal as biohazardous waste.

2.2.2.2.2 Lentivirus transduction – 'Spinfection'

Transductions were performed on 5×10^5 5TGM1 BF cells in 2.5 mL supplemented IMDM media with 16 μg/mL polybrene, seeded in 6 well trays. The filtered media was added dropwise to the cells. The trays were sealed with parafilm and centrifuged at 1000 RCF, RT for 60 minutes. Following a one-day incubation at 37°C, the media was changed by pelleting the cells at 300 RCF, RT for 5 minutes and resuspending the cell pellet in 6 mL of supplemented IMDM media. The cells were then transferred to a T25 flask.

Transduced cells were allowed to recover for at least two days and rinsed twice with supplemented IMDM media before FACS for successfully transduced cells.

2.2.2.2.3 FACS

Flow cytometry and FACS of cells were performed at SAHMRI's Flow Facility. 5TGM1 cells to be sorted were first pelleted at 300 RCF, RT for 5 min, washed with 1x PBS, and re-pelleted before resuspension in IMDM + 2% FCS. The cells were then filtered through a cell strainer snap cap of a Falcon™ test tube and kept on ice.

Flow operation was performed by facility staff, using the BD LSR Fortessa™ X-20 for cell analysis, and the BD FACSAria™ Fusion for FACS. Cell populations were sorted into test tubes containing IMDM + 2% FCS. The cells were pelleted at 300 RCF, RT for 5 minutes, before resuspension in supplemented IMDM media. Monoclones were directly sorted into round-bottom 96 well trays pre-filled with 200 µL supplemented IMDM media.

2.2.2.3 Treatment of cell lines

2.2.2.3.1 Doxycycline treatments

To induce the expression of gRNA *in-vitro*, doxycycline hyclate (dox) dissolved in MQ water, was added to a concentration of 1 µg/mL to cells seeded at 1×10^5 cells/mL. Cells were incubated at 37°C for 3 days before the cells were washed in PBS and resuspended in fresh media to remove dox.

2.2.2.3.2 2,2-Dipyridyl treatments

The hypoxia mimetic 2,2-Dipyridyl, dissolved in DMSO, was added to a concentration of 100 µM to cells seeded at 5×10^5 cells/mL. Negative treatment control samples were also set up with the addition of an equal volume of DMSO. Cells were incubated at 37°C between 2-48 hours and subsequently centrifuged at 300 RCF, RT for 5 minutes to harvest cell pellets.

2.2.2.3.3 Hypoxia treatments – for RNA-seq

Hypoxia treatments for RNA-seq were performed on one monoclonal cell line for each 5TGM1 HIF-α knockout genotype at a time (Table 2.1). Cells were seeded at 5×10^5 cells/mL in 6 mL, 6 cm dishes. Samples to be incubated in hypoxia were transferred to a hypoxia workstation that was maintained at 37°C, <1% O_2, 5% CO_2. Within the hypoxia workstation, cells were kept inside a humidified incubation box. Treatment samples were incubated in hypoxia for either 8 or 48 hours. Normoxic controls were set up alongside and cultured at 37°C with 5% CO_2 and humidified conditions, for 8 hours.

At the end of the treatment period, the cells were transferred into 10 mL graduated centrifuge tubes using transfer pipettes within the hypoxia workstation. The cultures were then pelleted at 300 RCF for 5 min, and the media was aspirated off. The cell pellets were then suspended in 250 μL RNA*later* and stored at -20°C.

Table 2.1: Treatment plan for monoclonal HIF-1α and HIF-2α knockout and control 5TGM1 cells.

Genotype	Treatment group 1	Treatment group 2	Treatment group 3	Treatment group 4	Treatment group 5
H1E2	KO 1	KO 2	KO 4	KO 5	KO 6
H1E3	KO 1	KO 2	KO 3	KO 4	KO 5
H2E2	KO 1	KO 2	KO 3	KO 4	KO 5
H2E3	KO 2	KO 3	KO 4	KO 5	KO 6
EV	EV 2	EV 3	EV 4	EV 5	EV 6

2.2.3 Bioinformatics (RNA-seq)

2.2.3.1 *RNA-seq analysis*

Initial analysis was performed by the SAHMRI Bioinformatics Facility using an in-house pipeline. Briefly, raw single-end FASTQ reads were trimmed by AdapterRemoval and aligned using the STAR transcriptome algorithm to the GRCh38/mm10 genome (Dobin et al. 2013). Quantification was performed by featureCounts/R, and QC assessment was performed by FastQC (Ward, To & Pederson 2018). Gene annotations were obtained from Ensembl and data was subsequently filtered for low counts, that are <1 CPM in >4 samples. Data exploratory analysis was performed by MDS plot and heatmap. Data linear modelling was done by limma voom (Ritchie et al. 2015), and differential gene analysis was performed by limma. Functional annotation was performed by gene ontology pathway enrichment analysis on GOrilla (Eden et al. 2009).

Results 1

Generation of HIF-1α and HIF-2α Knockout 5TGM1 Cells Using an Inducible CRISPR/Cas9 System

3 Results 1

3.1 Generation of HIF-1α and HIF-2α knockout 5TGM1 cells using an inducible CRISPR/Cas9 system

Aim 1: To generate HIF-1α and HIF-2α inducible-knockout 5TGM1 cells.

Aim 2: To generate and characterise HIF-1α and HIF-2α knockout 5TGM1 cells.

3.1.1 Background

Previous attempts by past members of the Peet laboratory to knockout HIF-1α and HIF-2α in the 5TGM1 murine MM cells have had limited success.

Initial efforts by Y. Ma (2015) and N. Martin (2018) employed a two-sgRNA CRISPR plasmid strategy to delete exon 2 of *Hif-1α* and *Hif-2α* by inducing simultaneous double-stranded breaks (DSBs) within the flanking introns. Non-homologous end joining (NHEJ) DNA repair of the two flanking introns 'excises' the deleted exon (Canver et al. 2014; Togashi et al. 2015). This truncates HIF-α as exon 2 does not code for a multiple of 3 base pairs (bp), causing a frameshift mutation that leads to a premature termination codon (PTC). Guides targeting intron 1 and 2 of *Hif-1α* or *Hif-2α* were cloned into PX458 CRISPR plasmids and were co-introduced into 5TGM1 B cells with a plasmid expressing dsRed by Polyfect transfection (Ran et al. 2013). Since an entire exon was expected to be removed by this modification, PCR amplification using primers flanking the cut sites and gel electrophoresis was used to detect for knockout monoclones by screening for smaller amplicons (Canver et al. 2014).

However, this strategy was inefficient at generating knockout monoclonal cell lines. Firstly, 5TGM1 cells were difficult to transfect, possessing a transfection efficiency of less

than 4% under optimised transfection conditions (Ma 2015). Secondly, transfected 5TGM1 cells recovered very poorly from single-cell fluorescence-activated cell sorting (FACS), with about 2-3% of single cells growing into monoclonal colonies (Ma 2015). This poor recovery was overcome by isolating sorted cells using limiting dilution, which yielded a higher survival rate of 13%. Lastly, the homozygous deletion of exon 2 was a rare event. From two attempts, no HIF-1α knockouts (out of a total of 83 clones) were detected by PCR screening, whereas only 2 HIF-2α knockouts (out of a total of 62 clones) were detected (Martin 2018).

There are possible explanations for these observations. 5TGM1 cells may not be particularly amenable to the use of transfection reagents as they are non-adherent in culture; non-adherent cells generally lowly express negatively-charged heparan sulphate proteoglycans on their plasma membranes that interact with positively-charged transfection complexes (Mislick & Baldeschwieler 1996). Several publications have reported on the low nucleic acid transfection efficiency of MM cells with conventional and 'easy-to-use' transfection reagents (Brito, Brown & Morgan 2010; Brito et al. 2008; Steinbrunn et al. 2014). This would ultimately lead to reduced Cas9 protein expression, and consequently, lowered CRISPR/Cas9 mediated gene-editing efficiency (Jinek et al. 2013). Additionally, the two guides targeting introns need high on-target efficiency as simultaneous DSBs would have to occur before NHEJ repair mediates exon 2 removal. Furthermore, the efficiency of the guides in practice was not known as no pre-testing, such as by T7E1 assay, was reported.

Subsequent efforts by J. Lum (2017) utilised a lentivirus system in an attempt to knockout HIF-α in 5TGM1s with better efficiency (Lum 2017). Lentiviral delivery of vectors into 5TGM1 cells has been previously used successfully by N. Martin, and by members of the Zannettino lab as reported in several of their publications (Cheong et al. 2015; Hewett et al. 2017; Martin 2018; Mrozik et al. 2015). J. Lum's strategy employed the use of the single gRNA CRISPR/Cas9 lentiCRISPRv2 vector to induce DSBs in an early exon, leading to its repair by error prone NHEJ. The indels introduced by NHEJ at the single cut site may cause frameshift mutations, leading to HIF-α protein truncation. In

addition, pre-testing of guides by T7 Endonuclease I assay was performed to test for the presence of on-target activity of selected guides.

Although lentivirus transduction of 5TGM1 cells was previously reported to be quite efficient, lentiviral transductions were unsuccessful in J. Lum's study (Lum 2017). Several reasons could account for this, such as low virus titres or problems with the selected viral packaging vectors (pCMV-dR8.2 dvpr, pRSV-Rev, pMD2.G). The use of lentiCRISPRv2 with 5TGM1 cells has also not been previously reported. However, due to time constraints, the exact nature of the problem was left unresolved.

Consequently, a different lentivirus strategy was formulated and employed in this study to overcome the problems previously encountered. The two-plasmid inducible lentiviral guide RNA expression system designed by the Herold laboratory was reported to be an efficient and temporally controllable CRISPR/Cas9 system, consisting of (i) a constitutively expressing *Streptococcus pyogenes* Cas9 (spCas9) and mCherry vector FuCas9Cherry, and (ii) a doxycycline (dox)-inducible sgRNA and constitutively expressing eGFP vector FgH1tUTG (Aubrey et al. 2015). The dox-inducible sgRNA system was favoured over constitutive expression to enable targeted editing of *Hif-α* genes *in-vivo.*

5TGM1 BMX1 (5TGM1 B) cells are 5TGM1 cells that have been transduced with the tri-modality reporter NES-TGL, that contains firefly luciferase for live *in-vivo* imaging, eGFP for cell sorting and thymidine kinase. These cells are a clonal subline that have also been recirculated and collected from the BM of a KaLwRij mouse once to ensure BM tropism (Hewett et al. 2017). 5TGM1 BMX1 FuCas9Cherry (5TGM1 BF) cells constitutively expressing spCas9 had been generated by the Zannetinno lab using an established transduction protocol, and characterised. Thus, to generate inducible knockout lines, the FgH1tUTG +guide vector would have to be transduced into these 5TGM1 BF cells, allowing for a range of alternative gene knockouts to be generated from this one cell line.

However, as the 5TGM1 B cells have already been transduced with a tri-modality reporter expressing eGFP, the transduction efficiency of FgH1tUTG into the cell line would be difficult to measure quantitatively as it also encodes eGFP. Therefore, FgH1tUTG would have to be re-engineered to express a different selection marker to enable the selection of successfully transduced cells.

This chapter first describes the generation of FgH1tUTP, which constitutively expresses the mPlum fluorescent protein instead of eGFP. This plasmid is valuable for MM research with applications beyond that of investigating the HIFs since it can be used with guides for any target of interest. This is followed by the description of the generation and characterisation of inducible-knockout and knocked-out HIF-1α and HIF-2α 5TGM1 cells lines using FgH1tUTP, valuable tools for the investigation into the roles of HIF-1α and HIF-2α in MM.

3.1.2   Cloning the FgH1tUTP dox-inducible gRNA vectors

To enable tri-colour fluorescent sorting for the selection of cells that have been successfully transduced with the guide vector, the FgH1tUTG plasmid was re-engineered to express the mPlum selection marker instead of eGFP (FgH1tUTP). mPlum is a far-red monomeric fluorescent protein derived from DsRed by somatic hypermutation and has a long emission wavelength (Wang et al. 2004) (Figure 3.1). Its emission spectra partially overlap that of mCherry, but since it has a different emission maximum to that of mCherry (609 nm vs 646 nm) the two colours should be distinguishable from each other by multi-colour flow cytometry. This would enable 5TGM1 BF cells which had been successfully transduced with FgH1tUTP (5TGM1 BFF) to be selectively isolated using fluorescence-activated cell sorting (FACS), gating for cells that are positive for GFP, mCherry and mPlum signals.

FgH1tUTP was generated from FgH1tUTG by replacing the *egfp* gene with a gBlock containing *mplum* by isothermal assembly (Figure 3.2A). Plasmids were screened by MscI restriction digestion (Figure 3.2B) and the sequence integrity of the inserted *mplum* gene was verified by Sanger sequencing (data not shown). The presence of mPlum activity was then confirmed by flow analysis of transiently transfected HEK293T cells with FgH1tUTP (Appendix, Figure 6.1). Thus, 5TGM1 BF cells transduced with FgH1tUTP could be selectively isolated using FACS, by gating for eGFP$^+$ mCherry$^+$ mPlum$^+$ cells. FgH1tUTP's mechanism for dox-inducible guide expression is shown and described in Figure 3.3.

To knockout HIF-1α and HIF-2α, early exons (between exons 1-3) were selected as target regions for sgRNA-directed CRISPR/Cas9 editing. The cleavage, repair by NHEJ, and induction of frameshift mutations at precise positions in the coding sequence of HIF-α, should lead to the introduction of early stop codons and consequent protein truncation (Hsu, Lander & Zhang 2014). This prevents essential functional domains that are downstream of the cut site from being translated, leading to abrogated protein function and activity. Three guides were selected for *Hif-1α*, one for each of exons 1, 2 and 3

(H1E1, H1E2 and H1E3 guides). Two guides were selected for *Hif-2α*, one for each of exons 2 and 3 (H2E2 and H2E3 guides). Multiple guides were used to control for potential off-target effects. Importantly, Exons 2 and 3 are present in all reported transcript variants of both *Hif-1α* and *Hif-2α*.

The H1E1 guide targets the early coding region of the protein. Whereas the exon 2 guides, H1E2 and H2E2, cut within the bHLH DNA binding domain that recognises and binds to the HRE DNA sequence, while the exon 3 guides, H1E3 and H2E3, cut within the PAS 1 domain that is for HIF-α binding with ARNT (Figure 3.4). Truncation of HIF-α in the DNA binding and dimerization domains also causes the loss of degradation and transactivation domains, leading to the putative loss of HIF-α function as the latter domains are important for coactivator interaction, binding and recruitment. Additionally, the generation of stop codon(s) in early exons increases the likelihood of nonsense mediated mRNA decay (Popp & Maquat 2016). On the other hand, in-frame (non-frameshift) mutations can still potentially disrupt protein function since the guides sit within essential functional domains.

Guide RNA sequences were designed on Benchling against the mm10 *Mus musculus* genome assembly and selected with considerations for their calculated on-target and off-target scores, as well as their potential off-target sites. These guides were also designed to be directly upstream of the SpCas9 protospacer adjacent motif (PAM) sequence, 5'-NGG-3', which is required for Cas9 recognition of a DNA binding site (Shah et al. 2013). On-target scores were based on a model which predicts gRNA on-target activity with considerations for gene positional information (Doench et al. 2016). Off-target scores were based on a separate model that predicts potential non-specific cleavage site within the genome (Hsu et al. 2013).

Synthesised guide oligonucleotides were annealed and ligated into the BsmbI restriction sites of FgH1tUTP and successful guide insertion was confirmed by Sanger sequencing (FgH1tUTP+gRNA).
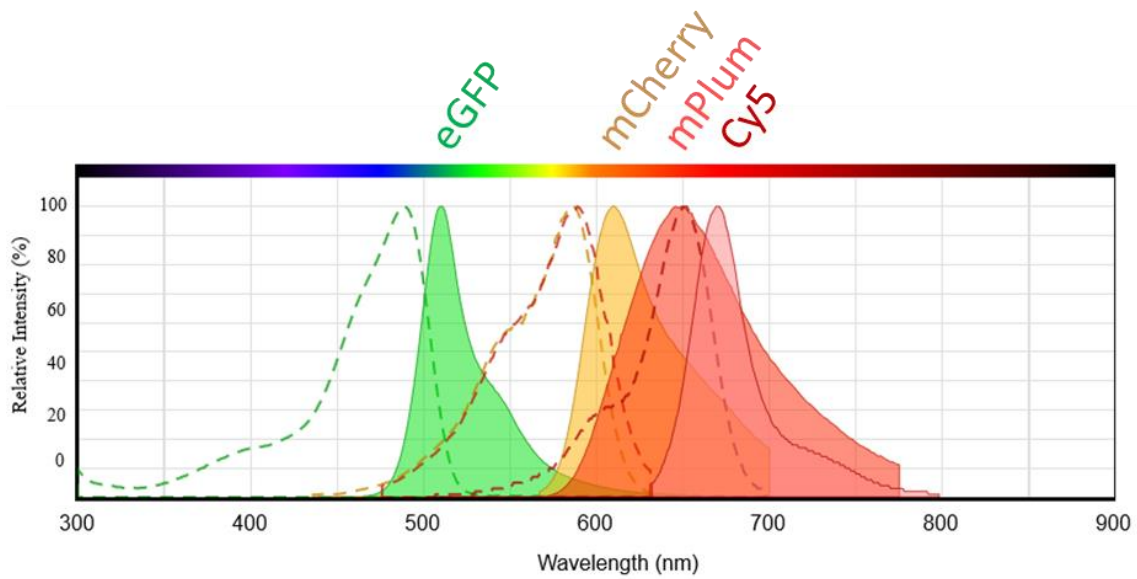
Figure 3.1: Excitation and emission spectra of eGFP, mCherry, mPlum and Cy5. The selection of successfully transduced 5TGM1 BF cells with FgH1tUTP was performed by gating for the presence of GFP, mCherry and mPlum emissions. Dotted plots indicate excitation spectra whereas solid plots indicate emission spectra. Emission spectra are also labelled above the plot. The emission spectrum of Cy5 has greater overlap of mPlum than mCherry. From left to right, eGFP, max 489/510 nm; mCherry, max 587/609 nm; mPlum, max 589/646 nm; Cy5, max 650/669 nm. Plot generated using AAT Bioquest® Spectrum Viewer, https://www.aatbio.com/spectrum/.

A
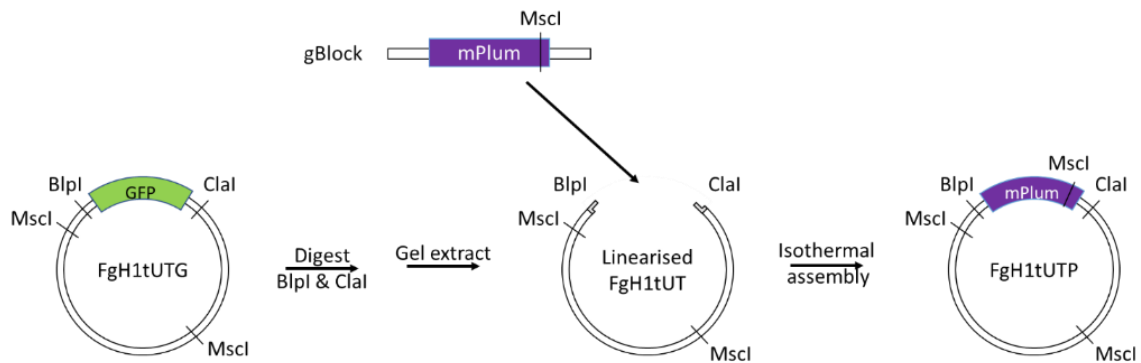
B
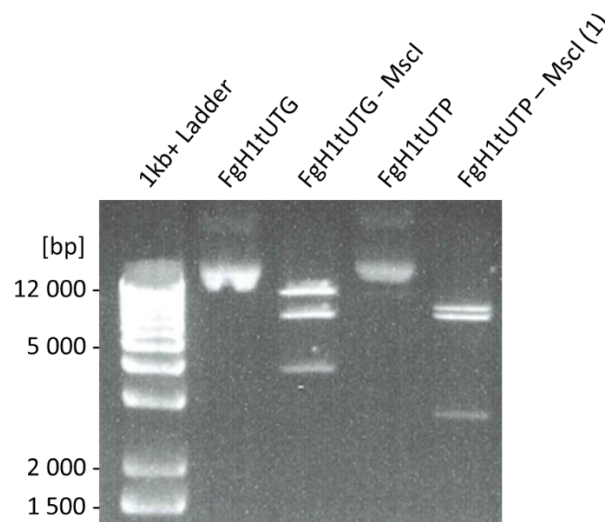
Figure 3.2: Assembly of FgH1tUTP. (A) Schematic summary of the Gibson Isothermal Assembly strategy used to create the FgH1tUTP mammalian inducible CRISPR/Cas9 vector. The *egfp* gene is flanked by single BlpI and ClaI cut sites on either side and was removed from FgH1tUTG by double restriction enzyme digest before purification of the plasmid backbone by gel extraction. Insertion of a synthesised double-stranded mPlum gBlock gene fragment (IDT) was performed by isothermal assembly. **(B)** Plasmids were then subsequently screened by MscI diagnostic digest. Plasmid minipreps from bacterial colonies transformed with Gibson assembly products of the FgH1tUT backbone and mPlum gBlock gene fragment were digested with the MscI restriction enzyme and

resolved on a 1% agarose gel. Digest products from all screened FgH1tUTP candidates have a different banding pattern as compared to the digested FgH1tUTG control. Successful insertion was confirmed by Sanger sequencing (AGRF).
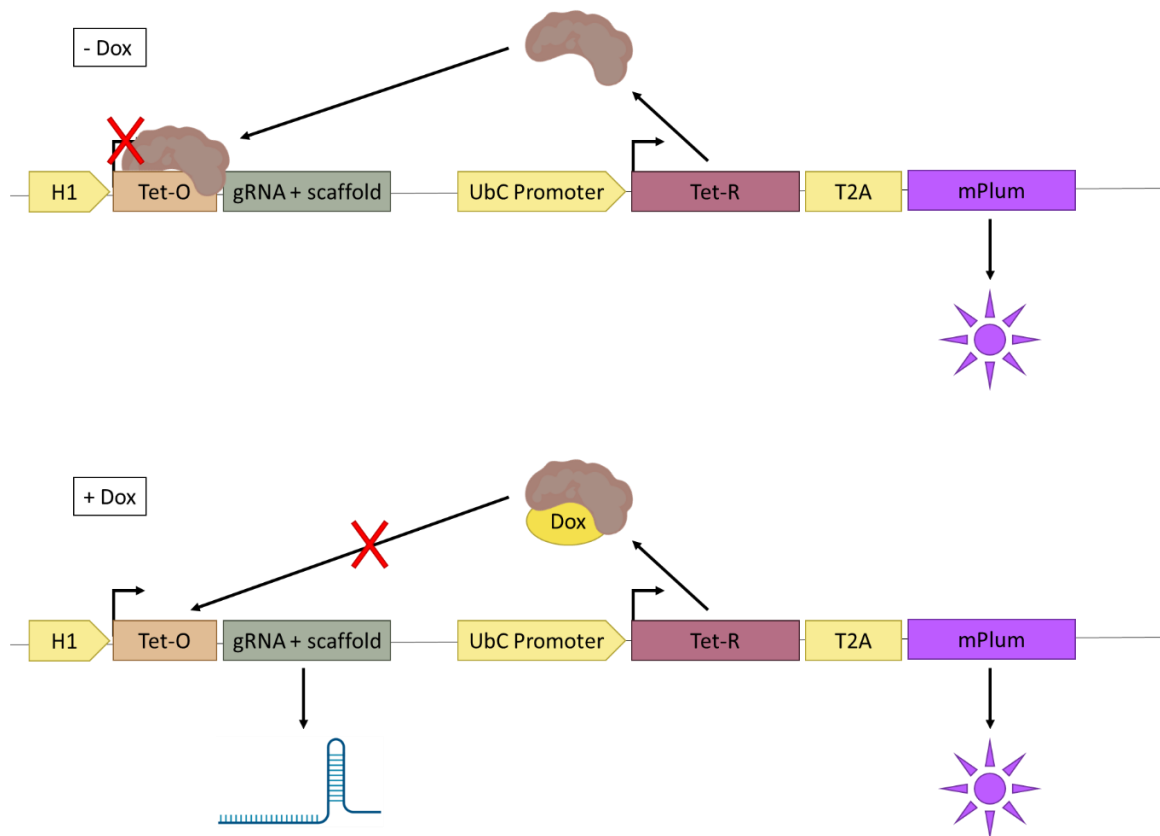
Figure 3.3: Schematic for the mechanism of dox-inducible guide RNA expression of the FgH1tUTP lentiviral vector. The constitutive UbC mammalian promoter drives the expression of the Tet-R and the mPlum fluorescent protein. Tet-R and mPlum are linked via a self-cleaving T2A peptide. In the absence of dox, Tet-R binds to Tet-O downstream and suppresses promoter activity of the constitutive H1 promoter that drives sgRNA expression. This suppression is alleviated in the presence of dox, leading to sgRNA expression. Tet-O, tetracycline operator; gRNA, guide RNA; Dox, doxycycline; UbC, ubiquitin C; Tet-R, tetracycline repressor.

A
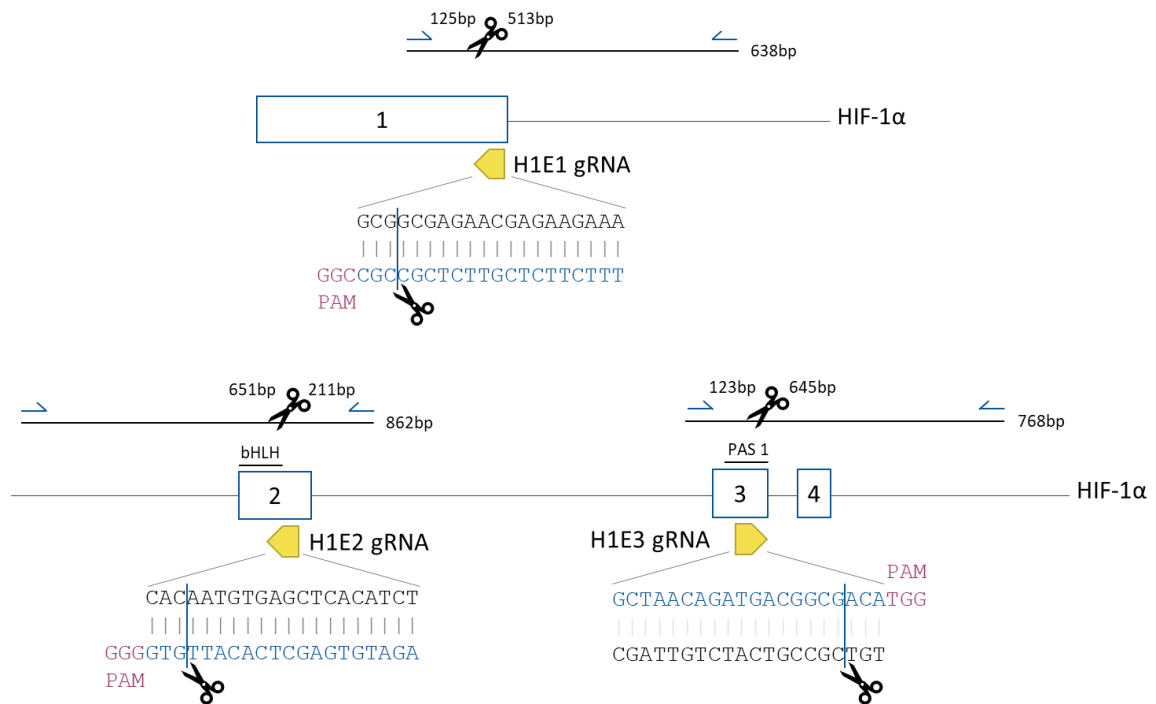
B
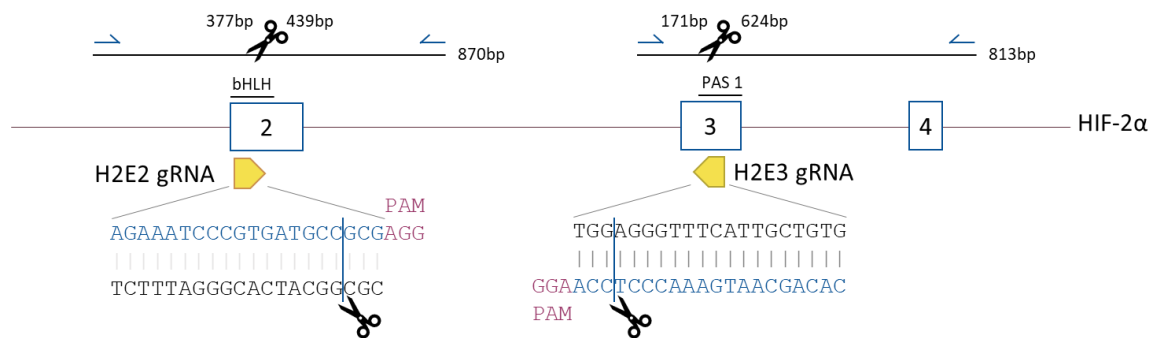
Figure 3.4: Schematic diagram of the *Hif-α* gRNA sequences. Yellow block arrows indicate the position and direction of gRNAs targeting **(A)** *Hif-1α* and **(B)** *Hif-2α*. Blue arrows indicate T7E1 primer positions, numbers to the right of PCR amplicons indicate their size and the numbers on top are expected T7E1 fragment sizes. Vertical blue lines indicate where spCas9 is expected to cut within the target sequences. PAM, Protospacer adjacent motif.

3.1.3   Generation of HIF-1α and HIF-2α inducible-knockout 5TGM1 cells

To generate HIF-α inducible knockout 5TGM1 lines (5TGM1 BFF), 5TGM1 BF cells, which constitutively express spCas9, were transduced with FgH1tUTP+gRNA. An empty vector control was also generated by transducing 5TGM1 BF cells with FgH1tUTP. FACS was optimised to achieve an effective sorting strategy as shown in Figure 3.5.

Inducible knockout 5TGM1 BFF cells were successfully isolated using the FACSAria™ Fusion cell sorter, by gating and sorting for eGFP[+], mCherry[+] and Cy5^{+} (for mPlum[+]). Transduction efficiency, measured by the proportion of 5TGM1 cells with mPlum fluorescence, was about 42% of all cells across all transduced lines (Table 3.1). Post-sort purity checks were performed on all samples to confirm successful sorting.
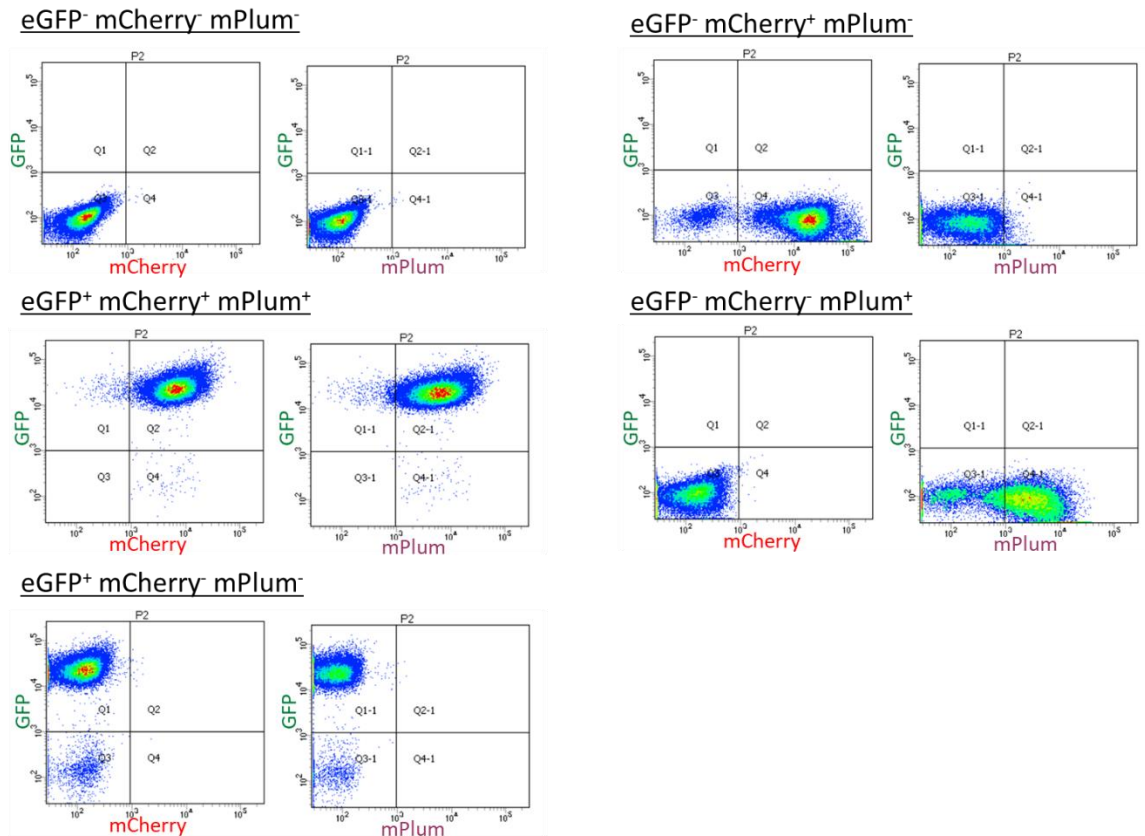
Figure 3.5: Flow cytometry analysis of 5TGM1 cells transduced with a combination of eGFP$^+$ (NES-TGL), mCherry$^+$ (FuCas9Cherry) and mPlum$^+$ (FgH1tUTP) plasmids. Analysis was performed using the BD LSRFortessa X20 analyser. The use of a multi-laser flow cytometer with the application of appropriate compensation settings was able to distinguish between mCherry$^+$ and mPlum$^+$ population of cells. Information on the cell lines used can be found in Methods, Section 2.1.12. FgH1tUTP was transduced using the spinfection method. Transduced cells were passaged twice and washed with PBS twice to remove live virus prior to flow analysis.

Table 3.1: Transduction efficiency of FgH1tUTP, measured as the proportion of all cells with mPlum⁺ fluorescence by FACS.

5TGM1 BFF Line / FgH1tUTP guide	Transduction efficiency (% of cells)
HIF-1α Exon 1 (H1E1)	42
HIF-1α Exon 2 (H1E2)	39
HIF-1α Exon 3 (H1E3)	54
HIF-2α Exon 2 (H2E2)	39
HIF-2α Exon 3 (H2E3)	40
Empty Vector (EV)	39
Average	42

3.1.4 Assaying the on-target activity of the guide RNAs

To assay for gRNA on-target activity, guide pretesting on 5TGM1 BFF cells was performed using the T7 Endonuclease I (T7E1) assay. As on-target scores are only predictive of guide activity, it was crucial to demonstrate guide activity experimentally. The T7E1 enzyme recognises and cleaves heteroduplexed DNA (Vouillot, Thélie & Pollet 2015). If guide on-target activity is present, various indels will arise from CRISPR/Cas9 editing and DNA repair in a pool of cells. Primers flanking the target region are used to amplify the different alleles by PCR. The subsequent annealing of two different alleles that are not perfectly matched within the edited segment of its sequence gives rise to heteroduplexed DNA. Heteroduplexed DNA is recognised and cleaved by T7E1 within the mismatched region. Mismatch cleavage leads to the formation of cleaved products of predictable size, which are easily distinguishable from the full amplicon by resolution on an agarose gel.

Before performing T7E1 assays, primers flanking the gRNA target sites were tested on the extracted gDNA for amplification and specificity. Optimal annealing temperatures were determined by gradient PCR. The optimal amplification condition for each set of primers is summarised in Methods, Section 2.1.8.2.

Guide pre-testing was performed for all 5TGM1 BFF lines with inducible gRNA. These cells were treated with 1 μg/mL dox for approximately 72 hours to induce gRNA expression alongside untreated controls. CRISPR/Cas9 mediated genome editing takes place during this treatment period. gDNA was then extracted from these treated cell lines using the salting out method (Methods, Section 2.2.1.15)

T7E1 assays performed on cells transduced with FgH1tUTP containing the H1E2, H1E3, H2E2 and H2E3 guides show the presence of on-target guide activity (Figure 3.6). For these guides, the expected cleavage products were produced from the T7E1 digest of amplicons from 3 day dox-treated cells. Furthermore, these cleavage products were only

observed when cells had been treated with dox, confirming that guide expression is dox-dependent.

On the other hand, the result from the T7E1 digest of cells transduced with FgH1tUTP containing the H1E1 guide was inconclusive (Figure 3.7A). Background bands produced from T7E1 digest running approximately the same size as the expected fragments were present in both dox-treated and untreated cell lines. Therefore, it was difficult to determine if the intended cleavage within the CRISPR target region has occurred.

3.1.4.1   Cloned insert sequencing

To determine if the H1E1 guide exhibited on-target activity, *Hif-1α* Exon 1 PCR products were cloned into the pGEM-T vector and sequenced. Sequencing results suggest that the H1E1 guide has low on-target efficiency. Only one sequence out of four samples had a +1 nucleotide (nt) insert at the target site. The remaining three samples were wildtype (wt) sequences.

Interestingly, Sanger sequencing also revealed a homopolymeric region of A/T nucleotides within 50 nt of the predicted cut site (Figure 3.7B). For the four products sequenced, this region had between 17-21 A/T nt. This observation may be explained by the occurrence of enzyme slippage during the PCR amplification steps, which leads to homopolymeric products of different lengths (Viguera, Canceill & Ehrlich 2001). The difference in lengths of these stretches explains the presence of background bands produced from the T7E1 digest of untreated (no dox) samples (Figure 3.8A). Given the ambiguity of the T7E1 assay results, and the inefficiency of on target efficency with the H1E1 guide, this guide was not used to generate monoclonal lines.

Similarly, the background bands from the T7E1 digest of untreated *Hif-1α* Exon 2 sample can be explained by the presence of homopolymeric regions within the amplicon (Figure

3.8B). The homopolymeric region within the intron upstream of *Hif-1α* Exon 2 had a range of between 11-15 A/T nt. Cleavage within this region produces the observed background fragments of approximately 350 and 500 bp. However, as these bands were distinguishable from the dox-dependent bands produced in the T7E1 assay of 200 and 650 bp, this guide was used for the generation of monoclonal cells lines.

A
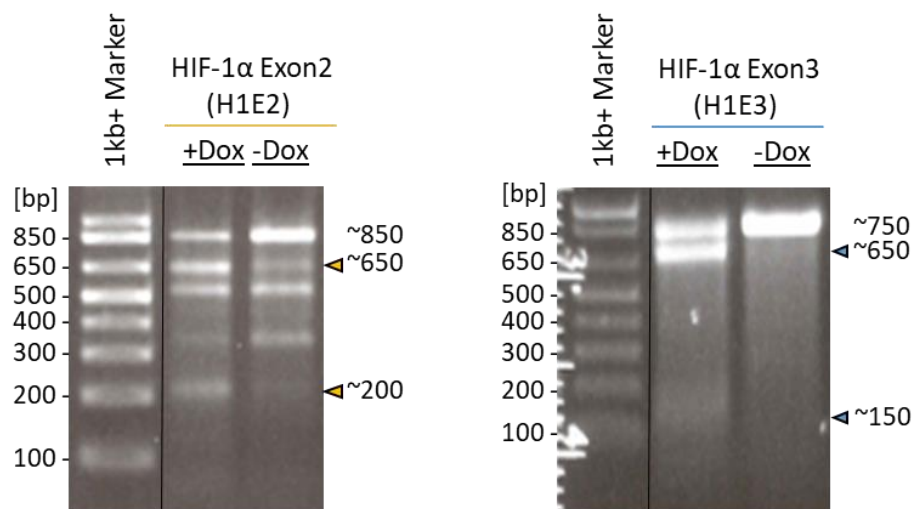
B
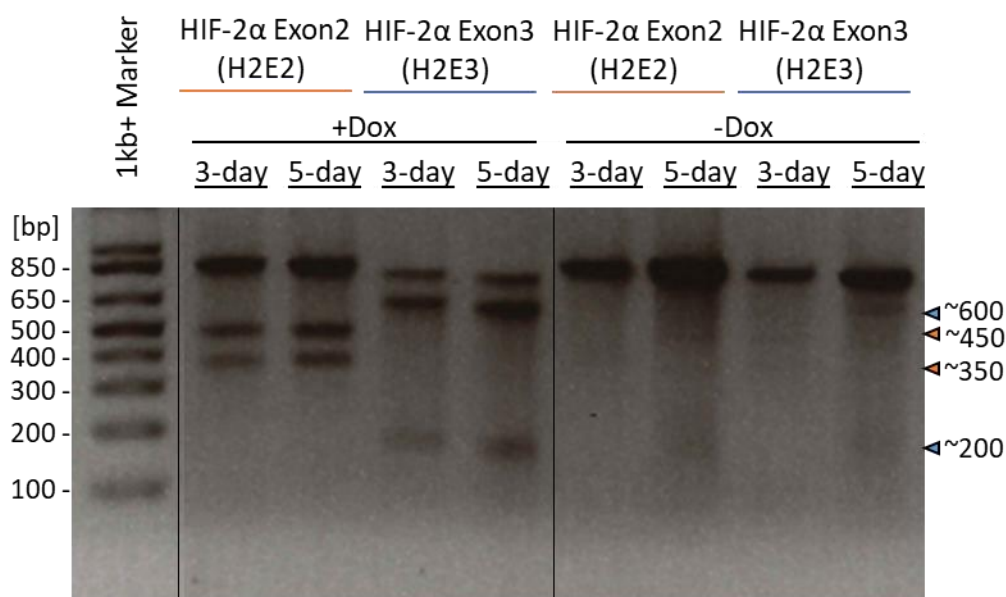
Figure 3.6: Pre-screening for on-target activity of dox-inducible gRNA. T7 Endonuclease (T7E1) assay performed on PCR-amplified gDNA from 1 μg/mL dox-treated (+dox) and untreated (-dox) 5TGM1 BFF cells. **(A)** Cells with guides H1E2 and H1E3 were treated for a period of 3 days, while **(B)** cells with guides H2E2 and H2E3 were treated for periods of 3 and 5 days. PCR amplification of all samples were performed on gDNA extract using Taq Polymerase with Standard Buffer and resolved by gel electrophoresis on 1% agarose gel. Coloured arrows indicate expected fragments produced from the T7E1 assay when

indels are generated by CRISPR/Cas9 editing. Black lines indicate where lanes are spliced together from the same gel for analysis.

A
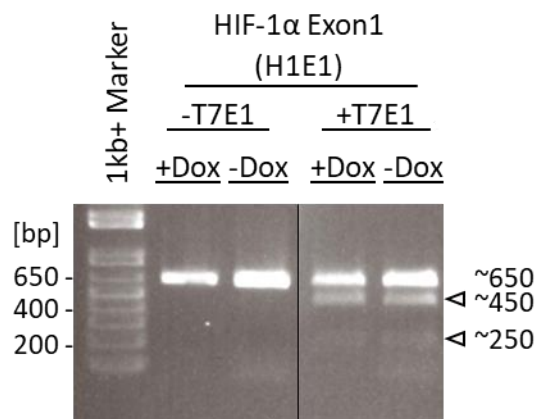
B

```
            951                                                    1000
Hif1a (E... GGCACCGATTCGCCATGGAGGGCGCCGGC-GGCGAGAACGAGAAGAAAAA
pGEM-T 1    GACACCGATTCGCCATGGAGGGCGCCGGC-GGCGAGAACGAGAAGAAAAA
pGEM-T 2    GGCACCGATTCGCCATGGAGGGCGCCGGC-GGCGAGAACGAGAAGAAAAA
pGEM-T 3    GGCACCGATTCGCCATGGAGGGCGCCGGCGGGCGAGAACGAGAAGAAAAA
pGEM-T 4    GGCACCGATTCGCCATGGAGGGCGCCGGC-GGCGAGAACGAGAAGAAAAA

            ........................................................

            1001                                                   1050
Hif1a (E... GTAAGCCGGGCCGCCGCGTTCCGTGGACTGGCtttttttttttttttttt
pGEM-T 1    GTAAGCCGGGCCGCCGCGTTCCGTGGACTGGC--TTTTTTTTTTTTTTTT
pGEM-T 2    GTAAGCCGGGCCGCCGCGTTCCGTGGACTGGC---TTTTTTTTTTTTTTT
pGEM-T 3    GTAAGCCGGGCCGCCGCGTTCCGTGGACTGGC----TTTTTTTTTTTTTT
pGEM-T 4    GTAAGCCGGGCCGCCGCGTTCCGTGGACTGGCTTTTTTTTTTTTTTTTTT

            ........................................................

            1051                                                   1100
Hif1a (E... tttGTCTCCGCTCCCCTTCCGTCCCCCCCAGCCTCACGCGCCGGGCTCCC
pGEM-T 1    TTTGTCTCCGCTCCCCTTCCGTCCCCCCCAGCCTCACGCGCCGGGCTCCC
pGEM-T 2    TTTGTCTCCGCTCCCCTTCCGTCCCCCCCAGCCTCACGCGCCGGGCTCCC
pGEM-T 3    TTTGTCTCCGCTCCCCTTCCGTCCCCCCCAGCCTCACGCGCCGGGCTCCC
pGEM-T 4    TTTGTCTCCGCTCCCCTTCCGTCCCCCCCAGCCTCACGCGCCGGGCTCCC
```

Figure 3.7: Homopolymeric regions give rise to background bands in T7E1 assay. (A) T7E1 assay performed on PCR-amplified gDNA from 1 µg/mL dox-treated (+dox, 3 days) and untreated (-dox) 5TGM1 BFF H1E1 cells. *Hif-1α* Exon 1 was PCR amplified and resolved by gel electrophoresis on 1% agarose gel. White arrows indicate amplicon fragments produced following T7E1 digest. Black lines indicate where lanes are spliced

together from the same gel for analysis. **(B)** *Hif-1α* Exon 1 amplicons were amplified from gDNA of dox-treated 5TGM1 BFF H1E1 cells and cloned into the pGEM-T vector. Cloned inserts were sanger sequenced using the T7prom_F primer. One out of the four amplicons sequenced contained a +1 nt insertion at the cut site (blue arrow). The orange box indicates the homopolymeric region (stretch of A/Ts) within proximity of the H1E1 gRNA cut site.

A

Length (nt)	Count
17	1
18	1
19	1
21	1

B

Length (nt)	Count
11	2
12	5
13	10
15	1
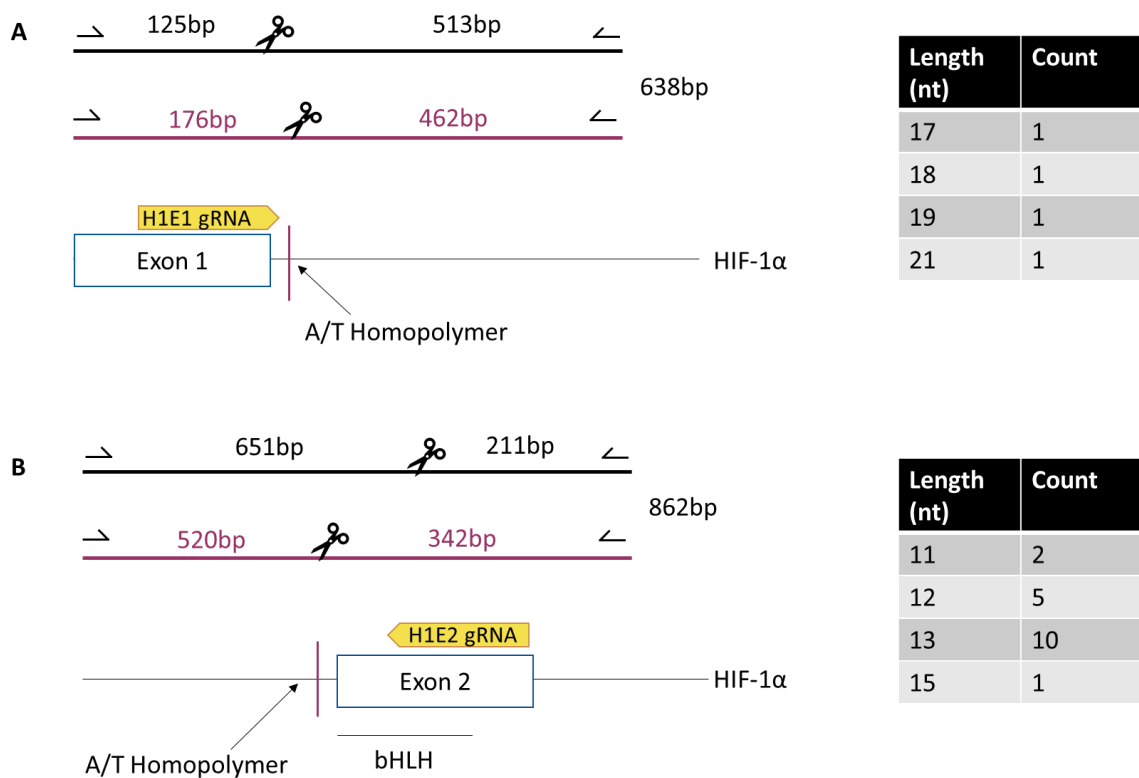
Figure 3.8: Schematic diagram indicating the position of homopolymeric regions in proximity to HIF-1α CRISPR/Cas9 editing sites. These homopolymer regions in proximity to *Hif-1α* (A) Exon 1 and (B) Exon 2 have different lengths of A/T single nucleotide repeats that are brought about by polymerase enzyme slippage during PCR. The black line indicates the intended T7E1 cleavage products that are produced if CRISPR/Cas9 editing occurs. The purple line indicates the products produced due to T7E1 cleavage at homopolymeric regions. These products give rise to the background bands observed in T7E1 assays. Tables on the right summarises the frequency of lengths of homopolymeric regions observed from Sanger sequencing of the cloned inserts.

3.1.5   Generation of monoclonal HIF-1α and HIF-2α inducible-knockout 5TGM1 Cells

To control for the effects brought about by the differences in FgH1tUTP vector integration in 5TGM1 BFF cells, monoclonal 5TGM1 BFF cells (5TGM1 BFF m) for H1E2, H1E3, H2E2 and H2E3 guides were generated by single-cells FACS on the FACSAria™ Fusion cell sorter (Figure 3.9). A summary of the established cell lines is presented in Table 3.2. Monoclonal EV controls were also similarly generated (Table 3.3). Single cells were isolated by gating for eGFP⁺ mCherry⁺ mPlum⁺ into 96 well trays and grown to confluency over two weeks. 12 monoclonal lines were selected for each guide or empty vector line and were tested for luciferase activity using Promega's Luciferase Assay System with the GloMax® 96 Microplate luminometer. This was necessary because luciferase activity is required to monitor the growth of tumours *in-vivo* by bioluminescent imaging. A total of 5 or 6 monoclonal lines that retained luciferase activity were selected for each guide or empty vector line (Appendix, Figure 6.2). The isolation of multiple monoclonal lines for each sgRNA controls for random effects associated with the generation and/or isolation of the edited cells. These monoclonal lines can then be analysed independently, or combined, to control for line-specific effects.

### 3.1.6   Generation of monoclonal HIF-1α and HIF-2α knockout 5TGM1 cells

Next, for the 5 monoclonal lines for each of the inducible sgRNAs (H1E2, H1E3, H2E2 and H2E3), CRISPR-Cas9 editing was induced by treating 5×10^5 cells with 1 µg/mL dox for 3 days. The dox-treated cells were then isolated by single-cell FACS into 96 well plates using the FACSAria™ Fusion cell sorter (Figure 3.9). To identify knockout lines, up to 12 monoclonal cell lines were generated from dox treatment of each of the original inducible sgRNA monoclonal lines. Then gDNA was extracted, the DNA region surrounding and including the guide target site was amplified by PCR using the same primers for T7E1 assays, and the amplified DNA was Sanger sequenced.

The indels for each monoclonal line were determined by manually resolving the overlapping Sanger sequencing traces or using the web-based CRISP-ID v1.1 program (Dehairs et al. 2016). A summary of observed alleles is presented in Figure 3.10. Various indels arose across the target sites from CRISPR/Cas9 editing, but a predominant indel of -1 nt deletion was observed for 3 out of the 4 guides. Furthermore, *Hif-1α* guides also appear to have better on-target activity compared to *Hif-2α* guides, as about a quarter of sequenced *Hif-2α* alleles are unedited at the target site.

Knockout lines with two different frameshift mutations (ie. one in each allele) were preferentially selected (5TGM1 BFF mK). One knockout line was selected from each of the original 5TGM1 BFF m inducible monoclonal lines for each guide or empty vector line. A summary of the established lines is presented in Table 3.2.
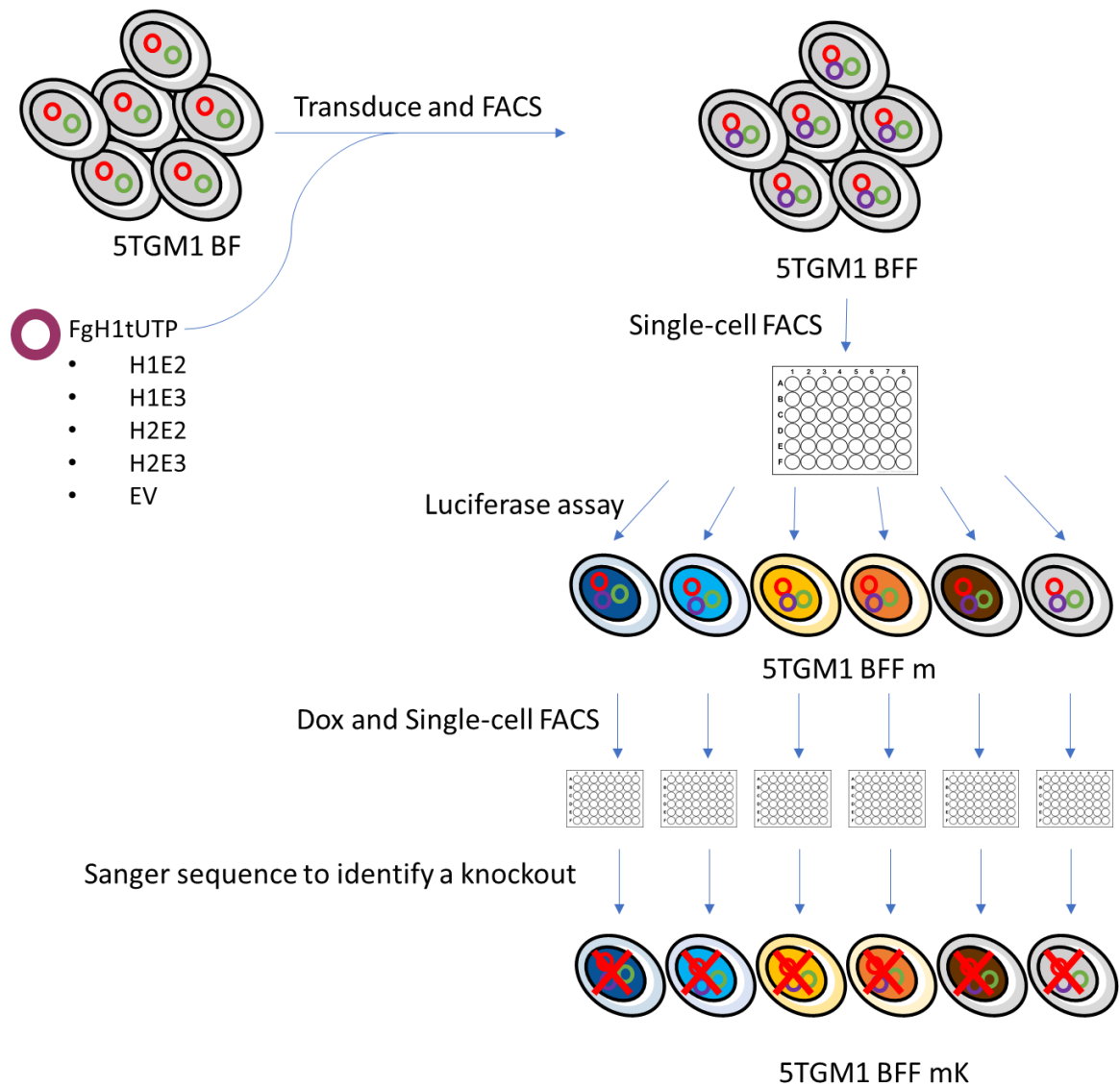
Figure: 3.9: Strategy for the generation of HIF-α inducible knockout and knocked out cell lines. SpCas9 expressing 5TGM1 cells (5TGM1 BF) cells were transduced with FgH1tUTP guide vectors, and inducible knockout cell lines (5TGM1 BFF) were isolated by FACS. A total of 5 to 6 monoclonal inducible knockout cell lines (5TGM1 BFF m) were isolated for each inducible guide line. A constitutively knocked-out monoclonal cell lines (5TGM1 BFF mK) was generated for each monoclonal inducible knockout cell line, by isolating doxocycline treated 5TGM1 BFF m cells to single cells and genotyping their CRISPR indels by Sanger sequencing.
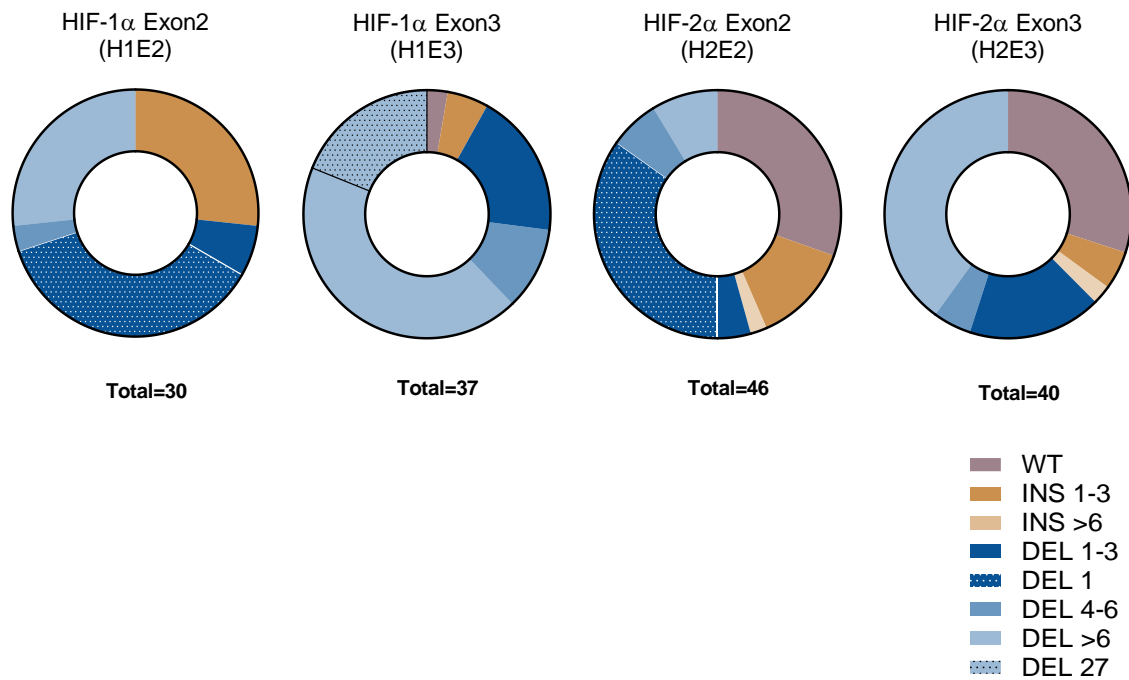
Figure 3.10: Profile of CRISPR/Cas9 induced indels. PCR amplicons flanking the gRNA target region of monoclonal knockout 5TGM1s were Sanger sequenced. Sequencing traces were aligned by MAFFT v7 on Benchling against *Hif-1α* and *Epas1* gene sequences from the GRCm38 (mm10) reference genome. Overlapping alleles were resolved by manually tracing back the peaks or by using CRISP-ID v1.1. The dotted pattern indicates the predominant allele induced by CRISPR/Cas9 editing for each gRNA. WT, wild type; INS, insert; DEL, deletion.

Table 3.2: Summary of all generated HIF-α knockout cell lines

	HIF-1α Exon 1 (H1E3)	HIF-1α Exon 2 (H1E2)	HIF-1α Exon 3 (H1E3)	HIF-2α Exon 2 (H2E2)	HIF-2α Exon 3 (H2E3)
On-target Activity	✗	✓	✓	✓	✓
Inducible Knockout Cells (5TGM1 BFF)		✓	✓	✓	✓
Monoclonal Inducible Knockout Cells (5TGM1 BFF m)		IK 1 (m1) IK 2 (m2) IK 3 (m3) IK 4 (m4) IK 5 (m7) IK 6 (m8)	IK 1 (m2) IK 2 (m4) IK 3 (m6) IK 4(m8) IK 5 (m9)	IK 1 (m1) IK 2 (m2) IK 3 (m6) IK 4 (m10) IK 5 (m11)	IK 1 (m1) IK 2 (m4) IK 3 (m5) IK 4 (m6) IK 5 (m9) IK 6 (m10)
Monoclonal HIF-α Knockout Cells (5TGM1 BFF mK)		KO 1 (m1/11k) KO 2 (m2/1k) KO 3 (m3/10k) KO 4 (m4/7k) KO 5 (m7/1k) KO 6 (m8/4k)	KO 1 (m2/3k) KO 2 (m4/5k) KO 3 (m6/9k) KO 4 (m8/2k) KO 5 (m9/5k)	KO 1 (m1/1k) KO 2 (m2/2k) KO 3 (m6/2k) KO 4 (m10/8k) KO 5 (m11/6k)	UNSK 1 (m1/1k) KO 2 (m4/5k) KO 3 (m5/3k) KO 4 (m6/1k) KO 5 (m9/4k) KO 6 (m10/1k)

Table 3.3: Summary of Monoclonal 5TGM1 BFF EV cell lines

	Empty Vector (EV)
Polyclonal EV Cells (5TGM1 BFF EV)	✓
Monoclonal EV Cells (5TGM1 BFF mEV)	EV 1 (m1) EV 2 (m3) EV 3 (m7) EV 4 (m8) EV 5 (m10) EV 6 (m12)

3.1.7 Characterisation of HIF-1α knockout 5TGM1 cells

3.1.7.1 Genetic characterisation

From Sanger sequencing monoclonal dox-induced 5TGM1 BFF H1E2 and H1E3 cell lines, one monoclonal HIF-1α knockout line was identified for each of the original monoclonal inducible-knockout lines. The indels which arose from CRISPR/Cas9 editing are summarised in Table 3.4. Six knockout lines were selected for the H1E2 guide lines whereas 5 knockout lines were selected for the H1E3 guide lines. Except for H1E2 KO 3, all the selected knockout lines have two different frameshift mutations, one for each allele, at the target region. H1E2 KO 3 only displayed a single trace of -5 nt which suggests that it either has the same indel on both alleles, has a large deletion in this region, or has only one copy of *Hif-1α*. In addition, the indels of two H1E2 KO samples (KO 1 and KO 2) were confirmed by cloning the amplified PCR products into the pGEM-T vector and sequencing multiple (>8) independent clones, confirming the presence of only the two copies of the *Hif-1α* gene containing the identified indels, and the reliability of the screening technique for HIF-1α knockout cells, as well as supporting the clonal nature of these lines.

3.1.7.2 HIF-1α mRNA levels

qRT-PCR was performed to determine the effects of HIF-1α knockout on the relative *Hif-1α* mRNA expression levels in the 5TGM1 cells. RNA from untreated 5TGM1 H1E2 KO and H1E3 KO cells as well as the parental 5TGM1 B cells were extracted and reverse transcribed. In comparison to the 5TGM1 B cells, the 5TGM1 H1E2 KO cells showed small but insignificant decreases in *Hif-1α* mRNA expression (Figure 3.11A). However, the majority of 5TGM1 H1E3 KO lines displayed a significant reduction of *Hif-1α* of up to 14 fold (Figure 3.11B). This reduced *Hif-1α* mRNA observed in the knockout cells is

consistent with the occurence of nonsense-mediated decay to degrade *Hif-1α* transcripts with a frameshift-induced PTC (Popp & Maquat 2016).

HIF-1α is known to be predominantly post-translationally regulated. 5TGM1 *Hif-1α* mRNA expression has previously shown no significant change in expression upon hypoxic treatment (Martin 2018). To confirm that HIF-1α knockout does not change *Hif-1α* expression in hypoxia, 5TGM1 H1E2 KO, H1E3 KO and parental 5TGM1 B cells were treated with the hypoxia mimetic 2,2-dipyridyl (DP) for 16 hours. In the 5TGM1 B cells, relative *Hif-1α* mRNA levels showed no significant change in expression upon DP treatment (Figure 3.11). Each of the 5TGM1 H1E2 KO and H1E3 KO cells also displayed a similar expression of *Hif-1α* mRNA in DP treatment as with their untreated equivalent (Figure 3.11).

3.1.7.3 *HIF-1α protein induction*

The accumulation of HIF-1α in response to hypoxia is post-translationally regulated, mediated by the oxygen-sensing PHD dioxygenases (Maxwell et al. 1999; Tanimoto et al. 2000). In HIF-1α knockout cells, the introduction of PTCs due to frameshift mutations would lead to the production of truncated HIF-1α protein. To determine if HIF-1α protein induction and accumulation in response to a hypoxia mimetic treatment is lost in HIF-1α knockout cells, western blotting was performed on vehicle and DP treated HIF-1α knockout 5TGM1 cells in comparison to control 5TGM1 B cells.

Therefore, western blotting was performed on whole cell extracts from control 5TGM1 B, the 5 monoclonal H1E2 KO lines, and the 5 monoclonal H1E3 KO lines. HIF-1α expression was induced in the control 5TGM1 B cells following a 16 hour treatment with DP, but this induction was absent in all of the H1E2 KO and H1E3 KO cell lines, confirming their HIF-1α knockout status (Figure 3.12).

3.1.7.4   HIF-1α target gene, BNIP3 induction

As HIF-α is a transcription factor, the loss of HIF-1α activity can be directly assessed by assaying for the induction of HIF-1-specific target genes in response to hypoxia using qRT-PCR. *BNIP3* has been previously identified as a HIF-1α target gene that is strongly upregulated in hypoxia (Choi, Oh & Park 2008; Wang et al. 2005). In 5TGM1 cells, it is strongly induced by hypoxia and remains consistently expressed from 16 through to 72 hours of hypoxic treatment (Martin et al. 2010).

To determine the expression profile of *BNIP3* in parental 5TGM1 B cells in response to treatment with the hypoxia mimetic DP, a timecourse experiment was performed. *BNIP3* was found to be highly induced between 2 to 8 hours of DP treatment and then remained elevated with treatment periods of up to 48 hours (Figure 3.13). The sustained expression of *BNIP3* during more extended periods of DP treatment is similar to that previously observed in 5TGM1 cells in hypoxia (Martin et al. 2010), which is consistent with the activation of HIF-1 in these cells.

Assessment of HIF-1α knockout 5TGM1 H1E2 KO and H1E3 KO cells revealed an absence of *BNIP3* mRNA induction in response to DP treatment for 16 hours in all knockout cell lines, in contrast to the 16-fold induction observed in the control 5TGM1 B cells, which indicates the loss of HIF-1α activity and further supports the successful HIF-1α knockout of these cell lines (Figure 3.14). This observed loss of *BNIP3* mRNA induction is specific to that of HIF-1α knockouts; the induction is still robust in all of the empty vector monoclonal cell lines (5TGM1 BFF mEV) when treated with DP for 16 hours (Figure 3.15).

Table 3.4: CRISPR/Cas9-induced indels of selected monoclonal HIF-1α knockout cell lines

HIF-1α Exon 2 (5TGM1 BFF H1E2 mK)	Indels	HIF-1α Exon 3 (5TGM1 BFF H1E3 mK)	Indels
KO 1 [†]	-2 nt -85 nt	KO 1	-2 nt -8 nt
KO 2 [†]	+1 nt -1 nt	KO 2	-7 nt -22 nt
KO 3	-5 nt (single)	KO 3	-34 nt -35 nt
KO 4	+1 nt -1 nt	KO 4	-2 nt -20 nt
KO 5	-1 nt -13 nt	KO 5	-1 nt -11 nt
KO 6	-1 nt -10 nt		

[†] Indels further verified by cloned insert sequencing of amplified gDNA using the pGEM-T vector system
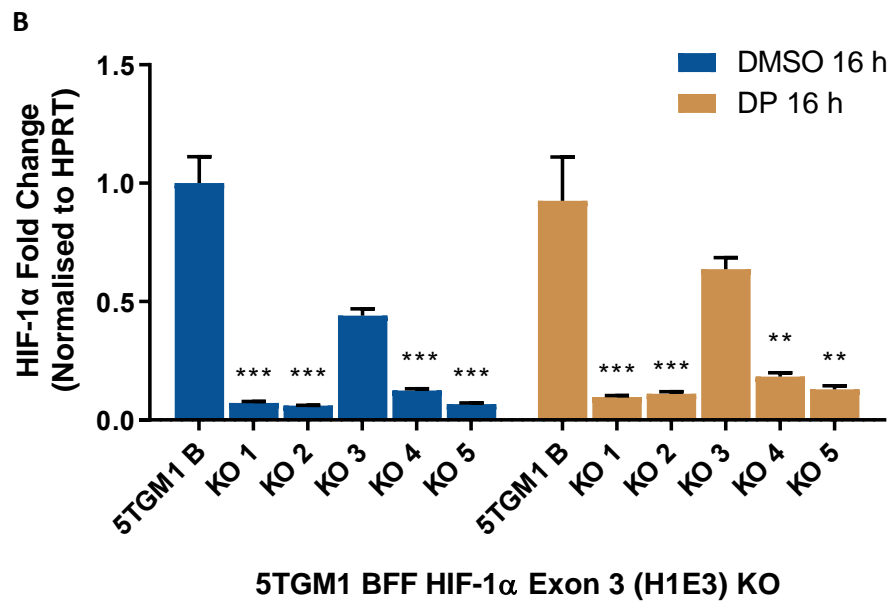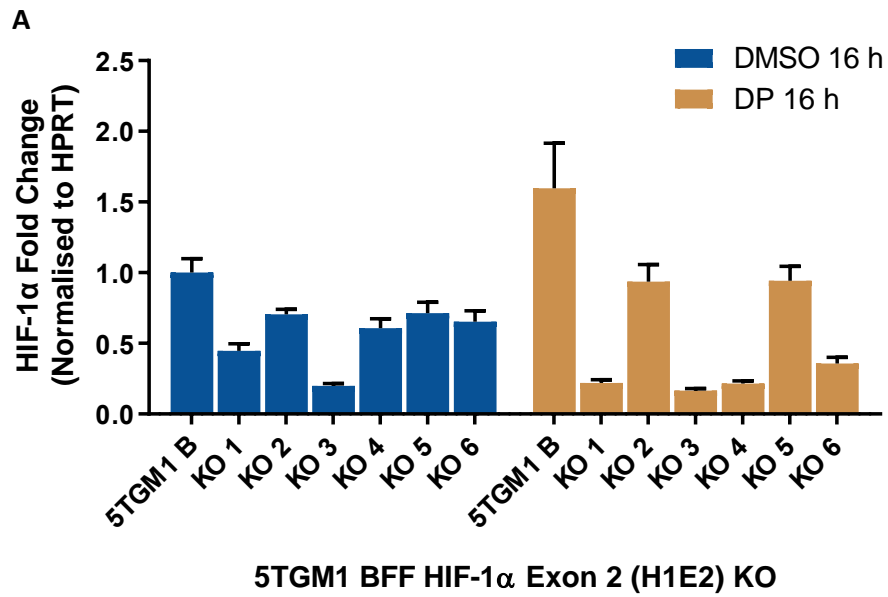
Figure 3.11: HIF-1α knockouts in 5TGM1 cells reduce *Hif-1α* mRNA expression. Control 5TGM1 B and HIF-1α knockout **(A)** 5TGM1 BFF H1E2 KO and **(B)** 5TGM1 BFF H1E3 KO cells were treated with 100 µM of the hypoxia mimetic DP or with an equivalent volume of DMSO for 16 hours. mRNA was extracted and reverse transcribed, and relative *Hif-1α* cDNA levels were examined by qRT-PCR. Data are presented as mean expression fold change in comparison to BMX1 treated with DMSO after normalisation against *Hprt* ($2^{-\Delta\Delta CT}$), ±95% CI. N=3 biological replicates. Sidak's multiple comparisons test was calculated

using mean ΔΔCT values, by comparing knockout samples to the BMX1 control within each treatment group. (** p ≤ 0.01, *** p ≤0.001)
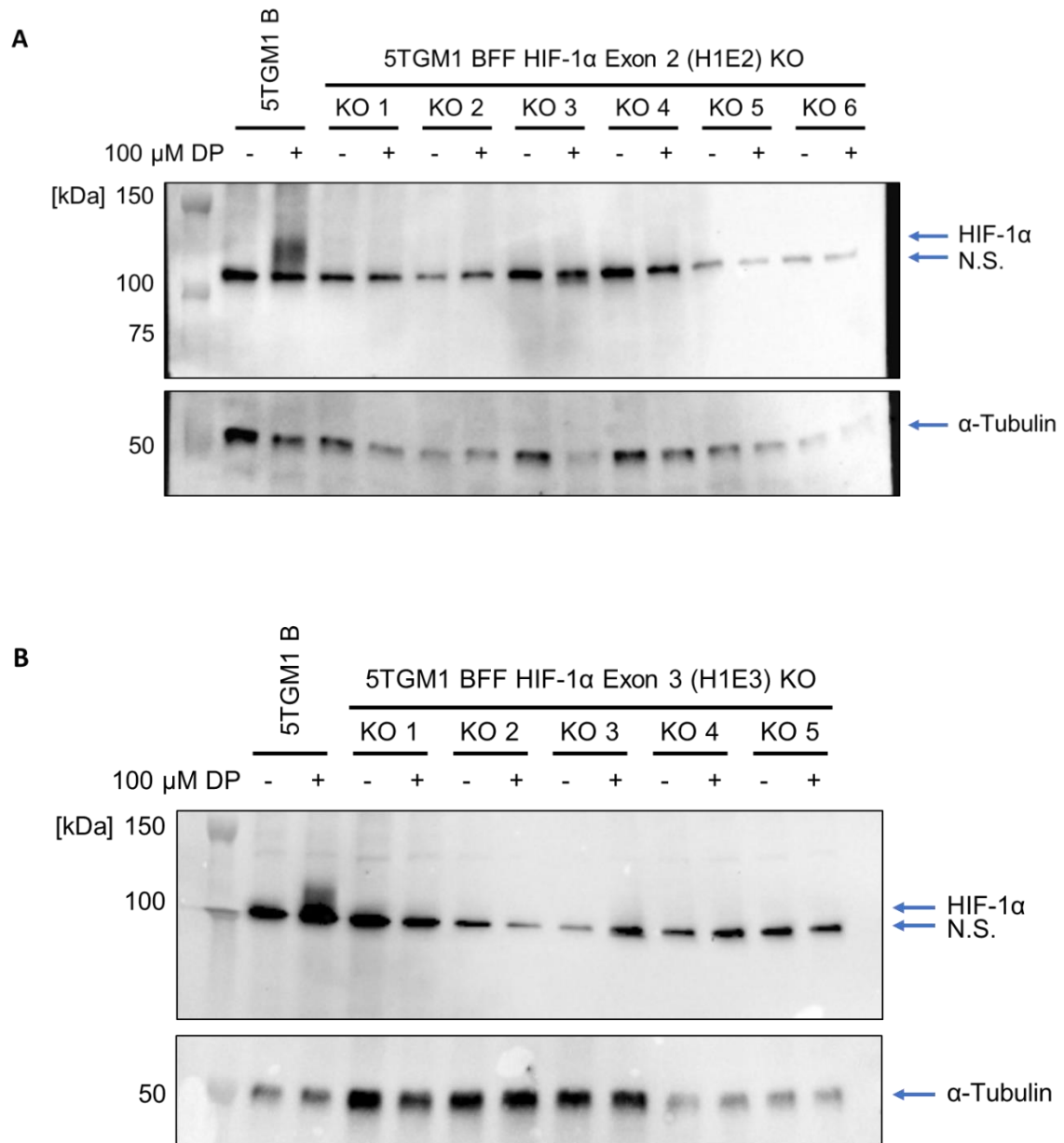
Figure 3.12: HIF-1α protein expression is absent in DP treated HIF-1α knockout 5TGM1 cells. Control 5TGM1 B, and HIF-1α knockout **(A)** 5TGM1 BFF H1E2 KO and **(B)** 5TGM1 BFF H1E3 KO cells were treated with 100 μM of the hypoxia mimetic DP (+) or with an equivalent amount of DMSO (-) for 16 hours, and whole cell lysates were extracted using RIPA buffer. Equivalent protein amounts were run on a 7.5% SDS-PAGE gel and transferred onto a nitrocellulose membrane and probed for HIF-1α protein expression. α-Tubulin was used as a loading control. Blots shown are representative of N=2

biological replicates (Appendix, Figure 6.3). H1E3 western blot was performed with C. Gallasch. HIF-1α, NB100-449, 1:1 000; α-Tubulin, NB600-506, 1:1 000. N.S., non-specific.
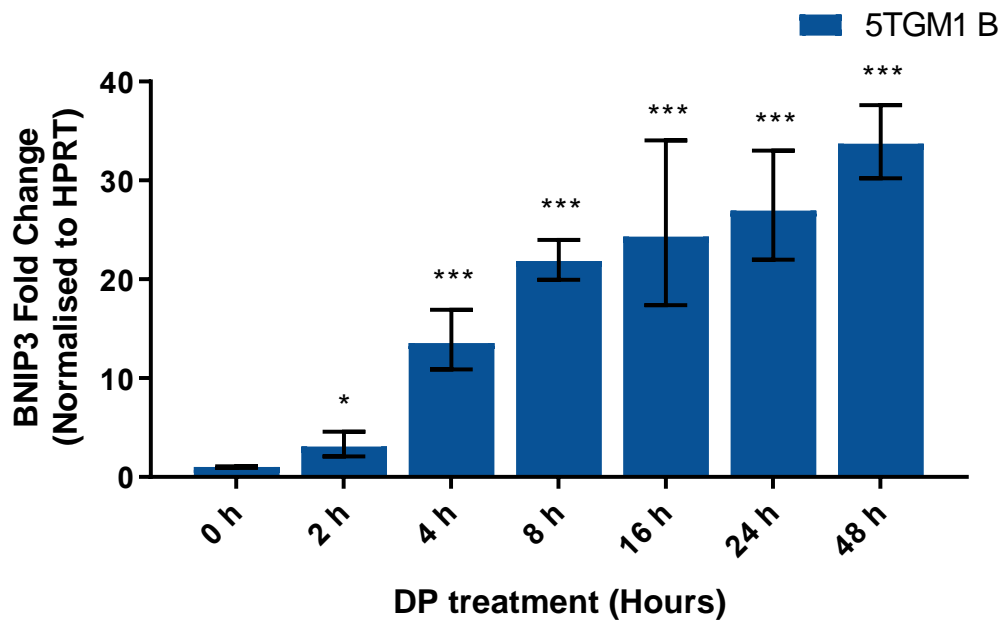
Figure 3.13: *Bnip3* mRNA induction in 5TGM1 cells in response to DP treatment.
Parental 5TGM1 B cells were treated with 100 µM of the hypoxia mimetic DP for 2 to 48
hours. mRNA was extracted and reverse transcribed. Relative *Bnip3* cDNA levels were
determined by qRT-PCR. Data are presented as mean expression fold change in
comparison to BMX1 DMSO after normalisation against *Hprt* ($2^{-\Delta\Delta CT}$), ±95% CI. N=3
biological replicates. Dunnett's multiple comparisons test was calculated using mean
ΔΔCT values, against the 0 hour DP treatment control column. (* p ≤0.05, *** p ≤0.001)
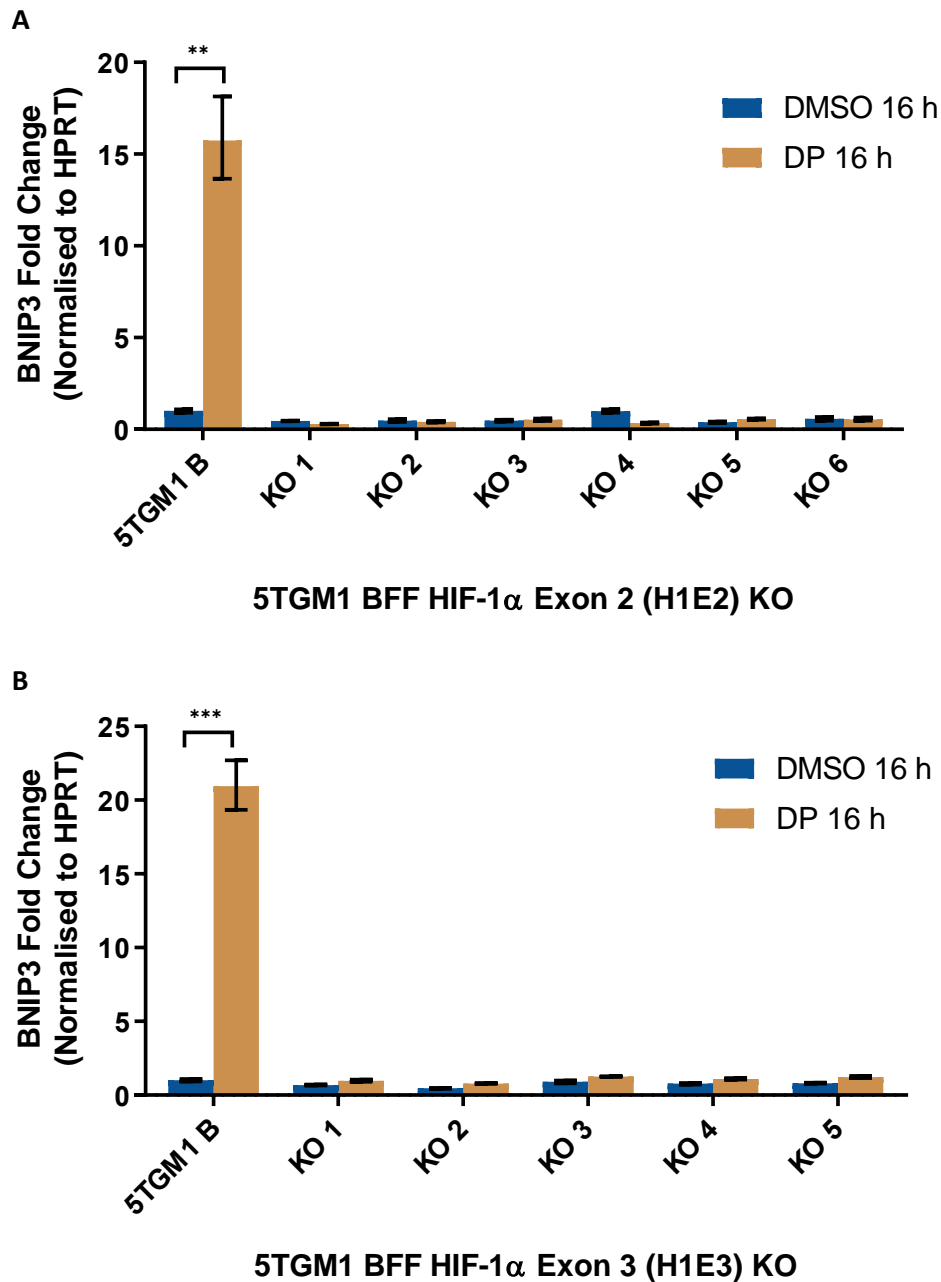
Figure 3.14: HIF-1α knockouts in 5TGM1 cells arrests *Bnip3* mRNA induction on DP treatment. Control 5TGM1 B and HIF-1α knockout **(A)** 5TGM1 BFF H1E2 KO and **(B)** 5TGM1 BFF H1E3 KO cells were treated with 100 μM of the hypoxia mimetic DP or DMSO for 16 hours. mRNA was extracted and reverse transcribed. Relative *Bnip3* cDNA levels were examined by qRT-PCR. Data are presented as mean expression fold change in comparison to BMX1 DMSO after normalisation against *Hprt* ($2^{-\Delta\Delta CT}$), ±95% CI. N=3 biological replicates. Sidak's multiple comparisons test was calculated using mean ΔΔCT

values, by comparing each sample's DP 16 hour treatment with its corresponding DMSO 16 hour treatment. (** $p \leq 0.01$, *** $p \leq 0.001$)

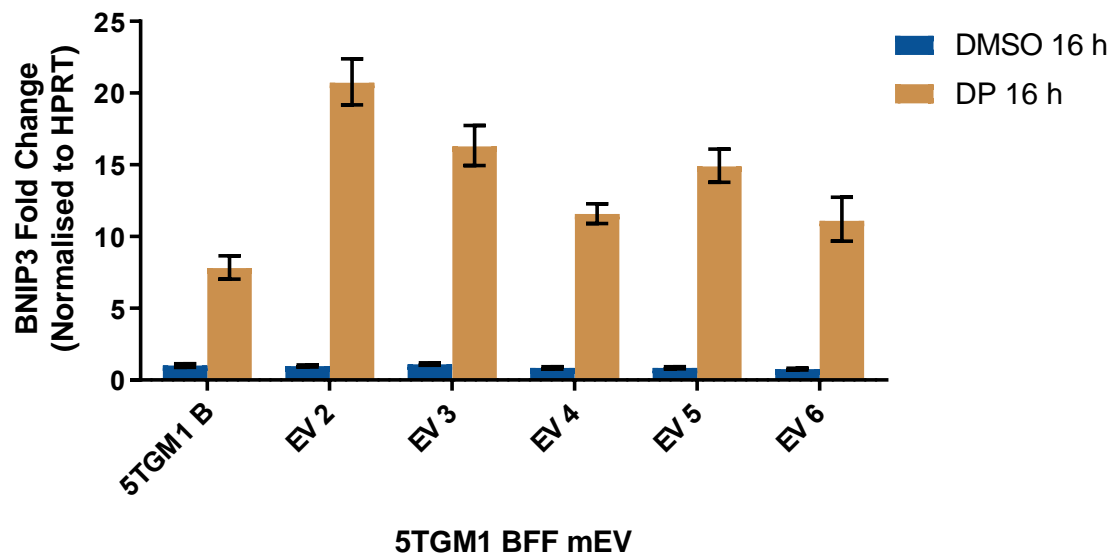**Figure 3.15: Empty vector control cells display normal *Bnip3* mRNA induction on DP treatment.** 5TGM1 BFF EV cells were treated with 100 µM of the hypoxia mimetic DP or DMSO for 16 hours. mRNA was extracted and reverse transcribed. Relative *Bnip3* cDNA levels were examined by qRT-PCR. Data are presented as mean expression fold change in comparison to BMX1 DMSO after normalisation against *Hprt* ($2^{-\Delta\Delta CT}$), ±95% CI. N=3 biological replicates. Sidak's multiple comparisons test was calculated using mean ΔΔCT values, by comparing each sample's DP 16 hour treatment with its corresponding DMSO 16 hour treatment.

3.1.8 Characterisation of HIF-2α knockout 5TGM1 cells

3.1.8.1 Genetic characterisation

From Sanger sequencing of amplified PCR products from monoclonal dox-induced 5TGM1 BFF H2E2 KO and H2E3 KO cell lines , one monoclonal HIF-2α knockout line was identified for each of the original monoclonal inducible-knockout lines. Knockout lines with two different frameshift mutations, one for each allele at the target region, were preferentially selected for further experiments (Table 3.5).

To further verify the indels for all HIF-2α knockout cell lines, mRNA was isolated and cDNA generated from each monoclonal knockout line. The targeted regions were amplified by PCR, cloned into the pGEM-T vector and multiple colonies (>4) from each Sanger sequenced. All selected knockout lines contained two different HIF-2α sequences, one frameshift mutation at the target region for each allele. H2E2 UNSK 1 was shown to contain a wildtype allele and was excluded from RNA sequencing.

3.1.8.2 HIF-2α mRNA levels

qRT-PCR was performed to determine the effects of HIF-2α knockout on the relative *Hif-2α* mRNA expression levels in 5TGM1 cells. The cells were treated with the hypoxia mimetic DP or vehicle (DMSO) for 16 hours, RNA extracted and cDNA analysed. *Hif-2α* transcripts were of relatively low abundance and were detected at high CTs (>30). In the control (DMSO treated) cell lines, 6 out of 10 HIF-2α knockout 5TGM1 cell lines showed a large, statistically significant decrease in expression of *Hif-2α* transcript when compared to 5TGM1 B cells, and the remaining 4 cell lines also exhibited smaller decreases in *Hif-2α* expression, consistent with NMD (Popp & Maquat 2016) (Figure 3.16). The relative *Hif-2α* mRNA expression in control 5TGM1 B cells was induced

approximately 8 fold upon DP-treatment for 48 hours, consistent with transcriptional induction of *Hif-2α* mRNA in other MM cells (D. Peet, personal communication). *Hif-2α* mRNA induction was also present across all HIF-2α knockout cell lines, but they generally had lower *Hif-2α* mRNA expression levels when compared to the 5TGM1 B line (Figure 3.16).

3.1.8.3   HIF-2α protein expression

To investigate corresponding loss of HIF-2α protein expression in the HIF-2α knockout 5TGM1 cell lines, western blots were performed. However, endogenous HIF-2α could not be detected in the in whole cell extracts from 5TGM1 BMX1 cells after hypoxia or DP treatments of up to 48 hours despite numerous optimisation attempts (Figure 3.17). Previous attempts by N. Martin using several methods including western blot, immunoprecipitation as well as mass-spectrometry, also failed to detect endogenous HIF-2α in 5TGM1 cells (Martin 2018). Difficulties in detecting HIF-2α protein in mouse samples is a common issue with commercially available primary antibodies (D. Peet, personal communication). These observations suggest that the HIF-2α protein is very lowly expressed in 5TGM1 cells, even after an extended period of DP treatment or hypoxia.

3.1.8.4   HIF-2α target gene induction

Several attempts were made to identify a HIF-2α specific target gene by qRT-PCR, to assay for the loss of HIF-2α functional activity in HIF-2α knockout cell lines. A suitable target gene would exhibit robust upregulation in 5TGM1 B cells upon DP treatment for 48 hours, but not in HIF-2α knockout cells. Among the reported HIF-2α specific target genes tested were the *Epo* (Haase 2013), *β-catenin* (Sun et al. 2015), *Endrb* (Westfall et

al. 2008), *Interleukin 1β* (Imtiyaz et al. 2010), *Oct-4* (*Pou5f1*) (Covello et al. 2006) and *Twist1* (Xu et al. 2012). However, none of these genes display a pattern of abrogated hypoxic induction in comparisons between the control 5TGM1 B cells and HIF-2α knockout lines (data not shown).

On the other hand, all of the HIF-2α knockout cell lines still retained HIF-1α functional activity, as they displayed similar *Bnip3* mRNA induction to the control 5TGM1 B cells following DP treatment for 16 hours (Figure 3.18).

In summary, although the loss of HIF-2α protein and HIF-2α functional activity in the knockout lines could not be ascertained, Sanger sequencing of both gDNA and cDNA confirmed that there are no wildtype HIF-2α alleles or transcripts in the selected monoclonal HIF-2α knockout cell lines.

Table 3.5: CRISPR/Cas9-induced indels of selected monoclonal HIF-2α knockout cell lines

HIF-2α Exon 2 (5TGM1 BFF H2E2 mK)	Indels	HIF-2α Exon 3 (5TGM1 BFF H2E3 mK)	Indels
KO 1 [†]	-1 nt -8 nt	KO 2 [†]	+11 nt -22 nt
KO 2	+1 nt -1 nt	KO 3	-1 nt -19 nt
KO 3 [†]	-1 nt -5 nt	KO 4	-7 nt -22 nt
KO 4	-1 nt -39 nt	KO 5	-1 nt -17 nt
KO 5	-1 nt -8 nt	KO 6	+1 nt -32 nt

[†] Indels further verified by cloned insert sequencing of amplified gDNA using the pGEM-T vector system

Indels for all monoclonal HIF-2α knockout cell lines were also further verified by cloned insert sequencing of amplified cDNA.
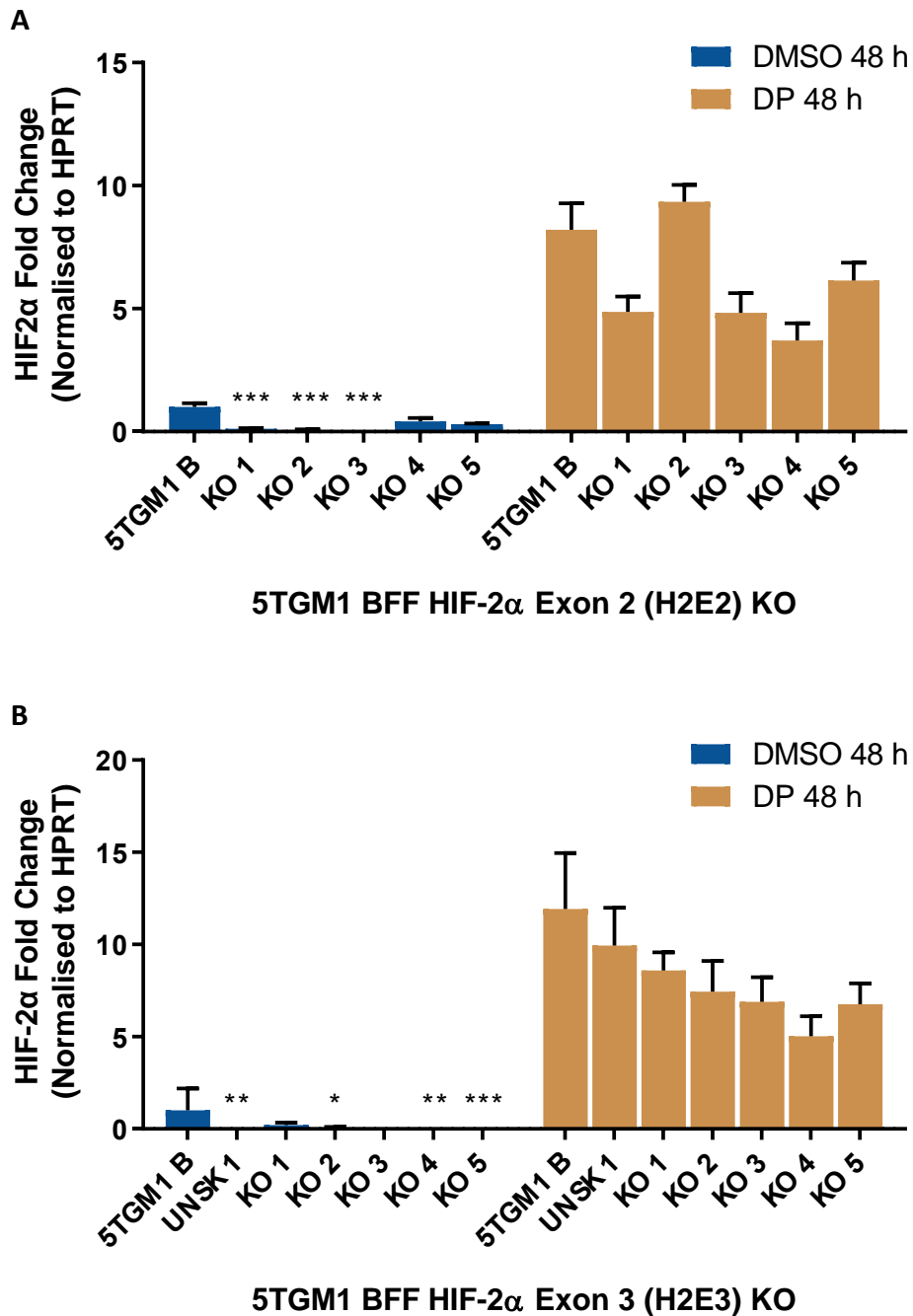
Figure 3.16: HIF-2α knockouts in 5TGM1 cells reduce *Hif-2α* mRNA expression. Control 5TGM1 B and HIF-2α knockout **(A)** 5TGM1 BFF H2E2 KO and **(B)** 5TGM1 BFF H2E3 cells were treated with 100 μM of the hypoxia mimetic DP or DMSO for 48 hours. mRNA was extracted and reverse transcribed. Relative *Hif-2α* cDNA levels were examined by qRT-PCR. Data are presented as mean expression fold change in comparison to BMX1 DMSO after normalisation against *Hprt* ($2^{-\Delta\Delta CT}$), ±95% CI. N=3 biological replicates. Sidak's

multiple comparisons test was calculated using mean ΔΔCT values, by comparing knockouts samples to the BMX1 control within each treatment group. (* p ≤ 0.05, ** p ≤ 0.01, *** p ≤0.001)
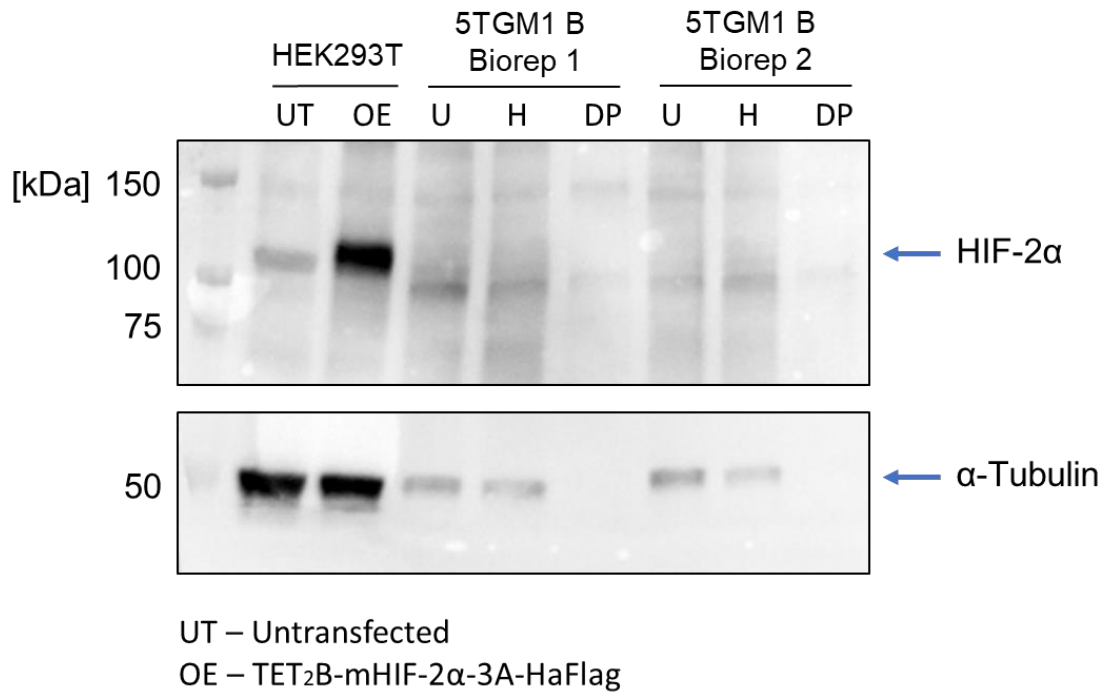
Figure 3.17: Endogenous HIF-2α was not detected in hypoxia-cultured or DP-treated 5TGM1 B cells. Parental 5TGM1 B cells were cultured in hypoxia (H) or treated with vehicle (U) or 100 µM DP (DP) for 48 hours. HEK293T cells overexpressing mouse HIF-2α (OE) were generated by L. Menicucci, by transfecting Tet$_2$Blast-mHIF-2α-3A-HaFlag and culturing them in the presence of dox in normoxia for 16 hours, alongside an un-transfected control (UT). Whole cell lysates were run on a 7.5% SDS-PAGE gel at 160 V for 1 hour 10 minutes and transferred onto a nitrocellulose membrane. HIF-2α protein expression was probed by western blot and α-Tubulin was used as a loading control. Western blot was performed with C. Gallasch. HIF-2α, NB100-122, 1:1 000; α-Tubulin, NB600-506, 1:1 000.
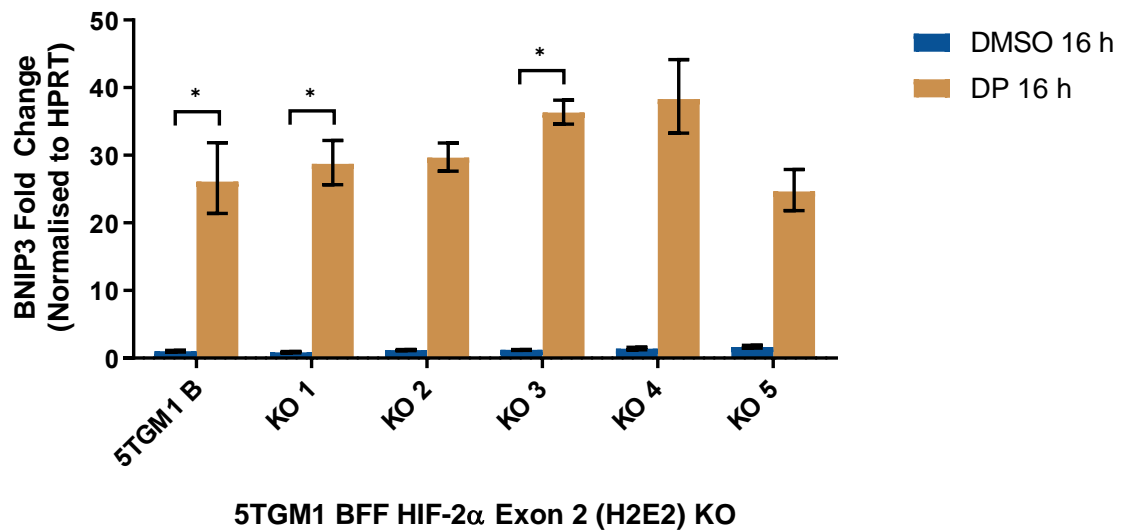
Figure 3.18: HIF-2α knockouts in 5TGM1 cells have no effect on *Bnip3* mRNA induction on DP treatment. Control 5TGM1 B and HIF-2α knockout 5TGM1 cells were treated with 100 μM of the hypoxia mimetic DP or DMSO for 16 hours. mRNA was extracted and reverse transcribed. Relative *Bnip3* cDNA levels were examined by qRT-PCR. Data are presented as mean expression fold change in comparison to BMX1 DMSO after normalisation against *Hprt* ($2^{-\Delta\Delta CT}$), ±95% CI. N=3 biological replicates. Sidak's multiple comparisons test was calculated using mean ΔΔCT values, by comparing each sample's DP 16 hour treatment with its corresponding DMSO 16 hour treatment. (* p ≤ 0.05)

3.2 Discussion

The harnessing of CRISPR/Cas9 technology in mammalian cells has paved the way for fast, simple and effective editing of gDNA (Cong et al. 2013; Mali et al. 2013). This technology has been extensively modified in many different ways to suit a wide variety of research applications (Knott & Doudna 2018). A two-plasmid inducible CRISPR/Cas9 lentiviral platform, designed by the Herold laboratory (Aubrey et al. 2015), was chosen to study the roles of HIF-1α and HIF-2α in MM development and progression using the 5TGM1/KaLwRij murine model. This CRISPR/Cas9 platform allows for the temporally-controllable deletion of either HIF-1α or HIF-2α both *in-vitro* or *in-vivo*, such that their roles can be assessed at different stages of disease development and progression. This system was successfully utilised to generate knockouts in other lymphocytic cancer cell lines, including *JAK2* knockout in MHH-CALL4 B-ALL cells and *ARID5B* knockout in Jurkat T-ALL cells (Kim et al. 2018; Leong et al. 2017).

The modifications performed to the Herold CRISPR/Cas9 system were described above, to broaden the system's compatibility to include cells that already express eGFP. Gibson assembly was employed to clone in a gBlock gene fragment encoding mPlum into the dox-inducible gRNA vector FgH1tUTG, replacing the eGFP reporter gene (Figure 3.2A). Gibson assembly was chosen over traditional cloning methods for its ability to perform scar-less and highly efficient cloning of large inserts (Gibson et al. 2009). The re-engineered FgH1tUTP plasmid is readily transducible with reasonable efficiency and expresses detectable levels of mPlum, which is discernible from eGFP and mCherry fluorescent markers by flow analysis (Figure 3.5). When used together with the 5TGM1 BF cell line that constitutively expresses spCas9, FgH1tUTP acts as a carrier of targeting information that allows for the temporally-controllable deletion of any gene in a 'mix & match' format. This system is currently being employed in the Zannettino laboratory to study other genes of interest in the context of MM (D. Hewett, personal communication).

HIF-1α and HIF-2α inducible knockout 5TGM1 cells were generated from the 5TGM1 BF cells to study the effects of their knockout on MM development and progression (Table 3.2). The guides were designed to target early exons which are conserved in all splice variants, within regions that encode essential functional domains (Figure 3.8). A similar strategy employed in a CRISPR screen for cancer drug targets found that targeting functional protein domains increases the probability of generating null mutations, where in-frame indels would likely disrupt the function of the targeted domain (Shi et al. 2015). The targeted amino acids are also highly conserved in mammals (Figure 3.19). The reduction in the activity of in-frame mutants would be favourable for inducible knockout experiments *in-vivo* as it would result in a greater overall 'knockdown' effect. In addition, the guides were selected to target different exons to prevent selected guides from overlapping and sharing potential off-targets. The use of multiple independent guides per target gene also serves for redundancy, so that the phenotypes brought about by the editing of a single guide can be tested for reproducibility with another independent one.

Guides H1E2, H1E3, H2E2 and H2E3 displayed the presence of on-target activity in the T7E1 assay (Figure 3.6). In the case of the H1E1 and H1E2 guides, background bands were generated from the T7E1 assay, both in the absence and presence of dox treatment (Figure 3.6 & 3.7A). The occurrence of background bands in T7E1 assays have been previously reported, but the cause of which remains unexplained in literature (Sentmanat et al. 2018). Background bands running a similar size to expected T7E1 fragments may potentially confound guide pretesting as they appear as false-positive results. From Sanger sequencing cloned PCR amplicons, it was found that homopolymeric regions coincide with the position where cleavage would occur to produce the background bands (Figure 3.7B & 3.8). Polymerase slippage during PCR amplification can give rise to single nucleotides repeats of different lengths, which is subsequently recognised and cleaved by the T7E1 enzyme. Therefore, when designing CRISPR/Cas9 guides, it would be important to note the presence and location of homopolymeric regions near the intended target site to account for false positive pretesting results.

132

The polyclonal inducible-knockout, monoclonal inducible-knockout and monoclonal knockout 5TGM1 cell lines were isolated by multicolour FACS. An initial technical problem with detecting the mPlum[+] signal was overcome by alternatively gating for Cy5, which is a detection strategy previously reported for visualising real-time influenza infection dynamics in live cells (Thompson 2018). A transduction efficiency of about 42%, calculated from FACS data, was achieved in 5TGM1 cells using the spinfection method which is higher than Polyfect transfection (4%) or other transduction methods (<20%) in the lab for these cells (Table 3.1). Previous attempts to produce knockout 5TGM1 cells by Y. Ma (2015) was not very efficient and only resulted in two HIF-2α knockout lines, a factor of which could be limited by low plasmid delivery from Polyfect transfection as well as the transient expression of the Cas9 nuclease and gRNAs (Ma 2015). The better transduction efficiency achieved in this project was likely a contributing factor to the high editing rates observed.

From screening dox-treated monoclonal inducible-knockout 5TGM1 cells for knockouts by Sanger sequencing, it was observed that almost all HIF-1α alleles and about ¾ of HIF-2α alleles harboured indels within targeted regions (Figure 3.10). The difference in the proportion of modified HIF-2α in comparison to HIF-1α alleles can be explained either by gRNA on-target activity or chromatin accessibility. Although the predicted on-target scores for HIF-1α (65.7 & 64.4) and HIF-2α (71.7 & 64.7) guides were somewhat similar, their actual activity may vary in experiments. The accuracy of on-target algorithms depends on the type and species being modified as well as the method for expressing or introducing the gRNA (Haeussler et al. 2016). For instance, the on-target algorithm (by Doench *et.al.*) used in this project is thought to perform best for constitutively expressing U6-driven gRNA. Since the H1 promoter in FgH1tUTP has a lower expression than the U6 promoter, additional factors like the stability of the gRNA may potentially have a more substantial influence on overall activity (Moreno-Mateos et al. 2015). On the other hand, since HIF-2α transcription is normally suppressed in normoxia, reduced chromatin accessibility due to the influence of chromatin structure may restrict Cas9 accessibility (Yarrington et al. 2018). While the difference in the efficiency of HIF-1α versus HIF-2α editing was not a significant hurdle for the generation and selection of

monoclonal knockout 5TGM1 cells *in-vitro* (this was overcome by screening more monoclonal lines), it would be an important consideration when comparing sample groups in future inducible-knockout experiments *in-vivo*.

At least five monoclonal inducible-knockout 5TGM1 cell lines were selected for each gRNA, as they can be pooled for further experiments to account for random FgH1tUTP integration. These monoclonal inducible-knockout lines were identified to retain luciferase activity by firefly luciferase assays on cell lysates. Live-cell luciferase activity would need to be performed on these cells using the Xenogen IVIS imager, for matching live-cell luciferase activity prior to *in-vivo* experiments. A monoclonal knockout line was identified for each monoclonal inducible-knockout line. The monoclonal knockout lines were selected with a preference for monoclones with two different frameshift mutations as there would be better confidence that they are genetically true knockouts. Cells which only one identified mutation could potentially either have the same indel on both alleles, a large deletion that removed a primer binding site (Adikusuma et al. 2018) or have a genetic aberration and are homozygous for that gene.

Genotyped monoclonal HIF-1α knockouts were further validated at the mRNA and protein levels by qRT-PCR and western blotting. Generally, HIF-1α knockout cell lines had a lower expression of *Hif-1α* mRNA, consistent with the action of NMD to degrade transcripts with frameshift-induced PTCs (Figure 3.11) (Popp & Maquat 2016). 4 out of 5 H1E3 knockout lines exhibited a statistically significant reduction of *Hif-1α* transcript level, whereas H1E2 knockout lines have a reduced trend of *Hif-1α* expression that was not statistically significant. The reduced action of NMD in *Hif-1α* transcript in H1E2 knockout lines can be explained by the proximity of PTCs to the start codon, which is known to be inefficient at triggering NMD (Popp & Maquat 2016). The circularisation of mRNA brought about by the interaction between the cap-binding complex and poly-A binding proteins is thought to inhibit the association of other NMD regulators to the ribonucleoprotein complex at the PTC (Peixeiro et al. 2012; Pereira et al. 2015). At the protein level, all HIF-1α knockouts displayed a loss of HIF-1α induction upon DP treatment when compared to the 5TGM1 B controls by western blotting, confirming the

absence of its expression (Figure 3.12). However, for blots probed with the Novus-449 α-HIF-1α antibody, there was a non-specific background band running just below the HIF-1α band.

HIF-1α knockout 5TGM1 cells also displayed a loss functional HIF-1 activity, whereby the induction of the target gene *Bnip3* was absent upon DP treatment (Figure 3.14). In hypoxia, BNIP3 mediates cellular pro-survival effects through its regulation of mitochondrial autophagy (Bellot et al. 2009; Zhang et al. 2008). BNIP3 induction was still observed in HIF-2α knockout and empty vector control 5TGM1 cells, which supports that *Bnip3* is a HIF-1α specific target gene in 5TGM1 cells (Figure 3.15 & 3.18). This observation was similar to that in mice forebrain neurons where HIF-1α, but not HIF-2α, was found to regulate the induction of *Bnip3* in response to exposure to hypoxia (Barteczek et al. 2017).

For monoclonal HIF-2α knockout cell lines, their genotypes were validated by sequencing both their gDNA and cDNA (Table 3.5). At the mRNA level, *Hif-2α* transcript was expressed in low levels, even in the parental 5TGM1 B cells, and was difficult to detect by qRT-PCR. *Hif-2α* transcripts were reduced in the knockout lines, consistent with NMD activation (Figure 3.16). However, *Hif-2α* transcripts in the HIF-2α knockout lines remained inducible by DP treatment. This could be due to the inhibition of NMD response due to hypoxia-like stresses from DP-treatment, allowing knockout transcripts to escape targeted degradation (Gardner 2008).

Further attempts to characterise the HIF-2α knockout cells at the protein level were unsuccessful. The expression of endogenous HIF-2α protein could not be detected in hypoxia-cultured, DMSO or DP-treated 5TGM1 B cells (Figure 3.17). Since murine HIF-2α was detectable in the overexpression control, the absence of endogenous HIF-2α bands could presumably be due to its low expression, below the detection limit of the assay. This is unsurprising, however, as TF expression tends to be lower than that of non-TF genes which makes them difficult to detect (Vaquerizas et al. 2009). Furthermore, difficulties in detecting endogenous mouse HIF-2α protein with commercially available

antibodies is a common problem in this field. Given that HIF-2α expression have been previously reported to be constitutive and oxygen-independent in several human MM cell lines (Mysore et al. 2016), it would have been of interest to compare HIF-2α expression in these compared to the 5TGM1 cells. This could be potentially performed in the future when better antibodies that have higher affinity to mouse HIF-2α become available.

Additional efforts to identify a HIF-2α specific target gene by screening for their loss-of-induction in HIF-2α knockout 5TGM1 cells were unsuccessful. Candidate target genes screened were either known or putative HIF-2α targets in other cell types. For instance, *Epo* is a characterised HIF-2α target gene in the kidney, retina and forebrain neurons (Barteczek et al. 2017; Haase 2013; Morita et al. 2003), while *Oct-4* expression is reported to be a HIF-2α dependent target in haematopoietic stem cells (Covello et al. 2006). However, the results from sequencing of both gDNA and cDNA adequately confirm the knockout of HIF-2α.

In summary, multiple HIF-1α and HIF-2α inducible-knockout and knockout 5TGM1 monoclonal cells were successfully generated via the transduction of a dox-inducible CRISPR/Cas9 system. Guide inducibility and on-target activity were confirmed by T7E1 assay. Monoclonal HIF-1α and HIF-2α knockout 5TGM1 cells were identified and genotyped by Sanger sequencing. Loss of HIF-1α protein expression and function in the monoclonal HIF-1α knockouts were confirmed by western blot and qRT-PCR respectively. While loss of HIF-2α protein expression and function in the monoclonal HIF-2α knockouts could not be determined at this stage, their knockout status was further confirmed at the RNA level by of their cDNA.

A
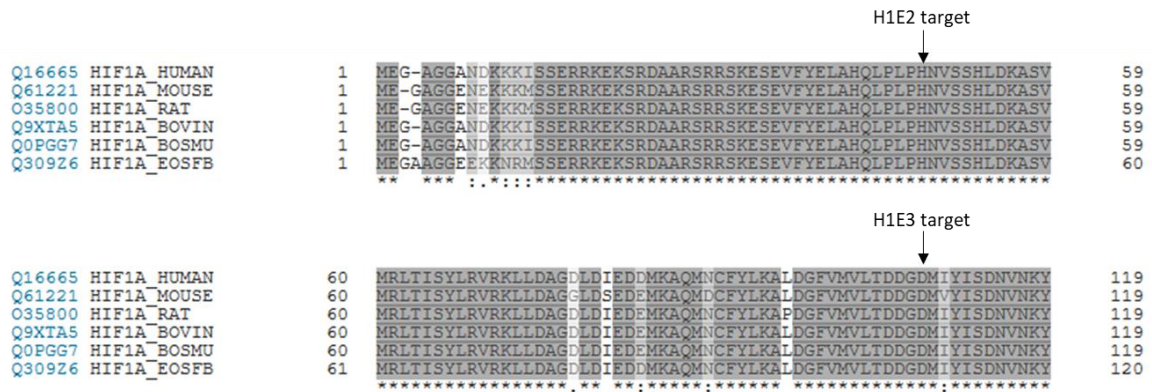
B
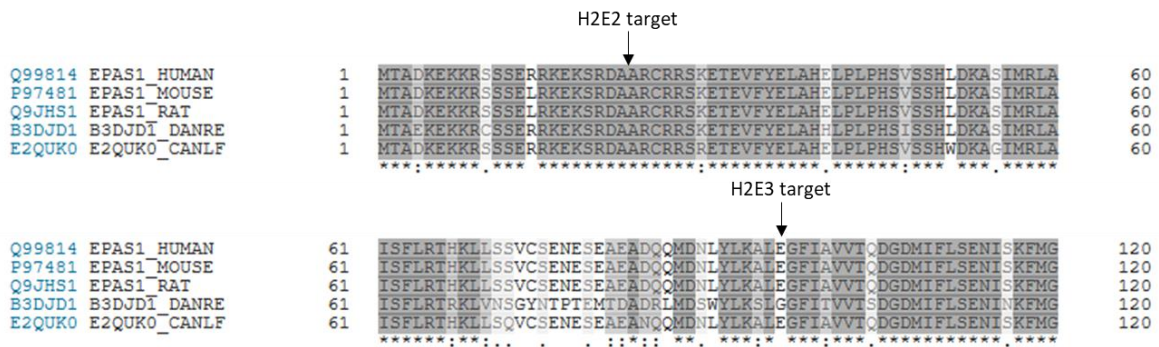
Figure 3.19: Position of guide target sites relative to protein sequences. (A) HIF-1α protein sequence alignments for human, mouse, rat, bovine, wild yak and Plateau zokor (burrowing rodent). (B) HIF-2α protein sequence alignments for human, mouse, rat, zebrafish and dog. Black arrows indicate the relative position of guide cut sites on the aligned protein sequences. Intensity of shading of amino acids indicate amino acid similarity and conservation between organisms

Results 2

Transcriptomic Analysis of HIF-1α and HIF-2α Knockout 5TGM1 Cells

4 Results 2

4.1 Transcriptomic analysis of HIF-1α and HIF-2α knockout 5TGM1 cells

Aim 3: To profile the transcriptomic changes in 5TGM1 cells in response to HIF-1α and HIF-2α knockout.

Transcriptomic analysis was performed to characterise the changes in gene expression that occur in 5TGM1 cells *in-vitro* in response to HIF-1α or HIF-2α knockout under both normoxic and hypoxic conditions. The transcriptomes of HIF-1α and HIF-2α knockout 5TGM1 cells, as well as EV control 5TGM1 cells, were profiled by RNA-seq. This is of great value to identify and delineate the specific target genes for each HIF-α isoform in the context of MM, especially for HIF-2α as it has very few known targets. Also, this analysis would help identify genes regulated by the hypoxic response that could support MM disease development and progression. Further gene ontology analysis would also assist in broadly characterising the functional roles of each HIF-α isoform in MM disease.

4.1.1 Determining hypoxic treatment times

Before carrying out the hypoxia treatments on the various 5TGM1 cell lines for RNA-seq, time-course experiments were performed to determine suitable treatment times to identify HIF-1α and HIF-2α specific target genes. For the first hypoxic timepoint, a short treatment time was preferred to delineate direct HIF-1α target genes responsible for acute or direct responses to hypoxia, while reducing overlap with the induction of chronic and indirect responses. To determine the best length of time to treat 5TGM1 cells to induce these responses, the transcript induction profile of *Bnip3* was determined in 5TGM1 B cells using qRT-PCR (Results 1, Figure 3.13). *Bnip3*, a pro-apoptotic and pro-autophagic gene, is a well-characterised direct HIF-1α target gene that is dramatically induced by hypoxia (Guo et al. 2001).

5TGM1 B cells were treated with 100 µM of the hypoxia mimetic DP for a range of treatment times between 2 to 48 hours. *Bnip3* was rapidly induced between 2 and 8 hours of treatment, after which its expression increased slowly until the 48 hour timepoint. The shortest treatment time required to induce a high induction of BNIP3 expression is preferable to determine direct HIF-1α responses, and thus 8 hours was chosen as the first hypoxia timepoint for the RNA-seq experiment. The expression of several HIF-1α dependent target genes have been reported to be strongly induced at 8 hours of hypoxic exposure in other cell types, such as *Bnip3* in rat neonatal cardiomyocytes (Guo et al. 2001) and *FoxP3* in primary mouse CD4 T-cells (Clambey et al. 2012). Other reported experiments looking at HIF-1α and HIF-2α binding sites by ChIP cultured MCF-7 breast cancer cells for a longer hypoxic treatment of 16 hours (Mole et al. 2009; Schödel et al. 2011).

For a suitable hypoxia treatment time to identify chronic responses to hypoxia mediated by HIF-2α in 5TGM1 cells, the time point with the highest *Hif-2α* transcript expression was used because a HIF-2α specific target gene has yet to be identified in the 5TGM1 cells. HIF-2α expression in LP1 human MM cells was previously found to be transcriptionally regulated, where *Hif-2α* mRNA was observed to be strongly induced

after 24 hours of hypoxic exposure and remained sustained with longer periods of treatment (S. Martin, personal communication). In 5TGM1 B cells treated with 100 µM DP, *Hif-2α* transcript expression was found to be very low and relatively constant up to 24 hours, and only significantly induced (p ≤0.001) after 48 hours of DP treatment (Figure 4.1). A similar trend where *Hif-2α* expression peaks at 48 hours was also observed in hypoxia-treated 5TGM1 BFF EV cells, however with much lower and non-significant induction (Figure 4.2). The absence of strong hypoxic *Hif-2α* mRNA induction in the 5TGM1 cells is different from what has previously been observed in human LP-1 MM cells, which could be due to differences between these cell lines. Nevertheless, 48 hours was selected as the second time point for RNA-seq sample preparation for chronic hypoxic responses.
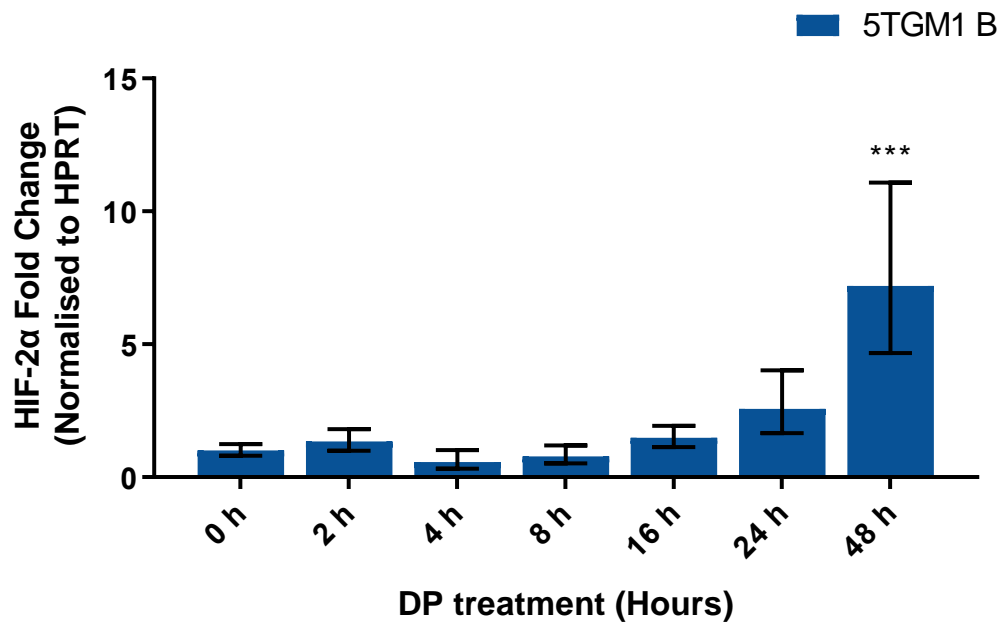
Figure 4.1: *Hif-2α* **mRNA induction in 5TGM1 cells in response to DP treatment.** 5TGM1 BMX1 cells were treated with 100 μM of the hypoxia mimetic DP for 2 to 48 hours. mRNA was extracted using TRIzol reagent, and equivalent amounts were reverse transcribed. Relative *Hif-2α* cDNA levels were examined by qRT-PCR. Data is presented as mean expression fold change in comparison to BMX1 DMSO after normalisation against *Hprt* ($2^{-\Delta\Delta CT}$), ±95% CI. N=3 biological replicates. Dunnett's multiple comparisons test was calculated using mean ΔΔCT values, against the 0 hour DP treatment control column. (*** p ≤0.001)
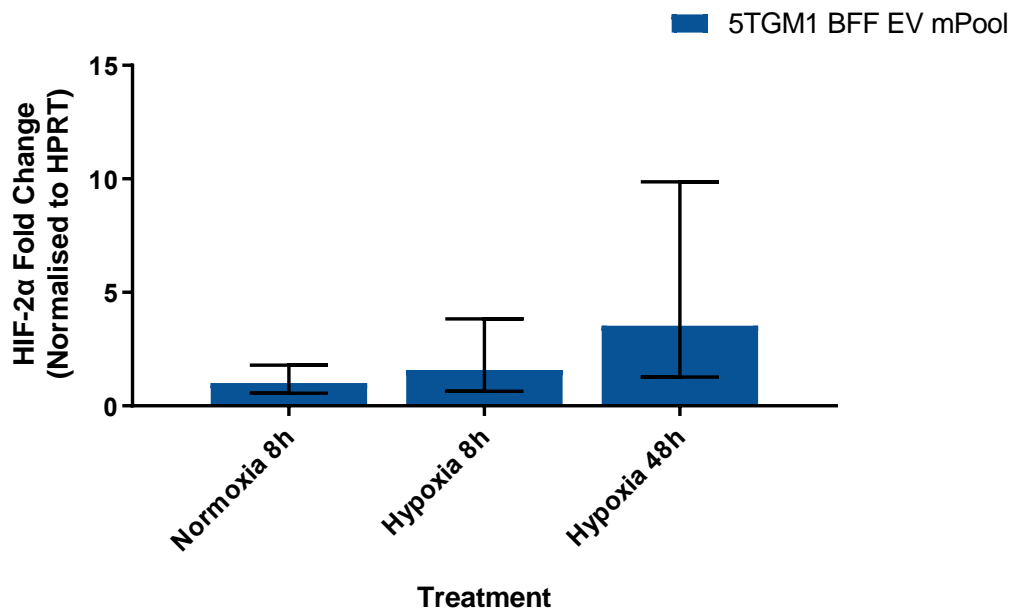
Figure 4.2: *Hif-2α* **mRNA induction in empty vector control cell in response to hypoxia treatment.** 5TGM1 BFF mEV monoclones (EV 2, EV 3, EV 4, EV 5, EV 6) were cultured in normoxia for 8 hours or hypoxia for 8 or 48 hours. Cell suspensions, preserved in *RNA-later*, were combined in equal volumes prior to extraction. mRNA was extracted using the mir-Vana extraction kit, and equivalent amounts were reverse transcribed. Relative *Hif-2α* cDNA levels were examined by qRT-PCR. Data is presented as mean expression fold change in comparison to 5TGM1 BFF EV mPool cultured in Normoxia for 8 hours after normalisation against *Hprt* ($2^{-\Delta\Delta CT}$), ±95% CI. N=3 biological replicates. Dunnett's multiple comparisons test was calculated using mean ΔΔCT values, against the Normoxia 8 hours treatment control column.

4.1.2   Cell treatment

Hypoxia and normoxia treatments were carried out as described in methods, section 2.2.2.3.2.

Five monoclonal knockouts for each of the H1E2, H1E3, H2E2 and H2E3 guides, as well as five monoclonal EV control lines, were selected for transcriptomic analysis. All the selected monoclonal lines were seeded at a fixed concentration for each of the treatment conditions; 8 hour normoxia, 8 hour hypoxia and 48 hour hypoxia. Given the substantial scale of the experiment, the cells were seeded and treated in a staggered fashion. One monoclonal line for each of the different guide and control lines were treated simultaneously to control for day-to-day effects within each guide or control group (Methods, Table 2.1). Following treatments, cell pellets were resuspended in *RNAlater* solution to stabilise and preserve the RNA for later processing. All treatments were repeated three times on different days within the same week as biological replicates to account for day-to-day variation. These steps were then repeated for subsequent sets of monoclonal lines.

Due to the complexity and prohibitive cost of sequencing each of the 25 cell lines with 3 treatment groups and 3 biological replicates (225 samples), the cell suspensions of all five monoclonal lines for each guide, or EV control lines, were pooled before RNA extraction (45 samples). Pooling the treated cells allows for the dilution of clone-specific differences, controls for random FgH1tUTP vector integration, and consolidates the number of sequencing samples to 45. The pooling was performed after treatments using a proportion of the preserved cell suspensions so that remaining monoclonal samples could be analysed independently to validate RNA-seq results and identify clonal differences between the lines.

Following isolation, DNase treated RNA was submitted to the David R Gunn Genomics Facility (SAHMRI) for quality assessment. The isolated RNA was determined to be of good quality (Appendix, Figure 6.4). The RNA was polyA enriched, reverse transcribed,

barcoded and sequenced on the Illumina NextSeq 500, with between 32.5 million and 45 million single-end reads obtained per sample. Sequencing data were processed and analysed by J. Breen and N. Aryamanesh from the SAHMRI Bioinformatics Facility using their in-house pipeline (Figure 4.3). Initial raw single-end FASTQ reads were aligned using the STAR transcriptome algorithm (Dobin et al. 2013) and, on average, 62.05% of the reads mapped to the GRCh38/mm10 mouse genome assembly (Table 4.1). The alignment rate was lower than the expected (>80%) but could be due to mapping 5TGM1 transcripts that were derived from the C57BL/KaLwRij strain to a C57BL/6 genome assembly. Other potential explanations for lower mapping rates are the high expression of exogenous transcripts like firefly luciferase and fluorescent proteins, and the accumulated genetic changes from *in-vitro* culture.

Read quality was assessed using FastQC (Ward, To & Pederson 2018), and the overall quality of the RNA-seq data was deemed acceptable (Appendix, Section 6.1).
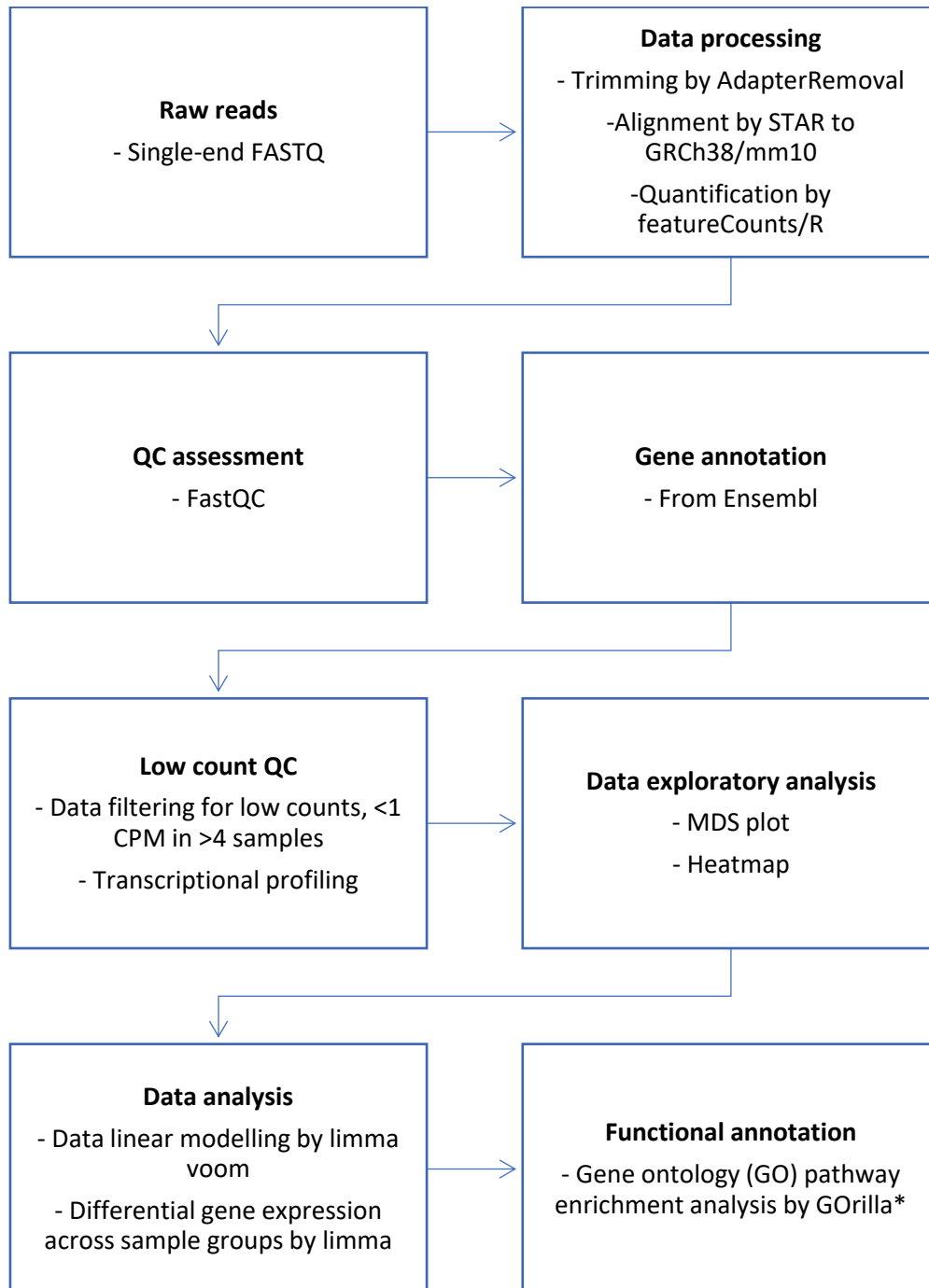
Figure 4.3: RNA-seq analysis pipeline. Pipeline developed and used by the SAHMRI Bioinformatics Facility. Arrows indicate data flow. Asterisk (*) indicates a modification from the original pipeline.

Table 4.1: Sample number and alignment rate for each RNA-seq sample against the GRCh38/mm10 mouse genome.

#	Genotype	Treatment	Bioreplicate	Alignment Rate (%)
1	HIF-1α Exon 2 KO	Normoxia 8h	1	61.73
2	(H1E2 KO)		2	62.82
3			3	61.99
4		Hypoxia 8h	1	62.68
5			2	62.27
6			3	61.71
7		Hypoxia 48h	1	62.58
8			2	62.98
9			3	63.13
10	HIF-1α Exon 3 KO	Normoxia 8h	1	62.75
11	(H1E3 KO)		2	61.99
12			3	62.18
13		Hypoxia 8h	1	62.05
14			2	62.46
15			3	62.55
16		Hypoxia 48h	1	63.26
17			2	62.77
18			3	63.11
19	HIF-2α Exon 2 KO	Normoxia 8h	1	61.51
20	(H2E2 KO)		2	62.07
21			3	61.95
22		Hypoxia 8h	1	61.50
23			2	60.37
24			3	62.29
25		Hypoxia 48h	1	62.16
26			2	62.65
27			3	61.85
28	HIF-2α Exon 3 KO	Normoxia 8h	1	61.20
29	(H2E3 KO)		2	60.97
30			3	62.51
31		Hypoxia 8h	1	61.87
32			2	62.35
33			3	61.78
34		Hypoxia 48h	1	61.65
35			2	62.46
36			3	62.27

37	Empty Vector Control	Normoxia 8h	1	61.79
38	(EV Control)		2	61.99
39			3	61.48
40		Hypoxia 8h	1	61.88
41			2	61.39
42			3	60.82
43		Hypoxia 48h	1	61.20
44			2	61.68
45			3	61.65
	Average (%)			62.05

### 4.1.3 Bioinformatics: Exploratory data analysis

Before exploratory data analysis, gene-annotated counts were filtered to reduce noise, by removing any genes expressed at <1 count per million (CPM) in more than four total samples, and normalised. A total of 10 265 genes remained post-filtering. A multidimensional scaling (MDS) plot was graphed to visualise the main data characteristics and sample similarity (Figure 4.4). Biological replicates for each genotype and treatment group cluster tightly, indicating highly similar transcriptomes within them. Between treatments, 48 hour hypoxia treated samples cluster further away from the 8 hour normoxia treated samples than the 8 hour hypoxia treated samples, suggesting that longer hypoxic treatments induce more significant transcriptomic responses, and are thus highly likely to have a higher number of differentially expressed genes (DEGs).

HIF-1α knockout samples cluster away from the EV control for hypoxic treatments, with H1E2 KOs showing more considerable differences in hypoxic gene expression than H1E3 KOs. Interestingly, H1E2 KOs treated in normoxia cluster far away from normoxic EV controls, suggesting potential roles for the HIFs in normoxia in 5TGM1 cells. Also, H1E2 KOs and H1E3 KOs do not cluster together, which could be due to potential downstream effects of CRISPR off-targeting. On the other hand, HIF-2α knockouts cluster tightly with EV controls even at 48 hours of hypoxia treatment, suggesting that HIF-2α may only play subtle roles in 5TGM1 cells.

Hierarchical clustering analysis showed that each of the EV control and the HIF-1α KOs has similar expression patterns within its genotype group (Figure 4.5). However, the H2E2 KOs and H2E3 KOs have a more similar expression pattern to each other than to the other samples within their genotype group that were cultured in normoxia or 8 hour hypoxia. There was also greater difference between the two HIF-1α cell lines under each condition, than between the two HIF-2α cell lines or between either of the two HIF-2α cell lines and the EV controls, suggesting that there may be off-targets effects in one or

both of the HIF-1α cell lines. Importantly, all the biological replicates cluster closely together which indicates good consistency in the generation of these samples.
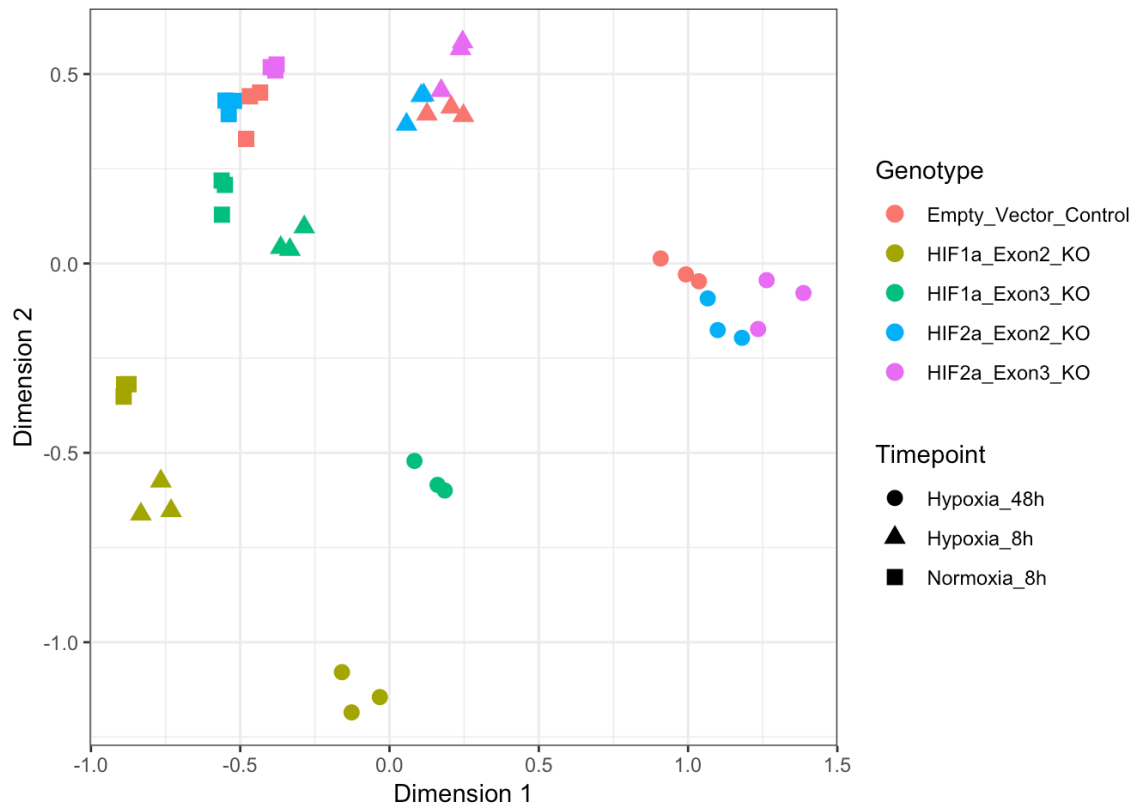
Figure 4.4: Multi-dimensional scaling plot of normalised data for all RNA-seq samples.
Plot generated using plot MDS function from the limma package. Distance between samples represents 'leading fold change', which provides unsupervised sample clustering.
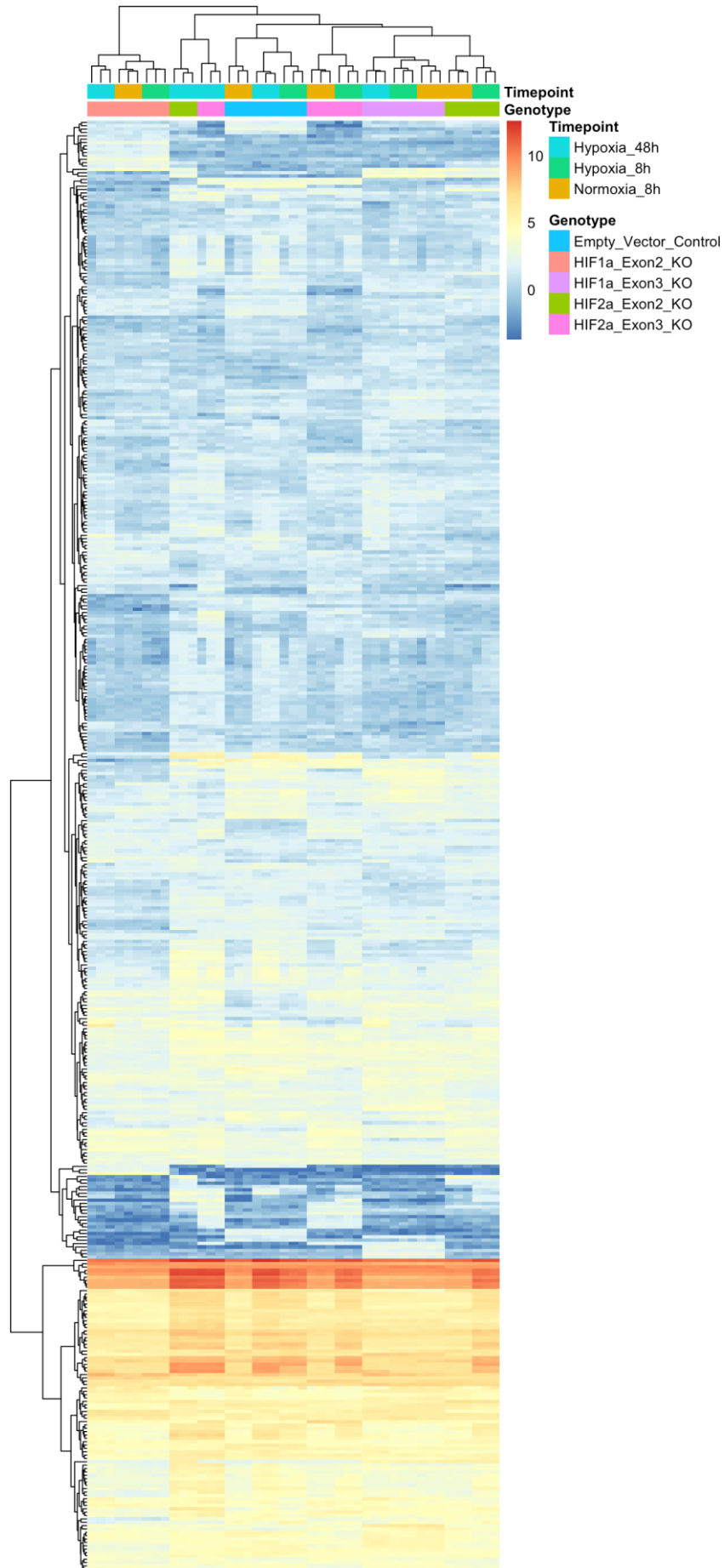
Figure 4.5: Heat map of hierarchical clustering analysis. Data plotted as log count per million. Each row represents one gene, and genes with similar expression patterns are linked by dendrogram on the y-axis. The dendrogram on the x-axis clusters samples with a higher degree of similarity.

4.1.4 Bioinformatics: Data analysis

4.1.4.1 Identification of DEGs within genotype groups

Differential analysis was performed between treatment groups for each sample genotype to determine DEGs in response to hypoxic treatments (Appendix, Tables 6.1, 6.2, 6.3, 6.4 & 6.5). The limma-voom method was employed to estimate variance and to linearize gene expression data (Ritchie et al. 2015). Genes with a ≥ 2-fold change and a false discovery rate (FDR) of < 0.05 were considered differentially expressed.

Comparing 8 hour hypoxia to 8 hour normoxia treatments, the H1E2 KO line had only 4 DEGs upregulated in response to acute hypoxia, while the H1E3 KO line did not have any DEGs (Figure 4.6A, B). The lack of transcriptional response to short-term hypoxia in the HIF-1α KOs is in line with HIF-1α being the critical mediator of acute hypoxic responses in these cells (Dengler, Galbraith & Espinosa 2014). In contrast, samples with wildtype HIF-1α displayed an upregulation of numerous genes, including many well-characterised HIF-1 target genes. EV control, H2E2 KOs and H2E3 KOs had 26, 23 and 28 DEGs upregulated by short-term hypoxia (Figure 4.6C, D, E).

Between 48 hour hypoxia and normoxia treatments, the EV control had 93 DEGs, 89 of which were upregulated (Figure 4.6E). The H2E2 KO line had 143 DEGs (136 upregulated), and the H2E3 KO line had 219 DEGs (200 upregulated) (Figure 4.6C, D). HIF-2α knockouts had a higher number of DEGs than the EV controls in response to long-term hypoxia, suggesting that HIF-2α could potentially be playing a role in tuning those responses. In contrast, HIF-1α knockouts had fewer DEGs than the EV control at 48 hours of hypoxia, with 64 and 36 DEGs for the H1E2 KO and H1E3 KO lines respectively (Figure 4.6A, B).

A

HIF-1a Exon 2 KO
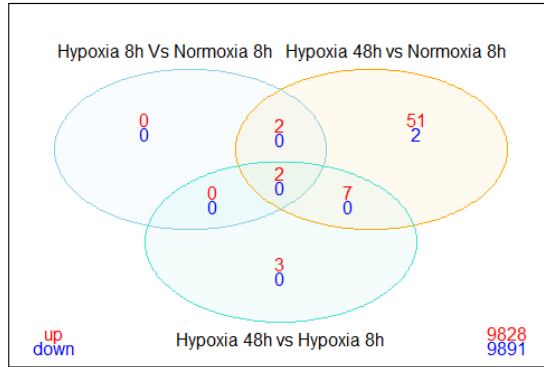
B

HIF-1a Exon 3 KO
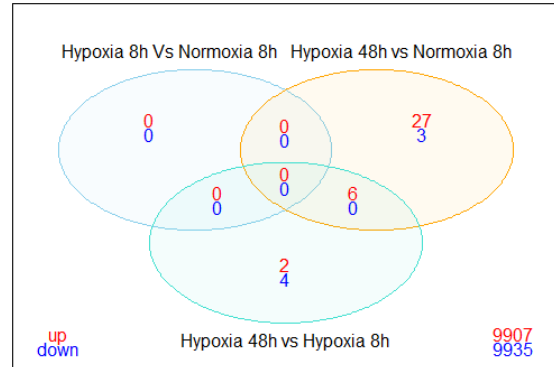
C

HIF-2a Exon 2 KO
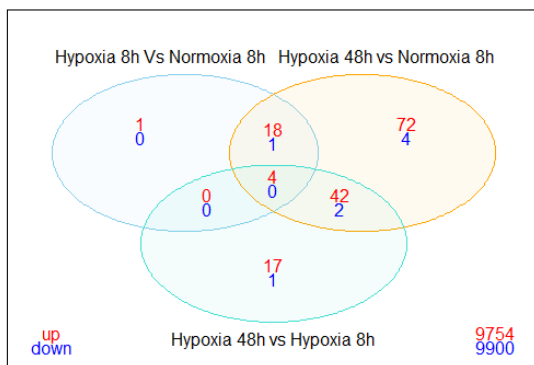
D

HIF-2a Exon 3 KO
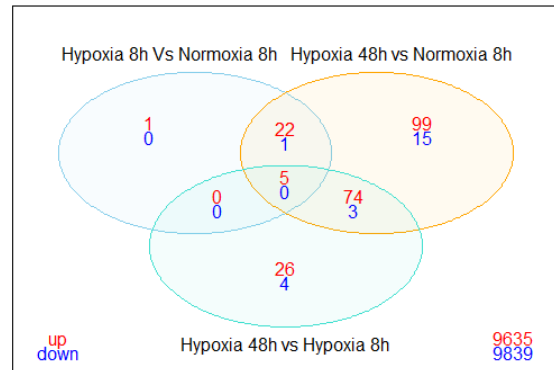
E

Empty Vector Control
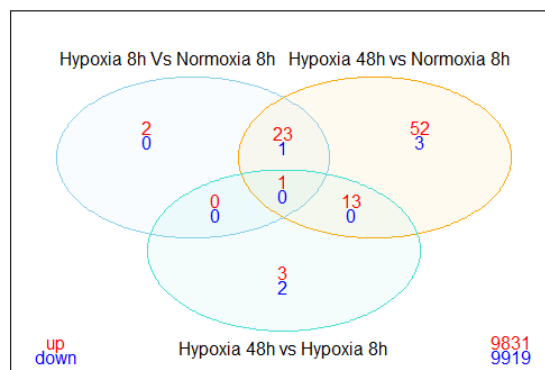
Figure 4.6: Venn diagrams of DEGs between treatments within each genotype group.
Red numbers are the number of upregulated genes whereas blue numbers are the number of downregulated genes. Differentially expressed genes were defined as having a LogFC >1 and FDR <0.05.

4.1.4.2 Identification of HIF-1α specific target genes

Differential analysis was performed by comparing the five different sample genotypes within each treatment group to identify HIF-α isoform-specific and dependent target genes, which may be directly or indirectly regulated. Like the previous comparison, genes with a ≥2-fold change and a false discovery rate (FDR) of < 0.05 were considered differentially expressed. HIF-1α-specific target genes were identified comparing the EV control to both HIF-1α KO lines, and any HIF-2α specific target genes were identified by comparing the EV control to both of the HIF-2α KO lines. HIF-1α appeared to control more transcriptional regulation, as the EV vs HIF-1α knockout comparisons had a higher number of DEGs than the EV vs HIF-2α knockout comparisons for both 8 hour and 48 hour hypoxia treatments, which was consistent with the MDS plot (Figure 4.7).

Only 1 gene displayed altered expression in both HIF-1α KO lines, but not the HIF-2α KO lines, in normoxia compared to the control EV lines (Figure 4.7A, blue arrow). This gene was identified as *Hapln1*, which encodes a secreted protein that stabilises proteoglycan monomers with hyaluronic acid (Table 4.2). This is interesting finding, as it suggests that HIF-1α protein that escapes oxygen-dependent degradation in normoxia may have some functional relevance in 5TGM1 cells. *Hapln1* is also similarly downregulated in the 8 hour and 48 hour hypoxia treated HIF-1α knockout samples. consistent with being HIF-1α-specific target genes that are regulated by hypoxia (Figure 4.7).

In the 8 hour hypoxia treatment, 30 genes were identified as HIF-1α specific target genes (Figure 4.7B, blue arrow). The majority of HIF-1α specific DEGs (30/31) were upregulated in the EV controls in comparison to the HIF-1α knockouts, consistent with being induced by HIF-1α in the acute response to hypoxia. The data are consistent with the well-established role of HIF-1α in metabolic reprogramming, as 13 out of the 30 identified HIF-1α target genes were associated with glucose transport, glucose metabolism and glycolysis (Table 4.2). HIF-1α also induced a broad range of other responses, with target genes having various associated roles including apoptotic signalling, cytoskeletal remodelling and histone modification. In addition, *Egln1* (PHD2),

another well-characterised HIF-1α target gene encoding a hydroxylase that preferentially hydroxylates HIF-1α (Berra et al. 2003), was also found to be positively regulated. Nearly all of these target genes (29/31) also remained differentially expressed after treatment with 48 hours of hypoxia (Figure 4.8).

The longer hypoxic treatment induced a greater number of HIF-1α specific target genes, with an even broader range of functional associations. A total of 59 upregulated and 5 downregulated HIF-1α targets were identified (Figure 4.7C, blue arrow). In addition to the previous roles discussed, additional target genes differentially expressed at 48 hour hypoxia were notably involved in collagen synthesis, transcriptional regulation and vesicle transport (Table 4.2). Interestingly, it appeared that HIF-1α activity also downregulates genes associated with adaptive immune responses. Strangely, given HIF-1α's canonical role in angiogenesis, no pro-angiogenic genes were found to be regulated by HIF-1α under these conditions in the 5TGM1 cells.

To visualise the induction patterns of upregulated HIF-1α target genes, the average log fold change (LogFC) in expression of all upregulated HIF-1α target genes at 8 hour and 48 hour hypoxia treatments were compared (Figure 4.9). Average LogFC was calculated as the mean LogFC of the EV vs H1E2 KO and EV vs H1E3 KO comparisons. Not surprisingly, most of the genes upregulated after 8 hours of hypoxia were upregulated to a similar or greater extent after 48 hours of hypoxia. Several genes displayed what appeared to be interesting temporal-specific expression.

Grin1, *Kif26a*, *Nipsnap1*, *Selenbp1* and several LncRNAs, appeared to show a unique 'second wave' of inductions in response to chronic exposure to hypoxia, with no induction observed after 8 hours of hypoxia, but only after 48 hours (Figure 4.9). However, more detailed analysis found that these genes did not pass the low gene cut-off filter at the 8 hour hypoxia treatment but did after the 48 hour hypoxia treatment. From checking the Log2 transcript count per million (CPM) plots, it appears that the expression of each of these genes was already somewhat elevated or 'primed' after 8 hours of exposure to hypoxia, but their transcript levels that were below the low gene

cut-off threshold (Appendix, Figure 6.8). So, these genes display a similar induction to most of the other HIF-1α target genes, but this is masked by their low levels of expression in normoxia and after exposure to 8 hours of hypoxia. Similarly, *Dhcr24* appeared to show a unique 'first wave' induction, where it was induced after 8 hours of hypoxia but not observed after 48 hours (Figure 4.9). This was because the gene did not pass the low gene cut-off filter at the 48 hour hypoxia treatment, and the CPM plot indicates that *Dhcr24* expression levels are similar after both 8 hours and 48 hours of hypoxia (Appendix, Figure 6.8).

To predict the subset of identified HIF-1α target genes that are directly regulated, as opposed to those indirectly regulated by HIF-1α, comparisons were made to HIF-1α chromatin immunoprecipitation with DNA microarray (ChIP-ChIP) and ChIP-sequencing (ChIP-seq) data generated from human MCF-7 breast cancer cells (Table 4.3) (Mole et al. 2009; Schödel et al. 2011). Almost a third (19/66) of these target genes were reported to be in proximity to HIF-1α binding sites in MCF-7 cells, all of which were positively regulated by HIF-1α. M*ost of these genes (13/19) were upregulated as an acute response to hypoxia and remained sustained at the 48 hour hypoxia treatment.* About half of the predicted direct HIF-1α target genes (11/19) were also reported to be shared targets with HIF-2α in MCF-7 cells. Surprisingly, *Ero1l*, which was identified as a HIF-1α target gene in 5TGM1 cells, was reported as a HIF-2α direct target in MCF-7 cells. The difference of HIF-α isoform dependent regulation of *Ero1l* could be due to cell-type or species-specific differences between 5TGM1 and MCF-7 cells.

It is preferable to perform comparisons to data obtained from mouse cells, specifically MM, but currently available ChIP-seq data for mouse HIF-1α binding profile may not be completely reliable (Guimarães-Camboa et al. 2015). This is because commercially available HIF-1α antibodies commonly bind to non-specific proteins in mouse samples (D. Peet, personal communication), similar to that observed in the western blots on HIF-1α knockout 5TGM1 cells that were previously described (Results 1, Figure 3.12). In comparison to RNA-seq and ChIP-seq analysis of fetal mouse hearts, about a third (23/66) of HIF-1α target genes in 5TGM1 cells appear to be also upregulated by HIF-1α

the in foetal mouse hearts (Table 4.4) (Guimarães-Camboa et al. 2015). Interestingly, *Hmox1*, which was hypoxically upregulated by HIF-1α in 5TGM1 cells, was reported to be downregulated in HIF-1α deficient foetal mouse hearts, indicating a cell-type dependent difference in its regulation (Table 4.4).

To identify potentially novel HIF-1α target genes, the list of identified HIF-1α target genes in 5TGM1 cells were checked online to determine if they have been previously found to be regulated by HIF-1α. Appendix Table 6.6 summarises known HIF-1α target genes, with references to the literature reporting on their regulation by HIF-1α. Notably, *Cox4i2*, *Klf10*, *Prelid1* and *Slc37a4* were identified as direct HIF-1α targets in ChIP studies (Tables 4.3, 4.4), but studies of their regulation by HIF-1α has not been reported. A total of 28 novel target genes were identified from the transcriptomic analysis of 5TGM1 cells (Appendix, Table 6.7), which have not been previously found to be regulated by HIF-1α.

To generate an overall representation of the biological process affected by HIF-1α knockout for each hypoxic treatment, gene ontology (GO) analysis was performed using *GOrilla* (Eden et al. 2009)*. In comparisons between EV controls and HIF-1α knockouts, terms associated with glycolysis and various metabolic processes were most strongly enriched in both the 8 hour and 48 hour hypoxia treatments (Figure 4.10).

A

EV control vs KO line, Normoxia 8h
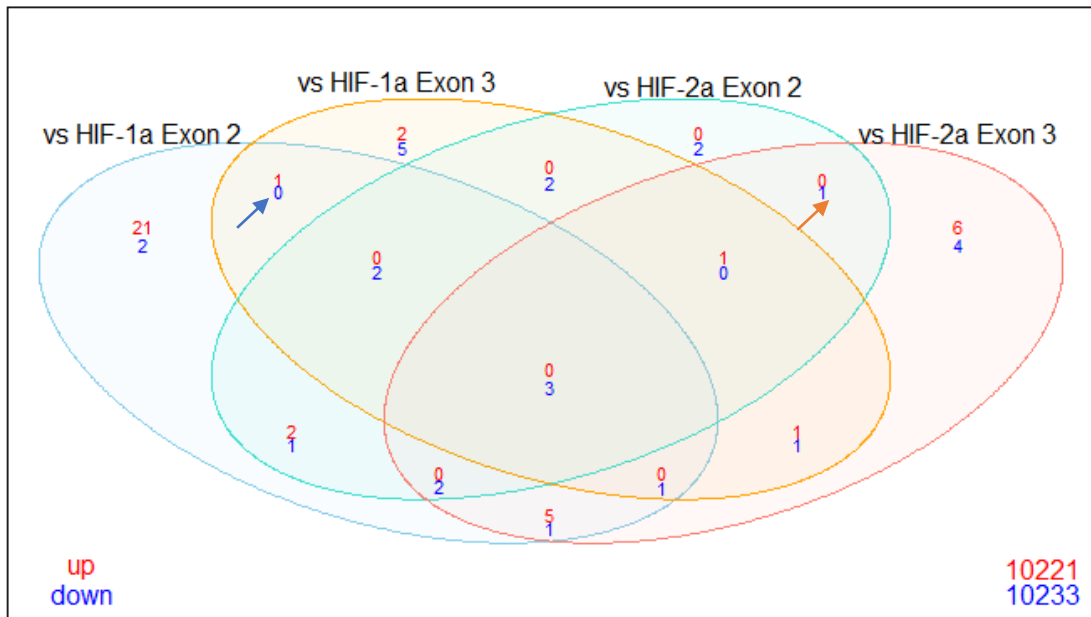
B

EV control vs KO line, Hypoxia 8h

163

C
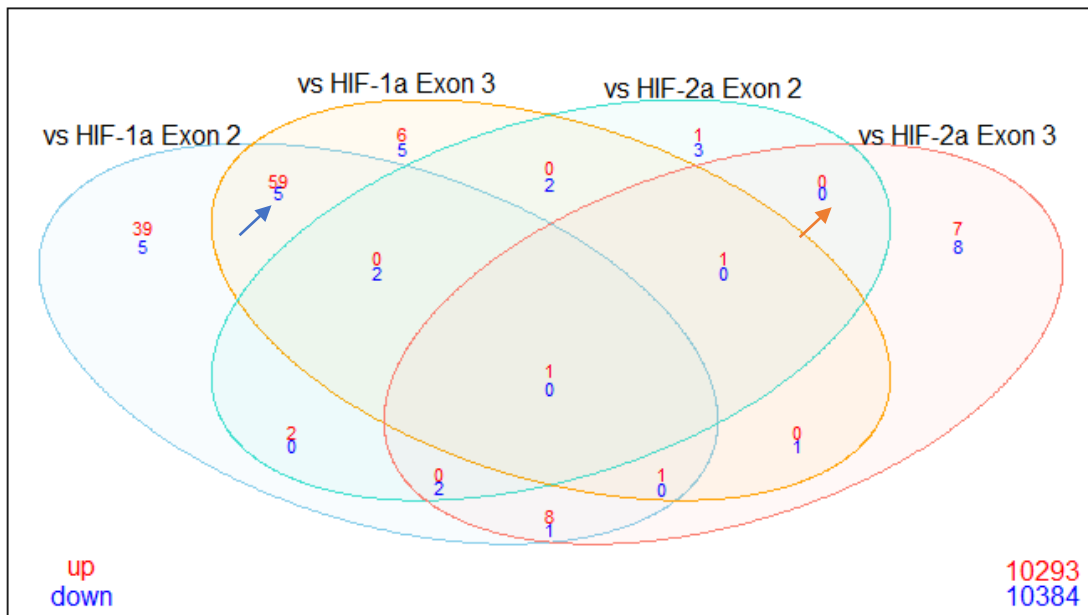
Figure 4.7: Identification of HIF-1α and HIF-2α specific target genes. Number of overlapping differentially expressed genes for EV controls in comparison to each knockout line within the **(A)** 8 hour normoxia, **(B)** 8 hour hypoxia, and **(C)** 48 hour hypoxia treatment groups. Differentially expressed genes were defined as having a LogFC >1 and FDR <0.05. The blue arrows indicate the position of the subset corresponding to HIF-1α specific target genes, whereas the orange arrow indicates the position of the subset corresponding to HIF-2α specific target genes.

Table 4.2: HIF-1α specific target genes in 5TGM1 cells. Multiple comparisons performed between genotypes within treatment groups, and genes listed are uniquely differentially expressed by EV controls in comparison to HIF-1α knockouts for each treatment condition.

Normoxia 8h

	#	ID	Gene	EV vs H1E2 KO LogFc	EV vs H1E3 KO LogFc	Associated Function	Note
Upregulated	1	ENSMUSG00000021613	*Hapln1*	2.29326	1.98638	Hyaluronan and proteoglycan linker	†,‡

Hypoxia 8h

	#	ID	Gene	EV vs H1E2 KO LogFc	EV vs H1E3 KO LogFc	Associated Function	Note
Downregulated	1	ENSMUSG00000028931	*Kcnab2*	-3.302952	-2.882842	Potassium ion channel	‡
Upregulated	1	ENSMUSG00000050914	*Ankrd37*	4.45521	3.96381		‡
	2	ENSMUSG00000078566	*Bnip3*	4.87793	4.43907	Apoptosis	‡
	3	ENSMUSG00000003955	*Fam162a*	1.67112	1.85902	Apoptosis	‡
	4	ENSMUSG00000034926	*Dhcr24*	4.08501	3.41095	Cholesterol biosynthesis	
	5	ENSMUSG00000045667	*Smtnl2*	5.96688	4.32557	Cytoskeleton - actin organisation	‡
	6	ENSMUSG00000062591	*Tubb4a*	2.26632	1.70806	Cytoskeleton - tubulin	‡
	7	ENSMUSG00000021668	*Polk*	1.45341	1.60505	DNA damage repair - polymerase	

8	ENSMUSG00000025791	*Pgm1*	1.50391	1.36381	Glucose metabolism	‡
9	ENSMUSG00000028645	*Slc2a1*	2.32431	2.09699	Glucose transport	‡
10	ENSMUSG00000032114	*Slc37a4*	1.68326	1.50673	Glucose transport	‡
11	ENSMUSG00000063229	*Ldha*	2.00587	1.9874	Glycolysis	‡
12	ENSMUSG00000023456	*Tpi1*	1.96265	1.91623	Glycolysis	‡
13	ENSMUSG00000011752	*Pgam1*	1.72114	1.66918	Glycolysis	‡
14	ENSMUSG00000021196	*Pfkp*	1.68611	1.27737	Glycolysis	‡
15	ENSMUSG00000030695	*Aldoa*	1.56805	1.46852	Glycolysis	‡
16	ENSMUSG00000062070	*Pgk1*	1.5424	1.53107	Glycolysis	‡
17	ENSMUSG00000020277	*Pfkl*	1.53823	1.7206	Glycolysis	‡
18	ENSMUSG00000063524	*Eno1*	1.43834	1.33168	Glycolysis	‡
19	ENSMUSG00000036427	*Gpi1*	1.4229	1.37704	Glycolysis	‡
20	ENSMUSG00000000628	*Hk2*	1.36782	1.41628	Glycolysis	‡
21	ENSMUSG00000031987	*Egln1*	1.86199	1.94348	HIF-α regulation	‡
22	ENSMUSG00000053470	*Kdm3a*	1.83756	1.78128	Histone demethylase	‡
23	ENSMUSG00000024201	*Kdm4b*	1.76258	1.62888	Histone demethylase	‡
24	ENSMUSG00000056962	*Jmjd6*	1.22027	1.28855	Histone demethylase, protein hydroxylase	‡
25	ENSMUSG00000021613	*Hapln1*	2.3212	2.07435	Hyaluronan and proteoglycan linker	*,‡
26	ENSMUSG00000079414	*Gm11110*	2.4566	2.05088	LncRNA	‡
27	ENSMUSG00000111394	*Gm49759*	1.94648	1.8821	LncRNA	‡

	#	ID	Gene			Associated Function	Note
	28	ENSMUSG00000009876	*Cox4i2*	1.74686	2.20677	Mitochondrial cytochrome activity	‡
	29	ENSMUSG00000000056	*Narf*	1.96021	1.82375	Nuclear binding	‡
	30	ENSMUSG00000020108	*Ddit4*	1.98002	2.19771	Stress response, mTOR signalling	‡

Hypoxia 48h

	#	ID	Gene	EV vs H1E2 KO LogFc	EV vs H1E3 KO LogFc	Associated Function	Note
Downregulated	1	ENSMUSG00000015143	*Actn1*	-2.70821762	-1.90230689	Cytoskeleton - actin organisation	
	2	ENSMUSG00000060586	*H2-Eb1*	-1.51927073	-1.58693959	Immune response – adaptive	
	3	ENSMUSG00000020395	*Itk*	-2.84091972	-1.82337818	Immune response - adaptive	
	4	ENSMUSG00000038463	*Olfml2b*	-1.5469534	-1.68844614		
	5	ENSMUSG00000028931	*Kcnab2*	-2.78526717	-2.69063805	Potassium ion channel	†
Upregulated	1	ENSMUSG00000078566	*Bnip3*	5.27709	5.17314	Apoptosis	†
	2	ENSMUSG00000003955	*Fam162a*	2.54098	2.73142	Apoptosis	†
	3	ENSMUSG00000022051	*Bnip3l*	1.81302	1.69113	Apoptosis	
	4	ENSMUSG00000021486	*Prelid1*	1.18986	1.15351	Apoptosis	
	5	ENSMUSG00000058966	*Fam57b*	2.21847	2.38964	Ceramide synthesis	
	6	ENSMUSG00000018906	*P4ha2*	1.89698	1.5855	Collagen synthesis	
	7	ENSMUSG00000019055	*Plod1*	1.62228	1.49716	Collagen synthesis	

8	ENSMUSG00000031637	*Lrp2bp*	1.82854	1.81294	Copper homeostasis	
9	ENSMUSG00000045667	*Smtnl2*	5.45941	6.25425	Cytoskeleton - actin organisation	†
10	ENSMUSG00000062591	*Tubb4a*	2.39935	1.74827	Cytoskeleton - tubulin	†
11	ENSMUSG00000034786	*Gpsm3*	1.83004	1.92558	G protein regulation	
12	ENSMUSG00000025791	*Pgm1*	1.94882	1.80114	Glucose metabolism	†
13	ENSMUSG00000028645	*Slc2a1*	2.5828	2.46499	Glucose transport	†
14	ENSMUSG00000032114	*Slc37a4*	1.69907	1.8596	Glucose transport	†
15	ENSMUSG00000026959	*Grin1*	7.75201	9.18125	Glutamate receptor channel	
16	ENSMUSG00000063229	*Ldha*	2.72315	2.69856	Glycolysis	†
17	ENSMUSG00000023456	*Tpi1*	2.72096	2.66078	Glycolysis	†
18	ENSMUSG00000030695	*Aldoa*	2.54616	2.41158	Glycolysis	†
19	ENSMUSG00000062070	*Pgk1*	2.52185	2.53863	Glycolysis	†
20	ENSMUSG00000063524	*Eno1*	2.31845	2.18891	Glycolysis	†
21	ENSMUSG00000059040	*Eno1b*	2.22053	2.02563	Glycolysis	
22	ENSMUSG00000036427	*Gpi1*	2.19714	2.15329	Glycolysis	†
23	ENSMUSG00000032294	*Pkm*	2.1631	2.04971	Glycolysis	
24	ENSMUSG00000011752	*Pgam1*	2.08581	2.1004	Glycolysis	†
25	ENSMUSG00000057666	*Gapdh*	1.88678	1.84709	Glycolysis	
26	ENSMUSG00000021196	*Pfkp*	1.58978	1.36396	Glycolysis	†
27	ENSMUSG00000020277	*Pfkl*	1.53527	1.79201	Glycolysis	†

28	ENSMUSG00000000628	*Hk2*	1.19667	1.25242	Glycolysis	†
29	ENSMUSG00000051615	*Rap2a*	1.51961	1.57889	GTP binding	
30	ENSMUSG00000005413	*Hmox1*	1.74038	1.35957	Heme catabolism	
31	ENSMUSG00000031987	*Egln1*	1.83254	1.97834	HIF-α regulation	†
32	ENSMUSG00000053470	*Kdm3a*	1.83878	1.73654	Histone demethylase	†
33	ENSMUSG00000024201	*Kdm4b*	1.61874	1.57416	Histone demethylase	†
34	ENSMUSG00000056962	*Jmjd6*	1.23799	1.36131	Histone demethylase, protein hydroxylase	†
35	ENSMUSG00000021613	*Hapln1*	2.04939	1.76191	Hyaluronan and proteoglycan linker	*,†
36	ENSMUSG00000033307	*Mif*	1.39477	1.50704	Immune response - cytokine	
37	ENSMUSG00000021831	*Ero1l*	1.99843	2.18794	Immunoglobulin folding	
38	ENSMUSG00000006494	*Pdk1*	1.44288	1.4797	Kinase - AKT signalling	
39	ENSMUSG00000021294	*Kif26a*	5.08063	6.50987	Kinesin (atypical), cell growth repressor	
40	ENSMUSG00000043421	*Hilpda*	1.92776	1.84511	Lipid accumulation	
41	ENSMUSG00000109881	*Gm45507*	5.38569	5.54094	LncRNA	
42	ENSMUSG00000097660	*Gm26762*	2.51393	2.60603	LncRNA	
43	ENSMUSG00000086225	*Gm8661*	2.18779	1.75645	LncRNA	
44	ENSMUSG00000111394	*Gm49759*	2.10122	2.08392	LncRNA	†
45	ENSMUSG00000079414	*Gm11110*	2.05174	2.16741	LncRNA	†

46	ENSMUSG00000082927	*Gm5863*	1.9186	1.72999	LncRNA	
47	ENSMUSG00000009876	*Cox4i2*	3.74538	4.39562	Mitochondrial cytochrome activity	†
48	ENSMUSG00000038412	*Higd1a*	1.44905	1.44812	Mitochondrial homeostasis	
49	ENSMUSG00000000056	*Narf*	1.76879	1.69014	Nuclear binding	†
50	ENSMUSG00000027333	*Smox*	1.92063	1.84599	Polyamine regulation	
51	ENSMUSG00000068874	*Selenbp1*	2.92687	2.80116	Selenium binding	
52	ENSMUSG00000020108	*Ddit4*	1.65201	1.93085	Stress response, mTOR signalling	†
53	ENSMUSG00000042622	*Maff*	1.56105	1.32937	Transcription factor	
54	ENSMUSG00000037465	*Klf10*	1.77778	1.67556	Transcriptional repressor	
55	ENSMUSG00000022754	*Tmem45a*	2.66051	1.85798	Transmembrane protein	
56	ENSMUSG00000009092	*Derl3*	2.53713	2.15084	Unfolded protein response	
57	ENSMUSG00000034799	*Unc13a*	2.69895	2.49118	Vesicle maturation, exocytosis	
58	ENSMUSG00000034285	*Nipsnap1*	3.65333	2.3585	Vesicle transport	
59	ENSMUSG00000050914	*Ankrd37*	5.28539	5.28603		†

* Also differentially expressed in Normoxia 8h

† Also differentially expressed in Hypoxia 8h

‡ Also differentially expressed in Hypoxia 48h

HIF-1α specific target genes
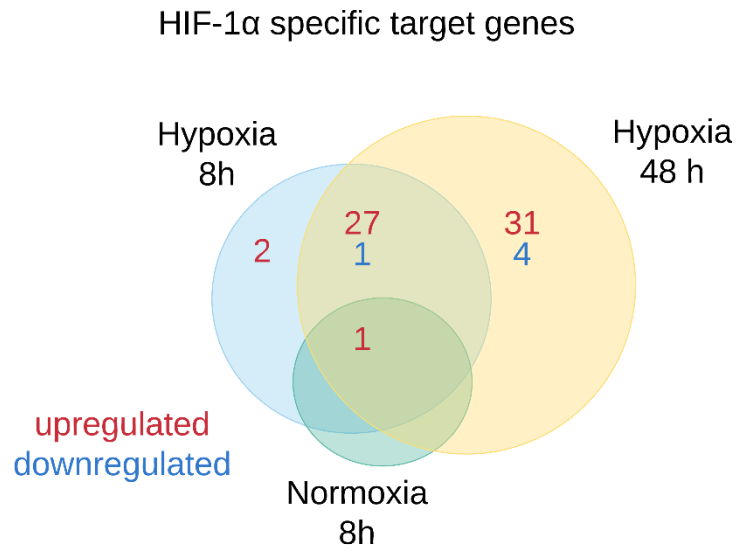
Figure 4.8: Venn diagram of HIF-1α dependent target genes. Red numbers are the number of HIF-1α upregulated genes and blue numbers are the number of HIF-1α downregulated genes. Overlaps indicate where target genes are differentially expressed in multiple treatment conditions.
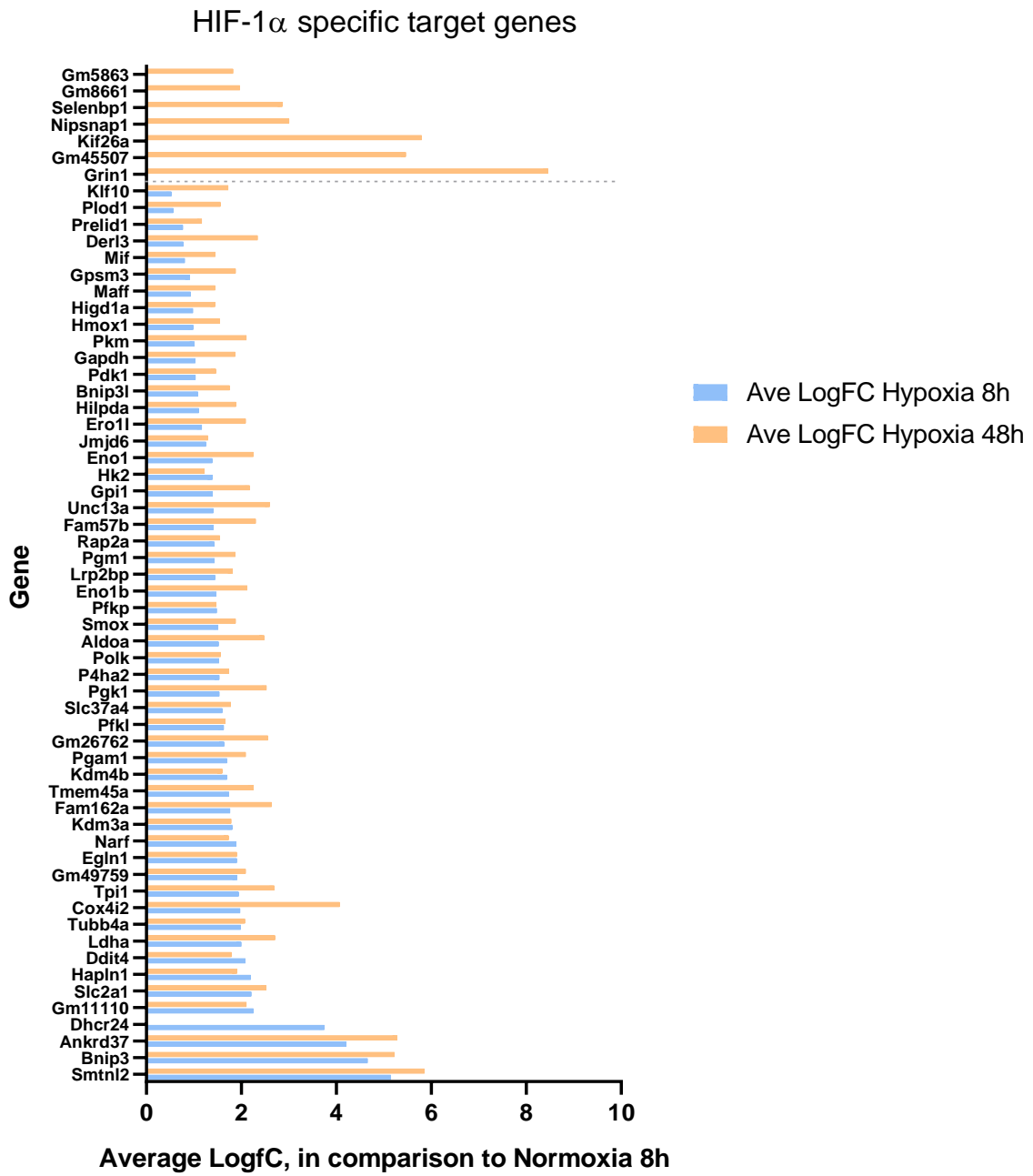
Figure 4.9: HIF-1α target gene induction profile. Plot shows the average LogFC for Hypoxia 8h and Hypoxia 48h treatments, in comparison to 8 hour normoxia for all upregulated HIF-1α target genes. For each treatment, genes with transcript CPM <1 in >4 samples were omitted from analysis.

Table 4.3: Comparison of HIF-1α dependent upregulated target genes in 5TGM1 cells with ChIP data for MCF-7 human breast cancer cells. These genes have been identified from RNA-seq to be positively regulated by HIF-1α in 5TGM1 cells.

#	5TGM1 HIF-1α target gene	8h	48h	MCF-7 HIF-1α ChIP-ChIP (Mole et al. 2009)	MCF-7 HIF-1α ChIP-seq (Schödel et al. 2011)	Note
1	*Aldoa*	✓	✓		✓	*
2	*Ankrd37*	✓	✓		✓	*
3	*Bnip3l*	✓	✓	✓		*
4	*Ddit4*	✓	✓		✓	*
5	*Eno1*	✓	✓		✓	*
6	*Gapdh*		✓	✓	✓	*
7	*Hk2*	✓	✓	✓	✓	*
8	*Klf10*		✓		✓	*
9	*Ldha*	✓	✓	✓	✓	*
10	*Mif*		✓		✓	
11	*Narf*	✓	✓	✓	✓	
12	*P4ha2*		✓		✓	
13	*Pdk1*		✓		✓	*
14	*Pfkl*	✓	✓		✓	
15	*Pfkp*	✓	✓		✓	
16	*Pgam1*	✓	✓	✓	✓	
17	*Pgk1*	✓	✓	✓		
18	*Slc2a1*	✓	✓	✓	✓	*
19	*Tmem45a*		✓	✓	✓	

* Also identified as HIF-2α direct target gene in MCF-7 ChIP-ChIP or ChIP-seq experiment.

Table 4.4: Comparison of HIF-1α dependent upregulated target genes in 5TGM1 cells with RNA-seq and ChIP-seq data for e12.5 foetal mouse hearts. These genes have been identified from RNA-seq to be positively regulated by HIF-1α in 5TGM1 cells.

#	5TGM1 HIF-1α target gene	8h	48h	Foetal mouse heart ChIP-seq, upregulated	Foetal mouse heart ChIP-seq, downregulated
1	*Aldoa*	✓	✓	✓	
2	*Ankrd37*	✓	✓	✓	
3	*Bnip3*	✓	✓	✓	
4	*Bnip3l*		✓	✓	
5	*Cox4i2*	✓	✓	✓	
6	*Egln1*	✓	✓	✓	
7	*Eno1*	✓	✓	✓	
8	*Gapdh*		✓	✓	
9	*Hk2*	✓	✓	✓	
10	*Hmox1*		✓		✓
11	*Ldha*	✓	✓	✓	
12	*Mif*		✓	✓	
13	*Narf*	✓	✓	✓	
14	*Pdk1*		✓	✓	
15	*Pfkl*	✓	✓	✓	
16	*Pfkp*	✓	✓	✓	
17	*Pgam1*	✓	✓	✓	
18	*Pgk1*	✓	✓	✓	
19	*Pkm*		✓	✓	
20	*Prelid1*		✓	✓	
21	*Selenbp1*		✓	✓	
22	*Slc37a4*	✓	✓	✓	
23	*Tmem45a*		✓	✓	

A

EV vs H1E2 KO, Hypoxia 8h

EV vs H1E3 KO, Hypoxia 8h

B

EV vs H1E2 KO, Hypoxia 48h

EV vs H1E3 KO, Hypoxia 48h

176
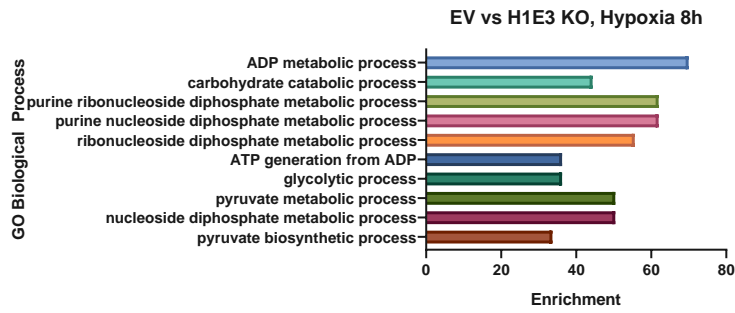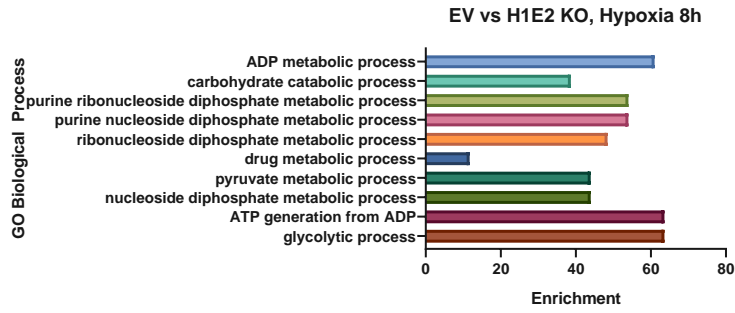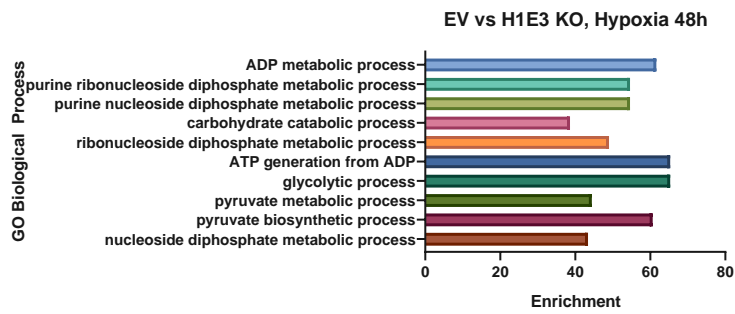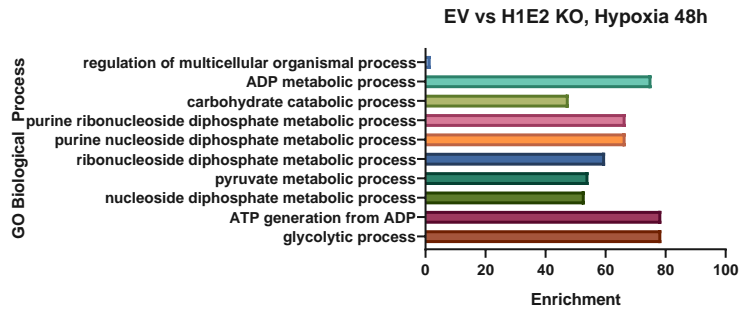
Figure 4.10: Top 10 enriched GO biological process terms for the (A) 8 hour and (B) 48 hour hypoxia treatments. Gene ontology analysis was performed on GOrilla, using a single ranked list of all genes (by their FDR) for each of the EV versus knockout line comparisons. The enrichment of top 10 terms with the lowest P-values are presented. Enrichment was calculated as the proportion of input genes in a particular GO term divided by the proportion of genes expected for that term in all genes.

4.1.4.3   Identification of HIF-1α independent hypoxic response genes

Several genes appeared to be similarly differentially expressed in both the HIF-1α knockouts and EV controls in response to hypoxic treatment (Figure 4.11). These genes could be regulated by non-HIF hypoxic-response pathways. To identify these HIF-1α-independent hypoxic responses, differential analysis was performed between each hypoxic treatment timepoint and normoxic treatment for the HIF-1α knockout and EV control lines. Like the previous comparisons, genes with a ≥ 2-fold change and a false discovery rate (FDR) of < 0.05 were considered differentially expressed. Shared DEGs for the H1E2 KO, H1E3 KO and EV control lines were subsequently identified.

No shared DEGs were identified for the H1E2 KO, H1E3 KO and EV control lines in the 8 hour hypoxia vs 8 hour normoxia comparison. This suggests that HIF-1α is the major cellular mediator for acute hypoxic responses in 5TGM1 cells. On the other hand, several shared DEGs were identified for the H1E2 KO, H1E3 KO and EV control lines in the 48 hour hypoxia vs 8 hour normoxia comparison (Table 4.5). Among these genes is *Angptl6*, which is thought to recruit endothelial cells and promote angiogenesis (Oike et al. 2004). Two genes in this list, *Ddit4* and *Itk*, were previously identified to be HIF-1α specific target genes and are thus differentially regulated by a combination of HIF-1α dependent and independent means.
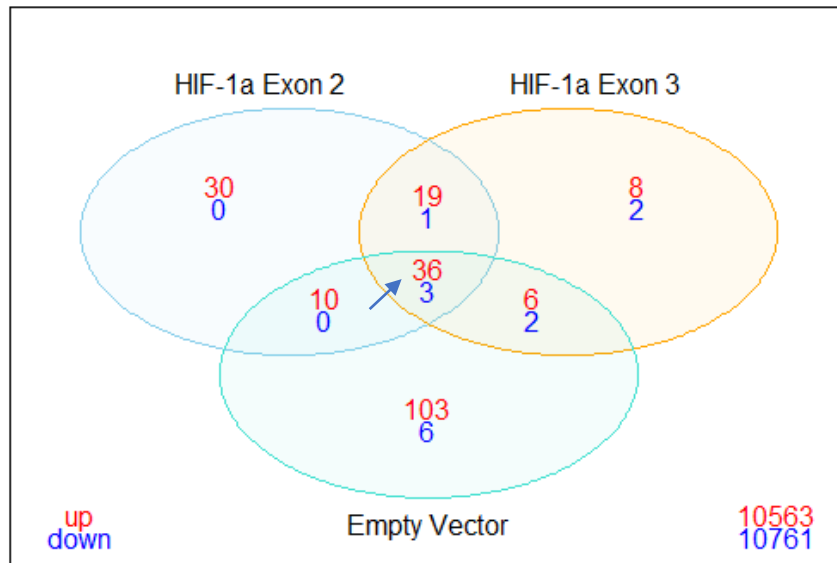
Figure 4.11: Identification of the number of HIF-1α independent hypoxic response genes. Venn diagram presents the number of DEGs between HIF-1α knockout 5TGM1 cells and EV control for the 48 hour hypoxia versus 8 hour normoxia comparison. Differentially expressed genes were defined as having a LogFC >1 and FDR <0.05. The blue arrow indicates the position of the subset corresponding to shared hypoxic response genes upregulated at 48 hours of hypoxia that is independent of HIF-1α regulation.

Table 4.5: HIF-1α independent genes differentially regulated in 48 hour hypoxia, in comparison to 8 hour normoxia. HIF-1α independent genes were defined as similar DEGs between H1E2 KO, H1E3 KO and EV controls.

#	GeneID	GeneName	H1E2 KO LogFC	H1E3 KO LogFC	EV LogFC	Note
1	ENSMUSG00000076934	Iglv1	2.157037243	2.383357543	2.20466992	
2	ENSMUSG00000034445	Cyb561a3	2.023092054	2.050628059	2.627416773	
3	ENSMUSG00000029657	Hsph1	1.413844583	1.442912223	1.773012166	
4	ENSMUSG00000033032	Afap1l1	-1.426795181	-1.469164934	-1.463853836	
5	ENSMUSG00000025203	Scd2	-1.64685848	-1.644046753	-2.32538765	
6	ENSMUSG00000021226	Acot2	-1.663393291	-1.741233172	-1.607876592	
7	ENSMUSG00000032193	Ldlr	-1.675810475	-1.618879535	-1.885113807	
8	ENSMUSG00000031841	Cdh13	-1.708267807	-1.831817707	-1.557384522	
9	ENSMUSG00000041642	Kif21b	-1.757249492	-1.349278548	-1.642837807	
10	ENSMUSG00000035504	Reep6	-1.804885605	-1.745401121	-1.241299138	
11	ENSMUSG00000019278	Dpep1	-1.80745233	-2.074745314	-2.252961158	
12	ENSMUSG00000030739	Myh14	-2.02949725	-1.64951213	-1.622551361	
13	ENSMUSG00000027737	Slc7a11	-2.118843992	-1.956653939	-1.471213311	
14	ENSMUSG00000086111	Gm15326	-2.130904835	-2.251866926	-2.480068416	
15	ENSMUSG00000044037	Als2cl	-2.135508337	-2.539797869	-2.68781005	
16	ENSMUSG00000097785	B230217O12Rik	-2.141638398	-1.994883042	-1.473718536	
17	ENSMUSG00000041444	Arhgap32	-2.155935851	-2.098293734	-2.078458661	

18	ENSMUSG00000020120	Plek	-2.183961212	-1.622683646	-1.983371482	
19	ENSMUSG00000037822	Smim14	-2.231465037	-1.940308399	-2.337047756	
20	ENSMUSG00000020108	Ddit4	-2.28613407	-1.844813712	-3.7504052	*,1
21	ENSMUSG00000105906	Iglc1	-2.446209229	-3.220360567	-3.183837198	
22	ENSMUSG00000026764	Kif5c	-2.634036272	-2.473990577	-1.929468672	
23	ENSMUSG00000042851	Zc3h6	-2.638869325	-2.544984946	-3.06585969	
24	ENSMUSG00000028179	Cth	-2.698147954	-2.287808853	-1.911394907	
25	ENSMUSG00000022421	Nptxr	-2.908710431	-3.015936702	-2.472350021	
26	ENSMUSG00000004698	Hdac9	-2.918989687	-2.972762502	-3.383611178	
27	ENSMUSG00000107344	Gm2559	-2.928781055	-2.696183109	-2.381148299	
28	ENSMUSG00000028838	Extl1	-3.054060858	-2.430799668	-2.230989957	
29	ENSMUSG00000047492	Inhbe	-3.067897324	-2.547821972	-2.250426248	
30	ENSMUSG00000054134	Umodl1	-3.301263694	-2.688739134	-2.649255905	
31	ENSMUSG00000026822	Lcn2	-3.355975497	-3.083269055	-2.378185676	
32	ENSMUSG00000054136	Adm2	-3.461139206	-3.163131025	-4.91374115	
33	ENSMUSG00000032572	Col6a4	-3.508970706	-2.237428692	-2.016663896	
34	ENSMUSG00000032715	Trib3	-3.632008229	-2.885258113	-2.629229486	
35	ENSMUSG00000024867	Pip5k1b	-3.632773407	-2.910291227	-3.324561699	
36	ENSMUSG00000038742	Angptl6	-3.833591486	-3.215023928	-2.5561182	
37	ENSMUSG00000020395	Itk	-3.89348797	-3.508254397	-2.101767948	*
38	ENSMUSG00000029094	Afap1	-4.078924695	-3.57956275	-3.259967058	
39	ENSMUSG00000024451	Arap3	-4.1780683	-2.974376604	-2.004059648	

* Also identified as HIF-1α dependent target gene

1 Identified to be near HIF-1α and HIF-2α binding sites from ChIP-seq of human MCF-7 cells (Schödel et al. 2011)

4.1.4.4 Identification of HIF-2α target genes

To identify HIF-2α specific target genes, further analysis was performed on the data generated in section 3.1.5.2. HIF-2α specific target genes were defined as the subset of shared DEGs that were unique to H2E2 KO and H2E3 KO samples in comparison to EV controls. A total of 1 and 3 DEGs were specific for HIF-2α for the 8 hour normoxia and 8 hour hypoxia treatments, respectively (Figure 4.7A, B, orange arrows). These genes encoded transcription factors and a B-cell antigen receptor signalling regulator (Table 4.6). Unexpectedly, given HIF-2α's role in mediating chronic responses to hypoxia, no HIF-2α-specific DEGs were identified for the 48 hour hypoxia treatment (Figure 4.7C). Assuming classical HIF-2α induction and function in long-term exposure to hypoxia, the absence of HIF-2α-specific responses may have been due to very low or no HIF-2α induction when cultured in hypoxia for 48 hours. Investigation into *Epas1* expression in these samples showed that it was filtered out at the low-expression cut-off step, and further checks into its raw counts revealed that it was undetected (equivalent to noise) across all samples. Thus HIF-2α's role in the 5TGM1 cells' response to chronic hypoxia under these conditions with cultured 5TGM1 cells appears to be, if any, very subtle.

There have been reports that HIF-2α may be atypically regulated in several human MM cell lines, whereby its protein expression is constitutive and predominantly regulated by PHD3 (Gastelum et al. 2017; Mysore et al. 2016). To determine *Egln3* (*Phd3*) transcript expression in 5TGM1 cells, *Egln3* Log2 transcript CPM was plotted against treatments for all cell genotypes (Figure 4.12). *Egln3* transcript was generally lowly expressed in EV controls and HIF-1α knockout cells. It was found that HIF-2α knockout upregulates the expression of *Egln3* across all treatments, although these differences are very small, consistent with HIF-2α supressing its expression in both normoxic and hypoxic conditions.

To identify potential HIF-2α target genes that are regulated across all treatment conditions in a manner like that of *Egln3*, differential analysis was performed between all genotypes, regardless of treatment conditions. HIF-2α specific genes were identified

as shared DEGs that were unique to the comparisons between EV control and HIF-2α knockouts. *Jakmip1* and *Utrn* were identified to be upregulated by HIF-2α, while *Tspan33*, *Mctp1*, *Eepd1*, *Aldoc*, *Adm2*, and *Egln3* were downregulated by HIF-2α (Table 4.6). The effect of HIF-2α knockouts on these genes appears to be subtle, consistent with the low HIF-2α expression in 5TGM1 cells (Figure 4.12)

Table 4.6: HIF-2α specific target genes in 5TGM1 cells. Multiple comparisons for Normoxia 8h and Hypoxia 8h were performed between genotypes within treatment groups, and genes listed are uniquely differentially expressed by EV controls in comparison to HIF-2α knockouts for each treatment condition. Multiple comparisons for Overall was performed between genotypes across all treatments, and genes listed are uniquely differentially expressed by EV controls in comparison to HIF-2α knockouts.

Normoxia 8h

	#	ID	Gene	EV vs H2E2 KO LogFc	EV vs H2E3 KO LogFc	Associated Function	Note
Downregulated	1	ENSMUSG00000031965	*Tbx20*	-2.113135202	-2.218981393	Transcription Factor	*

Hypoxia 8h

	#	ID	Gene	EV vs H2E2 KO LogFc	EV vs H2E3 KO LogFc	Associated Function	Note
Downregulated	1	ENSMUSG00000047143	*Dmrta2*	-1.774912518	-2.036491849	Transcription factor	
	2	ENSMUSG00000031965	*Tbx20*	-1.980123628	-1.884721508	Transcription Factor	†
	3	ENSMUSG00000039316	*Rftn1*	-2.668199902	-1.858006615	B-cell antigen receptor signalling regulator	

Overall

	#	ID	Gene	EV vs H2E2 KO LogFc	EV vs H2E3 KO LogFc	Associated Function	Note

Downregulated	1	ENSMUSG00000054136	*Adm2*	-3.3344097	-4.0103439	Calcitonin-related hormone	
	2	ENSMUSG00000021596	*Mctp1*	-3.0131771	-1.1630413	Calcium ion sensor	
	3	ENSMUSG00000001763	*Tspan33*	-1.7219541	-1.1111706	Cytoskeleton dynamics	
	4	ENSMUSG00000036611	*Eepd1*	-1.31928	-1.1640493	DNA damage repair	
	5	ENSMUSG00000017390	*Aldoc*	-1.2567007	-1.6003936	Glycolysis	1
	6	ENSMUSG00000035105	*Egln3*	-4.7174036	-4.0662321	HIF-2a regulation	2
Upregulated	1	ENSMUSG00000019820	*Utrn*	1.069637	1.261447	Cytoskeleton - anchor to PM	3
	2	ENSMUSG00000063646	*Jakmip1*	1.677397	1.498002	Cytoskeleton - microtubule regulator	

* Also differentially expressed in Normoxia 8h

† Also differentially expressed in Hypoxia 8h

1 Identified to be near HIF-1α binding site from ChIP-ChIP and ChIP-seq of human MCF-7 cells (Mole et al. 2009; Schödel et al. 2011)

2 Identified to be near HIF-1α and HIF-2α binding sites from ChIP-seq of human MCF-7 cells (Schödel et al. 2011)

3 Identified to be near HIF-1α binding site from Chip-Seq of human MCF-7 cells (Schödel et al. 2011)
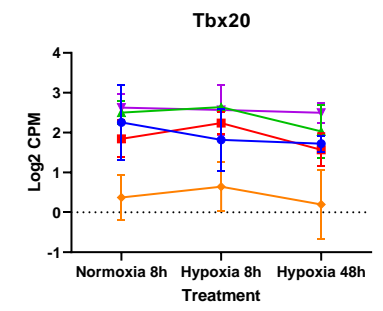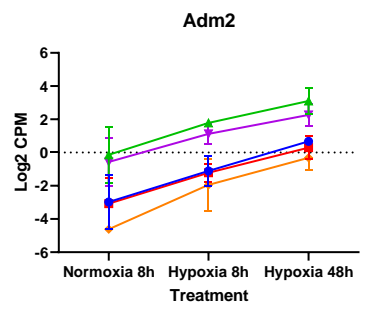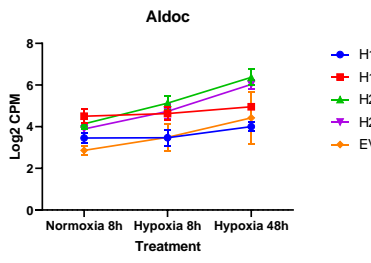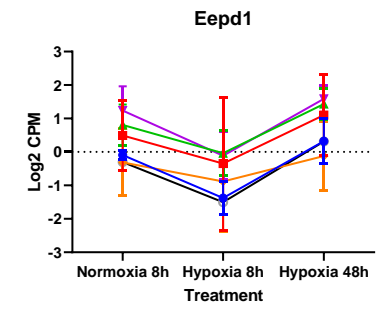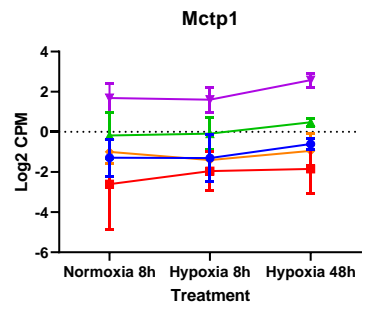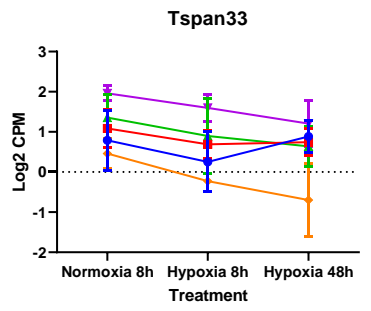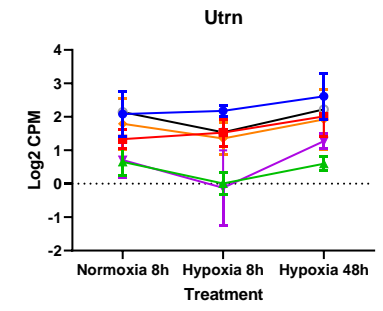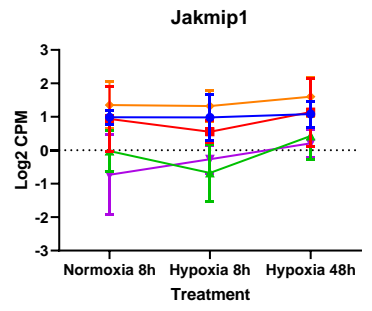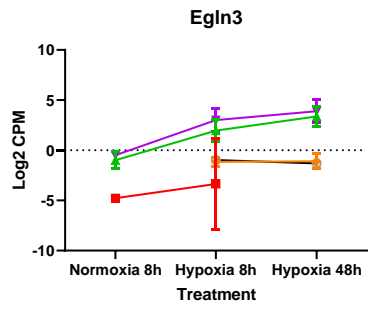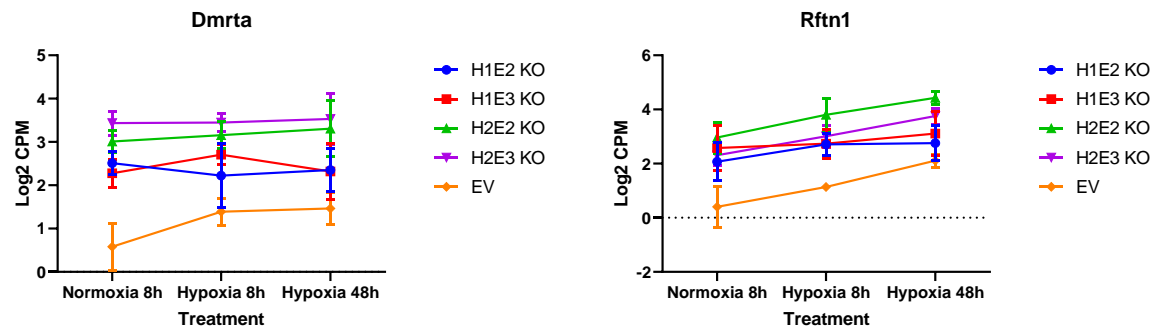
Figure 4.12: Expression of HIF-2α target genes. RNA-seq data are presented as Log2 transcript count per million (CPM) against treatments for each knockout line, ±SD. N=3 biological replicates.

4.2 Discussion

RNA-seq is a powerful technique that utilises next-generation sequencing platforms to profile cellular transcriptomes and to quantify changes in gene expression in response to genetic modifications and different treatment conditions (Chu & Corey 2012; Wang, Gerstein & Snyder 2009). This technique has been previously utilised to study different aspects of MM disease progression in 5TGM1 cells, such as for the identification of pro-migratory cell surface receptors and the identification of bone-related target genes regulated by the bone-specific transcription factor Runx2 (Opperman et al. 2019; Trotter et al. 2015). In this project, RNA-seq was employed to determine HIF-1α and HIF-2α target genes in 5TGM1 cells. This was performed by analysing the differences in gene expression of HIF-1α and HIF-2α knockout 5TGM1 cells in comparison to an EV control, in both normoxic and hypoxic culture conditions. Elucidating the distinct role of each HIF-α isoform in MM PCs would contribute to our understanding of how the hypoxic BM microenvironment, through the HIFs, supports MM disease development and progression.

Gene knockout is a standard method to study protein function (McKinley & Cheeseman 2017; Mehrabian et al. 2014). A requisite step in this process is the isolation and genetic characterisation of monoclonal cell lines to generate a homogenous population of knockout cells. However, a potential artefact of monoclonal isolation is the high clonal variation that could confound comparative analysis (Grav et al. 2018; Orellana et al. 2018). To account for this, cell suspensions of five individually treated, genetically unique knockout monoclones, generated with the same gRNA, were pooled in equal volumes prior to RNA extraction to dilute out clone-specific differences. While this did not capture the full heterogeneity of a polyclonal population, it achieved a middle ground between having to identify and isolate all successfully knocked-out cells in a polyclonal culture and to sequence a monoclonal knockout cell line which could bias sequencing outcomes.

DNase-treated RNA samples were poly-A selected to enrich for mRNA and for ribosomal RNA (rRNA) depletion. While poly-A selection provides better exonic coverage and quantification accuracy over other rRNA depletion methods(Zhao et al. 2018), many species of non-coding RNA, like micro RNA, polyA$^-$ long non-coding RNA (LncRNA) and small nucleolar RNA, would be lost from the starting material. While it would be also informative to elucidate HIF-dependent regulation of these non-coding RNA in 5TGM1 cells, focusing on the coding transcripts allowed for reasonable sequencing coverage at the selected sequencing depth (at least 30 million reads per sample).

Concerning the bioinformatic pipeline (Figure 4.3), it is important to note that it was one of many combinations of analysis tools that are commonly used to analyse the RNA-seq data. Small changes in findings may be observed with different bioinformatics methodologies, but robust changes should be independent.

Ideally, knockouts generated using different gRNAs targeting the same gene would be expected to produce the same phenotypes, given that in each case the function of the same protein is lost. However, in data exploratory analysis, H1E2 KO and H1E3 KO samples do not appear to cluster together on the MDS plot (Figure 4.4), suggesting that there are some differences in the transcriptomes of these two knockout lines. This could be due to off-target effects of CRISPR/Cas9 editing, whereby either one or both guides have inadvertently cleaved and disrupted the function of otherwise normal genes, inducing phenotypes in addition to the ones caused by HIF-1α knockout (Zhang, X-H et al. 2015). This is a key reason why multiple, non-overlapping gRNAs were used to target each gene. Nonetheless, in differential analysis, the DEGs due to off-target effects were removed from the list of DEGs that were HIF-1α specific by filtering and retaining overlapping DEGs in comparisons involving the EV control, H1E2 KO and H1E3 KO samples. Surprisingly, HIF-2α knockouts appeared to have very similar transcriptomes to EV controls, even in the 48 hour hypoxia treatment where HIF-2α is expected to mediate the expression of target genes in response to chronic hypoxia.

A key aim for the transcriptomic analysis of HIF-1α and HIF-2α knockout 5TGM1 cells was to identify HIF-1α and HIF-2α specific target genes in the 5TGM1 cells. As expected, HIF-1α was found to specifically regulate the expression of many different target genes in response to hypoxia (Table 4.2), and several notable targets are highlighted in this discussion. A large proportion the genes that were upregulated in hypoxia had associations with glycolysis and glucose metabolism. This was similarly observed in patient MM samples and human MM cell lines, whereby they display a significant activation of glycolytic genes in response to chronic hypoxia, which is vital for MM cell survival in hypoxic conditions (Ikeda et al. 2018). Glycolytic genes are common HIF-1α specific targets, and are exclusive HIF-1α targets in other cell lines like 786-O renal cell carcinoma cells and HEK293T human embryonic kidney cells (Hu et al. 2003; Wang et al. 2005).

The metabolic reprogramming of cancer cells to favour glycolysis in hypoxia is essential to sustain ATP production for energy when oxygen availability is limited, as well as to produce biosynthetic building blocks for nucleotide and protein synthesis (Eales, Hollinshead & Tennant 2016). Metabolomic profiling of the human MM1S MM cell line had previously shown that hypoxic MM1S cells had increased levels of intermediate glycolytic metabolites in comparison to normoxic cells (Maiso et al. 2015). In addition to metabolic reprogramming, increased *LDHA* expression was also associated with treatment resistance, and disrupting *LDHA* restores bortezomib and melphalan sensitivity in drug-resistant MM cells (Maiso et al. 2015). Given the magnitude and breadth of HIF-1α's regulation of glycolysis, it is presumably important for the metabolic adaptation of MM PCs to the hypoxic BM microenvironment.

Besides glycolytic genes, HIF-1α was also found to upregulate pro-apoptotic and pro-autophagic genes like *Bnip3* and *Bnip3l* in 5TGM1 cells. *BNIP3* is a well-characterised HIF-1α direct target gene that is also commonly epigenetically regulated by DNA methylation in many tumours (Ma et al. 2017). Methylation of the *BNIP3* promoter occurs in about 13.2% of MM patients and is correlated with reduced overall survival (Braggio et al. 2010; Heller et al. 2008). However, BNIP3 and BNIP3L have been reported to be highly

expressed in other cell types without causing cell death (Glick et al. 2012; O'Sullivan et al. 2015), and could instead be regulating autophagy as a pro-survival process to BM hypoxia in MM cells (Bellot et al. 2009; Oancea et al. 2004).

Besides, HIF-1α activity also elicits further transcriptional responses by regulating the expression of several histone modifiers, like *Kdm3a*, and transcription factors, like *Klf10*. HIF-1α driven KDM3a has been reported to positively feedback on HIF-1α expression which is thought to enhance glycolytic gene expression and provide apoptosis resistance in MM (Ikeda et al. 2018). KLF10 expression had been shown to decrease CXCL12 expression in pancreatic ductal adenocarcinoma (Weng et al. 2017). *Cxcl12* transcript was undetected in 5TGM1 cells from the RNA-seq, but high endogenous CXCL12 expression in human MM cells have been shown to downregulate their expression of CXCR4 and desensitise them to CXCL12, facilitating egress to the peripheral circulation (Vandyke et al. 2017). Therefore HIF-1α could be mediating bone-retention signals, in contrast to the action of HIF-2α that is thought to stimulate metastasis. Furthermore, HIF-1α also downregulates *Actn1* which could result in reduced cellular motility (Fife, McCarroll & Kavallaris 2014).

HIF-1α was also found to regulate the expression of *Hapln1* across all treatments, which indicates that, despite being actively targeted for proteasomal degradation, HIF-1α maintained some degree of regulatory activity in normoxia. HAPLN1 has been reported to mediate atypical NF-κB activation in human MM cell lines that confers bortezomib resistance (Huynh et al. 2018). This suggests that HIF-1α that escapes normoxic degradation can regulate a subset of its targets, which could exert pro-tumorigenic effects.

Several genes, including *Actn1*, *H2-Eb1* and *Itk* were identified to be downregulated by HIF-1α in 5TGM1 cells. HIF-1α is generally accepted to be a transcriptional activator (Choudhry & Harris 2018), and its ability to downregulate target genes may be indirect, through the regulation of transcriptional repressors like *Klf10*. Supporting this, ChIP-seq analysis of MCF-7 cells found no association between HIF-1α binding and the loci of

hypoxically downregulated transcripts (Schödel et al. 2011). In contrast, ChIP-seq data comparing wildtype and HIF-1α deficient foetal mouse hearts reported a subset of genes directly repressed by HIF-1α, which is atypical of HIF-1α function. However, there are concerns about the reliability of this data due to commonly observed non-specific binding of commercial HIF-1α antibodies in mouse samples (D. Peet, personal communication).

The HIF-1α specific target genes identified for 5TGM1 cells were also compared to published human HIF-1α ChIP-ChIP and ChIP-seq data as well as mouse HIF-1α ChIP-seq data to predict directly regulated genes (Table 4.3). A slightly larger proportion of HIF-1α target genes identified in 5TGM1 cells were reported to be directly regulated in foetal mouse hearts (23/66) than in MCF-7 cells (19/66). 15 of these genes are direct HIF-1α in both the foetal mouse hearts and MCF-7 cells, suggesting that while there is high concordance between HIF-1α binding in mouse and humans, as well as some species-specific or cell type dependent differences in HIF-1α binding sites between them. A proportion (11/19) of these HIF-1α target genes in MCF-7 cells were also found to be shared HIF-2α targets, but these genes were not differentially regulated in the HIF-2α knockout 5TGM1 cells. Additionally, the rest of the HIF-1α target genes that were not identified to be either HIF-1α direct targets in either MCF-7 cells or in foetal mouse hearts were also not identified at HIF-2α targets in the MCF-7 cells, suggesting that they may be indirectly regulated by HIF-1α.

In addition to HIF-1α dependent target genes, several HIF-1α independent target genes were also identified to be regulated in response to chronic hypoxia. With the exception of *Ddit4*, all these genes have not been reported to be in proximity to HIF-1α or HIF-2α binding sites in the MCF-7 ChIP-ChIP and ChIP-seq data, suggesting that they were HIF independent target genes that were regulated by other hypoxic response pathways. Both *Ddit4* and *Itk* were also identified to be HIF-1α dependent target genes, indicating that were regulated by other mechanisms in addition to HIF-1. No HIF-independent responses were identified at the 8 hour hypoxia timepoint, which suggests that HIF-1α mediates most acute hypoxic responses.

On the other hand, it was more challenging to identify HIF-2α specific target genes in the 5TGM1 cells as HIF-2α's expression pattern in these cells is still not known. While 5TGM1 cells demonstrated classical delayed *Epas1* induction when treated with DP for 48 hours, this did not simulate the activation of *Hif-2α* expression in response to chronic hypoxia in the BM. *Epas1* transcript in 5TGM1 cells did not appear to be strongly upregulated in response to long term hypoxia and was below the detectable limit for RNA-seq. The absence of a significant hypoxic *Epas1* induction was also seen in EV controls by qRT-PCR (Figure 4.2). No genes were found to be strongly induced by HIF-2α in response to chronic hypoxia in 5TGM1 cells. This raises the possibility that HIF-2α may not be expressed, or expressed at very low levels, by 5TGM1 cells.

There have been reports of HIF-2α being constitutively expressed in normoxia in some cancer cells (Lee et al. 2016; Pietras, Johnsson & Påhlman 2010),and in certain human MM cell lines (Gastelum et al. 2017; Mysore et al. 2016). While it is not known if 5TGM1 cells constitutively express low levels of HIF-2α, knocking out HIF-2α appeared to cause a small upregulation of the expression of *Egln3* in both normoxia and hypoxia. PHD3 has been previously described to preferentially downregulate HIF-2α (Bishop et al. 2008), and this result suggests that HIF-2α downregulated *Egln3* expression to positively feedback on its expression. HIF-2α also appeared to subtly regulate other target genes in an oxygen-independent manner, as they differ, to a similar degree, in expression when cultured in both normoxia and hypoxia.

In conclusion, the transcriptomic profiles of HIF-1α and HIF-2α knockout 5TGM1 cells in response to normoxia, acute hypoxia and chronic hypoxia were profiled *in-vitro*. Several HIF-1α and HIF-2α target genes were identified. Of the 66 HIF-1α target genes, 28 of them appear to be novel genes that have not been previously reported in the literature to be regulated in a HIF-1α dependent manner. HIF-1α regulates a broad range of target genes response hypoxia, many of which are involved in glycolysis. In contrast, HIF-2α's function appears to be constitutive, and the effect of HIF-2α loss in 5TGM1 cells is, if any, very subtle.

Chapter 5

Final Discussion and Future Directions

5 Final discussion and future directions

HIF signalling regulates an extensive range of target genes and is a driver of tumorigenesis (Ruan, Song & Ouyang 2009). While its role in solid tumours is extensively studied, it has only recently garnered increased appreciation for its role in driving the development and progression of liquid cancers (Schito, Rey & Konopleva 2017). In MM, disease features like angiogenesis, metastasis and MM PC survival have been linked to the HIFs, which identifies them as potential therapeutic targets (Martin et al. 2011).

The work in this thesis contributes towards addressing the paucity of published data comparing the roles of HIF-1α and HIF-2α in MM, especially of that in *in-vivo* models. An inducible CRISPR/Cas9 vector system was used to generate inducible knockout and constitutively knocked-out HIF-1α and HIF-2α 5TGM1 murine MM cell lines, to study their functions in MM disease. Following characterisation, the transcriptomes of HIF-1α and HIF-2α knockout 5TGM1 cells were profiled by RNA-seq. HIF-1α was identified to mediate acute responses to hypoxia, with prominent roles in metabolic programming, cell-survival and transcriptional regulation, that were sustained in extended hypoxic culture. HIF-2α on the other hand, appears to mediate more subtle roles, consistent with its very low level of expression in the 5TGM1 cells *in-vitro*.

5.1 Immediate future experiments: Further *in-vitro* characterisation of HIF-α knockout 5TGM1 cells

Several experiments can be carried out in the immediate future to further characterise the HIF-1α and HIF-2α knockout 5TGM1 cells. During knockout cell characterisation experiments, there were difficulties in detecting endogenous levels of HIF-2α in 5TGM1 cells. 5TGM1 cells may be expressing very low levels of HIF-2α, which could be a cell line or species specific characteristic, as HIF-2α protein have been reportedly detected in several human MM cell lines by western blot (Martin et al. 2010; Mysore et al. 2016). The commercial α-HIF-2α primary antibody used in this project can detect exogenously expressed mHIF-2α, and this issue could be thus due to the detection limit of the assay rather than antibody reactivity. Further attempts to detect HIF-2α could include performing nuclear extracts to separate and concentrate the nuclear fraction of 5TGM1 cells, together with immunoprecipitation. Successful optimisation of this assay will help identify if HIF-2α protein is constitutively or inducibly expressed in the 5TGM1 cells. Additionally, nuclear extractions can be attempted for further HIF-1α western blot optimisations to identify the localisation of the non-specific band that runs around the same size of the HIF-1α protein. If the non-specific protein is specifically cytoplasmic, it would dramatically improve the quality of the data obtained from western blots.

From qRT-PCR experiments, *Hif-2α* transcript was found to be expressed at very low levels in the 5TGM1 cells and was not induced by hypoxia *in-vitro.* HIF-2α was previously observed to be regulated differently in human LP-1 MM cells, in a hypoxically-inducible and transcriptional (rather than post-translational) manner, whereby both *Hif-2α* mRNA and HIF-2α protein expression were induced after 12 hours in hypoxia (Martin et al. 2010). Instead, a significant induction of *Hif-2α* levels was only observed upon DP treatment for 48 hours, suggesting that *Hif-2α* expression may be predominantly regulated by iron homeostasis than oxygen availability in the 5TGM1 cells. HIF-2α activity has been linked to the regulation of iron homeostasis and erythropoiesis in the kidney, liver and gut (Haase 2013; Renassia & Peyssonnaux 2019; Schwartz et al. 2019).

In MM patients, increased serum hepcidin, a hepatic hormone that blocks ferroportin iron efflux in gut enterocytes and macrophages, contributing to diminished plasma iron levels and anaemia (Maes et al. 2010). About 32% of MM patients was found to have iron deficiency (König et al. 2013). This could potentially induce HIF-2α expression in MM cells. Iron supplementation has been reported to sensitize human MM cell lines and primary MM PCs to Bortezomib treatment (Campanella et al. 2013). Thus, further experiments to investigate the effect of iron availability on Hif-2α expression on 5TGM1 cells can include qRT-PCR experiments on 5TGM1 cells treated with various iron chelating agents (like DP and deferoxamine) as well as iron supplementation.

The phenomenon of genetic compensation, whereby a gene knockout upregulates the expression of related genes, has been documented in many animal models and cells lines (El-Brolosy & Stainier 2017). The conditional deletion of HIF-1α in long term HSCs has been reported to strongly upregulate the *Epas1* transcript expression, by around 120 fold (Kocabas et al. 2012). While *Epas1* transcript was undetected in all samples from the RNA-seq, including the HIF-1α knockout 5TGM1 cells, it would be of interest to validate the absence of knockout compensation in these cells. Future experiments can include comparing HIF-1α and HIF-2α mRNA and protein levels in both HIF-1α and HIF-2α knockout 5TGM1 cells by qRT-PCR and western blot.

Furthermore, it would be valuable to perform follow up experiments and confirm several observations from the RNA-seq by qRT-PCR, especially for the genes associated with HIF-2α. While the read depth used for this RNA-seq experiment (30 million reads) is, by rule of thumb, enough for differential expression studies, it was insufficient to detect very lowly expressing transcripts like *Epas1* and its many of its potential target genes*.* A higher sequencing depth would better capture higher transcriptome diversity but would result in higher costs and increased data noise (Tarazona et al. 2011). Therefore, future experiments can include qRT-PCR to measure the relative transcript quantity of the HIF-2α target genes to confirm that HIF-2α regulates them. It would be of interest to confirm the negative regulation of *Egln3* by HIF-2α, which can positively feedback on HIF-2α expression by reducing its degradation. Also, qRT-PCR quantitation

of HIF-2α target gene expression can also be performed on the HIF-2α overexpression 5TGM1 cell lines previously generated by N. Martin, to verify that they are indeed HIF-2α targets.

The RNA-seq data indicates that glycolytic genes are strongly upregulated by HIF-1α in response to hypoxia, but the metabolic profile of 5TGM1 cells is not yet known. This can be determined by Seahorse live-cell metabolic assay (TeSlaa & Teitell 2014). By measuring the oxygen consumption and extracellular acidification of 5TGM1 cells in DMSO and DP treated (pseudohypoxia) cells, the levels of oxidative respiration and glycolysis can be determined in these cells. This will help identify if 5TGM1 display the Warburg effect (aerobic glycolysis), or if they switch from an oxidative phenotype to a glycolytic one depending on oxygen levels. Also, assaying HIF-1α and HIF-2α knockout cells can also help identify if either HIF-α isoform, especially HIF-1α, is the major driver for metabolic reprogramming of 5TGM1 cells in response to BM hypoxia.

Live-cell luciferase assays should be performed on the knockout cell lines to verify their luciferase activity. In some instances, the expression of virally integrated genes has been found to be completely lost or gradually reduced over time due to epigenetic silencing (Yao et al. 2004). While luciferase assays have been performed on the HIF-1α and HIF-2α lines to ensure that they retained luciferase activity, they were not quantitative and performed on cell lysates which may not be representative of how they would be used for *in-vivo* bioluminescence imaging. Thus, before conducting *in-vivo* experiments, the luciferase activity of these generated cell lines should have to be measured on the Xenogen IVIS, which is the same system used for live imaging. Since multiple knockout lines were generated, cells with similar luciferase levels can be subsequently pooled for animal experiments to ensure consistent reporter activity between them.

The use of mouse models in cancer studies recapitulates the intricate interactions between tumour cells and its surrounding microenvironment. However, despite sharing highly similar anatomies, mice and humans have subtle differences in their physiology and tissue architecture, which could yield different phenotypic outcomes in response to

cancer-causing genetic alterations (Rangarajan & Weinberg 2003). Thus, as research carried out on mouse models are only predictive of human response, it is crucial to determine if similar outcomes can be achieved in humans. Therefore, it would be of interest to generate HIF-1α and HIF-2α knockouts in human MM cell lines, to study if the findings from the transcriptomic analysis of HIF-1α and HIF-2α knockout 5TGM1 cells can be repeated in the human cells. The hypoxic induction of both HIF-1α HIF-2α expression in the LP-1 human MM cell line have been previously reported, and thus would be a suitable candidate cell line for future knockout experiments (Martin et al. 2010). Identifying the similarities and differences between the hypoxic response in human and mouse MM cell lines would help in evaluating the significance of findings from animal experiments, and how relevant these findings would be in the context of human disease.

5.2 Future *in-vivo* experiments

5TGM1 cells were derived from, and are syngeneic with, the C57BL/KaLwRij mouse model (Hu et al. 2012). *In-vivo* experiments with the generated HIF-1α and HIF-2α knockout cell lines are planned for the near future. Initial experiments can be performed by the intratibial injection of HIF-1α and HIF-2α knockout 5TGM1 cells into young KaLwRij mice to assess the effects of HIF-1α and HIF-2α knockouts on the tumour development and progression. Although *Hif-2α* does not appear to be significantly induced by hypoxia *in-vitro*, the more complex interactions in the BM microenvironment *in-vivo* may result in higher and/or inducible levels of HIF-2α. Thus, HIF-2α may play more important roles in the BM microenvironment that is not reflected in *in-vitro* culture, which warrants further investigation in animal models.

The different measurable aspects of disease progression in the KaLwRij mice can be assessed by several methods. Firstly, tumour growth and metastasis can be visualised weekly by live *in-vivo* bioluminescence imaging on the Xenogen IVIS. Indirect measures of tumour burden can be performed by weekly paraprotein quantification on isolated peripheral blood samples. The degree of tumour angiogenesis can be determined on bone sections by IHC, staining for angiogenic markers like CD34^{+} and VEGF, while bone osteolysis can be assessed on fixed long bones by microCT. This experiment will provide insight into how the different HIF-α isoforms contribute to establishing and supporting MM disease in the BM microenvironment in the 5TGM1/KaLwRij model. Additionally, these experiments can be repeated with the inducible HIF-1α and HIF-2α knockout 5TGM1 cells, to allow tumours to develop normally before studying the effects of HIF-1α and HIF-2α knockouts at any time of disease progression.

Further *in-vivo* experiments can include the intravenous inoculation of HIF-1α and HIF-2α knockout 5TGM1 cells into young KaLwRij mice to assess the effects of HIF-1α and HIF-2α knockout on 5TGM1 cell homing to the BM. Following a short time to allow homing to occur, the tibial BM can be harvested by flushing cells using a syringe into

sterile media. The number of cells that successfully migrate into the BM can be quantified by flow cytometry. Given the use of pooled monoclonal lines, each with a unique genetic identify, analysis of the isolated cells can explore the occurrence of clonal selectivity in bone marrow tumours.

It would also be informative to relate the obtained RNA-seq results with the various measurable features of disease progression in this MM mouse model, to formulate hypotheses before carrying out the animal experiments. Previous preliminary animal experiments by N. Martin with HIF-2α knockout 5TGM1 cells indicated that the loss of HIF-2α function may delay tumour growth and reduce tumour burden (Martin 2018).

5TGM1 cells exhibit bone tropism in the KaLwRij mouse model and thus would need to alter cellular metabolism to adapt to hypoxia in the BM microenvironment. The majority of HIF-1α regulated genes in 5TGM1 cells were identified to be involved in glycolysis and glucose metabolism, consistent with HIF-1α being a major metabolic re-programmer in response to hypoxia. Given the limited oxygen available for oxidative phosphorylation in the BM microenvironment, glycolysis is presumably an important source of ATP for MM PCs. Several human MM cell lines, like RPMI8226 and JJN3, are reliant on aerobic glycolysis, as glycolytic inhibition by dichloroacetate treatment induces apoptosis and inhibits their proliferation (Sanchez et al. 2013). The suppression of HIF-1α in the subcutaneous xenograft of JJN3 cells in SCID-NOD mice have been previously shown to reduce the development in the size and weight of plasmacytomas (Storti et al. 2013). In the context of other blood cancers, glycolytic inhibition using the HKII inhibitor 3-bromopyruvate have been previously shown to increase levels of cell death under hypoxic conditions in HL-60 human leukemia cells and Raji human lymphoma cells (Xu et al. 2005). Therefore, it is expected that HIF-1α knockout in the 5TGM1 cells would slow down or inhibit tumour growth in the KaLwRij mouse model, that would be observed as a delayed detection and reduced intensity of bioluminescence signal during live luciferase imaging. Additionally, the reduced tumour burden will also be reflected as a reduction in the levels of circulating paraprotein.

HIF-2α has been implicated in promoting human MM cell metastasis, by stimulating MM PC egress from the bone marrow through the regulation of the CXCL12/CXCR4 and CCL3/CCR1 cytokine axes (Vandyke et al. 2017). CXCR4 is thought to detect the retention signal by CXCL12, and CCR1 induces migration towards high levels of CCL3 in the peripheral blood. However, the mechanisms controlling 5TGM1 cell dissemination may be different from that in human disease. From the RNA-seq, 5TGM1 cells were found to highly express *Cxcr4* but do not express *Ccr1*, similar to that previously reported by the Zannettino laboratory (Opperman et al. 2019). The levels of *Cxcr4* in the 5TGM1 cells did not decrease in exposure to chronic hypoxia, suggesting it may not be hypoxically regulated in these cells. 5TGM1 cells also do not express detectable *Cxcl12*, which is thought to be a driver of bone osteolysis (Diamond et al. 2009; Zannettino et al. 2005). Moreover, IGF-1R has been identified as a mediator of 5TGM1 cell homing and retention in response to IGF-1 expressed by BM macrophages (Opperman et al. 2019). Hypoxic treatment of 5TGM1 cells does not affect *Igf-1r* transcript levels, which suggests that hypoxia does not abrogate this retention signalling axis. It would thus be valuable to identify if HIF-2α knockouts affect the ability of 5TGM1 cells to metastasize in the intratibial syngeneic KaLwRij mouse model, by monitoring for the establishment of tumours in the contralateral tibia. This information would help determine if further interrogation of other receptor signalling pathways is required for 5TGM1 cells, to determine novel hypoxia-regulated pathways for MM cell dissemination and metastasis.

As an angiogenic switch is associated with malignant and symptomatic MM disease progression, the HIFs are thought to play a role in stimulating increased BM angiogenesis (Giuliani et al. 2011; Manier et al. 2012; Vacca et al. 1994). However, from RNA-seq data, HIF's roles in regulating the expression of pro-angiogenic genes in the 5TGM1 cells are somewhat unclear. From analysis, no proangiogenic genes were identified to be HIF-1α or HIF-2α specific, and only *Angptl6* was identified to be upregulated in a HIF-1α independent manner in response to hypoxia. 5TGM1 cells were found to express high levels of *Vegfa* transcript in normoxia, that increases in exposure to hypoxia. Knocking out either HIF-1α and HIF-2α did not have a significant effect on its upregulation, suggesting that it is controlled by a combination of multiple factors. While

206

the HIFs, especially HIF-1α, are well accepted to be major angiogenic regulators in many cancers including MM (Giuliani et al. 2011), their role in regulating the expression of proangiogenic genes in 5TGM1 cells appear to be less pronounced. The knockdown of HIF-1α in subcutaneously engrafted and intratibially injected JJN3 human MM cells in SCID-NOD mice are reported to result in reduced tumour angiogenesis (Storti et al. 2013), but it is unclear if these observations are due to the reduced HIF-1α regulated expression of pro-angiogenic molecules, slower tumour growth and subsequent reduced need for higher oxygen delivery, or a combination of both factors. For future 5TGM1 *in-vivo* experiments, HIF-1α and HIF-2α knockouts are both hypothesized to have reduced blood vessel formation when measured by IHC, but the mechanisms affecting this may require further investigation.

Potential future experiments should also include the transcriptomic analysis of 5TGM1 tumours developed in KaLwRij mice to complement the *in-vitro* RNA-seq data that have been generated for the 5TGM1 cells. In the BM, 5TGM1 cells would interact with and receive stimuli from the many other BM residents, which is unlike the static hypoxic conditions *in-vitro*. It has been suggested that the transcriptome of cancer cells may vary depending on the culture method. For example, it had been observed that mouse mammary carcinoma cells in a monolayer culture had enriched gene pathways for cell growth, cell cycle progression and protein synthesis, but when grown *in-vivo* had enriched gene pathways for migration, inflammation and angiogenesis (Hum et al. 2019). Differences in *in-vitro* and *in-vivo* transcriptomes have also been reported for other cell types, such as human bladder cancer cells and bovine blastocysts (Driver et al. 2012; Ord et al. 2005). HIF-α knockout and control 5TGM1 cells can be isolated from the BM at any point of disease progression by FACS, and their RNA can be extracted *ex-vivo.* By using RNA-seq, their transcriptomes can be profiled and analysed to identify HIF-α isoform-specific changes in gene expression in the hypoxic BM microenvironment, which can be compared against the data generated for the 5TGM1 cells cultured in hypoxia *in-vitro*. In addition to the comparative analysis between 5TGM1 exposure to artificial hypoxia and the physiological hypoxia of the BM microenvironment, hypoxically regulated genes can also be identified for different stages of MM disease progression in

the 5TGM1/KaLwRij model. This would potentially identify important HIF-regulated pathways that can help promote and drive MM disease progression, which can be further investigated.

Overall, while the 5TGM1/KaLwRij mouse model recapitulates most human MM disease symptoms, there may be some differences in the mechanisms driving disease progression and development. In the 5TGM1 cells, HIF-1α appears to be important in hypoxic cell survival, mediating metabolic reprogramming to enable cellular adaptation to limited oxygen availability. Thus, this model appears suitable for investigating metabolic disruption, using glycolytic or HIF-1α inhibitors, as potential therapy for MM patients. Although RNA-seq data indicates that HIF-2α mediates subtle transcriptional roles in the 5TGM1 cells, it may still be important in supporting the establishment and development of MM disease within the complex BM microenvironment in an *in-vivo* system (Martin 2018). But given the greater breadth of HIF-1α regulation as compared to HIF-2α, disrupting HIF-1α appears to be potentially a more effective therapeutic strategy for the treatment of MM disease.

5.3 HIF-inhibitor experiments

Despite advancements in treatment therapies contributing to increased median patient survival, MM still remains an incurable disease (Kumar et al. 2014). MM is recognised as a genetically heterogenous disease at clinical, cytogenic and molecular levels (Corre, Munshi & Avet-Loiseau 2015), so the identification and development of treatments that target common disease features appears to be a promising research strategy. A notable example is the recently approved (July 2019) selective inhibitor Selinexor which binds to exportin 1 and blocks nuclear export (Gandhi et al. 2018). Nuclear transport is a fundamental system in cells for intracellular signalling, and is often co-opted in cancer to prevent apoptotic and cell cycle signals from being transported into the nucleus (Senapedis, Baloglu & Landesman 2014). This drug is approved as a drug of last resort for the treatment of patients with relapsed or refractory MM, who do not respond to 4 or more different therapies (quad- or penta- refractory MM) (Chim et al. 2018).

As the BM microenvironment is well accepted to be physiologically hypoxic, the HIFs represent potential therapeutic targets for treating MM disease (Murugesan et al. 2018; Semenza 2003). It would be of interest to pre-clinically evaluate HIF-α inhibitors in the 5TGM1/KaLwRij model. This would contribute towards the rationale for clinically investigating the repurposing of HIF inhibitors for the treatment of MM disease. Examples of inhibitors that can be evaluated are the HIF-1α specific RNA antisense oligonucleotide EZN-2968 and the HIF-2α specific small molecule inhibitor PT2385, which are both in the clinical stages of development. EZN-2968 has recently completed a phase 1b clinical trial in previously treated adult hepatocellular carcinoma patients to evaluate its potential clinical benefit and safety, where it was reported to reduce *Hif-1α* transcript expression at a tolerated dose of 10 mg/kg (Wu et al. 2019). PT2385 was evaluated in a phase 1 dose escalation trial in previously treated advanced clear cell RCC patients, and was reported to have a favourable safety profile and activity (Courtney et al. 2018). These drugs could be tested on the 5TGM1/KaLwRij model to determine if the

use of selective HIF-α inhibitors could potentially delay MM progression and reduce tumour burden.

5.4   Concluding remarks

As the major mediators of cellular transcriptional responses to hypoxia, the HIFs are potential therapeutic targets for the treatment of cancers. HIF isoform-specific inhibitors are currently being developed and tested in the clinic, and it would be valuable to evaluate if they can be repurposed for MM treatment. The work in this thesis was performed to develop HIF-1α and HIF-2α inducible knockout and knocked-out 5TGM1 cell lines that are syngeneic with the KaLwRij mouse model, as well as to identify HIF-1α and HIF-2α target genes in the 5TGM1 cells by transcriptomic analysis. It was found that HIF-1α mediates a broad range of transcriptomic responses to hypoxia in the 5TGM1 cells, with a major role in metabolic reprogramming through the upregulation of pro-glycolytic genes. HIF-1α also notably regulates genes associated with apoptosis, further transcriptional regulation and cytoskeletal modification. On the other hand, HIF-2α mediates more subtle roles and may possibly have a constitutive function in the 5TGM1 cells. These data, and future experiments to be carried out with the generated HIF-α knockout cells, would contribute towards our understanding of the shared and unique roles of HIF-1α and HIF-2α in MM, as well as provide support for the rationale to pre-clinically evaluate the efficacy of HIF isoform-specific inhibitors for the treatment of MM disease. Overall, the development of targeted and more efficacious therapies would optimistically lead to improved patient survival, prognoses and disease outcomes.

Chapter 6

Appendices

6 Appendices

A
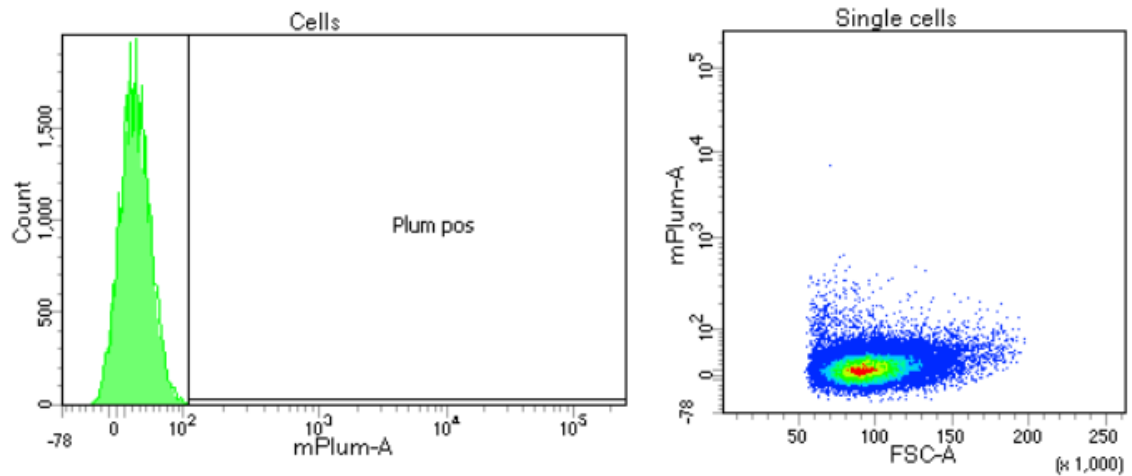
B
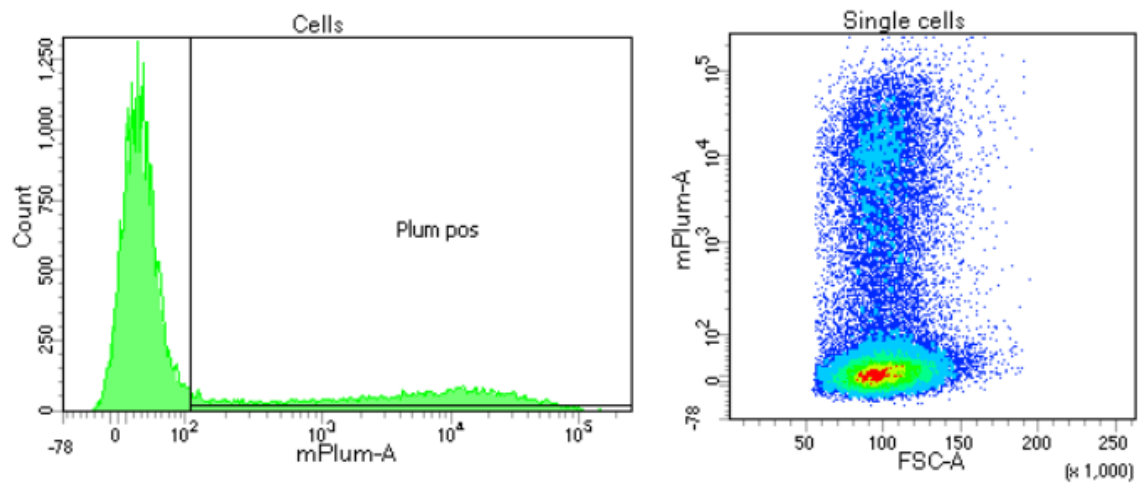
Figure 6.1: mPlum⁺ activity detected in FgH1tUTP transiently transfected HEK293T cells. (A) Control and **(B)** FgH1tUTP transfected HEK293Ts were analysed on the BD FACSAria™ Fusion. Cells were transfected using Lipofectamine-2000.
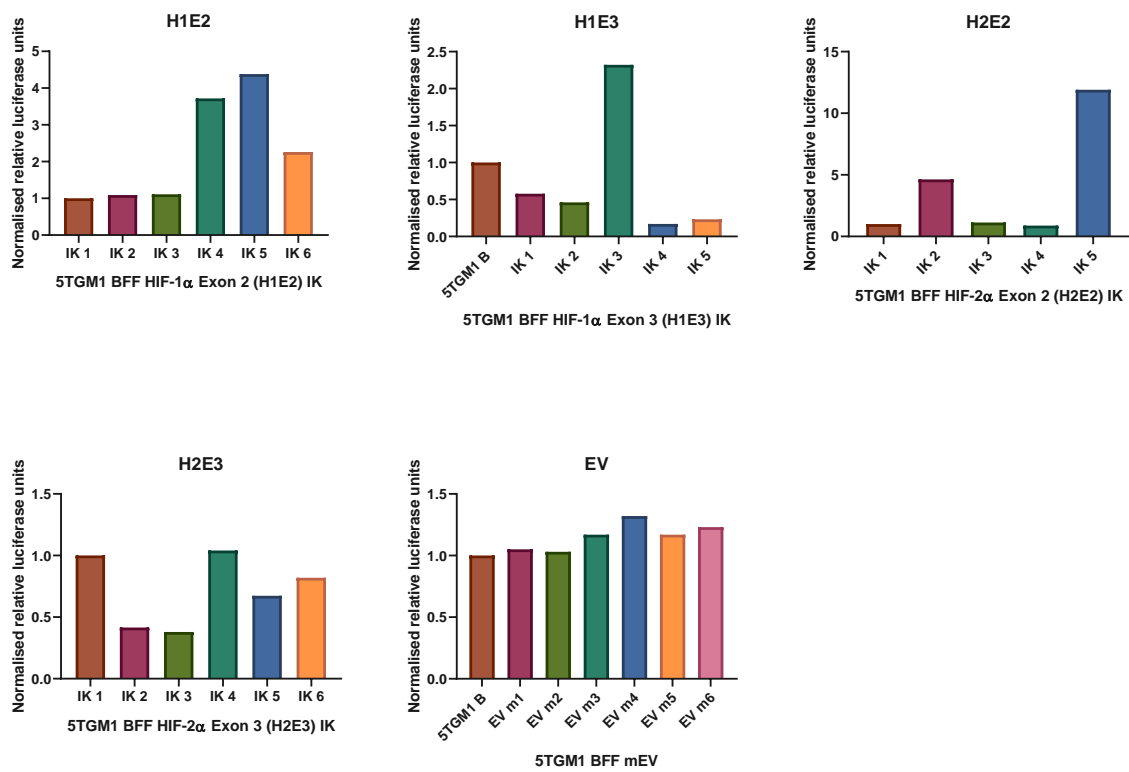
Figure 6.2: 5TGM1 monoclonal inducible knockout cells retain firefly luciferase activity.
Firefly luciferase activity was measured using the GloMax® 96 Microplate luminometer
on cell lysates. Data presented as relative luciferase units normalised against cell
number. n=1.

A
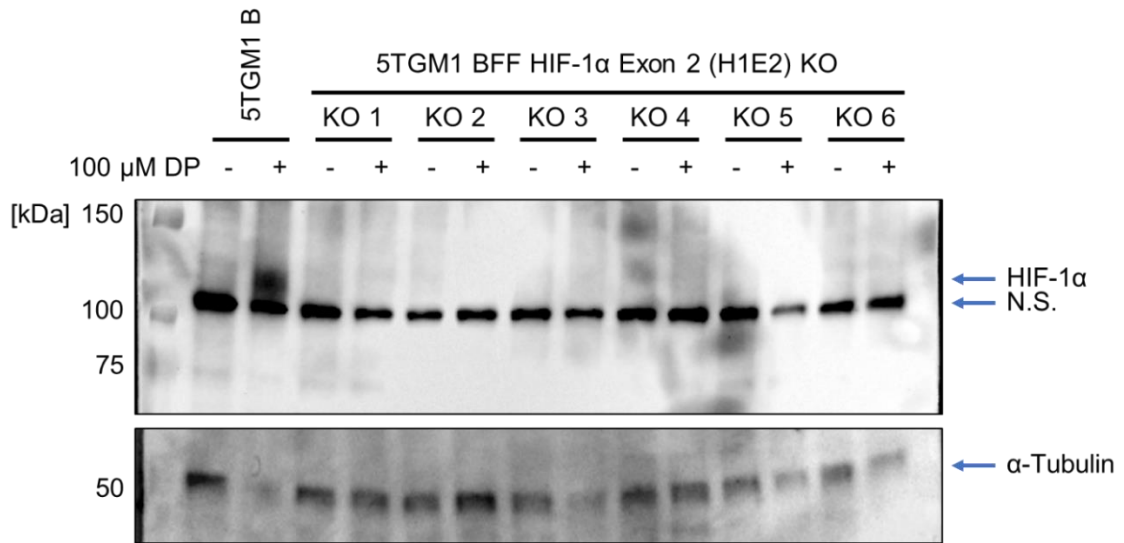
B
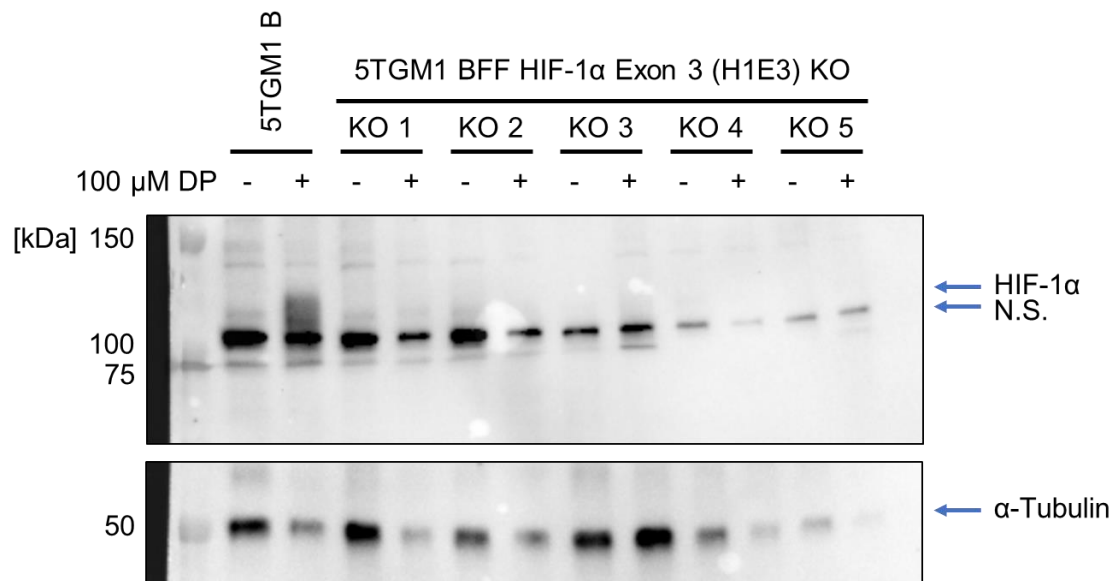
Figure 6.3: Second independent biological replicates for HIF-1α protein expression in DP treated HIF-1α knockout 5TGM1 cells. Representative western blots presented in Figure 3.12. Control 5TGM1 B, and HIF-1α knockout **(A)** 5TGM1 BFF H1E2 KO and **(B)** 5TGM1 BFF H1E3 KO cells were treated with 100 µM of the hypoxia mimetic DP (+) or with an equivalent amount of DMSO (-) for 16 hours, and whole cell lysates were extracted using RIPA buffer. Equivalent protein amounts were run on a 7.5% SDS-PAGE

gel and transferred onto a nitrocellulose membrane and probed for HIF-1α protein expression. α-Tubulin was used as a loading control. Blots shown are one of N=2 biological replicates. HIF-1α, NB100-449, 1:1 000; α-Tubulin, NB600-506, 1:1 000. N.S., non-specific.
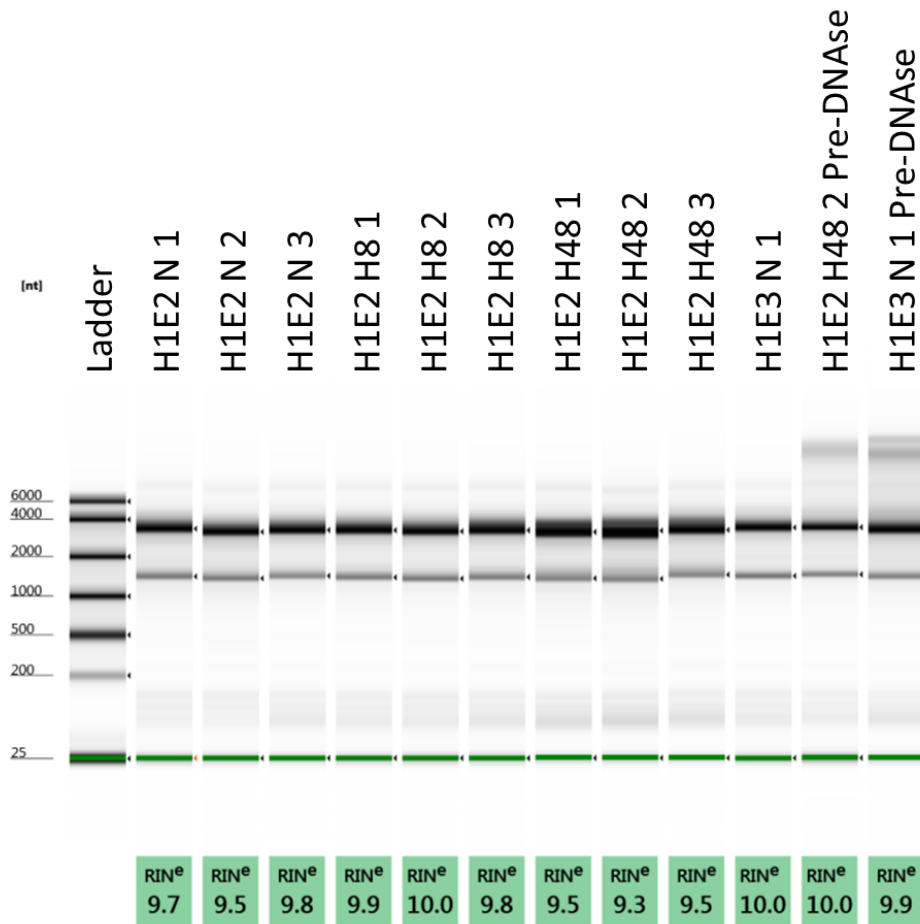
Figure 6.4: RNA samples submitted for RNA-seq are of good quality. RNA quality was measured by automated electrophoresis on the 2200 TapeStation. Lanes 2 to 10 are DNase-treated RNA for 10 out of 45 submitted samples. DNase treatment reduces the intensity of bands above the 28s ribosomal band, consistent with the reduction in DNA contamination.

6.1   QC assessment for RNA-seq

Read quality was assessed using FastQC (Ward, To & Pederson 2018), and the overall quality of the RNA-seq data was deemed acceptable. While all samples passed 6 out of the 11 modules, the remaining 2 and 3 were assigned 'fail' and 'warning' flags, respectively, for potential issues (Figure 6.5). However, the parameters for which FastQC assigns these flags are calibrated for gDNA shotgun sequencing, and these flagged modules were thus re-examined in the context of RNA-seq according to the FastQC Help website (*Index of /projects/fastqc/Help* n.d.).

All samples had 'fail' flags for the *Per base sequence content* and *Sequence duplication level* modules and were examined first. For *Per base sequence content,* all samples did not have a uniform distribution of nucleotides for their first 12-13 sequenced bases (Figure 6.6A). This inconsistent distribution is almost always observed in RNA-seq libraries, due to the fragmentation bias introduced by most commercial library kits(Hansen, Brenner & Dudoit 2010). The random priming during the cDNA synthesis step is bias-prone, as it favours certain random hexamers (not wholly random priming) (Hansen, Brenner & Dudoit 2010). Regardless, most RNA-seq libraries do not show strong locational biases within a transcript, and any artefacts should cancel themselves out during differential analysis. Secondly, the failed *Sequence duplication level* module indicates a lack of diversity in the sequenced library. About 60% of reads were identified as duplicates (Figure 6.7). However, cellular transcripts usually are present in a wide range of expressed levels and given the sequencing depth required to detect lowly expressed transcripts, over-sequencing of highly expressed transcripts occurs which appears as duplicated reads. To account for this, differential analysis was performed on both duplicated and de-duplicated counts to assess if they have any substantial impact on the analysis performed.

With all 'fail' modules manually checked and deemed of acceptable quality, modules with 'warning' flags were next examined. Sample 27 had a warning for *Per sequence GC content*, but on closer inspection appeared to have a mean GC content that is normally distributed, similar to the expected theoretical distribution (Figure 6.6B). Next, Warning

flags for *Sequence length distribution* indicated the presence of sequences of different lengths and was safely ignored because certain sequencing platforms, including the NextSeq, generates some reads of different lengths. Also, most sequences obtained were of the expected length (75/76 nt). Lastly, samples 11, 13, 14, 15 and 16 had moderately overrepresented (0.1 to 0.7%) sequences but were identified as possible adapter sequences and were highly unlikely to be contaminants. Hence all modules with 'warning' flags were also deemed of acceptable quality after being manually checked. Together, these checks confirm the acceptable quality of all the samples for subsequent analyses.
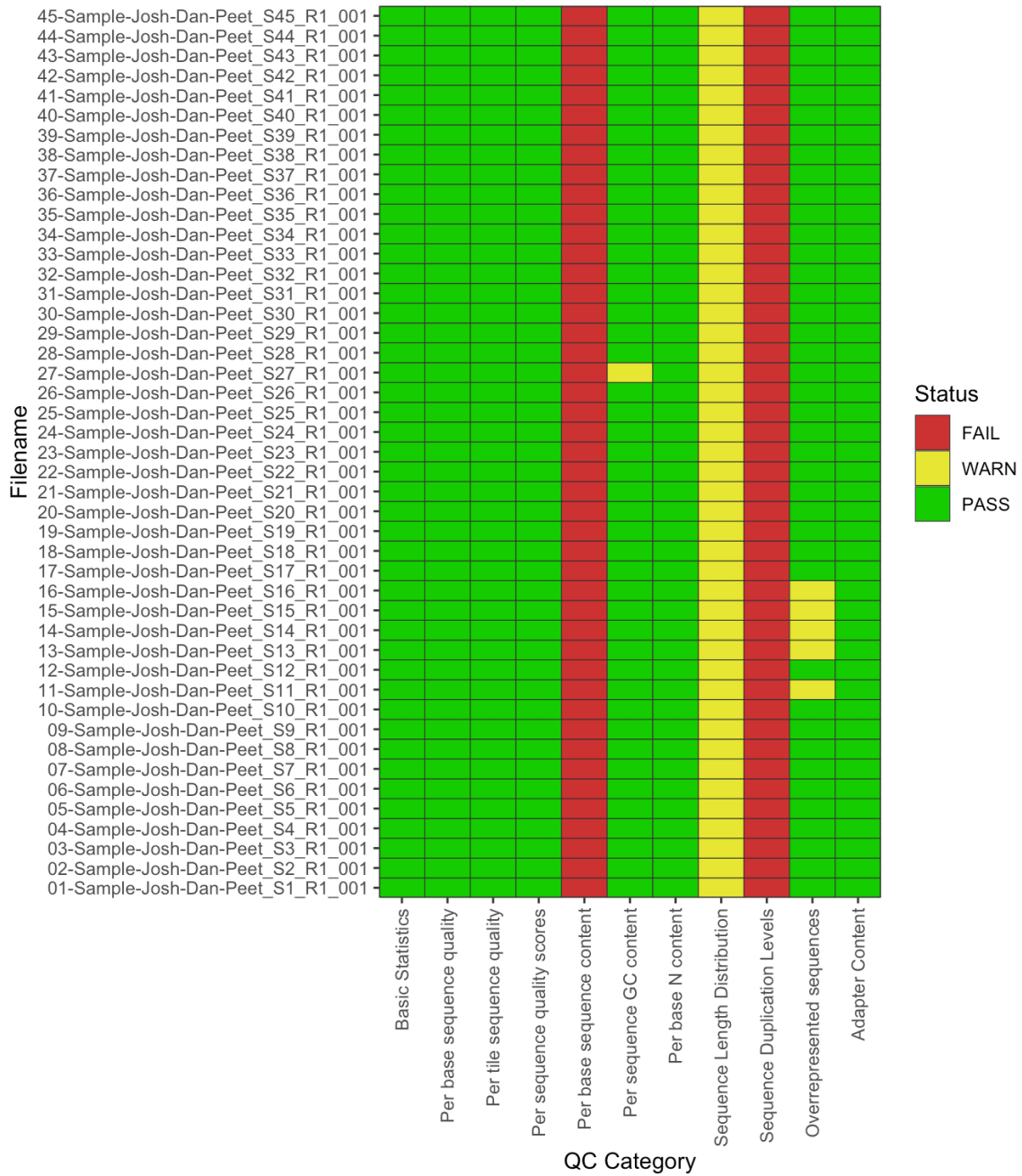
Figure 6.5: Result summary of FastQC quality control performed on all RNA-seq samples. Sample numbers are as listed in Results 2, Table 4.1. Plot generated using ngsReports(Ward, To & Pederson 2018).

A
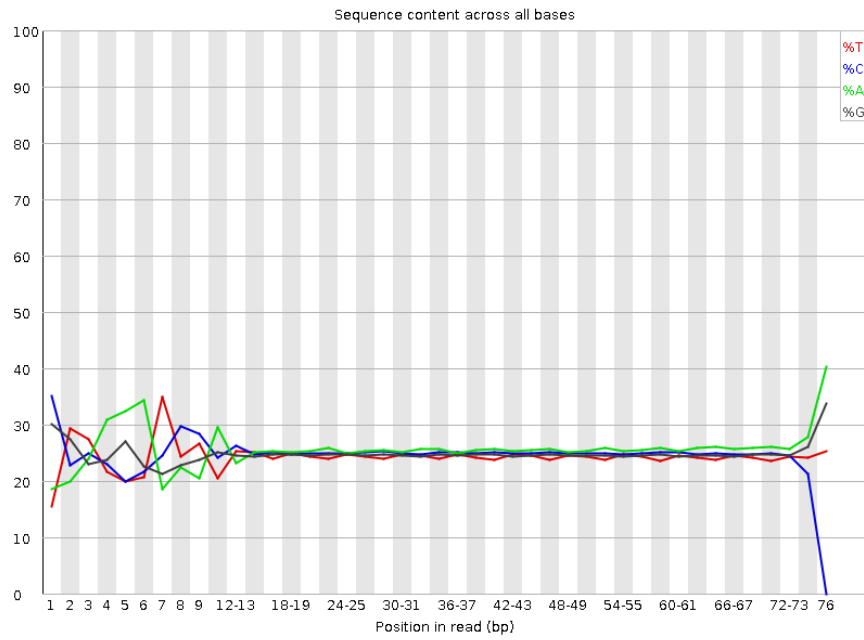
B
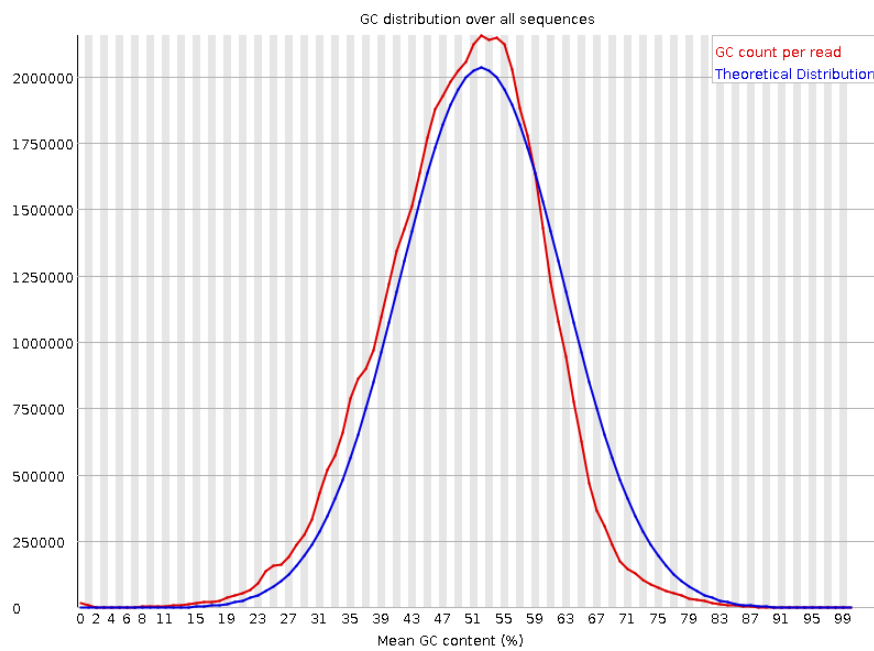
Figure 6.6: Flagged modules from FastQC analysis. (A) Per base sequence content plot

with bias in nucleotide content for the first 12-13 bp. Uniform sequence content after

the first 12-13 bp is discerned as parallel lines across all four nucleotides. Representative

plot (sample 1) shown, and a similar bias was observed in all other samples. **(B)** Per sequence GC content for sample 27 (red curve) in comparison to a theoretical normal distribution (blue curve).
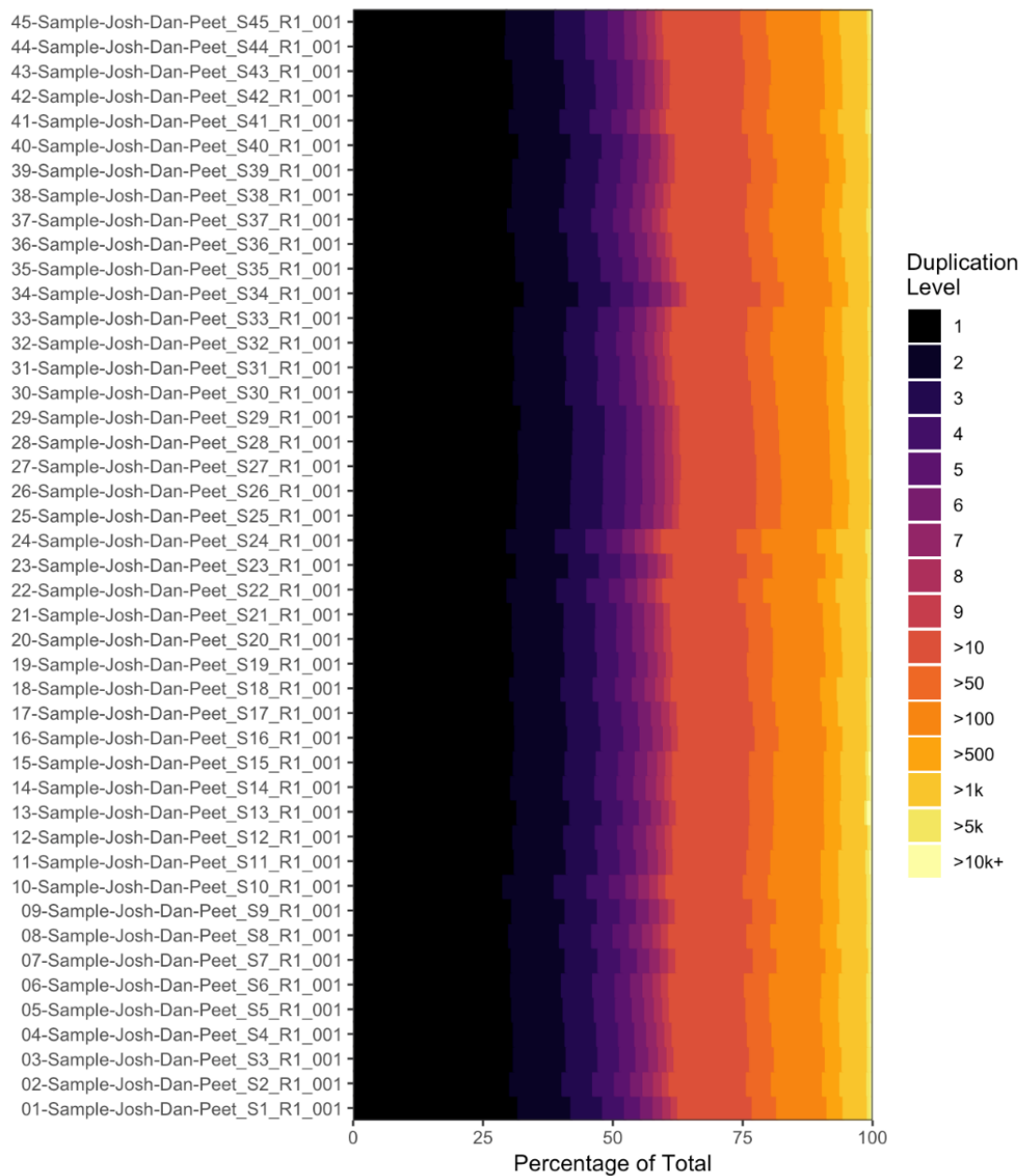
Figure 6.7: Proportion of duplicated reads in RNA-seq samples. Sample numbers are as listed in Results 2, Table 4.1. Plot generated using ngsReports(Ward, To & Pederson 2018).

Table 6.1: Top 10 DEGs between treatments for HIF-1α Exon 2 KO 5TGM1 cells, ranked by FDR.

HIF-1α Exon 2 KO

Comparison	#	GeneID	GeneName	logFC	FDR	Associated function
Hypoxia 8h Vs Normoxia 8h	1	ENSMUSG00000047492	*Inhbe*	1.64E+00	3.23E-03	Hormone regulation
	2	ENSMUSG00000028179	*Cth*	1.48E+00	3.94E-03	Cystine biosynthesis
	3	ENSMUSG00000027737	*Slc7a11*	1.33E+00	6.07E-03	Cysteine/Glutamate transport
	4	ENSMUSG00000032715	*Trib3*	1.80E+00	3.39E-02	Protein kinase regulator
Hypoxia 48h vs Normoxia 8h	1	ENSMUSG00000047492	*Inhbe*	3.08E+00	2.52E-12	Hormone regulation
	2	ENSMUSG00000028179	*Cth*	2.71E+00	2.52E-12	Cystine biosynthesis
	3	ENSMUSG00000027737	*Slc7a11*	2.13E+00	1.23E-11	Cysteine/Glutamate transport
	4	ENSMUSG00000028838	*Extl1*	3.06E+00	3.26E-11	Glycosyltransferase
	5	ENSMUSG00000020108	*Ddit4*	2.30E+00	1.00E-10	Apoptosis, mTOR signalling
	6	ENSMUSG00000032715	*Trib3*	3.64E+00	1.00E-10	Protein kinase regulator
	7	ENSMUSG00000020395	*Itk*	3.90E+00	1.20E-10	Tyrosine kinase
	8	ENSMUSG00000035504	*Reep6*	1.81E+00	3.01E-09	Receptor transport
	9	ENSMUSG00000027313	*Chac1*	1.74E+00	5.42E-09	Apoptosis, unfolded protein response
	10	ENSMUSG00000028893	*Sesn2*	1.56E+00	7.53E-09	Metabolic homeostasis
Hypoxia 48h Vs Hypoxia 8h	1	ENSMUSG00000020395	*Itk*	2.30E+00	1.42E-06	Tyrosine kinase
	2	ENSMUSG00000028838	*Extl1*	1.82E+00	3.78E-06	Glycosyltransferase
	3	ENSMUSG00000040258	*Nxph4*	2.06E+00	1.98E-05	Signalling molecule

4	ENSMUSG00000032715	*Trib3*	1.84E+00	4.08E-05	Protein kinase regulator
5	ENSMUSG00000047492	*Inhbe*	1.44E+00	3.25E-04	Hormone regulation
6	ENSMUSG00000041642	*Kif21b*	1.48E+00	5.60E-04	Kinesin motor protein
7	ENSMUSG00000049422	*Chchd10*	1.75E+00	3.84E-03	Mitochondrial cytochrome activity
8	ENSMUSG00000056749	*Nfil3*	1.93E+00	5.27E-03	Transcriptional regulator
9	ENSMUSG00000018166	*Erbb3*	1.53E+00	1.24E-02	Receptor tyrosine kinase
10	ENSMUSG00000025203	*Scd2*	1.42E+00	1.53E-02	Cytokinesis

Table 6.2: Top 10 DEGs between treatments for HIF-1α Exon 3 KO 5TGM1 cells, ranked by FDR.

HIF-1α Exon 3 KO

Comparison	#	GeneID	GeneName	logFC	FDR	Associated function
Hypoxia 48h vs Normoxia 8h	1	ENSMUSG00000032715	*Trib3*	2.89E+00	1.54E-10	Protein kinase regulator
	2	ENSMUSG00000020395	*Itk*	3.51E+00	1.54E-10	Tyrosine kinase
	3	ENSMUSG00000028179	*Cth*	2.29E+00	2.85E-10	Cystine biosynthesis
	4	ENSMUSG00000035504	*Reep6*	1.75E+00	1.86E-09	Receptor transport
	5	ENSMUSG00000047492	*Inhbe*	2.55E+00	1.90E-09	Hormone regulation
	6	ENSMUSG00000028838	*Extl1*	2.44E+00	6.31E-09	Glycosyltransferase
	7	ENSMUSG00000027737	*Slc7a11*	1.96E+00	8.68E-09	Cysteine/Glutamate transport
	8	ENSMUSG00000004698	*Hdac9*	2.98E+00	8.96E-08	Histone deactylase
	9	ENSMUSG00000041444	*Arhgap32*	2.10E+00	8.96E-08	GTPase regulation
	10	ENSMUSG00000044037	*Als2cl*	2.54E+00	8.96E-08	Endosome organisation
Hypoxia 48h Vs Hypoxia 8h	1	ENSMUSG00000020395	*Itk*	2.29E+00	3.67E-07	Tyrosine kinase
	2	ENSMUSG00000004698	*Hdac9*	2.48E+00	1.07E-05	Histone deactylase
	3	ENSMUSG00000032715	*Trib3*	1.62E+00	1.01E-04	Protein kinase regulator
	4	ENSMUSG00000044037	*Als2cl*	1.93E+00	1.01E-04	Endosome organisation
	5	ENSMUSG00000047492	*Inhbe*	1.66E+00	1.01E-04	Hormone regulation
	6	ENSMUSG00000021624	*Cd180*	-1.75E+00	4.96E-04	Innate immunity
	7	ENSMUSG00000037685	*Atp8a1*	1.40E+00	6.98E-03	Phospholipid translocation

8	ENSMUSG00000028838	*Extl1*	1.46E+00	6.98E-03	Glycosyltransferase
9	ENSMUSG00000086324	*Gm15564*	-1.95E+00	1.19E-02	LncRNA
10	ENSMUSG00000076258	*Gm23935*	-2.00E+00	3.20E-02	LncRNA

Table 6.3: Top 10 DEGs between treatments for HIF-2α Exon 2 KO 5TGM1 cells, ranked by FDR.

HIF-2α Exon 2 KO

Comparison	#	GeneID	GeneName	logFC	FDR	Associated function
Hypoxia 8h Vs Normoxia 8h	1	ENSMUSG00000078566	*Bnip3*	4.67E+00	7.59E-11	Apoptosis
	2	ENSMUSG00000028645	*Slc2a1*	2.39E+00	5.88E-10	Glucose transport
	3	ENSMUSG00000063229	*Ldha*	1.73E+00	1.48E-08	Glycolysis
	4	ENSMUSG00000020108	*Ddit4*	3.17E+00	1.20E-07	Apoptosis, mTOR signalling
	5	ENSMUSG00000050914	*Ankrd37*	3.24E+00	1.26E-07	
	6	ENSMUSG00000031987	*Egln1*	1.87E+00	1.28E-07	HIF-α regulation
	7	ENSMUSG00000000628	*Hk2*	1.50E+00	1.38E-07	Glycolysis
	8	ENSMUSG00000111394	*Gm49759*	1.80E+00	1.38E-07	LncRNA
	9	ENSMUSG00000053470	*Kdm3a*	1.55E+00	1.38E-07	Histone demethylase
	10	ENSMUSG00000032114	*Slc37a4*	1.95E+00	4.45E-07	Glucose transport
Hypoxia 48h vs Normoxia 8h	1	ENSMUSG00000078566	*Bnip3*	5.80E+00	1.38E-12	Apoptosis
	2	ENSMUSG00000063229	*Ldha*	2.32E+00	3.98E-12	Glycolysis
	3	ENSMUSG00000028645	*Slc2a1*	2.82E+00	7.13E-12	Glucose transport
	4	ENSMUSG00000021196	*Pfkp*	2.86E+00	8.86E-12	Glycolysis
	5	ENSMUSG00000023456	*Tpi1*	2.34E+00	8.86E-12	Glycolysis
	6	ENSMUSG00000021831	*Ero1l*	4.02E+00	1.21E-11	Apoptosis, electron transport
	7	ENSMUSG00000062070	*Pgk1*	2.62E+00	1.21E-11	Glycolysis

8	ENSMUSG00000036427	*Gpi1*	2.46E+00	1.74E-11	Glycolysis
9	ENSMUSG00000020108	*Ddit4*	4.67E+00	1.94E-11	Apoptosis, mTOR signalling
10	ENSMUSG00000025791	*Pgm1*	2.38E+00	3.36E-11	Glucose metabolism

Hypoxia 48h Vs Hypoxia 8h	1	ENSMUSG00000078566	*Bnip3*	5.80E+00	1.38E-12	Apoptosis
	2	ENSMUSG00000063229	*Ldha*	2.32E+00	3.98E-12	Glycolysis
	3	ENSMUSG00000028645	*Slc2a1*	2.82E+00	7.13E-12	Glucose transport
	4	ENSMUSG00000021196	*Pfkp*	2.86E+00	8.86E-12	Glycolysis
	5	ENSMUSG00000023456	*Tpi1*	2.34E+00	8.86E-12	Glycolysis
	6	ENSMUSG00000021831	*Ero1l*	4.02E+00	1.21E-11	Apoptosis, electron transport
	7	ENSMUSG00000062070	*Pgk1*	2.62E+00	1.21E-11	Glycolysis
	8	ENSMUSG00000036427	*Gpi1*	2.46E+00	1.74E-11	Glycolysis
	9	ENSMUSG00000020108	*Ddit4*	4.67E+00	1.94E-11	Apoptosis, mTOR signalling
	10	ENSMUSG00000025791	*Pgm1*	2.38E+00	3.36E-11	Glucose metabolism

Table 6.4: Top 10 DEGs between treatments for HIF-2α Exon 3 KO 5TGM1 cells, ranked by FDR.

HIF-2α Exon 3 KO

Comparison	#	GeneID	GeneName	logFC	FDR	Associated function
Hypoxia 8h Vs Normoxia 8h	1	ENSMUSG00000078566	*Bnip3*	4.71E+00	5.10E-16	Apoptosis
	2	ENSMUSG00000028645	*Slc2a1*	2.42E+00	4.27E-14	Glucose transport
	3	ENSMUSG00000063229	*Ldha*	1.76E+00	2.74E-11	Glycolysis
	4	ENSMUSG00000024201	*Kdm4b*	1.74E+00	4.83E-10	Histone demethylase
	5	ENSMUSG00000023456	*Tpi1*	1.64E+00	5.23E-10	Glycolysis
	6	ENSMUSG00000031987	*Egln1*	1.83E+00	5.36E-10	HIF-α regulation
	7	ENSMUSG00000020108	*Ddit4*	3.00E+00	5.46E-10	Apoptosis, mTOR signalling
	8	ENSMUSG00000050914	*Ankrd37*	3.25E+00	5.77E-10	
	9	ENSMUSG00000111394	*Gm49759*	2.11E+00	1.05E-09	LncRNA
	10	ENSMUSG00000000628	*Hk2*	1.47E+00	6.48E-09	Glycolysis
Hypoxia 48h vs Normoxia 8h	1	ENSMUSG00000078566	*Bnip3*	5.81E+00	4.36E-18	Apoptosis
	2	ENSMUSG00000021831	*Ero1l*	4.21E+00	1.40E-17	Apoptosis, electron transport
	3	ENSMUSG00000021196	*Pfkp*	2.91E+00	3.41E-17	Glycolysis
	4	ENSMUSG00000028645	*Slc2a1*	2.86E+00	1.60E-16	Glucose transport
	5	ENSMUSG00000041444	*Arhgap32*	2.68E+00	1.09E-15	GTPase regulation
	6	ENSMUSG00000036427	*Gpi1*	2.41E+00	1.90E-15	Glycolysis
	7	ENSMUSG00000023456	*Tpi1*	2.24E+00	3.31E-15	Glycolysis

	8	ENSMUSG00000063229	*Ldha*	2.16E+00	5.54E-15	Glycolysis
	9	ENSMUSG00000020108	*Ddit4*	4.56E+00	1.05E-14	Apoptosis, mTOR signalling
	10	ENSMUSG00000062070	*Pgk1*	2.66E+00	1.05E-14	Glycolysis
Hypoxia 48h Vs Hypoxia 8h	1	ENSMUSG00000041444	*Arhgap32*	2.26E+00	2.89E-13	GTPase regulation
	2	ENSMUSG00000021831	*Ero1l*	2.55E+00	3.08E-12	Apoptosis, electron transport
	3	ENSMUSG00000028838	*Extl1*	2.75E+00	4.28E-11	Glycosyltransferase
	4	ENSMUSG00000041642	*Kif21b*	2.03E+00	6.13E-11	Kinesin motor protein
	5	ENSMUSG00000056749	*Nfil3*	2.44E+00	7.81E-10	Transcriptional regulator
	6	ENSMUSG00000032715	*Trib3*	2.91E+00	1.73E-09	Protein kinase regulator
	7	ENSMUSG00000040258	*Nxph4*	2.81E+00	3.65E-09	Signalling molecule
	8	ENSMUSG00000037465	*Klf10*	2.24E+00	5.87E-09	Transcriptional repressor
	9	ENSMUSG00000047492	*Inhbe*	2.34E+00	8.42E-09	Hormone regulation
	10	ENSMUSG00000017314	*Mpp2*	2.15E+00	1.34E-08	Synaptic signalling

Table 6.5: Top 10 DEGs between treatments for Empty Vector control 5TGM1 cells, ranked by FDR.

Empty Vector Control

Comparison	#	GeneID	GeneName	logFC	FDR	Associated function
Hypoxia 8h Vs Normoxia 8h	1	ENSMUSG00000028645	*Slc2a1*	2.38E+00	4.61E-14	Glucose transport
	2	ENSMUSG00000020108	*Ddit4*	2.92E+00	1.88E-13	Apoptosis, mTOR signalling
	3	ENSMUSG00000078566	*Bnip3*	4.35E+00	1.88E-13	Apoptosis
	4	ENSMUSG00000050914	*Ankrd37*	3.24E+00	6.35E-11	
	5	ENSMUSG00000031987	*Egln1*	1.86E+00	9.21E-11	HIF-α regulation
	6	ENSMUSG00000024201	*Kdm4b*	1.75E+00	1.43E-09	Histone demethylase
	7	ENSMUSG00000063229	*Ldha*	1.74E+00	1.43E-09	Glycolysis
	8	ENSMUSG00000053470	*Kdm3a*	1.58E+00	1.85E-08	Histone demethylase
	9	ENSMUSG00000023456	*Tpi1*	1.52E+00	1.13E-07	Glycolysis
	10	ENSMUSG00000025791	*Pgm1*	1.58E+00	1.24E-07	Glucose metabolism
Hypoxia 48h vs Normoxia 8h	1	ENSMUSG00000020108	*Ddit4*	3.76E+00	9.39E-16	Apoptosis, mTOR signalling
	2	ENSMUSG00000078566	*Bnip3*	5.44E+00	2.05E-15	Apoptosis
	3	ENSMUSG00000028645	*Slc2a1*	2.56E+00	2.05E-15	Glucose transport
	4	ENSMUSG00000021831	*Ero1l*	3.29E+00	3.87E-14	Apoptosis, electron transport
	5	ENSMUSG00000023456	*Tpi1*	2.33E+00	9.91E-14	Glycolysis
	6	ENSMUSG00000063229	*Ldha*	2.36E+00	1.39E-13	Glycolysis
	7	ENSMUSG00000021196	*Pfkp*	2.27E+00	9.24E-13	Glycolysis

	8	ENSMUSG00000050914	*Ankrd37*	3.67E+00	1.49E-12	
	9	ENSMUSG00000025791	*Pgm1*	2.17E+00	1.49E-12	Glucose metabolism
	10	ENSMUSG00000062070	*Pgk1*	2.53E+00	1.89E-12	Glycolysis
Hypoxia 48h Vs Hypoxia 8h	1	ENSMUSG00000009876	*Cox4i2*	1.74E+00	1.36E-04	Mitochondrial cytochrome activity
	2	ENSMUSG00000021831	*Ero1l*	1.56E+00	1.36E-04	Apoptosis, electron transport
	3	ENSMUSG00000044037	*Als2cl*	1.99E+00	1.55E-04	Endosome organisation
	4	ENSMUSG00000047492	*Inhbe*	1.98E+00	1.55E-04	Hormone regulation
	5	ENSMUSG00000041642	*Kif21b*	1.41E+00	2.00E-04	Kinesin motor protein
	6	ENSMUSG00000079559	*Colca2*	1.65E+00	3.84E-04	
	7	ENSMUSG00000056749	*Nfil3*	1.84E+00	3.50E-03	Transcriptional regulator
	8	ENSMUSG00000017314	*Mpp2*	1.33E+00	1.11E-02	Synaptic signalling
	9	ENSMUSG00000021624	*Cd180*	-1.70E+00	1.11E-02	Innate immunity
	10	ENSMUSG00000028838	*Extl1*	1.71E+00	1.31E-02	Glycosyltransferase
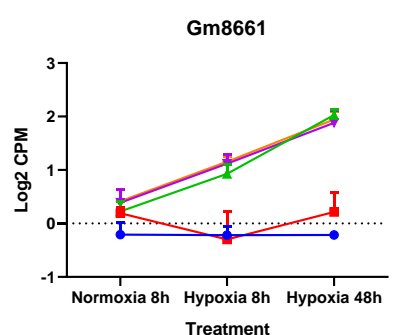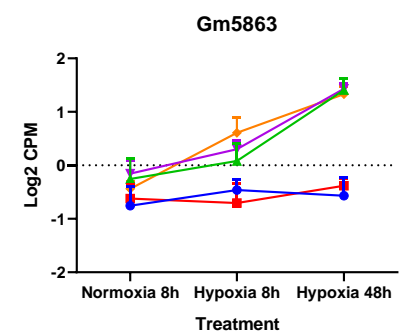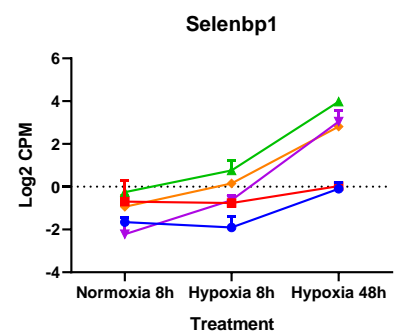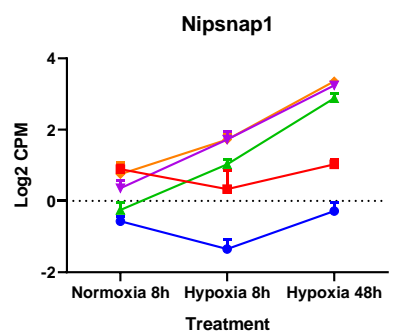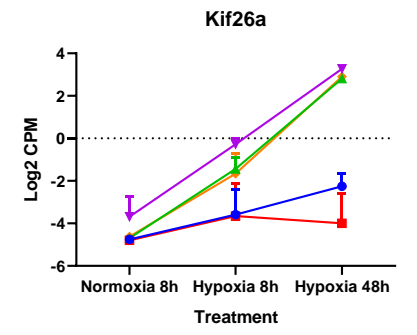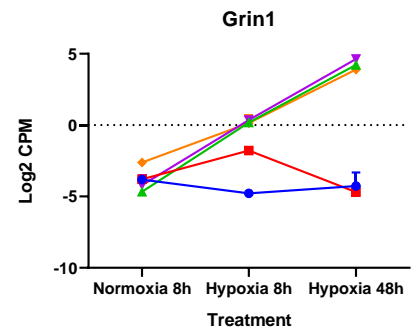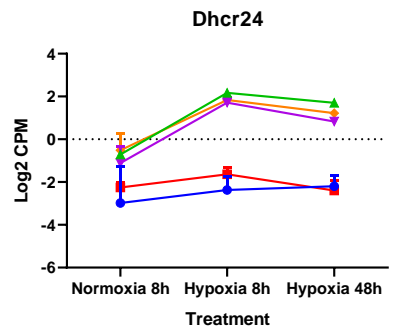
Figure 6.8: Expression of select HIF-1α target genes. RNA-seq data are presented as Log2 transcript count per million (CPM) against treatments for each knockout line, ±SD. N=3 biological replicates.

Table 6.6: Known HIF-1α target genes from the list of identified HIF-1α target genes in 5TGM1 cells. List adapted and updated from (Benita et al. 2009).

#	Known HIF-1α target gene	HIF-1α ChIP (re: Tables 4.3, 4.4)	Pubmed reference ID
1	Aldoa	✓	8955077
2	Ankrd37		19491311
3	Bnip3	✓	12879018
4	Bnip3l	✓	19273585
5	Cox4i2	✓	
6	Ddit4	✓	11884613
7	Egln1	✓	15563275
8	Eno1	✓	8955077
9	Ero1l		15592500
10	Gapdh	✓	10542317
11	Gpi1		24099156
12	Higd1a		23646141
13	Hilpda		20624928
14	Hk2	✓	13130303
15	Hmox1	✓	13130303
16	Jmjd6		19491311, *
17	Kdm3a		19858293
18	Kdm4b		22745382
19	Klf10	✓	
20	Ldha	✓	13130303
21	Mif	✓	27509135
22	Narf	✓	16956324
23	P4ha2	✓	23423382

24	*Pdk1*	✓	16517405
25	*Pfkl*	✓	13130303
26	*Pfkp*	✓	30850587
27	*Pgam1*	✓	26028220
28	*Pgk1*	✓	8089148
29	*Pgm1*		14645546
30	*Pkm*	✓	9436976
31	*Plod1*		14622280
32	*Prelid1*	✓	
33	*Selenbp1*	✓	19276359
34	*Slc2a1*	✓	13130303
35	*Slc37a4*	✓	
36	*Smtnl2*		29666476
37	*Tmem45a*	✓	22954140
38	*Tpi1*		13130303

* *In-silico* predicted HIF-1α target gene

Table 6.7: Novel HIF-1α target genes from the list of identified HIF-1α target genes in 5TGM1 cells.

#	Novel HIF-1α target gene
1	*Actn1*
2	*Derl3*
3	*Dhcr24*
4	*Eno1b*
5	*Fam162a*
6	*Fam57b*
7	*Gm11110*
8	*Gm26762*
9	*Gm45507*
10	*Gm49759*
11	*Gm5863*
12	*Gm8661*
13	*Gpsm3*
14	*Grin1*
15	*H2-Eb1*
16	*Hapln1*
17	*Itk*
18	*Kcnab2*
19	*Kif26a*
20	*Lrp2bp*
21	*Maff*
22	*Nipsnap1*
23	*Olfml2b*
24	*Polk*
25	*Rap2a*

26	*Smox*
27	*Tubb4a*
28	*Unc13a*

References

References

Adikusuma, F, Piltz, S, Corbett, MA, Turvey, M, McColl, SR, Helbig, KJ, Beard, MR, Hughes, J, Pomerantz, RT & Thomas, PQ 2018, 'Large deletions induced by Cas9 cleavage.', *Nature*, vol. 560, no. 7717, pp. E8–E9.

Appelhoff, RJ, Tian, Y-M, Raval, RR, Turley, H, Harris, AL, Pugh, CW, Ratcliffe, PJ & Gleadle, JM 2004, 'Differential function of the prolyl hydroxylases PHD1, PHD2, and PHD3 in the regulation of hypoxia-inducible factor.', *The Journal of Biological Chemistry*, vol. 279, no. 37, pp. 38458–38465.

Aranda, PS, LaJoie, DM & Jorcyk, CL 2012, 'Bleach gel: a simple agarose gel for analyzing RNA quality.', *Electrophoresis*, vol. 33, no. 2, pp. 366–369.

Asosingh, K, De Raeve, H, de Ridder, M, Storme, GA, Willems, A, Van Riet, I, Van Camp, B & Vanderkerken, K 2005, 'Role of the hypoxic bone marrow microenvironment in 5T2MM murine myeloma tumor progression.', *Haematologica*, vol. 90, no. 6, pp. 810–817.

Asosingh, K, De Raeve, H, Menu, E, Van Riet, I, Van Marck, E, Van Camp, B & Vanderkerken, K 2004, 'Angiogenic switch during 5T2MM murine myeloma tumorigenesis: role of CD45 heterogeneity.', *Blood*, vol. 103, no. 8, pp. 3131–3137.

Aubrey, BJ, Kelly, GL, Kueh, AJ, Brennan, MS, O'Connor, L, Milla, L, Wilcox, S, Tai, L, Strasser, A & Herold, MJ 2015, 'An inducible lentiviral guide RNA platform enables the identification of tumor-essential genes and tumor-promoting mutations in vivo.', *Cell reports*, vol. 10, no. 8, pp. 1422–1432.

Ayala, F, Dewar, R, Kieran, M & Kalluri, R 2009, 'Contribution of bone microenvironment to leukemogenesis and leukemia progression.', *Leukemia*, vol. 23, no. 12, pp. 2233–2241.

Azab, AK, Hu, J, Quang, P, Azab, F, Pitsillides, C, Awwad, R, Thompson, B, Maiso, P, Sun, JD, Hart, CP, Roccaro, AM, Sacco, A, Ngo, HT, Lin, CP, Kung, AL, Carrasco, RD, Vanderkerken, K & Ghobrial, IM 2012, 'Hypoxia promotes dissemination of multiple

myeloma through acquisition of epithelial to mesenchymal transition-like features.',
Blood, vol. 119, no. 24, pp. 5782–5794.

Barteczek, P, Li, L, Ernst, A-S, Böhler, L-I, Marti, HH & Kunze, R 2017, 'Neuronal HIF-1α
and HIF-2α deficiency improves neuronal survival and sensorimotor function in the early
acute phase after ischemic stroke.', *Journal of Cerebral Blood Flow and Metabolism*, vol.
37, no. 1, pp. 291–306.

Befani, CD, Vlachostergios, PJ, Hatzidaki, E, Patrikidou, A, Bonanou, S, Simos, G,
Papandreou, CN & Liakos, P 2012, 'Bortezomib represses HIF-1α protein expression and
nuclear accumulation by inhibiting both PI3K/Akt/TOR and MAPK pathways in prostate
cancer cells.', *Journal of Molecular Medicine*, vol. 90, no. 1, pp. 45–54.

Bellot, G, Garcia-Medina, R, Gounon, P, Chiche, J, Roux, D, Pouysségur, J & Mazure, NM
2009, 'Hypoxia-induced autophagy is mediated through hypoxia-inducible factor
induction of BNIP3 and BNIP3L via their BH3 domains.', *Molecular and Cellular Biology*,
vol. 29, no. 10, pp. 2570–2581.

Benita, Y, Kikuchi, H, Smith, AD, Zhang, MQ, Chung, DC & Xavier, RJ 2009, 'An integrative
genomics approach identifies Hypoxia Inducible Factor-1 (HIF-1)-target genes that form
the core response to hypoxia.', *Nucleic Acids Research*, vol. 37, no. 14, pp. 4587–4602.

Bergsagel, PL & Kuehl, WM 2005, 'Molecular pathogenesis and a consequent
classification of multiple myeloma.', *Journal of Clinical Oncology*, vol. 23, no. 26, pp.
6333–6338.

Berra, E, Benizri, E, Ginouvès, A, Volmat, V, Roux, D & Pouysségur, J 2003, 'HIF prolyl-
hydroxylase 2 is the key oxygen sensor setting low steady-state levels of HIF-1alpha in
normoxia.', *The EMBO Journal*, vol. 22, no. 16, pp. 4082–4090.

Bhaskar, A & Tiwary, BN 2016, 'Hypoxia inducible factor-1 alpha and multiple myeloma.',
International journal of advanced research, vol. 4, no. 1, pp. 706–715.

Bhatti, SS, Kumar, L, Dinda, AK & Dawar, R 2006, 'Prognostic value of bone marrow
angiogenesis in multiple myeloma: use of light microscopy as well as computerized
image analyzer in the assessment of microvessel density and total vascular area in

multiple myeloma and its correlation with various clinical, histological, and laboratory parameters.', *American Journal of Hematology*, vol. 81, no. 9, pp. 649–656.

Bishop, T, Gallagher, D, Pascual, A, Lygate, CA, de Bono, JP, Nicholls, LG, Ortega-Saenz, P, Oster, H, Wijeyekoon, B, Sutherland, AI, Grosfeld, A, Aragones, J, Schneider, M, van Geyte, K, Teixeira, D, Diez-Juan, A, Lopez-Barneo, J, Channon, KM, Maxwell, PH, Pugh, CW, Davies, AM, Carmeliet, P & Ratcliffe, PJ 2008, 'Abnormal sympathoadrenal development and systemic hypotension in PHD3-/- mice.', *Molecular and Cellular Biology*, vol. 28, no. 10, pp. 3386–3400.

Bishop, T & Ratcliffe, PJ 2014, 'Signaling hypoxia by hypoxia-inducible factor protein hydroxylases: a historical overview and future perspectives.', *Hypoxia*, vol. 2, pp. 197–213.

Blimark, CH, Turesson, I, Genell, A, Ahlberg, L, Björkstrand, B, Carlson, K, Forsberg, K, Juliusson, G, Linder, O, Mellqvist, U-H, Nahi, H, Kristinsson, SY & Swedish Myeloma Registry 2018, 'Outcome and survival of myeloma patients diagnosed 2008-2015. Real-world data on 4904 patients from the Swedish Myeloma Registry.', *Haematologica*, vol. 103, no. 3, pp. 506–513.

Braggio, E, Maiolino, A, Gouveia, ME, Magalhães, R, Souto Filho, JT, Garnica, M, Nucci, M & Renault, IZ 2010, 'Methylation status of nine tumor suppressor genes in multiple myeloma.', *International Journal of Hematology*, vol. 91, no. 1, pp. 87–96.

Brito, JLR, Brown, N & Morgan, GJ 2010, 'Transfection of siRNAs in multiple myeloma cell lines.', *Methods in Molecular Biology*, vol. 623, pp. 299–309.

Brito, JLR, Davies, FE, Gonzalez, D & Morgan, GJ 2008, 'Streptolysin-O reversible permeabilisation is an effective method to transfect siRNAs into myeloma cells.', *Journal of Immunological Methods*, vol. 333, no. 1-2, pp. 147–155.

Campanella, A, Santambrogio, P, Fontana, F, Frenquelli, M, Cenci, S, Marcatti, M, Sitia, R, Tonon, G & Camaschella, C 2013, 'Iron increases the susceptibility of multiple myeloma cells to bortezomib.', *Haematologica*, vol. 98, no. 6, pp. 971–979.

Camps, C, Buffa, FM, Colella, S, Moore, J, Sotiriou, C, Sheldon, H, Harris, AL, Gleadle, JM & Ragoussis, J 2008, 'hsa-miR-210 Is induced by hypoxia and is an independent prognostic factor in breast cancer.', *Clinical Cancer Research*, vol. 14, no. 5, pp. 1340–1348.

Cancer Australia 2019, *Myeloma statistics*, viewed 29 May 2018, <https://myeloma-cancer.canceraustralia.gov.au/statistics>.

Canver, MC, Bauer, DE, Dass, A, Yien, YY, Chung, J, Masuda, T, Maeda, T, Paw, BH & Orkin, SH 2014, 'Characterization of genomic deletion efficiency mediated by clustered regularly interspaced short palindromic repeats (CRISPR)/Cas9 nuclease system in mammalian cells.', *The Journal of Biological Chemistry*, vol. 289, no. 31, pp. 21312–21324.

Chen, C, Pore, N, Behrooz, A, Ismail-Beigi, F & Maity, A 2001, 'Regulation of glut1 mRNA by hypoxia-inducible factor-1. Interaction between H-ras and hypoxia.', *The Journal of Biological Chemistry*, vol. 276, no. 12, pp. 9519–9525.

Cheong, CM, Chow, AWS, Fitter, S, Hewett, DR, Martin, SK, Williams, SA, To, LB, Zannettino, ACW & Vandyke, K 2015, 'Tetraspanin 7 (TSPAN7) expression is upregulated in multiple myeloma patients and inhibits myeloma tumour development in vivo.', *Experimental Cell Research*, vol. 332, no. 1, pp. 24–38.

Chi, J-T, Wang, Z, Nuyten, DSA, Rodriguez, EH, Schaner, ME, Salim, A, Wang, Y, Kristensen, GB, Helland, A, Børresen-Dale, A-L, Giaccia, A, Longaker, MT, Hastie, T, Yang, GP, van de Vijver, MJ & Brown, PO 2006, 'Gene expression programs in response to hypoxia: cell type specificity and prognostic significance in human cancers.', *PLoS Medicine*, vol. 3, no. 3, p. e47.

Chim, CS, Kumar, SK, Orlowski, RZ, Cook, G, Richardson, PG, Gertz, MA, Giralt, S, Mateos, MV, Leleu, X & Anderson, KC 2018, 'Management of relapsed and refractory multiple myeloma: novel agents, antibodies, immunotherapies and beyond.', *Leukemia*, vol. 32, no. 2, pp. 252–262.

Cho, H & Kaelin, WG 2016, 'Targeting HIF2 in clear cell renal cell carcinoma.', *Cold Spring Harbor Symposia on Quantitative Biology*, vol. 81, pp. 113–121.

Choi, SM, Oh, H & Park, H 2008, 'Microarray analyses of hypoxia-regulated genes in an aryl hydrocarbon receptor nuclear translocator (Arnt)-dependent manner.', *The FEBS Journal*, vol. 275, no. 22, pp. 5618–5634.

Choudhry, H & Harris, AL 2018, 'Advances in Hypoxia-Inducible Factor Biology.', *Cell Metabolism*, vol. 27, no. 2, pp. 281–298.

Chu, Y & Corey, DR 2012, 'RNA sequencing: platform selection, experimental design, and data interpretation.', *Nucleic acid therapeutics*, vol. 22, no. 4, pp. 271–274.

Cipolleschi, MG, Dello Sbarba, P & Olivotto, M 1993, 'The role of hypoxia in the maintenance of hematopoietic stem cells.', *Blood*, vol. 82, no. 7, pp. 2031–2037.

Clambey, ET, McNamee, EN, Westrich, JA, Glover, LE, Campbell, EL, Jedlicka, P, de Zoeten, EF, Cambier, JC, Stenmark, KR, Colgan, SP & Eltzschig, HK 2012, 'Hypoxia-inducible factor-1 alpha-dependent induction of FoxP3 drives regulatory T-cell abundance and function during inflammatory hypoxia of the mucosa.', *Proceedings of the National Academy of Sciences of the United States of America*, vol. 109, no. 41, pp. E2784–93.

Colla, S, Storti, P, Donofrio, G, Todoerti, K, Bolzoni, M, Lazzaretti, M, Abeltino, M, Ippolito, L, Neri, A, Ribatti, D, Rizzoli, V, Martella, E & Giuliani, N 2010, 'Low bone marrow oxygen tension and hypoxia-inducible factor-1α overexpression characterize patients with multiple myeloma: role on the transcriptional and proangiogenic profiles of CD138(+) cells.', *Leukemia*, vol. 24, no. 11, pp. 1967–1970.

Compernolle, V, Brusselmans, K, Franco, D, Moorman, A, Dewerchin, M, Collen, D & Carmeliet, P 2003, 'Cardia bifida, defective heart development and abnormal neural crest migration in embryos lacking hypoxia-inducible factor-1alpha.', *Cardiovascular Research*, vol. 60, no. 3, pp. 569–579.

Cong, L, Ran, FA, Cox, D, Lin, S, Barretto, R, Habib, N, Hsu, PD, Wu, X, Jiang, W, Marraffini, LA & Zhang, F 2013, 'Multiplex genome engineering using CRISPR/Cas systems.', *Science*, vol. 339, no. 6121, pp. 819–823.

Corre, J, Munshi, N & Avet-Loiseau, H 2015, 'Genetics of multiple myeloma: another heterogeneity level?', *Blood*, vol. 125, no. 12, pp. 1870–1876.

Courtney, KD, Infante, JR, Lam, ET, Figlin, RA, Rini, BI, Brugarolas, J, Zojwalla, NJ, Lowe, AM, Wang, K, Wallace, EM, Josey, JA & Choueiri, TK 2018, 'Phase I Dose-Escalation Trial of PT2385, a First-in-Class Hypoxia-Inducible Factor-2α Antagonist in Patients With Previously Treated Advanced Clear Cell Renal Cell Carcinoma.', *Journal of Clinical Oncology*, vol. 36, no. 9, pp. 867–874.

Covello, KL, Kehler, J, Yu, H, Gordan, JD, Arsham, AM, Hu, C-J, Labosky, PA, Simon, MC & Keith, B 2006, 'HIF-2alpha regulates Oct-4: effects of hypoxia on stem cell function, embryonic development, and tumor growth.', *Genes & Development*, vol. 20, no. 5, pp. 557–570.

Danet, GH, Pan, Y, Luongo, JL, Bonnet, DA & Simon, MC 2003, 'Expansion of human SCID-repopulating cells under hypoxic conditions.', *The Journal of Clinical Investigation*, vol. 112, no. 1, pp. 126–135.

Dehairs, J, Talebi, A, Cherifi, Y & Swinnen, JV 2016, 'CRISP-ID: decoding CRISPR mediated indels by Sanger sequencing.', *Scientific Reports*, vol. 6, p. 28973.

Dengler, VL, Galbraith, MD & Espinosa, JM 2014, 'Transcriptional regulation by hypoxia inducible factors.', *Critical Reviews in Biochemistry and Molecular Biology*, vol. 49, no. 1, pp. 1–15.

Diamond, P, Labrinidis, A, Martin, SK, Farrugia, AN, Gronthos, S, To, LB, Fujii, N, O'Loughlin, PD, Evdokiou, A & Zannettino, ACW 2009, 'Targeted disruption of the CXCL12/CXCR4 axis inhibits osteolysis in a murine model of myeloma-associated bone loss.', *Journal of Bone and Mineral Research*, vol. 24, no. 7, pp. 1150–1161.

Dispenzieri, A & Kyle, RA 2005, 'Multiple myeloma: clinical features and indications for therapy.', *Best Practice & Research. Clinical Haematology*, vol. 18, no. 4, pp. 553–568.

Djunic, I, Elezovic, I, Ilic, V, Milosevic-Jovcic, N, Bila, J, Suvajdzic-Vukovic, N, Antic, D, Vidovic, A & Tomin, D 2014, 'The effect of paraprotein on platelet aggregation.', *Journal of clinical laboratory analysis*, vol. 28, no. 2, pp. 141–146.

Dobin, A, Davis, CA, Schlesinger, F, Drenkow, J, Zaleski, C, Jha, S, Batut, P, Chaisson, M & Gingeras, TR 2013, 'STAR: ultrafast universal RNA-seq aligner.', *Bioinformatics*, vol. 29, no. 1, pp. 15–21.

Doench, JG, Fusi, N, Sullender, M, Hegde, M, Vaimberg, EW, Donovan, KF, Smith, I, Tothova, Z, Wilen, C, Orchard, R, Virgin, HW, Listgarten, J & Root, DE 2016, 'Optimized sgRNA design to maximize activity and minimize off-target effects of CRISPR-Cas9.', *Nature Biotechnology*, vol. 34, no. 2, pp. 184–191.

Driver, AM, Peñagaricano, F, Huang, W, Ahmad, KR, Hackbart, KS, Wiltbank, MC & Khatib, H 2012, 'RNA-Seq analysis uncovers transcriptomic variations between morphologically similar in vivo- and in vitro-derived bovine blastocysts.', *BMC Genomics*, vol. 13, p. 118.

Dunwoodie, SL 2009, 'The role of hypoxia in development of the Mammalian embryo.', *Developmental Cell*, vol. 17, no. 6, pp. 755–773.

Dutta, AK, Fink, JL, Grady, JP, Morgan, GJ, Mullighan, CG, To, LB, Hewett, DR & Zannettino, ACW 2018, 'Subclonal evolution in disease progression from MGUS/SMM to multiple myeloma is characterised by clonal stability.', *Leukemia*, vol. 33, no. 2, pp. 457–468.

Dutta, AK, Hewett, DR, Fink, JL, Grady, JP & Zannettino, ACW 2017, 'Cutting edge genomics reveal new insights into tumour development, disease progression and therapeutic impacts in multiple myeloma.', *British Journal of Haematology*, vol. 178, no. 2, pp. 196–208.

Eales, KL, Hollinshead, KER & Tennant, DA 2016, 'Hypoxia and metabolic adaptation of cancer cells.', *Oncogenesis*, vol. 5, p. e190.

Eden, E, Navon, R, Steinfeld, I, Lipson, D & Yakhini, Z 2009, 'GOrilla: a tool for discovery and visualization of enriched GO terms in ranked gene lists.', *BMC Bioinformatics*, vol. 10, p. 48.

Ehrismann, D, Flashman, E, Genn, DN, Mathioudakis, N, Hewitson, KS, Ratcliffe, PJ & Schofield, CJ 2007, 'Studies on the activity of the hypoxia-inducible-factor hydroxylases using an oxygen consumption assay.', *The Biochemical Journal*, vol. 401, no. 1, pp. 227–234.

El-Brolosy, MA & Stainier, DYR 2017, 'Genetic compensation: A phenomenon in search of mechanisms.', *PLoS Genetics*, vol. 13, no. 7, p. e1006780.

Elvert, G, Kappel, A, Heidenreich, R, Englmeier, U, Lanz, S, Acker, T, Rauter, M, Plate, K, Sieweke, M, Breier, G & Flamme, I 2003, 'Cooperative interaction of hypoxia-inducible factor-2alpha (HIF-2alpha) and Ets-1 in the transcriptional activation of vascular endothelial growth factor receptor-2 (Flk-1).', *The Journal of Biological Chemistry*, vol. 278, no. 9, pp. 7520–7530.

Ema, M, Taya, S, Yokotani, N, Sogawa, K, Matsuda, Y & Fujii-Kuriyama, Y 1997, 'A novel bHLH-PAS factor with close sequence similarity to hypoxia-inducible factor 1alpha regulates the VEGF expression and is potentially involved in lung and vascular development.', *Proceedings of the National Academy of Sciences of the United States of America*, vol. 94, no. 9, pp. 4273–4278.

Fatrai, S, Wierenga, ATJ, Daenen, SMGJ, Vellenga, E & Schuringa, JJ 2011, 'Identification of HIF2alpha as an important STAT5 target gene in human hematopoietic stem cells.', *Blood*, vol. 117, no. 12, pp. 3320–3330.

Ferlay, J, Soerjomataram, I, Dikshit, R, Eser, S, Mathers, C, Rebelo, M, Parkin, DM, Forman, D & Bray, F 2015, 'Cancer incidence and mortality worldwide: sources, methods and major patterns in GLOBOCAN 2012.', *International Journal of Cancer*, vol. 136, no. 5, pp. E359–86.

Fife, CM, McCarroll, JA & Kavallaris, M 2014, 'Movers and shakers: cell cytoskeleton in cancer metastasis.', *British Journal of Pharmacology*, vol. 171, no. 24, pp. 5507–5523.

Frolova, O, Samudio, I, Benito, JM, Jacamo, R, Kornblau, SM, Markovic, A, Schober, W, Lu, H, Qiu, YH, Buglio, D, McQueen, T, Pierce, S, Shpall, E, Konoplev, S, Thomas, D, Kantarjian, H, Lock, R, Andreeff, M & Konopleva, M 2012, 'Regulation of HIF-1α signaling and chemoresistance in acute lymphocytic leukemia under hypoxic conditions of the bone marrow microenvironment.', *Cancer Biology & Therapy*, vol. 13, no. 10, pp. 858–870.

Fujita, N, Markova, D, Anderson, DG, Chiba, K, Toyama, Y, Shapiro, IM & Risbud, MV 2012, 'Expression of prolyl hydroxylases (PHDs) is selectively controlled by HIF-1 and HIF-2 proteins in nucleus pulposus cells of the intervertebral disc: distinct roles of PHD2 and PHD3 proteins in controlling HIF-1α activity in hypoxia.', *The Journal of Biological Chemistry*, vol. 287, no. 20, pp. 16975–16986.

Gandhi, UH, Senapedis, W, Baloglu, E, Unger, TJ, Chari, A, Vogl, D & Cornell, RF 2018, 'Clinical Implications of Targeting XPO1-mediated Nuclear Export in Multiple Myeloma.', *Clinical lymphoma, myeloma & leukemia*, vol. 18, no. 5, pp. 335–345.

Gardner, LB 2008, 'Hypoxic inhibition of nonsense-mediated RNA decay regulates gene expression and the integrated stress response.', *Molecular and Cellular Biology*, vol. 28, no. 11, pp. 3729–3741.

Gastelum, G, Poteshkina, A, Veena, M, Artiga, E, Weckstein, G & Frost, P 2017, 'Restoration of the prolyl-hydroxylase domain protein-3 oxygen-sensing mechanism is responsible for regulation of HIF2α expression and induction of sensitivity of myeloma cells to hypoxia-mediated apoptosis.', *Plos One*, vol. 12, no. 12, p. e0188438.

Ghobrial, IM 2012, 'Myeloma as a model for the process of metastasis: implications for therapy.', *Blood*, vol. 120, no. 1, pp. 20–30.

Giatromanolaki, A, Bai, M, Margaritis, D, Bourantas, KL, Koukourakis, MI, Sivridis, E & Gatter, KC 2010, 'Hypoxia and activated VEGF/receptor pathway in multiple myeloma.', *Anticancer Research*, vol. 30, no. 7, pp. 2831–2836.

Gibson Assembly – Samuel Miller Lab, UW, Seattle n.d., viewed 15 April 2019, <http://miller-lab.net/MillerLab/protocols/molecular-biology-and-cloning/gibson-assembly/>.

Gibson, DG, Young, L, Chuang, R-Y, Venter, JC, Hutchison, CA & Smith, HO 2009, 'Enzymatic assembly of DNA molecules up to several hundred kilobases.', *Nature Methods*, vol. 6, no. 5, pp. 343–345.

Giuliani, N, Storti, P, Bolzoni, M, Palma, BD & Bonomini, S 2011, 'Angiogenesis and multiple myeloma.', *Cancer Microenvironment*, vol. 4, no. 3, pp. 325–337.

Glick, D, Zhang, W, Beaton, M, Marsboom, G, Gruber, M, Simon, MC, Hart, J, Dorn, GW, Brady, MJ & Macleod, KF 2012, 'BNip3 regulates mitochondrial function and lipid metabolism in the liver.', *Molecular and Cellular Biology*, vol. 32, no. 13, pp. 2570–2584.

Grant, WC & Root, WS 1947, 'The relation of oxygen tension in bone marrow blood to the erythropoiesis following hemorrhage.', *Federation Proceedings*, vol. 6, no. 1 Pt 2, p. 114.

Grassi, F, Cristino, S, Toneguzzi, S, Piacentini, A, Facchini, A & Lisignoli, G 2004, 'CXCL12 chemokine up-regulates bone resorption and MMP-9 release by human osteoclasts: CXCL12 levels are increased in synovial and bone tissue of rheumatoid arthritis patients.', *Journal of Cellular Physiology*, vol. 199, no. 2, pp. 244–251.

Grav, LM, Sergeeva, D, Lee, JS, Marin de Mas, I, Lewis, NE, Andersen, MR, Nielsen, LK, Lee, GM & Kildegaard, HF 2018, 'Minimizing Clonal Variation during Mammalian Cell Line Engineering for Improved Systems Biology Data Generation.', *ACS synthetic biology [electronic resource]*, vol. 7, no. 9, pp. 2148–2159.

Guimarães-Camboa, N, Stowe, J, Aneas, I, Sakabe, N, Cattaneo, P, Henderson, L, Kilberg, MS, Johnson, RS, Chen, J, McCulloch, AD, Nobrega, MA, Evans, SM & Zambon, AC 2015, 'Hif1α represses cell stress pathways to allow proliferation of hypoxic fetal cardiomyocytes.', *Developmental Cell*, vol. 33, no. 5, pp. 507–521.

Guitart, AV, Subramani, C, Armesilla-Diaz, A, Smith, G, Sepulveda, C, Gezer, D, Vukovic, M, Dunn, K, Pollard, P, Holyoake, TL, Enver, T, Ratcliffe, PJ & Kranc, KR 2013, 'Hif-2α is

not essential for cell-autonomous hematopoietic stem cell maintenance.', *Blood*, vol. 122, no. 10, pp. 1741–1745.

Guo, K, Searfoss, G, Krolikowski, D, Pagnoni, M, Franks, C, Clark, K, Yu, KT, Jaye, M & Ivashchenko, Y 2001, 'Hypoxia induces the expression of the pro-apoptotic gene BNIP3.', *Cell Death and Differentiation*, vol. 8, no. 4, pp. 367–376.

Gustafsson, MV, Zheng, X, Pereira, T, Gradin, K, Jin, S, Lundkvist, J, Ruas, JL, Poellinger, L, Lendahl, U & Bondesson, M 2005, 'Hypoxia requires notch signaling to maintain the undifferentiated cell state.', *Developmental Cell*, vol. 9, no. 5, pp. 617–628.

Haase, VH 2013, 'Regulation of erythropoiesis by hypoxia-inducible factors.', *Blood Reviews*, vol. 27, no. 1, pp. 41–53.

Haeussler, M, Schönig, K, Eckert, H, Eschstruth, A, Mianné, J, Renaud, J-B, Schneider-Maunoury, S, Shkumatava, A, Teboul, L, Kent, J, Joly, J-S & Concordet, J-P 2016, 'Evaluation of off-target and on-target scoring algorithms and integration into the guide RNA selection tool CRISPOR.', *Genome Biology*, vol. 17, no. 1, p. 148.

Hansen, KD, Brenner, SE & Dudoit, S 2010, 'Biases in Illumina transcriptome sequencing caused by random hexamer priming.', *Nucleic Acids Research*, vol. 38, no. 12, p. e131.

Harrison, JS, Rameshwar, P, Chang, V & Bandari, P 2002, 'Oxygen saturation in the bone marrow of healthy volunteers.', *Blood*, vol. 99, no. 1, p. 394.

He, N, Zhang, L, Cui, J & Li, Z 2014, 'Bone marrow vascular niche: home for hematopoietic stem cells.', *Bone marrow research*, vol. 2014, p. 128436.

Heller, G, Schmidt, WM, Ziegler, B, Holzer, S, Müllauer, L, Bilban, M, Zielinski, CC, Drach, J & Zöchbauer-Müller, S 2008, 'Genome-wide transcriptional response to 5-aza-2'-deoxycytidine and trichostatin a in multiple myeloma cells.', *Cancer Research*, vol. 68, no. 1, pp. 44–54.

Hewett, DR, Vandyke, K, Lawrence, DM, Friend, N, Noll, JE, Geoghegan, JM, Croucher, PI & Zannettino, ACW 2017, 'DNA barcoding reveals habitual clonal dominance of myeloma plasma cells in the bone marrow microenvironment.', *Neoplasia*, vol. 19, no. 12, pp. 972–981.

Hose, D, Seckinger, A, Goldschmidt, H, Meiβner, T, Rebacz, B, Moreaux, J, Benes, V, Neben, K, Hillengass, J, Bertsch, U, Jauch, A, Rossi, JF, Möhler, T, Zimmermann, J, von Kalle, C, Lewis, J, Klein, B & Schultes, C 2009, 'Inhibition of HIF1A Signaling by a Novel Class of Sulfonanilides for Targeted Treatment of Multiple Myeloma.', *Blood*.

Hsu, PD, Lander, ES & Zhang, F 2014, 'Development and applications of CRISPR-Cas9 for genome engineering.', *Cell*, vol. 157, no. 6, pp. 1262–1278.

Hsu, PD, Scott, DA, Weinstein, JA, Ran, FA, Konermann, S, Agarwala, V, Li, Y, Fine, EJ, Wu, X, Shalem, O, Cradick, TJ, Marraffini, LA, Bao, G & Zhang, F 2013, 'DNA targeting specificity of RNA-guided Cas9 nucleases.', *Nature Biotechnology*, vol. 31, no. 9, pp. 827–832.

Hu, C-J, Wang, L-Y, Chodosh, LA, Keith, B & Simon, MC 2003, 'Differential roles of hypoxia-inducible factor 1alpha (HIF-1alpha) and HIF-2alpha in hypoxic gene regulation.', *Molecular and Cellular Biology*, vol. 23, no. 24, pp. 9361–9374.

Hu, J, Handisides, DR, Van Valckenborgh, E, De Raeve, H, Menu, E, Vande Broek, I, Liu, Q, Sun, JD, Van Camp, B, Hart, CP & Vanderkerken, K 2010, 'Targeting the multiple myeloma hypoxic niche with TH-302, a hypoxia-activated prodrug.', *Blood*, vol. 116, no. 9, pp. 1524–1527.

Hu, J, Van Valckenborgh, E, Menu, E, De Bruyne, E & Vanderkerken, K 2012, 'Understanding the hypoxic niche of multiple myeloma: therapeutic implications and contributions of mouse models.', *Disease Models & Mechanisms*, vol. 5, no. 6, pp. 763–771.

Hu, J, Van Valckenborgh, E, Xu, D, Menu, E, De Raeve, H, De Bruyne, E, Xu, S, Van Camp, B, Handisides, D, Hart, CP & Vanderkerken, K 2013, 'Synergistic induction of apoptosis in multiple myeloma cells by bortezomib and hypoxia-activated prodrug TH-302, in vivo and in vitro.', *Molecular Cancer Therapeutics*, vol. 12, no. 9, pp. 1763–1773.

Hu, Y, Kirito, K, Yoshida, K, Mitsumori, T, Nakajima, K, Nozaki, Y, Hamanaka, S, Nagashima, T, Kunitama, M, Sakoe, K & Komatsu, N 2009, 'Inhibition of hypoxia-

inducible factor-1 function enhances the sensitivity of multiple myeloma cells to melphalan.', *Molecular Cancer Therapeutics*, vol. 8, no. 8, pp. 2329–2338.

Huang, Y, Kempen, MB, Munck, AB, Swagemakers, S, Driegen, S, Mahavadi, P, Meijer, D, van Ijcken, W, van der Spek, P, Grosveld, F, Günther, A, Tibboel, D & Rottier, RJ 2012, 'Hypoxia-inducible factor 2α plays a critical role in the formation of alveoli and surfactant.', *American Journal of Respiratory Cell and Molecular Biology*, vol. 46, no. 2, pp. 224–232.

Hum, N, Sebastian, A, He, W, Moya, ML, Hynes, WF, Adorno, JJ, Hinckley, A, Wheeler, EK, Coleman, MA & Loots, GG 2019, 'Abstract 37: RNA-seq comparisons of *in vitro* and *in vivo* cancer model platforms: Monolayer, spheroids, immunodeficient, and syngeneic mouse model', in *Tumor Biology*, American Association for Cancer Research, pp. 37–37.

Huynh, M, Pak, C, Markovina, S, Callander, NS, Chng, KS, Wuerzberger-Davis, SM, Bakshi, DD, Kink, JA, Hematti, P, Hope, C, Asimakopoulos, F, Rui, L & Miyamoto, S 2018, 'Hyaluronan and proteoglycan link protein 1 (HAPLN1) activates bortezomib-resistant NF-κB activity and increases drug resistance in multiple myeloma.', *The Journal of Biological Chemistry*, vol. 293, no. 7, pp. 2452–2465.

Ikeda, S, Kitadate, A, Abe, F, Takahashi, N & Tagawa, H 2018, 'Hypoxia-inducible KDM3A addiction in multiple myeloma.', *Blood advances*, vol. 2, no. 4, pp. 323–334.

Imanirad, P, Solaimani Kartalaei, P, Crisan, M, Vink, C, Yamada-Inagawa, T, de Pater, E, Kurek, D, Kaimakis, P, van der Linden, R, Speck, N & Dzierzak, E 2014, 'HIF1α is a regulator of hematopoietic progenitor and stem cell development in hypoxic sites of the mouse embryo.', *Stem Cell Research*, vol. 12, no. 1, pp. 24–35.

Imtiyaz, HZ, Williams, EP, Hickey, MM, Patel, SA, Durham, AC, Yuan, L-J, Hammond, R, Gimotty, PA, Keith, B & Simon, MC 2010, 'Hypoxia-inducible factor 2alpha regulates macrophage function in mouse models of acute and tumor inflammation.', *The Journal of Clinical Investigation*, vol. 120, no. 8, pp. 2699–2714.

Index of /projects/fastqc/Help n.d., viewed 23 September 2019, <https://www.bioinformatics.babraham.ac.uk/projects/fastqc/Help/>.

Iyer, NV, Kotch, LE, Agani, F, Leung, SW, Laughner, E, Wenger, RH, Gassmann, M, Gearhart, JD, Lawler, AM, Yu, AY & Semenza, GL 1998, 'Cellular and developmental control of O2 homeostasis by hypoxia-inducible factor 1 alpha.', *Genes & Development*, vol. 12, no. 2, pp. 149–162.

Jinek, M, East, A, Cheng, A, Lin, S, Ma, E & Doudna, J 2013, 'RNA-programmed genome editing in human cells.', *eLife*, vol. 2, p. e00471.

Keith, B, Johnson, RS & Simon, MC 2011, 'HIF1α and HIF2α: sibling rivalry in hypoxic tumour growth and progression.', *Nature Reviews. Cancer*, vol. 12, no. 1, pp. 9–22.

Kim, KJ, Li, B, Winer, J, Armanini, M, Gillett, N, Phillips, HS & Ferrara, N 1993, 'Inhibition of vascular endothelial growth factor-induced angiogenesis suppresses tumour growth in vivo.', *Nature*, vol. 362, no. 6423, pp. 841–844.

Kim, S-K, Knight, DA, Jones, LR, Vervoort, S, Ng, AP, Seymour, JF, Bradner, JE, Waibel, M, Kats, L & Johnstone, RW 2018, 'JAK2 is dispensable for maintenance of JAK2 mutant B-cell acute lymphoblastic leukemias.', *Genes & Development*, vol. 32, no. 11-12, pp. 849–864.

Knott, GJ & Doudna, JA 2018, 'CRISPR-Cas guides the future of genetic engineering.', *Science*, vol. 361, no. 6405, pp. 866–869.

Kocabas, F, Xie, L, Xie, J, Yu, Z, DeBerardinis, RJ, Kimura, W, Thet, S, Elshamy, AF, Abouellail, H, Muralidhar, S, Liu, X, Chen, C, Sadek, HA, Zhang, CC & Zheng, J 2015, 'Hypoxic metabolism in human hematopoietic stem cells.', *Cell & bioscience*, vol. 5, p. 39.

Kocabas, F, Zheng, J, Thet, S, Copeland, NG, Jenkins, NA, DeBerardinis, RJ, Zhang, C & Sadek, HA 2012, 'Meis1 regulates the metabolic phenotype and oxidant defense of hematopoietic stem cells.', *Blood*, vol. 120, no. 25, pp. 4963–4972.

Koh, MY & Powis, G 2012, 'Passing the baton: the HIF switch.', *Trends in Biochemical Sciences*, vol. 37, no. 9, pp. 364–372.

König, C, Kleber, M, Ihorst, G, Gropp, A, Reinhardt, H, Koch, B, Wäsch, R & Engelhardt, M 2013, 'Prevalence of iron overload vs iron deficiency in multiple myeloma: resembling or

different from MDS--and stem cell transplant (SCT)--patients?', *Clinical lymphoma, myeloma & leukemia*, vol. 13, no. 6, pp. 671–680.e3.

Korde, N, Kristinsson, SY & Landgren, O 2011, 'Monoclonal gammopathy of undetermined significance (MGUS) and smoldering multiple myeloma (SMM): novel biological insights and development of early treatment strategies.', *Blood*, vol. 117, no. 21, pp. 5573–5581.

Koshiji, M, Kageyama, Y, Pete, EA, Horikawa, I, Barrett, JC & Huang, LE 2004, 'HIF-1alpha induces cell cycle arrest by functionally counteracting Myc.', *The EMBO Journal*, vol. 23, no. 9, pp. 1949–1956.

Krock, BL, Skuli, N & Simon, MC 2011, 'Hypoxia-induced angiogenesis: good and evil.', *Genes & cancer*, vol. 2, no. 12, pp. 1117–1133.

Kulshreshtha, R, Ferracin, M, Wojcik, SE, Garzon, R, Alder, H, Agosto-Perez, FJ, Davuluri, R, Liu, C-G, Croce, CM, Negrini, M, Calin, GA & Ivan, M 2007, 'A microRNA signature of hypoxia.', *Molecular and Cellular Biology*, vol. 27, no. 5, pp. 1859–1867.

Kumar, SK, Dispenzieri, A, Lacy, MQ, Gertz, MA, Buadi, FK, Pandey, S, Kapoor, P, Dingli, D, Hayman, SR, Leung, N, Lust, J, McCurdy, A, Russell, SJ, Zeldenrust, SR, Kyle, RA & Rajkumar, SV 2014, 'Continued improvement in survival in multiple myeloma: changes in early mortality and outcomes in older patients.', *Leukemia*, vol. 28, no. 5, pp. 1122–1128.

Kyle, RA & Rajkumar, SV 2004, 'Multiple myeloma.', *The New England Journal of Medicine*, vol. 351, no. 18, pp. 1860–1873.

Laderoute, KR, Calaoagan, JM, Gustafson-Brown, C, Knapp, AM, Li, G-C, Mendonca, HL, Ryan, HE, Wang, Z & Johnson, RS 2002, 'The response of c-jun/AP-1 to chronic hypoxia is hypoxia-inducible factor 1 alpha dependent.', *Molecular and Cellular Biology*, vol. 22, no. 8, pp. 2515–2523.

Lamouille, S, Xu, J & Derynck, R 2014, 'Molecular mechanisms of epithelial-mesenchymal transition.', *Nature Reviews. Molecular Cell Biology*, vol. 15, no. 3, pp. 178–196.

Lando, D, Peet, DJ, Gorman, JJ, Whelan, DA, Whitelaw, ML & Bruick, RK 2002, 'FIH-1 is an asparaginyl hydroxylase enzyme that regulates the transcriptional activity of hypoxia-inducible factor.', *Genes & Development*, vol. 16, no. 12, pp. 1466–1471.

Laubach, JP, Liu, C-J, Raje, NS, Yee, AJ, Armand, P, Schlossman, RL, Rosenblatt, J, Hedlund, J, Martin, M, Reynolds, C, Shain, KH, Zackon, I, Stampleman, L, Henrick, P, Rivotto, B, Hornburg, KTV, Dumke, HJ, Chuma, S, Savell, A, Handisides, DR, Kroll, S, Anderson, KC, Richardson, PG & Ghobrial, IM 2019, 'A Phase I/II Study of Evofosfamide, A Hypoxia-activated Prodrug with or without Bortezomib in Subjects with Relapsed/Refractory Multiple Myeloma.', *Clinical Cancer Research*, vol. 25, no. 2, pp. 478–486.

Lee, M-C, Huang, H-J, Chang, T-H, Huang, H-C, Hsieh, S-Y, Chen, Y-S, Chou, W-Y, Chiang, C-H, Lai, C-H & Shiau, C-Y 2016, 'Genome-wide analysis of HIF-2α chromatin binding sites under normoxia in human bronchial epithelial cells (BEAS-2B) suggests its diverse functions.', *Scientific Reports*, vol. 6, p. 29311.

Lemaire, M, Deleu, S, De Bruyne, E, Van Valckenborgh, E, Menu, E & Vanderkerken, K 2011, 'The microenvironment and molecular biology of the multiple myeloma tumor.', *Advances in cancer research*, vol. 110, pp. 19–42.

Leong, WZ, Tan, SH, Ngoc, PCT, Amanda, S, Yam, AWY, Liau, W-S, Gong, Z, Lawton, LN, Tenen, DG & Sanda, T 2017, 'ARID5B as a critical downstream target of the TAL1 complex that activates the oncogenic transcriptional program and promotes T-cell leukemogenesis.', *Genes & Development*, vol. 31, no. 23-24, pp. 2343–2360.

Lévesque, J-P, Winkler, IG, Hendy, J, Williams, B, Helwani, F, Barbier, V, Nowlan, B & Nilsson, SK 2007, 'Hematopoietic progenitor cell mobilization results in hypoxia with increased hypoxia-inducible transcription factor-1 alpha and vascular endothelial growth factor A in bone marrow.', *Stem Cells*, vol. 25, no. 8, pp. 1954–1965.

Lu, H, Forbes, RA & Verma, A 2002, 'Hypoxia-inducible factor 1 activation by aerobic glycolysis implicates the Warburg effect in carcinogenesis.', *The Journal of Biological Chemistry*, vol. 277, no. 26, pp. 23111–23115.

Lu, L, Payvandi, F, Wu, L, Zhang, L-H, Hariri, RJ, Man, H-W, Chen, RS, Muller, GW, Hughes, CCW, Stirling, DI, Schafer, PH & Bartlett, JB 2009, 'The anti-cancer drug lenalidomide inhibits angiogenesis and metastasis via multiple inhibitory effects on endothelial cell function in normoxic and hypoxic conditions.', *Microvascular Research*, vol. 77, no. 2, pp. 78–86.

Lum, J 2017, 'Generation of HIF-1α and HIF-2α knockouts in 5TGM1 cell lines to investigate their role in Multiple Myeloma', Undergraduate thesis.

Luo, F, Liu, X, Yan, N, Li, S, Cao, G, Cheng, Q, Xia, Q & Wang, H 2006, 'Hypoxia-inducible transcription factor-1alpha promotes hypoxia-induced A549 apoptosis via a mechanism that involves the glycolysis pathway.', *BMC Cancer*, vol. 6, p. 26.

Ma, Y 2015, 'Generation of HIF-α deficient cell lines for analyses of their roles in cancer', Master thesis, The University of Adelaide.

Ma, Z, Chen, C, Tang, P, Zhang, H, Yue, J & Yu, Z 2017, 'BNIP3 induces apoptosis and protective autophagy under hypoxia in esophageal squamous cell carcinoma cell lines: BNIP3 regulates cell death.', *Diseases of the Esophagus*, vol. 30, no. 9, pp. 1–8.

Maes, K, Nemeth, E, Roodman, GD, Huston, A, Esteve, F, Freytes, C, Callander, N, Katodritou, E, Tussing-Humphreys, L, Rivera, S, Vanderkerken, K, Lichtenstein, A & Ganz, T 2010, 'In anemia of multiple myeloma, hepcidin is induced by increased bone morphogenetic protein 2.', *Blood*, vol. 116, no. 18, pp. 3635–3644.

Magliulo, D & Bernardi, R 2018, 'HIF-α factors as potential therapeutic targets in leukemia.', *Expert Opinion on Therapeutic Targets*, vol. 22, no. 11, pp. 917–928.

Maiso, P, Huynh, D, Moschetta, M, Sacco, A, Aljawai, Y, Mishima, Y, Asara, JM, Roccaro, AM, Kimmelman, AC & Ghobrial, IM 2015, 'Metabolic signature identifies novel targets for drug resistance in multiple myeloma.', *Cancer Research*, vol. 75, no. 10, pp. 2071–2082.

Makino, Y, Cao, R, Svensson, K, Bertilsson, G, Asman, M, Tanaka, H, Cao, Y, Berkenstam, A & Poellinger, L 2001, 'Inhibitory PAS domain protein is a negative regulator of hypoxia-inducible gene expression.', *Nature*, vol. 414, no. 6863, pp. 550–554.

Mali, P, Yang, L, Esvelt, KM, Aach, J, Guell, M, DiCarlo, JE, Norville, JE & Church, GM 2013, 'RNA-guided human genome engineering via Cas9.', *Science*, vol. 339, no. 6121, pp. 823–826.

Manier, S, Sacco, A, Leleu, X, Ghobrial, IM & Roccaro, AM 2012, 'Bone marrow microenvironment in multiple myeloma progression.', *Journal of Biomedicine & Biotechnology*, vol. 2012, p. 157496.

Martin, NM 2018, 'Investigating the Role of HIF-1 and HIF-2 Transcription Factors in Multiple Myeloma', Doctoral dissertation, The University of Adelaide.

Martin, SK, Diamond, P, Gronthos, S, Peet, DJ & Zannettino, ACW 2011, 'The emerging role of hypoxia, HIF-1 and HIF-2 in multiple myeloma.', *Leukemia*, vol. 25, no. 10, pp. 1533–1542.

Martin, SK, Diamond, P, Williams, SA, To, LB, Peet, DJ, Fujii, N, Gronthos, S, Harris, AL & Zannettino, ACW 2010, 'Hypoxia-inducible factor-2 is a novel regulator of aberrant CXCL12 expression in multiple myeloma plasma cells.', *Haematologica*, vol. 95, no. 5, pp. 776–784.

Masoud, GN & Li, W 2015, 'HIF-1α pathway: role, regulation and intervention for cancer therapy.', *Acta pharmaceutica Sinica. B*, vol. 5, no. 5, pp. 378–389.

Matsunaga, T, Imataki, O, Torii, E, Kameda, T, Shide, K, Shimoda, H, Kamiunten, A, Sekine, M, Taniguchi, Y, Yamamoto, S, Hidaka, T, Katayose, K, Kubuki, Y, Dobashi, H, Bandoh, S, Ohnishi, H, Fukai, F & Shimoda, K 2012, 'Elevated HIF-1α expression of acute myelogenous leukemia stem cells in the endosteal hypoxic zone may be a cause of minimal residual disease in bone marrow after chemotherapy.', *Leukemia Research*, vol. 36, no. 6, pp. e122–4.

Maxwell, PH, Wiesener, MS, Chang, GW, Clifford, SC, Vaux, EC, Cockman, ME, Wykoff, CC, Pugh, CW, Maher, ER & Ratcliffe, PJ 1999, 'The tumour suppressor protein VHL targets hypoxia-inducible factors for oxygen-dependent proteolysis.', *Nature*, vol. 399, no. 6733, pp. 271–275.

Maynard, MA, Evans, AJ, Hosomi, T, Hara, S, Jewett, MAS & Ohh, M 2005, 'Human HIF-3alpha4 is a dominant-negative regulator of HIF-1 and is down-regulated in renal cell carcinoma.', *The FASEB Journal*, vol. 19, no. 11, pp. 1396–1406.

McDonald, DM & Baluk, P 2002, 'Significance of blood vessel leakiness in cancer.', *Cancer Research*, vol. 62, no. 18, pp. 5381–5385.

McKinley, KL & Cheeseman, IM 2017, 'Large-Scale Analysis of CRISPR/Cas9 Cell-Cycle Knockouts Reveals the Diversity of p53-Dependent Responses to Cell-Cycle Defects.', *Developmental Cell*, vol. 40, no. 4, pp. 405–420.e2.

Mehrabian, M, Brethour, D, MacIsaac, S, Kim, JK, Gunawardana, CG, Wang, H & Schmitt-Ulms, G 2014, 'CRISPR-Cas9-based knockout of the prion protein and its effect on the proteome.', *Plos One*, vol. 9, no. 12, p. e114594.

Michiels, C 2004, 'Physiological and pathological responses to hypoxia.', *The American Journal of Pathology*, vol. 164, no. 6, pp. 1875–1882.

Mislick, KA & Baldeschwieler, JD 1996, 'Evidence for the role of proteoglycans in cation-mediated gene transfer.', *Proceedings of the National Academy of Sciences of the United States of America*, vol. 93, no. 22, pp. 12349–12354.

Möglich, A, Ayers, RA & Moffat, K 2009, 'Structure and signaling mechanism of Per-ARNT-Sim domains.', *Structure*, vol. 17, no. 10, pp. 1282–1294.

Mohyeldin, A, Garzón-Muvdi, T & Quiñones-Hinojosa, A 2010, 'Oxygen in stem cell biology: a critical component of the stem cell niche.', *Cell Stem Cell*, vol. 7, no. 2, pp. 150–161.

Mole, DR, Blancher, C, Copley, RR, Pollard, PJ, Gleadle, JM, Ragoussis, J & Ratcliffe, PJ 2009, 'Genome-wide association of hypoxia-inducible factor (HIF)-1alpha and HIF-2alpha DNA binding with expression profiling of hypoxia-inducible transcripts.', *The Journal of Biological Chemistry*, vol. 284, no. 25, pp. 16767–16775.

Moreno-Mateos, MA, Vejnar, CE, Beaudoin, J-D, Fernandez, JP, Mis, EK, Khokha, MK & Giraldez, AJ 2015, 'CRISPRscan: designing highly efficient sgRNAs for CRISPR-Cas9 targeting in vivo.', *Nature Methods*, vol. 12, no. 10, pp. 982–988.

Morgan, GJ, Walker, BA & Davies, FE 2012, 'The genetic architecture of multiple myeloma.', *Nature Reviews. Cancer*, vol. 12, no. 5, pp. 335–348.

Morita, M, Ohneda, O, Yamashita, T, Takahashi, S, Suzuki, N, Nakajima, O, Kawauchi, S, Ema, M, Shibahara, S, Udono, T, Tomita, K, Tamai, M, Sogawa, K, Yamamoto, M & Fujii-Kuriyama, Y 2003, 'HLF/HIF-2alpha is a key factor in retinopathy of prematurity in association with erythropoietin.', *The EMBO Journal*, vol. 22, no. 5, pp. 1134–1146.

Mrozik, KM, Cheong, CM, Hewett, D, Chow, AWS, Blaschuk, OW, Zannettino, ACW & Vandyke, K 2015, 'Therapeutic targeting of N-cadherin is an effective treatment for multiple myeloma.', *British Journal of Haematology*, vol. 171, no. 3, pp. 387–399.

Murugesan, T, Rajajeyabalachandran, G, Kumar, S, Nagaraju, S & Jegatheesan, SK 2018, 'Targeting HIF-2α as therapy for advanced cancers.', *Drug Discovery Today*, vol. 23, no. 7, pp. 1444–1451.

Mylonis, I, Chachami, G, Samiotaki, M, Panayotou, G, Paraskeva, E, Kalousi, A, Georgatsou, E, Bonanou, S & Simos, G 2006, 'Identification of MAPK phosphorylation sites and their role in the localization and activity of hypoxia-inducible factor-1alpha.', *The Journal of Biological Chemistry*, vol. 281, no. 44, pp. 33095–33106.

Mysore, VS, Szablowski, J, Dervan, PB & Frost, PJ 2016, 'A DNA-binding Molecule Targeting the Adaptive Hypoxic Response in Multiple Myeloma Has Potent Antitumor Activity.', *Molecular Cancer Research*, vol. 14, no. 3, pp. 253–266.

Noguera, R, Fredlund, E, Piqueras, M, Pietras, A, Beckman, S, Navarro, S & Påhlman, S 2009, 'HIF-1alpha and HIF-2alpha are differentially regulated in vivo in neuroblastoma: high HIF-1alpha correlates negatively to advanced clinical stage and tumor vascularization.', *Clinical Cancer Research*, vol. 15, no. 23, pp. 7130–7136.

Noll, JE, Hewett, DR, Williams, SA, Vandyke, K, Kok, C, To, LB & Zannettino, ACW 2014, 'SAMSN1 is a tumor suppressor gene in multiple myeloma.', *Neoplasia*, vol. 16, no. 7, pp. 572–585.

O'Sullivan, TE, Johnson, LR, Kang, HH & Sun, JC 2015, 'BNIP3- and BNIP3L-Mediated Mitophagy Promotes the Generation of Natural Killer Cell Memory.', *Immunity*, vol. 43, no. 2, pp. 331–342.

Oancea, M, Mani, A, Hussein, MA & Almasan, A 2004, 'Apoptosis of multiple myeloma.', *International Journal of Hematology*, vol. 80, no. 3, pp. 224–231.

Oike, Y, Ito, Y, Maekawa, H, Morisada, T, Kubota, Y, Akao, M, Urano, T, Yasunaga, K & Suda, T 2004, 'Angiopoietin-related growth factor (AGF) promotes angiogenesis.', *Blood*, vol. 103, no. 10, pp. 3760–3765.

Opperman, KS, Vandyke, K, Clark, KC, Coulter, EA, Hewett, DR, Mrozik, KM, Schwarz, N, Evdokiou, A, Croucher, PI, Psaltis, PJ, Noll, JE & Zannettino, AC 2019, 'Clodronate-Liposome Mediated Macrophage Depletion Abrogates Multiple Myeloma Tumor Establishment In Vivo.', *Neoplasia*, vol. 21, no. 8, pp. 777–787.

Ord, JJ, Streeter, EH, Roberts, ISD, Cranston, D & Harris, AL 2005, 'Comparison of hypoxia transcriptome in vitro with in vivo gene expression in human bladder cancer.', *British Journal of Cancer*, vol. 93, no. 3, pp. 346–354.

Orellana, CA, Marcellin, E, Palfreyman, RW, Munro, TP, Gray, PP & Nielsen, LK 2018, 'RNA-Seq Highlights High Clonal Variation in Monoclonal Antibody Producing CHO Cells.', *Biotechnology Journal*, vol. 13, no. 3, p. e1700231.

Ouiddir, A, Planès, C, Fernandes, I, VanHesse, A & Clerici, C 1999, 'Hypoxia upregulates activity and expression of the glucose transporter GLUT1 in alveolar epithelial cells.', *American Journal of Respiratory Cell and Molecular Biology*, vol. 21, no. 6, pp. 710–718.

Parangi, S, O'Reilly, M, Christofori, G, Holmgren, L, Grosfeld, J, Folkman, J & Hanahan, D 1996, 'Antiangiogenic therapy of transgenic mice impairs de novo tumor growth.', *Proceedings of the National Academy of Sciences of the United States of America*, vol. 93, no. 5, pp. 2002–2007.

Parmar, K, Mauch, P, Vergilio, J-A, Sackstein, R & Down, JD 2007, 'Distribution of hematopoietic stem cells in the bone marrow according to regional hypoxia.',

Proceedings of the National Academy of Sciences of the United States of America, vol. 104, no. 13, pp. 5431–5436.

Peixeiro, I, Inácio, Â, Barbosa, C, Silva, AL, Liebhaber, SA & Romão, L 2012, 'Interaction of PABPC1 with the translation initiation complex is critical to the NMD resistance of AUG-proximal nonsense mutations.', *Nucleic Acids Research*, vol. 40, no. 3, pp. 1160–1173.

Pellat-Deceunynck, C & Bataille, R 2004, 'Normal and malignant human plasma cells: proliferation, differentiation, and expansions in relation to CD45 expression.', *Blood Cells, Molecules & Diseases*, vol. 32, no. 2, pp. 293–301.

Peng, J, Zhang, L, Drysdale, L & Fong, GH 2000, 'The transcription factor EPAS-1/hypoxia-inducible factor 2alpha plays an important role in vascular remodeling.', *Proceedings of the National Academy of Sciences of the United States of America*, vol. 97, no. 15, pp. 8386–8391.

Pereira, FJC, Teixeira, A, Kong, J, Barbosa, C, Silva, AL, Marques-Ramos, A, Liebhaber, SA & Romão, L 2015, 'Resistance of mRNAs with AUG-proximal nonsense mutations to nonsense-mediated decay reflects variables of mRNA structure and translational activity.', *Nucleic Acids Research*, vol. 43, no. 13, pp. 6528–6544.

Pichiule, P, Chavez, JC & LaManna, JC 2004, 'Hypoxic regulation of angiopoietin-2 expression in endothelial cells.', *The Journal of Biological Chemistry*, vol. 279, no. 13, pp. 12171–12180.

Pietras, A, Johnsson, AS & Påhlman, S 2010, 'The HIF-2α-driven pseudo-hypoxic phenotype in tumor aggressiveness, differentiation, and vascularization.', *Current Topics in Microbiology and Immunology*, vol. 345, pp. 1–20.

Ponomarev, V, Doubrovin, M, Serganova, I, Vider, J, Shavrin, A, Beresten, T, Ivanova, A, Ageyeva, L, Tourkova, V, Balatoni, J, Bornmann, W, Blasberg, R & Gelovani Tjuvajev, J 2004, 'A novel triple-modality reporter gene for whole-body fluorescent, bioluminescent, and nuclear noninvasive imaging.', *European Journal of Nuclear Medicine and Molecular Imaging*, vol. 31, no. 5, pp. 740–751.

Popp, MW & Maquat, LE 2016, 'Leveraging Rules of Nonsense-Mediated mRNA Decay for Genome Engineering and Personalized Medicine.', *Cell*, vol. 165, no. 6, pp. 1319–1322.

Radl, J, Hollander, CF, van den Berg, P & de Glopper, E 1978, 'Idiopathic paraproteinaemia. I. Studies in an animal model--the ageing C57BL/KaLwRij mouse.', *Clinical and Experimental Immunology*, vol. 33, no. 3, pp. 395–402.

Rajkumar, SV 2016, 'Multiple myeloma: 2016 update on diagnosis, risk-stratification, and management.', *American Journal of Hematology*, vol. 91, no. 7, pp. 719–734.

Rajkumar, SV, Dimopoulos, MA, Palumbo, A, Blade, J, Merlini, G, Mateos, M-V, Kumar, S, Hillengass, J, Kastritis, E, Richardson, P, Landgren, O, Paiva, B, Dispenzieri, A, Weiss, B, LeLeu, X, Zweegman, S, Lonial, S, Rosinol, L, Zamagni, E, Jagannath, S, Sezer, O, Kristinsson, SY, Caers, J, Usmani, SZ, Lahuerta, JJ, Johnsen, HE, Beksac, M, Cavo, M, Goldschmidt, H, Terpos, E, Kyle, RA, Anderson, KC, Durie, BGM & Miguel, JFS 2014, 'International Myeloma Working Group updated criteria for the diagnosis of multiple myeloma.', *The Lancet Oncology*, vol. 15, no. 12, pp. e538–48.

Rajkumar, SV, Mesa, RA, Fonseca, R, Schroeder, G, Plevak, MF, Dispenzieri, A, Lacy, MQ, Lust, JA, Witzig, TE, Gertz, MA, Kyle, RA, Russell, SJ & Greipp, PR 2002, 'Bone marrow angiogenesis in 400 patients with monoclonal gammopathy of undetermined significance, multiple myeloma, and primary amyloidosis.', *Clinical Cancer Research*, vol. 8, no. 7, pp. 2210–2216.

Ran, FA, Hsu, PD, Wright, J, Agarwala, V, Scott, DA & Zhang, F 2013, 'Genome engineering using the CRISPR-Cas9 system.', *Nature Protocols*, vol. 8, no. 11, pp. 2281–2308.

Rangarajan, A & Weinberg, RA 2003, 'Opinion: Comparative biology of mouse versus human cells: modelling human cancer in mice.', *Nature Reviews. Cancer*, vol. 3, no. 12, pp. 952–959.

Renassia, C & Peyssonnaux, C 2019, 'New insights into the links between hypoxia and iron homeostasis.', *Current Opinion in Hematology*, vol. 26, no. 3, pp. 125–130.

Del Rey, MJ, Valín, Á, Usategui, A, García-Herrero, CM, Sánchez-Aragó, M, Cuezva, JM, Galindo, M, Bravo, B, Cañete, JD, Blanco, FJ, Criado, G & Pablos, JL 2017, 'Hif-1α Knockdown Reduces Glycolytic Metabolism and Induces Cell Death of Human Synovial Fibroblasts Under Normoxic Conditions.', *Scientific Reports*, vol. 7, no. 1, p. 3644.

Ribatti, D 2009, 'Is angiogenesis essential for the progression of hematological malignancies or is it an epiphenomenon?', *Leukemia*, vol. 23, no. 3, pp. 433–434.

Ritchie, ME, Phipson, B, Wu, D, Hu, Y, Law, CW, Shi, W & Smyth, GK 2015, 'limma powers differential expression analyses for RNA-sequencing and microarray studies.', *Nucleic Acids Research*, vol. 43, no. 7, p. e47.

Roccaro, AM, Mishima, Y, Sacco, A, Moschetta, M, Tai, Y-T, Shi, J, Zhang, Y, Reagan, MR, Huynh, D, Kawano, Y, Sahin, I, Chiarini, M, Manier, S, Cea, M, Aljawai, Y, Glavey, S, Morgan, E, Pan, C, Michor, F, Cardarelli, P, Kuhne, M & Ghobrial, IM 2015, 'CXCR4 Regulates Extra-Medullary Myeloma through Epithelial-Mesenchymal-Transition-like Transcriptional Activation.', *Cell reports*, vol. 12, no. 4, pp. 622–635.

Rouault-Pierre, K, Lopez-Onieva, L, Foster, K, Anjos-Afonso, F, Lamrissi-Garcia, I, Serrano-Sanchez, M, Mitter, R, Ivanovic, Z, de Verneuil, H, Gribben, J, Taussig, D, Rezvani, HR, Mazurier, F & Bonnet, D 2013, 'HIF-2α protects human hematopoietic stem/progenitors and acute myeloid leukemic cells from apoptosis induced by endoplasmic reticulum stress.', *Cell Stem Cell*, vol. 13, no. 5, pp. 549–563.

Ruan, K, Song, G & Ouyang, G 2009, 'Role of hypoxia in the hallmarks of human cancer.', *Journal of Cellular Biochemistry*, vol. 107, no. 6, pp. 1053–1062.

Saba, F, Soleimani, M & Abroun, S 2018, 'New role of hypoxia in pathophysiology of multiple myeloma through miR-210.', *EXCLI journal*, vol. 17, pp. 647–662.

Sanchez, WY, McGee, SL, Connor, T, Mottram, B, Wilkinson, A, Whitehead, JP, Vuckovic, S & Catley, L 2013, 'Dichloroacetate inhibits aerobic glycolysis in multiple myeloma cells and increases sensitivity to bortezomib.', *British Journal of Cancer*, vol. 108, no. 8, pp. 1624–1633.

Sang, N, Stiehl, DP, Bohensky, J, Leshchinsky, I, Srinivas, V & Caro, J 2003, 'MAPK signaling up-regulates the activity of hypoxia-inducible factors by its effects on p300.', *The Journal of Biological Chemistry*, vol. 278, no. 16, pp. 14013–14019.

Schito, L, Rey, S & Konopleva, M 2017, 'Integration of hypoxic HIF-α signaling in blood cancers.', *Oncogene*, vol. 36, no. 38, pp. 5331–5340.

Schito, L & Semenza, GL 2016, 'Hypoxia-Inducible Factors: Master Regulators of Cancer Progression.', *Trends in cancer*, vol. 2, no. 12, pp. 758–770.

Schödel, J, Oikonomopoulos, S, Ragoussis, J, Pugh, CW, Ratcliffe, PJ & Mole, DR 2011, 'High-resolution genome-wide mapping of HIF-binding sites by ChIP-seq.', *Blood*, vol. 117, no. 23, pp. e207–17.

Schoenhals, M, Jourdan, M, Bruyer, A, Kassambara, A, Klein, B & Moreaux, J 2017, 'Hypoxia favors the generation of human plasma cells.', *Cell Cycle*, vol. 16, no. 11, pp. 1104–1117.

Schofield, CJ & Ratcliffe, PJ 2004, 'Oxygen sensing by HIF hydroxylases.', *Nature Reviews. Molecular Cell Biology*, vol. 5, no. 5, pp. 343–354.

Schwartz, AJ, Das, NK, Ramakrishnan, SK, Jain, C, Jurkovic, MT, Wu, J, Nemeth, E, Lakhal-Littleton, S, Colacino, JA & Shah, YM 2019, 'Hepatic hepcidin/intestinal HIF-2α axis maintains iron absorption during iron deficiency and overload.', *The Journal of Clinical Investigation*, vol. 129, no. 1, pp. 336–348.

Semenza, G 2002, 'Signal transduction to hypoxia-inducible factor 1.', *Biochemical Pharmacology*, vol. 64, no. 5-6, pp. 993–998.

Semenza, GL 2003, 'Targeting HIF-1 for cancer therapy.', *Nature Reviews. Cancer*, vol. 3, no. 10, pp. 721–732.

Senapedis, WT, Baloglu, E & Landesman, Y 2014, 'Clinical translation of nuclear export inhibitors in cancer.', *Seminars in Cancer Biology*, vol. 27, pp. 74–86.

Sentmanat, MF, Peters, ST, Florian, CP, Connelly, JP & Pruett-Miller, SM 2018, 'A Survey of Validation Strategies for CRISPR-Cas9 Editing.', *Scientific Reports*, vol. 8, no. 1, p. 888.

Sezer, O, Niemöller, K, Eucker, J, Jakob, C, Kaufmann, O, Zavrski, I, Dietel, M & Possinger, K 2000, 'Bone marrow microvessel density is a prognostic factor for survival in patients with multiple myeloma.', *Annals of Hematology*, vol. 79, no. 10, pp. 574–577.

Shah, SA, Erdmann, S, Mojica, FJM & Garrett, RA 2013, 'Protospacer recognition motifs: mixed identities and functional diversity.', *RNA Biology*, vol. 10, no. 5, pp. 891–899.

Shen, C, Beroukhim, R, Schumacher, SE, Zhou, J, Chang, M, Signoretti, S & Kaelin, WG 2011, 'Genetic and functional studies implicate HIF1α as a 14q kidney cancer suppressor gene.', *Cancer discovery*, vol. 1, no. 3, pp. 222–235.

Shi, J, Wang, E, Milazzo, JP, Wang, Z, Kinney, JB & Vakoc, CR 2015, 'Discovery of cancer drug targets by CRISPR-Cas9 screening of protein domains.', *Nature Biotechnology*, vol. 33, no. 6, pp. 661–667.

Shin, DH, Chun, Y-S, Lee, DS, Huang, LE & Park, J-W 2008, 'Bortezomib inhibits tumor adaptation to hypoxia by stimulating the FIH-mediated repression of hypoxia-inducible factor-1.', *Blood*, vol. 111, no. 6, pp. 3131–3136.

Siegel, R, Naishadham, D & Jemal, A 2012, 'Cancer statistics, 2012.', *CA: A Cancer Journal for Clinicians*, vol. 62, no. 1, pp. 10–29.

Simsek, T, Kocabas, F, Zheng, J, Deberardinis, RJ, Mahmoud, AI, Olson, EN, Schneider, JW, Zhang, CC & Sadek, HA 2010, 'The distinct metabolic profile of hematopoietic stem cells reflects their location in a hypoxic niche.', *Cell Stem Cell*, vol. 7, no. 3, pp. 380–390.

Singh, D, Arora, R, Kaur, P, Singh, B, Mannan, R & Arora, S 2017, 'Overexpression of hypoxia-inducible factor and metabolic pathways: possible targets of cancer.', *Cell & bioscience*, vol. 7, p. 62.

Smythies, JA, Sun, M, Masson, N, Salama, R, Simpson, PD, Murray, E, Neumann, V, Cockman, ME, Choudhry, H, Ratcliffe, PJ & Mole, DR 2019, 'Inherent DNA-binding specificities of the HIF-1α and HIF-2α transcription factors in chromatin.', *EMBO Reports*, vol. 20, no. 1.

Son, H & Moon, A 2010, 'Epithelial-mesenchymal Transition and Cell Invasion.', *Toxicological research*, vol. 26, no. 4, pp. 245–252.

Spencer, JA, Ferraro, F, Roussakis, E, Klein, A, Wu, J, Runnels, JM, Zaher, W, Mortensen, LJ, Alt, C, Turcotte, R, Yusuf, R, Côté, D, Vinogradov, SA, Scadden, DT & Lin, CP 2014, 'Direct measurement of local oxygen concentration in the bone marrow of live animals.', *Nature*, vol. 508, no. 7495, pp. 269–273.

Steinbrunn, T, Chatterjee, M, Bargou, RC & Stühmer, T 2014, 'Efficient transient transfection of human multiple myeloma cells by electroporation--an appraisal.', *Plos One*, vol. 9, no. 6, p. e97443.

Storti, P, Bolzoni, M, Donofrio, G, Airoldi, I, Guasco, D, Toscani, D, Martella, E, Lazzaretti, M, Mancini, C, Agnelli, L, Patrene, K, Maïga, S, Franceschi, V, Colla, S, Anderson, J, Neri, A, Amiot, M, Aversa, F, Roodman, GD & Giuliani, N 2013, 'Hypoxia-inducible factor (HIF)-1α suppression in myeloma cells blocks tumoral growth in vivo inhibiting angiogenesis and bone destruction.', *Leukemia*, vol. 27, no. 8, pp. 1697–1706.

Suan, D, Sundling, C & Brink, R 2017, 'Plasma cell and memory B cell differentiation from the germinal center.', *Current Opinion in Immunology*, vol. 45, pp. 97–102.

Sun, X, Pang, L, Shi, M, Huang, J & Wang, Y 2015, 'HIF2α induces cardiomyogenesis via Wnt/β-catenin signaling in mouse embryonic stem cells.', *Journal of Translational Medicine*, vol. 13, p. 88.

Takeda, K, Aguila, HL, Parikh, NS, Li, X, Lamothe, K, Duan, L-J, Takeda, H, Lee, FS & Fong, G-H 2008, 'Regulation of adult erythropoiesis by prolyl hydroxylase domain proteins.', *Blood*, vol. 111, no. 6, pp. 3229–3235.

Takeda, N, O'Dea, EL, Doedens, A, Kim, J, Weidemann, A, Stockmann, C, Asagiri, M, Simon, MC, Hoffmann, A & Johnson, RS 2010, 'Differential activation and antagonistic function of HIF-{alpha} isoforms in macrophages are essential for NO homeostasis.', *Genes & Development*, vol. 24, no. 5, pp. 491–501.

Takubo, K, Goda, N, Yamada, W, Iriuchishima, H, Ikeda, E, Kubota, Y, Shima, H, Johnson, RS, Hirao, A, Suematsu, M & Suda, T 2010, 'Regulation of the HIF-1alpha level is essential for hematopoietic stem cells.', *Cell Stem Cell*, vol. 7, no. 3, pp. 391–402.

Tanimoto, K, Makino, Y, Pereira, T & Poellinger, L 2000, 'Mechanism of regulation of the hypoxia-inducible factor-1 alpha by the von Hippel-Lindau tumor suppressor protein.', *The EMBO Journal*, vol. 19, no. 16, pp. 4298–4309.

Tarazona, S, García-Alcalde, F, Dopazo, J, Ferrer, A & Conesa, A 2011, 'Differential expression in RNA-seq: a matter of depth.', *Genome Research*, vol. 21, no. 12, pp. 2213–2223.

Tarhonskaya, H, Hardy, AP, Howe, EA, Loik, ND, Kramer, HB, McCullagh, JSO, Schofield, CJ & Flashman, E 2015, 'Kinetic Investigations of the Role of Factor Inhibiting Hypoxia-inducible Factor (FIH) as an Oxygen Sensor.', *The Journal of Biological Chemistry*, vol. 290, no. 32, pp. 19726–19742.

Terpos, E, Politou, M, Szydlo, R, Goldman, JM, Apperley, JF & Rahemtulla, A 2003, 'Serum levels of macrophage inflammatory protein-1 alpha (MIP-1alpha) correlate with the extent of bone disease and survival in patients with multiple myeloma.', *British Journal of Haematology*, vol. 123, no. 1, pp. 106–109.

TeSlaa, T & Teitell, MA 2014, 'Techniques to monitor glycolysis.', *Methods in Enzymology*, vol. 542, pp. 91–114.

Thompson, E 2018, 'Generation of an H3N2 Influenza A Reporter Virus to Visualize Modern Infection Dynamics'.

Tian, H, Hammer, RE, Matsumoto, AM, Russell, DW & McKnight, SL 1998, 'The hypoxia-responsive transcription factor EPAS1 is essential for catecholamine homeostasis and protection against heart failure during embryonic development.', *Genes & Development*, vol. 12, no. 21, pp. 3320–3324.

Tian, H, McKnight, SL & Russell, DW 1997, 'Endothelial PAS domain protein 1 (EPAS1), a transcription factor selectively expressed in endothelial cells.', *Genes & Development*, vol. 11, no. 1, pp. 72–82.

Togashi, Y, Mizuuchi, H, Tomida, S, Terashima, M, Hayashi, H, Nishio, K & Mitsudomi, T 2015, 'MET gene exon 14 deletion created using the CRISPR/Cas9 system enhances

cellular growth and sensitivity to a MET inhibitor.', *Lung Cancer*, vol. 90, no. 3, pp. 590–597.

Treins, C, Giorgetti-Peraldi, S, Murdaca, J, Semenza, GL & Van Obberghen, E 2002, 'Insulin stimulates hypoxia-inducible factor 1 through a phosphatidylinositol 3-kinase/target of rapamycin-dependent signaling pathway.', *The Journal of Biological Chemistry*, vol. 277, no. 31, pp. 27975–27981.

Trotter, TN, Li, M, Pan, Q, Peker, D, Rowan, PD, Li, J, Zhan, F, Suva, LJ, Javed, A & Yang, Y 2015, 'Myeloma cell-derived Runx2 promotes myeloma progression in bone.', *Blood*, vol. 125, no. 23, pp. 3598–3608.

Umezu, T, Tadokoro, H, Azuma, K, Yoshizawa, S, Ohyashiki, K & Ohyashiki, JH 2014, 'Exosomal miR-135b shed from hypoxic multiple myeloma cells enhances angiogenesis by targeting factor-inhibiting HIF-1.', *Blood*, vol. 124, no. 25, pp. 3748–3757.

Uprety, D, Adhikari, J, Arjyal, L, Naglak, MC & Seidman, M 2017, 'Racial differences in the survival of elderly patients with multiple myeloma in pre- and post-novel agent era', *Journal of Geriatric Oncology*, vol. 8, no. 2, pp. 125–127.

Vacca, A, Ribatti, D, Presta, M, Minischetti, M, Iurlaro, M, Ria, R, Albini, A, Bussolino, F & Dammacco, F 1999, 'Bone marrow neovascularization, plasma cell angiogenic potential, and matrix metalloproteinase-2 secretion parallel progression of human multiple myeloma.', *Blood*, vol. 93, no. 9, pp. 3064–3073.

Vacca, A, Ribatti, D, Roncali, L, Ranieri, G, Serio, G, Silvestris, F & Dammacco, F 1994, 'Bone marrow angiogenesis and progression in multiple myeloma.', *British Journal of Haematology*, vol. 87, no. 3, pp. 503–508.

Vandyke, K, Zeissig, MN, Hewett, DR, Martin, SK, Mrozik, KM, Cheong, CM, Diamond, P, To, LB, Gronthos, S, Peet, DJ, Croucher, PI & Zannettino, ACW 2017, 'HIF-2α Promotes Dissemination of Plasma Cells in Multiple Myeloma by Regulating CXCL12/CXCR4 and CCR1.', *Cancer Research*, vol. 77, no. 20, pp. 5452–5463.

Vaquerizas, JM, Kummerfeld, SK, Teichmann, SA & Luscombe, NM 2009, 'A census of human transcription factors: function, expression and evolution.', *Nature Reviews. Genetics*, vol. 10, no. 4, pp. 252–263.

Vaupel, P & Harrison, L 2004, 'Tumor hypoxia: causative factors, compensatory mechanisms, and cellular response.', *The Oncologist*, vol. 9 Suppl 5, pp. 4–9.

Verstovsek, S, Kantarjian, H, Manshouri, T, Cortes, J, Giles, FJ, Rogers, A & Albitar, M 2002, 'Prognostic significance of cellular vascular endothelial growth factor expression in chronic phase chronic myeloid leukemia.', *Blood*, vol. 99, no. 6, pp. 2265–2267.

Viguera, E, Canceill, D & Ehrlich, SD 2001, 'In vitro replication slippage by DNA polymerases from thermophilic organisms.', *Journal of Molecular Biology*, vol. 312, no. 2, pp. 323–333.

Viziteu, E, Grandmougin, C, Goldschmidt, H, Seckinger, A, Hose, D, Klein, B & Moreaux, J 2016, 'Chetomin, targeting HIF-1α/p300 complex, exhibits antitumour activity in multiple myeloma.', *British Journal of Cancer*, vol. 114, no. 5, pp. 519–523.

Vouillot, L, Thélie, A & Pollet, N 2015, 'Comparison of T7E1 and surveyor mismatch cleavage assays to detect mutations triggered by engineered nucleases.', *G3 (Bethesda, Md.)*, vol. 5, no. 3, pp. 407–415.

Wang, GL, Jiang, BH, Rue, EA & Semenza, GL 1995, 'Hypoxia-inducible factor 1 is a basic-helix-loop-helix-PAS heterodimer regulated by cellular O2 tension.', *Proceedings of the National Academy of Sciences of the United States of America*, vol. 92, no. 12, pp. 5510–5514.

Wang, L, Jackson, WC, Steinbach, PA & Tsien, RY 2004, 'Evolution of new nonantibody proteins via iterative somatic hypermutation.', *Proceedings of the National Academy of Sciences of the United States of America*, vol. 101, no. 48, pp. 16745–16749.

Wang, V, Davis, DA, Haque, M, Huang, LE & Yarchoan, R 2005, 'Differential gene up-regulation by hypoxia-inducible factor-1alpha and hypoxia-inducible factor-2alpha in HEK293T cells.', *Cancer Research*, vol. 65, no. 8, pp. 3299–3306.

Wang, Z, Gerstein, M & Snyder, M 2009, 'RNA-Seq: a revolutionary tool for transcriptomics.', *Nature Reviews. Genetics*, vol. 10, no. 1, pp. 57–63.

Ward, CM, To, H & Pederson, SM 2018, 'ngsReports: An R Package for managing FastQC reports and other NGS related log files.', *BioRxiv*.

Watanabe, Y, Terashima, Y, Takenaka, N, Kobayashi, M & Matsushita, T 2007, 'Prediction of avascular necrosis of the femoral head by measuring intramedullary oxygen tension after femoral neck fracture.', *Journal of Orthopaedic Trauma*, vol. 21, no. 7, pp. 456–461.

Wellmann, S, Guschmann, M, Griethe, W, Eckert, C, von Stackelberg, A, Lottaz, C, Moderegger, E, Einsiedel, HG, Eckardt, KU, Henze, G & Seeger, K 2004, 'Activation of the HIF pathway in childhood ALL, prognostic implications of VEGF.', *Leukemia*, vol. 18, no. 5, pp. 926–933.

Weng, CC, Hawse, JR, Subramaniam, M, Chang, VHS, Yu, WCY, Hung, WC, Chen, LT & Cheng, KH 2017, 'KLF10 loss in the pancreas provokes activation of SDF-1 and induces distant metastases of pancreatic ductal adenocarcinoma in the KrasG12D p53flox/flox model.', *Oncogene*, vol. 36, no. 39, pp. 5532–5543.

Wenger, RH, Stiehl, DP & Camenisch, G 2005, 'Integration of oxygen signaling at the consensus HRE.', *Science's STKE: Signal Transduction Knowledge Environment*, vol. 2005, no. 306, p. re12.

Westfall, SD, Sachdev, S, Das, P, Hearne, LB, Hannink, M, Roberts, RM & Ezashi, T 2008, 'Identification of oxygen-sensitive transcriptional programs in human embryonic stem cells.', *Stem Cells and Development*, vol. 17, no. 5, pp. 869–881.

Wiesener, MS, Jürgensen, JS, Rosenberger, C, Scholze, CK, Hörstrup, JH, Warnecke, C, Mandriota, S, Bechmann, I, Frei, UA, Pugh, CW, Ratcliffe, PJ, Bachmann, S, Maxwell, PH & Eckardt, K-U 2003, 'Widespread hypoxia-inducible expression of HIF-2alpha in distinct cell populations of different organs.', *The FASEB Journal*, vol. 17, no. 2, pp. 271–273.

Wu, J, Contratto, M, Shanbhogue, KP, Manji, GA, O'Neil, BH, Noonan, A, Tudor, R & Lee, R 2019, 'Evaluation of a locked nucleic acid form of antisense oligo targeting HIF-1α in

advanced hepatocellular carcinoma.', *World journal of clinical oncology*, vol. 10, no. 3, pp. 149–160.

Xie, C, Gao, X, Sun, D, Zhang, Y, Krausz, KW, Qin, X & Gonzalez, FJ 2018, 'Metabolic Profiling of the Novel Hypoxia-Inducible Factor 2α Inhibitor PT2385 In Vivo and In Vitro.', *Drug Metabolism and Disposition: the Biological Fate of Chemicals*, vol. 46, no. 4, pp. 336–345.

Xu, R-H, Pelicano, H, Zhou, Y, Carew, JS, Feng, L, Bhalla, KN, Keating, MJ & Huang, P 2005, 'Inhibition of glycolysis in cancer cells: a novel strategy to overcome drug resistance associated with mitochondrial respiratory defect and hypoxia.', *Cancer Research*, vol. 65, no. 2, pp. 613–621.

Xu, Y, Li, Y, Pang, Y, Ling, M, Shen, L, Yang, X, Zhang, J, Zhou, J, Wang, X & Liu, Q 2012, 'EMT and stem cell-like properties associated with HIF-2α are involved in arsenite-induced transformation of human bronchial epithelial cells.', *Plos One*, vol. 7, no. 5, p. e37765.

Yang, J, Zhang, L, Erbel, PJA, Gardner, KH, Ding, K, Garcia, JA & Bruick, RK 2005, 'Functions of the Per/ARNT/Sim domains of the hypoxia-inducible factor.', *The Journal of Biological Chemistry*, vol. 280, no. 43, pp. 36047–36054.

Yao, S, Sukonnik, T, Kean, T, Bharadwaj, RR, Pasceri, P & Ellis, J 2004, 'Retrovirus silencing, variegation, extinction, and memory are controlled by a dynamic interplay of multiple epigenetic modifications.', *Molecular Therapy*, vol. 10, no. 1, pp. 27–36.

Yarrington, RM, Verma, S, Schwartz, S, Trautman, JK & Carroll, D 2018, 'Nucleosomes inhibit target cleavage by CRISPR-Cas9 in vivo.', *Proceedings of the National Academy of Sciences of the United States of America*, vol. 115, no. 38, pp. 9351–9358.

Yu, X, Huang, Y, Collin-Osdoby, P & Osdoby, P 2003, 'Stromal cell-derived factor-1 (SDF-1) recruits osteoclast precursors by inducing chemotaxis, matrix metalloproteinase-9 (MMP-9) activity, and collagen transmigration.', *Journal of Bone and Mineral Research*, vol. 18, no. 8, pp. 1404–1418.

Zahoor, M, Westhrin, M, Aass, KR, Moen, SH, Misund, K, Psonka-Antonczyk, KM, Giliberto, M, Buene, G, Sundan, A, Waage, A, Sponaas, A-M & Standal, T 2017, 'Hypoxia promotes IL-32 expression in myeloma cells, and high expression is associated with poor survival and bone loss.', *Blood Advances*, vol. 1, no. 27, pp. 2656–2666.

Zannettino, ACW, Farrugia, AN, Kortesidis, A, Manavis, J, To, LB, Martin, SK, Diamond, P, Tamamura, H, Lapidot, T, Fujii, N & Gronthos, S 2005, 'Elevated serum levels of stromal-derived factor-1alpha are associated with increased osteoclast activity and osteolytic bone disease in multiple myeloma patients.', *Cancer Research*, vol. 65, no. 5, pp. 1700–1709.

Zhang, H, Bosch-Marce, M, Shimoda, LA, Tan, YS, Baek, JH, Wesley, JB, Gonzalez, FJ & Semenza, GL 2008, 'Mitochondrial autophagy is an HIF-1-dependent adaptive metabolic response to hypoxia.', *The Journal of Biological Chemistry*, vol. 283, no. 16, pp. 10892–10903.

Zhang, W, Shi, X, Peng, Y, Wu, M, Zhang, P, Xie, R, Wu, Y, Yan, Q, Liu, S & Wang, J 2015, 'HIF-1α Promotes Epithelial-Mesenchymal Transition and Metastasis through Direct Regulation of ZEB1 in Colorectal Cancer.', *Plos One*, vol. 10, no. 6, p. e0129603.

Zhang, X, Xu, Y, Liu, H, Zhao, P, Chen, Y, Yue, Z, Zhang, Z & Wang, X 2018, 'HIF-2α-ILK Is Involved in Mesenchymal Stromal Cell Angiogenesis in Multiple Myeloma Under Hypoxic Conditions.', *Technology in Cancer Research & Treatment*, vol. 17, p. 1533033818764473.

Zhang, X-H, Tee, LY, Wang, X-G, Huang, Q-S & Yang, S-H 2015, 'Off-target Effects in CRISPR/Cas9-mediated Genome Engineering.', *Molecular therapy. Nucleic acids*, vol. 4, p. e264.

Zhao, S, Zhang, Y, Gamini, R, Zhang, B & von Schack, D 2018, 'Evaluation of two main RNA-seq approaches for gene quantification in clinical RNA sequencing: polyA+ selection versus rRNA depletion.', *Scientific Reports*, vol. 8, no. 1, p. 4781.